PROCEEDINGS OF THE ELEVENTH WORKING MEETING ON EUROPEAN VLBI FOR GEODESY AND ASTROMETRY

Edited by

G Elgered

Research Report No 177
1996

DEPARTMENT OF RADIO AND SPACE SCIENCE
WITH ONSALA SPACE OBSERVATORY
CHALMERS UNIVERSITY OF TECHNOLOGY
GÖTEBORG, SWEDEN

CHALMERS TEKNISKA HÖGSKOLA
AVANCEZ
GÖTEBORG

PROCEEDINGS OF THE ELEVENTH WORKING MEETING ON EUROPEAN VLBI FOR GEODESY AND ASTROMETRY

published as

Research Report No 177

ISSN 1100-5564

edited by

Gunnar Elgered

Onsala Space Observatory
Chalmers University of Technology
Göteborg
September 1996

Preface

What do you expect to find in the preface of a conference proceedings? I never thought about that until today. In order to investigate this matter I have now read more prefaces to conference proceedings than ever before! I have found that you typically write that it was a great meeting. However, if you think about that for a while you realize that this is useless information because all of you that were here already know that it was a great meeting; and those that were not will not believe it, because such a statement is always written in the preface to any proceedings.

We appreciate the efforts of many staff members at the Chalmers University of Technology and the Onsala Space Observatory for the arrangements. Especially we would like to thank Mrs Barbro Lindberg whose flexibility and enthusiasm is greatly appreciated.

Finally, the work related to this meeting is over and the results and plans discussed are archived so that future generations can benefit from all our findings. Can you imagine your grandchildren reading your paper from this report some time in the future? Anyway, we can now look forward to the twelfth working meeting in Norway next summer and until then we can study these proceedings during the long and dark winter nights.

Onsala 1996-09-27
Gunnar Elgered

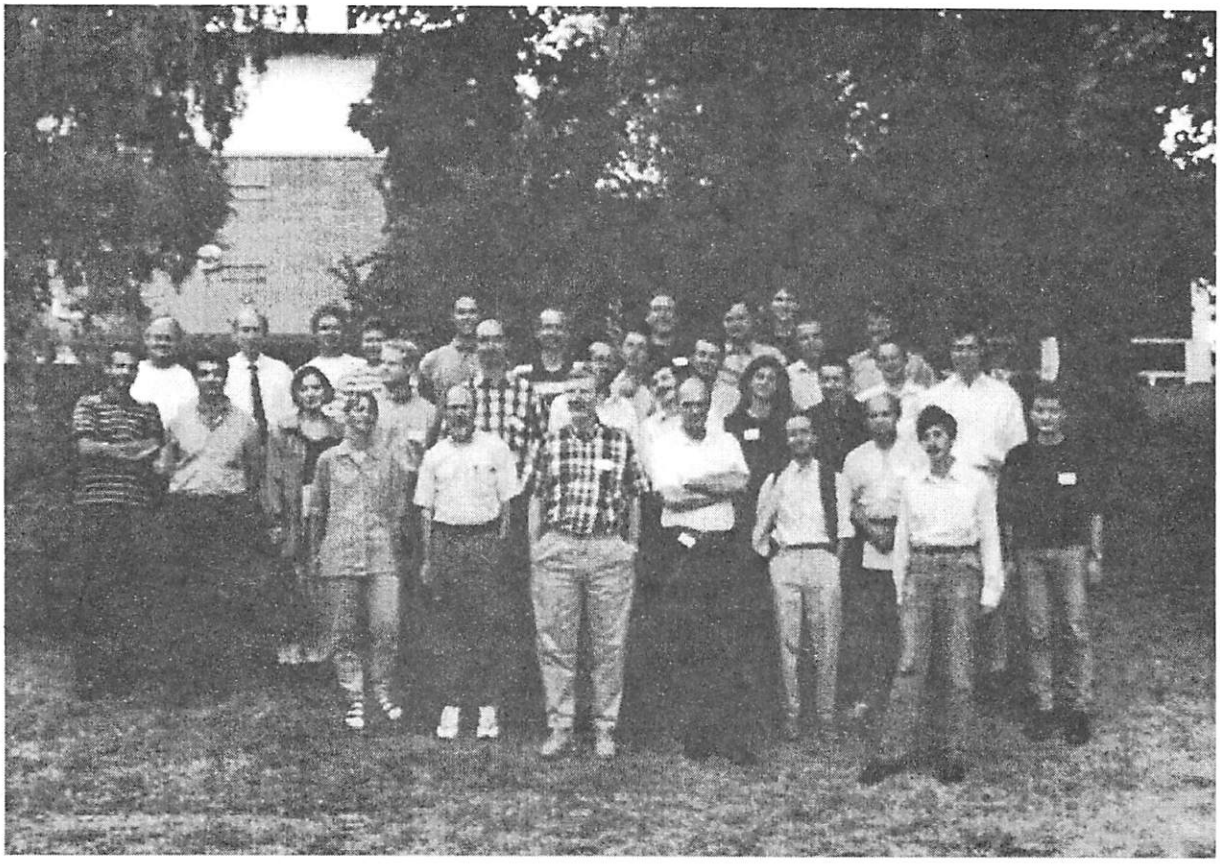

Meeting participants on the library hill.

TABLE OF CONTENTS

STATUS REPORT SESSION

Status Report on the Geodetic VLBI European Network 1
M. Sorgente

Status Report From MPIfR Correlator, August 1996 6
R. Porcas and W. Alef

Status of ERS/VLBI Station O'Higgins - Antarctica 7
A. Reinhold, J. Ihde, V. Thorandt, and R. Wojdziak

Effelsberg Status Report, August 1996 13
R. Porcas

Status Report at OAN — Yebes VLBI Station 14
OAN-Yebes VLBI group

Status Report of RT-Wettzell 18
R. Kilger

Radioastronomy at the NASA Madrid Deep Space Communications Complex 21
A. Rius, A. Alberdi, and J.A. Perea

Status Report on Noto VLBI Station 31
V. Tornatore, G. Tuccari, G. Nicotra, S. Buttaccio, C. Contavalle, and C. Stanghellini

Matera VLBI Station: Status Report 40
G. Bianco, D. DelRosso, L. Garramone, and G. Colucci

Geodesy and VLBI in the Netherlands: A Status Report 43
R. Molendijk

VLBI at Ny-Ålesund Space Geodetic Observatory Station Report 1995–1996 . 44
B.R. Pettersen

Status of the TIGO-Project 49
H. Hase, A. Böer, W. Schlüter, R. Dassing, P. Sperber, and R. Kilger

Geodetic Very-Long-Baseline Interferometry at the Onsala Space Observatory 1995–1996 55
G. Elgered

TECHNICAL SESSION

A New S/X Receiver For Noto Antenna 62
G. Tuccari, A. Orfei, and V. Tornatore

Time Transfer With VLBI Better Than 1ns Accuracy 68
H. Hase, T. Yoshino, S. Hama, H. Kiuchi, A. Kaneko Y. Takahashi, and R. Kilger

Yebes Phase Calibration Unit: Design, Construction, Performance and Tests on Thermal Influence 76
I. López-Fernández

ATMOSPHERIC EFFECTS IN GEODETIC VLBI

Propagation Delay Fluctuations in the Earth Troposphere: Random and Regular Components 83
A.A. Stotskii

A Quality Assessment of the Wet Path-Delay Estimated From GPS Data 89
T.R. Carlsson, G. Elgered, and J.M. Johansson

Measurement of Water Vapor by GPS, WVR, and Radiosonde 96
A.E. Niell, A.J. Coster, F.S. Solheim, V.B. Mendes, P.C. Toor, R.B. Langley, C.A. Ruggles

Strategies For Spatial and Temporal Extrapolation and Interpolation of Wet Path Delay 102
P.O.J. Jarlemark and T.R. Carlsson

VLBI ANALYSIS SESSION

Update on European Geodetic VLBI Analyses at the Geodetic Institute of the University of Bonn 110
A. Nothnagel

A Comprehensive and Tentatively Complete Summary of Oceanic Effects In Space Geodetic Baseline Measurements 121
H.-G. Scherneck

Spectral Analysis of the Baselength Time Series 134
O. Titov and E. Yakovleva

Determination of Height Changes in Regional GPS Networks 143
B. Görres

Service of VLBI Data Analysis at the Institute of Applied Astronomy 153
L. Petrov

Determination of Tidal Parameters From VLBI Data 162
R. Haas, H. Schuh, and J. Wünsch

Status Report on the Combination of VLBI and Other Space Geodetic Data . 172
P. H. Andersen

Determination of Metric Coefficients With VLBI 181
K. Boerger

The CGS VLBI EUR96 Geodetic Solution 187
R. Lanotte, G. Bianco, M. Fermi, P. Rutigliano, and G.R. Verdone

International Radio Interferometric Surveying — South: Results of the First 100 Sessions 194
A. Nothnagel, R. Haas, and H. Seeger

The Geodetic VLBI Observations at CRIMEA Station and Some Results of the Analysis 200
A. Bajkova, A. Finkelstein, A. Ipatov, D. Ivanov, V. Mardyshkin, and T. Pyatunina

A New Mapping Method For Astrometry of Close Source Pairs 209
R.W. Porcas and M.J. Rioja

Comparative VLBI Astrometric Analysis of the Pair 1308+326 and 1308+328 219
M.J. Rioja and R.W. Porcas

FUTURE EUROPEAN GEODESY VLBI SESSION

Measurement of Vertical Crustal Motion in Europe by VLBI—Further Support of the European Geodetic VLBI Network by the European Union 227
J. Campbell

APPENDIX A: The Competition: Questions and Answers A.1–A.2

APPENDIX B: List of Participants B.1–B.4

When you steal from one author it is plagiarism,
but when you steal from many it is research.

Wilson Mizner

Status Report on the Geodetic VLBI European Network

Mauro SORGENTE
Geodetic Institute of the University of Bonn (GIUB), Germany

Abstract

Presently the European Network is composed of seven core stations (Wettzell, Onsala, Madrid, Ny Alesund, Noto, Matera, Bologna) plus other two stations that occasionally take part in the network (Effelsberg and Crimea). The station at Yebes will join this network as soon as possible.

A period of transition started since the last meeting. For this reason the standard configuration of the network was changed (with the exception of the Europe6-95 campaign) and the number of antennas was limited to 5-6. This was due to many factors, but mainly the limitation created in correlating staffing by the leaving of Dr. Kurt Standke.

Introduction

Presently the European Network is composed of seven core stations (Wettzell, Onsala, Madrid, Ny Alesund, Noto, Matera, Bologna) plus other two stations that occasionally take part in the network (Effelsberg and Crimea) [see Fig.1]. The station at Yebes will join this network as soon as possible.

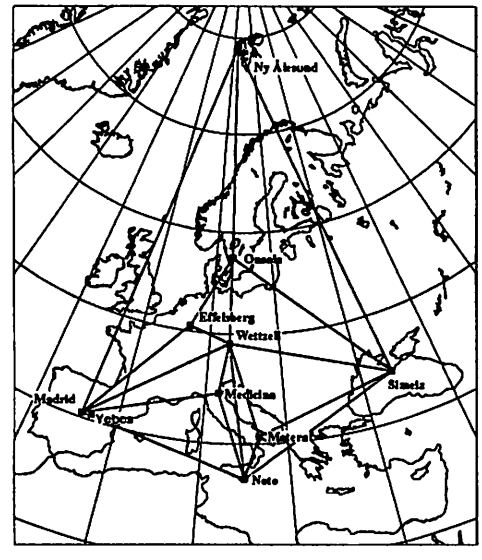

Figure 1: European Network

A period of transition started since the last meeting. For this reason the standard configuration of the network was changed (with the exception of the Europe6-95 campaign) and the number of antennas was limited to 5-6. This was due to many factors, but mainly the limitation created in correlating staffing by the leaving of Dr. Kurt Standke. As successor in this job I have started in Dec.'95.

Presented at the 11th Working Meeting on European VLBI for Geodesy and Astrometry, Onsala, Sweden, 1996

In table 1 can be seen the campaigns conducted in the years 1995/96 and the others planned untill the end the year. The campaigns between Europe6-95 and Europe3-96 are those I correlated and about which I will report some notes.

Experiment	date	Stations
Europe-1/95	01Feb95	Wet-Ons-Med-Mad-Not-Mat-Cri-Nya
Europe-2/95	12Apr95	Wet-Ons-Med-Mad-Not-Mat-Efl-Cri-Nya
Europe-3/95	08Jun95	Wet-Ons-Med-Mad-Not-Mat-Cri-Nya-Yeb
Europe-4/95	31Aug95	Wet-Ons-Mad-Nya
Europe-5/95	09Nov95	Wet-Ons-Med-Mad-Not-Mat
Europe-6/95	06Dec95	Wet-Ons-Med-Mad-Not-Mat-Efl-Nya
Europe-1/96	07Feb96	Wet-Ons-Med-Mad-Not-Mat
Europe-2/96	25Apr96	Wet-Ons- Mad-Cri-Nya
Europe-3/96	12Jun96	Wet-Ons-Mad-Not-Mat
Europe-4/96	09Sep96	Wet-Ons-Mad-Not-Mat
Europe-5/96	03Nov96	Wet-Ons-Med-Mad-Not-Mat-Cri-Nya-Yeb
Europe-6/96	05Dec96	Wet-Ons-Med-Mad-Not-Mat-Efl-Cri-Nya-Wtb

Table 1: European campaigns in 95/96

Notes about the latest correlated experiments

Here we suumarize the problems that were found in the last Campaigns:

EUROPE6-95

Effelsberg : For several hours data quality were not completely good (fringe quality plot 5-7) due an operator error. As a consequence 30 sec of observation was lost for each scan.

Madrid : The Logfile had to be edited in many points because missed the scan-time or the start/end time or the start/end footage or the name of the source were omitted.

Noto : In the last part of the experiment there were high parity errors in recording tracks of S-Band (Quality Factor D as a result on fringe plots).

Matera : Too many high parity errors during recording data on several tracks and also in many scans some tracks were lost. For this reason Matera data was not correlated.

Onsala : Occasional high parity error rates, most of the time on the reverse pass of recording.

EUROPE1-96

Madird : Several parts of Log-file were improperly recorded and had to be edited before the input to standard processing software.

Onsala : Sometime the signal at freq 8550.99 (X-Band) beteewn 8:00 and 10:20 U.T. was not recorded. Also recorded track spacing was often very narrow and caused correlation problems.

Noto : Problems in the first two hours freq 8570.99 (X-Band) missed or with RF interference.

Matera : High parity errors during recording data, but not as many as in the Europe6-95. Sometimes there was interference at freq 2222.99 (S-Band) (Quality Factor 2 as a result). 10% of Matera baselines have no detection (fringe quality plot 0, reason unknown).

EUROPE2-96

Crimea : 10% of all processed data have no detection (Quality Factor 0 as a result). The phase was completely undeterminate on all channels and there was scatter in the fringe amplitudes.

Madrid : Same problems as Europe1-96 in the Logfile.

Nyalesund : More than 50% of all data showed fringe amplitude less than half of the others at freq 2212.99 (S-Band). For this reason, the entire experiment was refringed.

Onsala : More than 30% of the data had problems on freq 8550.99 (X-band), especially in the first half of the experiment.

EUROPE3-96

Madrid : Some scans have no detections (snr lower then 7) for reasons unknown. No more problems in the Logfiles.

Matera : Interference at freq 2297.99 (S-Band) during the whole experiment. For this reason all scans were refringed without this track. Sometimes freq 2222.99 (S-Band) have fringe amplitude lower than 50% of the others (reason of QF=2 in Matera baselines).

Onsala : The playback error rate at freq 8550.99 (X-Band) was quite high, most notably on the forward passes. On first and third tapes, the recording was bad enough to generate many quality factor codes "D". This may have been due to poor tape quality. For this reason the experiment was refringed while decreasing the acceptable error threshold. This did not have a negative effect on the final results, but it improve the quality factor of many of these scans.

Conclusions about European Network and recommendations for all participating stations:

Unfortunately in each of these experiments there were one or more stations which did not work properly. This has to be avoided in the future to improve the quality of the results of each individual campaign.

For example the phase-cal phase is not always stable or with very well defined behaviour [see Fig.2].

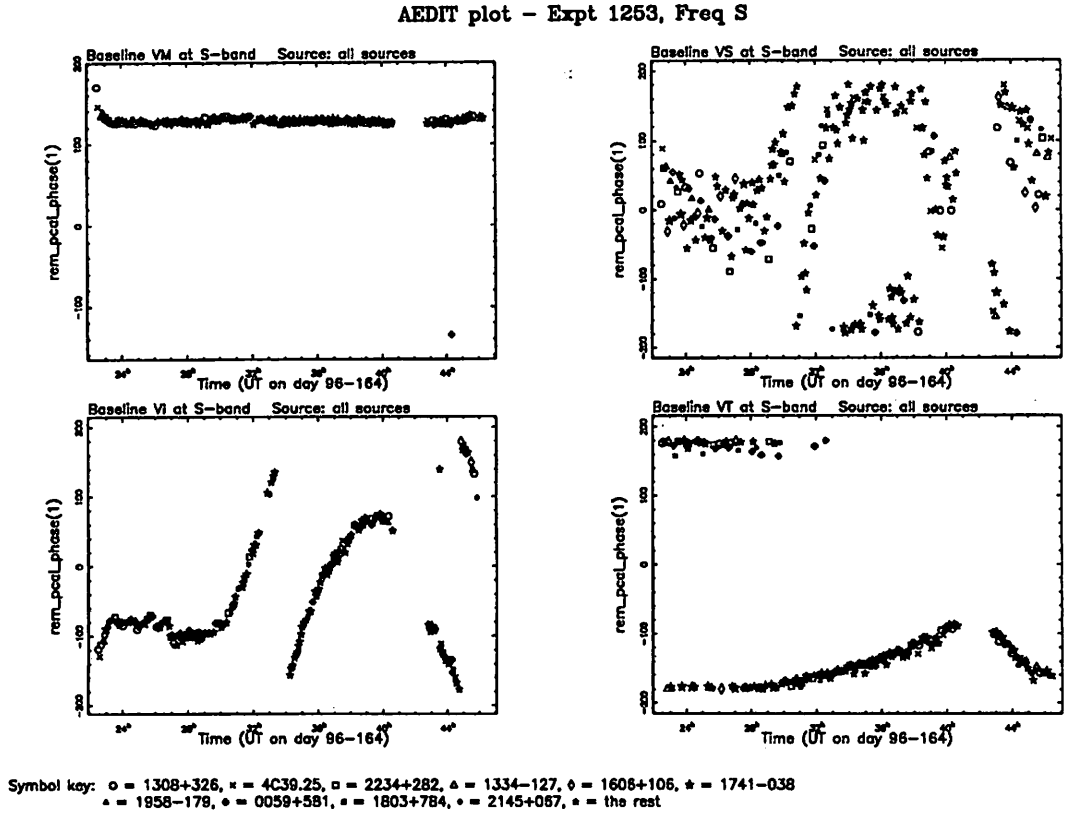

Figure 2: Phase-Cal Phase (Europe3-96)

For this reason it is essential that some basic check procedures are done before each experiment. In the following there is a list of the points that have to be checked:

- Computer
- IF Distibutor
- Formatter
- Antenna (pointing, focus)
- System temperature
- Receiver LO frequency
- BBC (bandwidth should be set properly)

- Phase cal signal
- Cable cal
- Prepass Tapes / Recorder Check

After this meeting a more detailed check-list will be sent to every station including more specific requests concerning the set-up before each campaign.

It is also important that comments are added into Logs because all information (e.g. vacum lost, footage errors, late start, source lost, etc.) is important for preparing and performing correlation. (Non standard Logs cause a great number of problems).

Another important aspect is to insert in the Logs comments about the comparison between MK3 and GPS times at least at the beginning and at the end of observations.

Tapes should be shipped as soon as possible!

The Logs have to be copied via ftp to 'FTP.MPIFR-BONN.MPG.DE' (user: anonymous, passw: e-mail addr. directory pub/user/geodesy/europeN_YY) within one week of the observation.

It is obvious that most of these things are known, but it is important that they are not forgotten.

In spite of this problems the percentage of the scheduled data that could be correlated for each of these experiments is still rather good [see Fig.3].

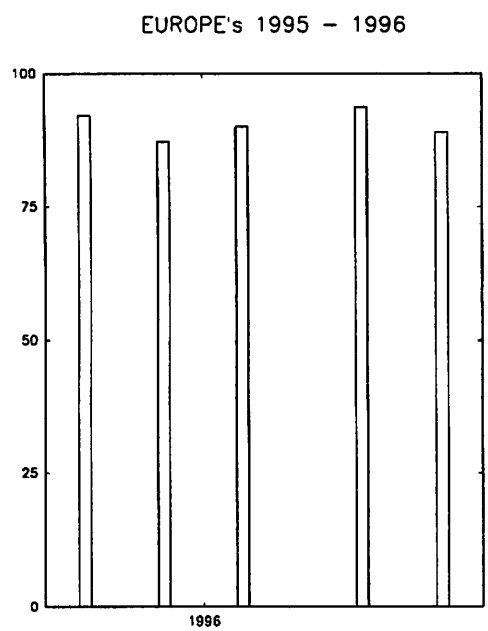

Figure 3: % of Correlated Data for each Experiment

STATUS REPORT FROM MPIfR CORRELATOR AUGUST 1996

Richard Porcas and Walter Alef (MPIfR, Bonn)

Hardware

Upgrading of the playback drives to VLBA/MK4 compatible playback electronics continues. Four of the "old" drives have now been upgraded, leaving two more to be done. Together with the "new" drives provided by IFAG, there is a total of nine Honeywell/Metrum playback units, which will be used together with the MK4 correlator, to be delivered in mid-1998 (?). The Penny and Giles experimental playback drive continues to be used for special purposes.

The seven drives with VLBA electronics have also been upgraded to allow thin tape operation. This includes an adjustment of the vacuum switch. The EVN and the MPIfR have purchased a batch of 232 thin tapes from Sony, and these are still waiting for glass reels (which have been ordered)

Operations

Throughput is stable and is measured by the percentage of time for which the correlation program COREL is running on either the old or the new MK3 correlator. This measure gives 60% operational efficiency. Geodesy correlation accounts for some 40% of the time, and is supervised by Arno Muskens and Mauro Sorgente. The remaining time is divided between in-house use, and outside EVN projects supervised by the JIVE support scientist, Luca Moscadelli, who stays in Bonn until the end of September. A replacement has been appointed by JIVE.

We have made the access to the A-file archive easier for outside users. These are now automatically stored on a Unix workstation, under an experiment directory, and can be accessed by anonymous FTP, after a request to the correlator: mpicor@mpifr-bonn.mpg.de

Software development

Two developments are underway in AIPS. One will allow the correlator tar archive to be read directly into AIPS (the present task MK3IN only reads the SAVEM archive). The second task will allow a better correlator model to replace that actually used at correlation, which will facilitate better use of the phase-referencing technique.

Presented at the 11th Working Meeting on European VLBI for Geodesy and Astrometry, Onsala, Sweden, 1996

Status of ERS/VLBI Station O'Higgins - Antarctica

Andreas Reinhold,
Johannes Ihde, Volkmar Thorandt, Reiner Wojdziak

Institut für Angewandte Geodäsie
Außenstelle Leipzig
Karl-Rothe-Straße 10-14
D-04 105 Leipzig
Tel./Fax: +49 341 5634 400 / 415

Summary

IfAG is responsible for the geodetic operations at O'Higgins research station. O'Higgins is equipped with VLBI and permanent GPS receiver thus contributing to the global IERS and IGS networks. Since 1992 O'Higgins participated in 34 international VLBI experiments. Step by step the infrastructure and the station equipment has been extended and additional geodetic instruments have been installed. A permanent working tide gauge sensor and an automatically working PRARE ground unit were installed near the radiotelescope during the last two years.

VLBI Projects

At present O'Higgins is the only VLBI-station at Antarctica in operation. Since 1992 O'Higgins was involved in 34 international VLBI-experiments with different goals.
The radiotelescope antenna and the receiver electronics are the most important geodetic tools of the station. A detailed report on structure, technical VLBI equipment, the operation and working conditions at the station O'Higgins was given in Hase et al., 1993.
VLBI observations are performed at O'Higgins to support the construction of a precise terrestrial reference network and its extension to the Antarctic continent. Of special interest is the motion behaviour of Antarctica with regard to the neighbouring tectonic plates. Some of the experiments have been performed to improve the coordinates of fixed stars in the southern hemisphere. These experiments - organized and managed by the U.S.Naval Observatory (USNO) have been ceased since 1995.
The geodetic VLBI experiments are performed within the framework of the project DOSE (Dynamics of the Solid Earth) and are prepared and managed by Goddard Space Flight Center (GSFC). Activities within the project are during the whole year, the station O'Higgins takes part in campaigns twice a year. Besides the stations Santiago, Fortaleza, Hartebeesthoek, Hobart and Tidbinbilla, since 1995 also the station Kauai at Hawaii is integrated into experiments in which O'Higgins participates. In January 1996 a global experiment was performed (GTRF8) in which O'Higgins par-

Presented at the 11th Working Meeting on European VLBI for Geodesy and Astrometry, Onsala, Sweden, 1996

VLBI Experiments at ERS/VLBI Station O'Higgins— Antarctica

date	experiments	involved stations											status
20.01.92	SHS-26	O -	S -	H -	T								[1]
27.01.92	POLAR-S1	O -	S -	H -	T -	D							[1]
04.02.92	SOREF-1	O -	S -	H -	T								[1]
10.02.92	SURVEY-S1	O -	S -	H -		D							[1]
11.02.92	SHS-27	O -	S -	H -	T								[1] fringes, not analysed
08.06.92	SOREF-3	O -	S -	H -	T								[2]
10.06.92	SHS-X30	O -	S -	H -									[2]
11.06.92	SOREF-4	O -	S -	H -	T								[2]
13.06.92	POLAR S3	O -	S -	H -	T								[2]
25.01.93	SHS-38	O -	S -	H -	T								analysed
27.01.93	SURVEY-S1	O -	S -	H -		D							analysed
01.02.93	SOREF-5	O -	S -	H -	T								analysed
04.02.93	SHS-39	O -	S -	H -	T								analysed
10.02.93	POLAR-S1	O -	S -	H -	T								analysed
21.09.93	POLAR-S3	O -	S -	H -	T -	D							analysed
23.09.93	SHS-46	O -	S -	H -	T -		F						analysed
27.09.93	SHS-48	O -	S -	H -	T -		F						analysed
29.09.93	POLAR-S4	O -	S -	H -	T -	D-							analysed
30.09.93	SHS-47	O -	S -	H -	T -		F						analysed
14.02.94	SHS-52	O -	S -	H -	T -		F						analysed
16.02.94	POLAR-S2	O -	S -	H -	T -	D							analysed
21.02.94	SHS-51	O -	S -	H -	T -		F						analysed
23.02.94	SURVEY-S1	O -	S -	H -		D							analysed
26.01.95	STRF-01	O -	S -	H -	T -		F -	K					analysed
30.01.95	POLAR-S1	O -	S -	H -	T -								analysed
13.02.95	POLAR-S2	O -	S -	H -	T -	D							analysed
23.02.95	STRF-02	O -	S -	H -	T -	D -	F -	K					analysed
05.10.95	STRF-10	O -	S -	H -	T -	D -	F -	K					analysed
09.10.95	STRF-08-ALT	O -	S -	H -	T -			K					[3] analysed
12.10.95	STRF-11	O -	S -	H -	T -	D -	F -	K					analysed
25.01.96	STRF-13	O -	S -	H -	T -	D -	F -	K					in analysis
29.01.96	GTRF-8	O -	S -	H -		D -	F -	K-	A-	Q-	E-	V-	analysed
05.02.96	STRF-14	O -	S -	H -	T -	D -	F -	K					in analysis
15.02.96	POLAR-S1	O -	S -	H -	T -	D							[4]

A - Gilmore Creck
Q - Kashima (26) Space Research Center, Kashima/Japan
E - Westford/USA
V - Fundamentalstation Wettzell/Germany
O - ERS/VLBI-Station O'Higgins, Germany - Chile
S - Center for Space Studies (CEE) Universität Santiago, Peldehue/Chile
H - Hartebeesthoek Radio Astronomy Observatory Johannesburg/South Africa
T - University of Tasmania, Hobart/Australia
D - DSS45 Deep Space Network Tidbinbilla/Australia
F - Fortaleza/Brasil
K - CDP Kokee Park Geophysical Obervatory, Kauai, Hawai/USA

1) not analysed, LO-lock-status at 2015 MHz instead of 2020 MHz
2) no correlation possible, no GPS-timing system (GPS antenna was destroyed by storm) — unknown absolute offset
3) alternative experiment, logistical problems, maser reached lock-status too late
4) upconverter did not work, no correlation possible

ticipated. For the first time it observed simultaneously with stations in the northern hemisphere.

Figure 1: The Chilenean Base and German annex-Station O'Higgins - September 1995

The extreme weather conditions in Antarctica and the salty air from the sea have influence on the technical equipment in place.

Other Projects

Besides the VLBI technology, also other geodetic measuring methods have been employed in the last years. These activities are part of nationally and internationally coordinated projects and programs.

GPS Projects:

O'Higgins participated in different GPS projects initiated by SCAR (Scientific Committee on Antarctic Research); data have been recorded with TRIMBLE GPS receivers in 1990, 1992 and 1993.
In 1995 O'Higgins was included into the GPS measurements for determination of a geodetic reference network Antarctica - performed as a joint venture of several German research institutions under the auspices of SCAR. This network is layed out with the objective to deliver coordinates of geodetic points with high (cm) accuracy in Antarctica and to create the prerequisites for geodynamic investigations into the fine

GEODETIC OBSERVATORY O'HIGGINS — overview

	VLBI Observations		GPS Measurements		Ocean Tide Registrations	Other Geodetic Works
			in campaigns	permanent		
1992	January/ February:	5 experiments	January/pillar K4 SCAR-campaign			
	June:	4 experiments	AUSLIG			
1993	January/ February:	5 experiments	January/pillar K4 SCAR-campaign			
	September:	5 experiments	AUSLIG			
1994	February:	4 experiments				Measurement of the terrestrial fixed point field with classical geodetic and GPS methods
1995	January/ February:	4 experiments	19.01.-24.02./pillar K1 GAP/SCAR-campaign	February: Start of data recording with a TURBO ROGUE-GPS-receiver and automatical data transfer via INMARSAT to Germany	February-June: Data recording with a Tide Gauge Sensor	February: Measurement of the axis of the radiotelescope and of additional fixed points. Test measurements with a gravity meter for determination of earth tides.
	October:	3 experiments		Integration of a weather station in the system	Restart of data recording on 29.09.95	Test measurements with a PRARE ground unit.
1996	January/ February:	4 experiments	22.01.-10.02./pillar K1 GAP/SCAR Sub'campaign		Installation of two additional sensors and organisation of automatical data transfer via INMARSAT to Germany.	Permanent installation of a PRARE ground unit in communication with ERS-2

SCAR: Scientific Committee on Antarctic Research
AUSLIG: Australian Land Information Group
GAP: German Antarctic GPS Project

structure of tectonic plates in the region between middle and southern South America and the Antarctic Peninsula.
Since February 1995 a TURBO ROGUE GPS receiver is observing permanently at O'Higgins. For the antenna a pillar on bedrock was constructed and a radom to protect the antenna against snow, ice and storm was installed. Data collection is done on a PC, the daily data transfer to Germany is done automatically via INMARSAT to the fundamental station Wettzell and from there to the IGS at Paris.

Gauge Measurements:

The determination of tides in the region of the Bransfield Street in the north of the Antarctic Peninsula is of great interest for various geodetic questions. Therefore, in February 1995 a stationary gauge measurement system with pressure sensors was permanently installed near the radiotelescope in a water depth of about 4 m and extended in 1996. The sensors are screwed to rock on the bottom of the sea.
A long-term recording shall allow to derive a height datum for O'Higgins.

Installation of a PRARE Ground Unit:

The 9m antenna of the station O'Higgins is used to receive SAR data of the European remote sensing satellites ERS1 and ERS2 and other satellites. The evaluation of the remote sensing data (e.g. altimetry data) requires the precise knowledge of their orbit data.

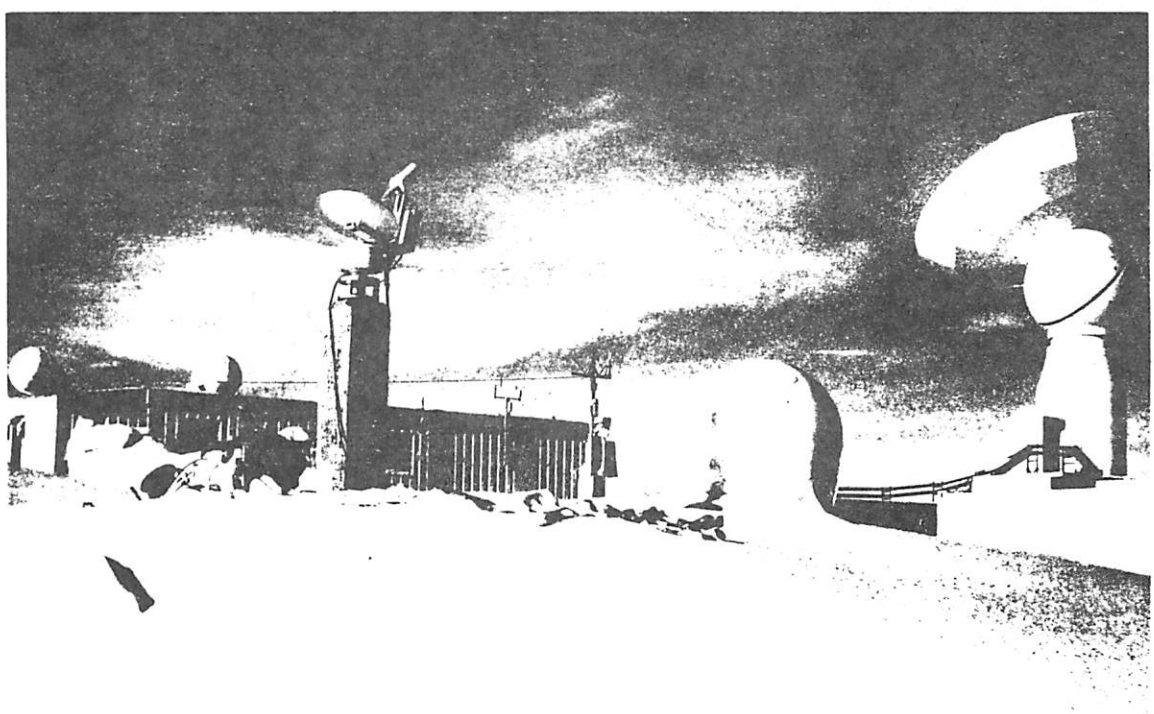

Figure 2: The 9m ERS/VLBI antenna system, the PRARE ground unit, in September 1995 provisionally mounted on pillar K4, the radom with the antenna of the TURBO ROGUE GPS system inside and parts of working, service and living containers of the German Station O'Higgins

For this purpose the PRARE (Precise Range and Range Rate Equipment) system was developed and consists of the space segment and ground units. One of the ground units has been installed at O'Higgins and plays its role for orbit determination in the Antarctic region. The installation has been done in January 1996 and was brought into communication with ERS2. Since that time the system works automatically and continuously - also in times when the station is unmanned.

Gravimetric Measurements:

Test measurements with a recording LaCoste&Romberg gravity meter have been performed in January/February 1995. The objective of this registration was to get knowledge about the disturbances of the gravimetric signal due to oceanic waves and other causes. Planned are gravity recordings over longer periods at O'Higgins.

In order to be able to relate the different observing systems to each other a geodetic control network has been established. The geodetic relations have been observed by precise terrestrial techniques and by GPS.

References

Hase, Hayo; Nothnagel, Axel: The ERS/VLBI Station O'Higgins in Antarctica. Proceedings of the 9th Working Meeting on European VLBI for Geodesy and Astronomy, Bad Neuenahr,30.Sept.-01.Oct.1993.

Beyer,L., Ihde,J., Reinhold,A., Soltau,G.: Sea Level Registration at O'Higgins (Antarctica). Presented at the XXI General Assembly of European Geophysical Society, The Hague, 06-10 Mai 1996

Dietrich, R.; Schenke, H.W., Soltau, G.; Seeber, G.; Niemeier, W.; Lindner, K.: The SCAR 95 GPS Campaign: Objectives, Data Analysis and Final Solution. Presented at the XXIV Meeting of SCAR, Cambridge August 7, 1996

EFFELSBERG STATUS REPORT, AUGUST 1996

Richard Porcas (MPIfR, Bonn)

The most important news is that the Effelsberg 100m telescope is now back in operation on a completely new azimuth track. During the period 21 February to 27 June this year, the 3200 ton antenna was lifted off the old track using hydraulic jacks for the replacement work. The new track is some 12mm higher, thus producing a shift in the vertical component of the position !

The Effelsberg MK3 terminal is being upgraded to MK4 standard as part of the EVN MK4 upgrade (EMU) project. New filters and single-sideband circuitry for the video-converters, and new ceramic inserts to support thin tape recording were added in November 1995. New read-write electronics and MK4 formatter are due to be installed after the October–November EVN observing session. We have now abandoned our old, home-grown PC Field system, in favour of the standard FS9.

A new 8.4 GHz low noise receiver is under construction, which will be optimised for VLBI and should have better polarisation characteristics.

A new receiver-switching control system has been brought into operation. This allows schedule-driven changes between all the receivers mounted at the secondary focus. In addition, the long-awaited 3-frequency receiver has now been mounted at the secondary focus. A new interface program connects the MK3/4 or VLBA control program to the telescope and receiver control computer, permitting automatic changing between 2.3, 5.0, 8.4, 15, 22 and 43 GHz receivers.

GPS time comparisons from the VLBA terminal are logged automatically at the VLBA correlator in Socorro. GPS comparisons from the MK3/4 terminal are logged during VLBI sessions.

In order to simplify observing at Effelsberg together with the VLBA, the VLBA terminal now records using thin tape in high-density mode.

Presented at the 11th Working Meeting on European VLBI for Geodesy and Astrometry, Onsala, Sweden, 1996

Status Report at OAN - Yebes VLBI Station

OAN-Yebes VLBI group[1] (presented by I. López-Fernández)

Centro Astronómico de Yebes, Observatorio Astronómico Nacional, Guadalajara, Spain

Abstract

We briefly present the current status of Yebes station concerning Geodetic VLBI, reporting recent technical upgrades and future trends and overviewing its problems during the last year.

1 Operational activities

Yebes Observatory (Observatorio Astronómico Nacional – OAN) has succesfully participated in its first geodetic VLBI experiment in June 8 - 9, 1995 (EUROPE3-95). Fringe detection was reported and Yebes was scheduled for the next session within the EUROPE campaign, EUROPE4-95 (August 31 - September 1, 1995). The observations where carried out without major trouble.

Preliminary analysis from the correlator of this later data showed extreme sudden and simultaneous phase (and amplitude) variations at both S and X bands of nearly 90°. This pinpointed to a problem at baseband, which caused a global time shift of one bit. After a careful inspection of the VLBA DAR, the formatter was sent to Interferometrics, were several defective chips (FIFO's) were replaced.

Yebes data form EUROPE4-95 was then mostly useless. Our participation in the subsequent EUROPE sessions, and in the GTRF campaign (where we were also scheduled) were frustrated due to the repairs that our formatter underwent.

2 Technical upgrades

- A new active **hydrogen maser** was purchased from KVARZ, model CH-75. We previously had a maser from the *Laboratorie de L'Horloge Atomique*, on loan by the CNRS. Its behaviour is continuously monitored against GPS, and it has shown an excellent performance during the last seven months, since its reception (Demidov [1]).
- A **Phase Calibration Unit**, based on Haystack '91 design, provided with a buit-in thermal control was constructed and tested at our station, substituting an old NASA unit with insufficient power level at X band. A communication about its performance and the improvements on phase stability has been presented in this meeting (see also López-Fernández [2]).

[1]Presently formed by (in alphabetical order): J. Alcolea, A. Barcia, F. Colomer (coordinator), P. de Vicente, J. D. Gallego, J. Gómez-González (director), I. López-Fernández.

Presented at the 11th Working Meeting on European VLBI for Geodesy and Astrometry, Onsala, Sweden, 1996

- We also have a new **meteorological station** connected to the Field System PC and to a dedicated PC which records temperature, humidity and pressure statistics. This solves the inconvinience of our meteo data not being incorporated to the log files.

- Several **software** upgrades have been accomplished lately. The operating system of our Field system PC has been changed from Venix to Linux. Simultaneously, the Field System version was updated to 9.1.

  The HP1000 tracking software and communications protocol with the HP2100 was modified to reduce the time lost between scans in measuring system temperature and synchronizing the HP1000 with the Field System. This yields now a delay time of approximately *36 seconds* between the end of one scan and the start of the antenna movement towards the next source, that must be taken into account when scheduling for Yebes.

- The **formatter firmware** was upgraded to version 2.92 as a result of its stay at Interferometrics. It enables the barrel roll track switching, thus now our data could be correlated at the VLBA.

- **Antenna efficiency** at Q band has improved considerably as a result of patching the milimiter subreflector according to the results of holographic measurements (Garrido [3]).

There are presently works in progress in the control room to set up a new air conditioning system.

3 Present Situation

Tables 1 and 2 summarize the main characteristics of our station. In table 1, the parameters of the 13.7 m antenna an feeders, at X, S and Q bands are given, while table 2 refers to the VLBI receivers features, including the VLBA terminal. All receivers, including HEMT amplifiers were designed and built at Yebes.

The VLBA DAR and recorder is commanded by version 9.1 of the Field System running on a 486-33 PC under slackware version 1.2.13 of Linux. This PC is not controlling the antenna; an old HP1000 is in charge, and as we mentioned before, both computers are not synchronized yet.

The timing system includes the KVARZ CH1-75 hydrogen active maser, a TRIMBLE 5000A GPS (locked to the maser 5 MHz) with a 1 pps comparator, and an OAY-11 (in house) 1 pps synthesizer. A 286 PC records every 15 minutes the output of the pps comparison from the GPS. Another 286 monitors the meteorological data.

The OAY-15 and OAY-16 Ground an Antenna Units of the phase calibration system are complemented by an HP 52131 A counter to measure the cable delay.

The overall performance of our system is condensed in Table 3.

		S BAND	*X BAND*	*Q BAND*
Structure	Type	Cassegrain, radome enclosed		
	Slew rate (°/sg)	< 1 (azimut and elevation)		
	Pointing (″)	10		
Main ref.	Diameter (m)			13.7
	rms (μm)	313		228 [1]
	η_s (%)	65		80 [1]
Subreflector	Diameter (cm)	220 [2]		108.6
Feeder	Horn type	Coaxial [2]	Conical [2]	Corrugated [3]
	Polarization	RCP	RCP	LCP

[1] after reshaping the secondary from holographic measurements

[2] tilted subreflector (6.29°) and off axis multiangled shaped feeders for S ($\phi = 46$ cm) & X ($\phi = 10$ cm) bands

[3] sole horn cooled ($\phi = 6.8$ cm)

Table 1: *Antenna characteristics*

4 Future plans

Several improvements are planned at Yebes dealing with VLBI. A new 22 GHz dual polarization receiver is under construction. The telescope control system is planned to be upgraded, enabling commanding the antenna from the Field System PC. Finally, we will modify our receiver to have wideband capability.

On the observational side, we will take part on the last EUROPE-96 sessions and on EUROPE-97 as a core station. We intend to participate in the pre-CORE experiments of 1997.

		S BAND	*X BAND*	*Q BAND*
Front-end	Type	HEMT - 15 K	HEMT - 15 K	Schottky-20 K
	T_{rec} [1] (K)	12	22	
	T_{sys} [1] (K)	62	55	110
	Freq. range (GHz)	2.21 - 2.35	8 - 9	41 - 49
Back-end	BW (MHz)	140	500	400
	Terminal	VLBA, 14 BBC		
	Recorder	Narrow track, Mark IIIa compatible		

[1] T_{rec} measured at vacuum window and T_{sys} includes waveguides, polarizers and horns

Table 2: *Recievers characteristics*

Sky frequencies (GHz)	2.21 - 2.35	8.13 - 8.63	41 - 49
η_A (%)	38	50	34
$\mathbf{T}_{sys}$ (K)	87	77	250
SEFD (Jy)	3800 [2]	3300 [2]	10500

[1] η_A, T_{sys} and SEFD measurements include radome effects (not optimized for S & X bands)

[2] measured using *Tau A* with assumed flux density of 810 Jy (S) and 563 Jy (X)

Table 3: *Overall performance*

References

[1] N.A. Demidov *et al.*, Investigations of the frequency instability of CH-75 hydrogen masers, Proc. of the 22nd Anual Precise Time and Time Interval (PTTI) Aplications and Planning Meeting, 1990.

[2] I. López Fernández *et al.*, Phase Calibrator: Antenna Unit, Technical Report 1996-4, Centro Astronómico de Yebes, 1996.

[3] J. E. Garrido, A. Barcia, J. M. Páez, Medidas de la superficie del reflector primario del radiotelescopio del CAY mediante técnicas holográficas IV: Correcciones en el secundario, Technical Report 1995-9, Centro Astronómico de Yebes, 1995.

Status Report of RT-Wettzell

Richard Kilger

Presenting the activities of the Radiotelescope in Wettzell since our last meeting in Matera has two parts; the first part shows our activities in VLBI-measurements, the second our activities in upgrading hard- and software.

Our main acivities in geodetic VLBI-observation are still:

IRIS-A or NEOS-A or POLARIS,
INTENSIVE or DELTA (UT1)
IRIS-S
EUROPE
GSFC (R&D, GLOBAL-TRF, GOLDEN GLOBAL, XASIA)
USNO (NAVEX, NVSAT)

Special activities were:
JAPAN (Time transfer measurement:
- Short Baseline Interferometer with
  : 1m-antenna and 20m-Wettzell,
  : local survey of the geometric distance between the 2 antennas,
  : determining the internal offset of this interferometer,

- Repeating this measurement with the 1m antenna and a 34m-antenna in Japan,

- Doing a 24h session between RT-Wettzell and the 34m-antenna in Japan.

The measurement has not been completed upto now. It has been our first measurement in K4 technique.

Regarding hardware the activities being interesting to the community are the installation of a new S-X-feedhorn in Wettzell and the measurement of the height of the reference point of the antenna [point of intersection of Az-, El- and boresightaxis] over ground.
Wettzell operated from the beginning of VLBI-operation in 1983 with a S-X-feedhorn, designed from the S-X-feedhorn, JPL worked on their 64m-antennas. This horn has been adapted to the geometry of the Wettzell Cassegrain antenna and operated fine. After increasing of the bandwidth in S+X-band since the R&D-experiments we experienced a decline of performance in the higher part of S and especially X-band.
We asked commercial companies for an offer of a S+X-feedhorn and received two appropriate offers. But the feedhorn we got first in late autumn 1995 didnot fulfil our specification by far. The second edition of the feedhorn was installed in early July 1996

Presented at the 11th Working Meeting on European VLBI for Geodesy and Astrometry, Onsala, Sweden, 1996

and showed significantly better performance in S-band and SEFD (System Equivalent Flux Density) over the extended S+X-band. We performed a lot of single dish measurements, determining over the whole frequency band:
- overall antenna efficiency ,
- overall antenna system temperature,
- SEFD.

A full set of single dish measurements has been performed with calibration sources CYGNUS-A, CASIOPEIA-A, TAURUS-A; by doing this the fluxes for these calibration sources had to be recalibrated over the frequency band of S+X-band, compared to the fluxes in the publications of Baars and also the Field System manual. Some results with CYGNUS-A are shown in the diagrams.

A second interesting activity was the measurement of the height of the antenna reference point over ground. The center of the Az-axis within the antenna is free of material. So, we could mount an Invar-wire from the intersection point of Az, El and boresight axis and loading the wire with a 1kg weight near the ground. The weight is guided in a precise cylinder. The distance of the cylinder over the ground is measured with an inductive sensor continuously and protocolled by a computerprogram. The length of the INVAR instrumentation should not change (much) with temperature. The length of the antenna tower will change with temperature. There is a temperature cycle every day and many of our VLBI-session last one day. There is a temperature cycle every year.

Accordingly two sets of diagrams are shown; a first set refers to a longer period in the spring 1996 from doy 80 to 120 and a second set refers to only 24h; at this day there was a large temperature change in the spring. The diagrams show:
- the temperatures during this time periods,
  Tu: a temperature in the lower part of the vicinity of the INVAR-wire,
  To: a temperature in the upper part of the vicinity of the INVAR-wire,
  Tw: a temperature in the inner part of the concrete tower.
- the measured change of the height of the antenna tower,
- calculated height changes on the basis of the temperature coefficient of concrete or steel and these measured temperatures
- and the difference of measured-calculated height differences.

One should consider, that the antenna height in RT-Wettzell
- is 12m,
- consists of a lower part of thick concrete with 8m and
- a higher part of steel structure made of thin steel with 4m.

Further one should consider, that during a short period of 24 days a thick concrete building does not change temperature more than 1 °C and therefore height does not change in this part of the structure significantly. Most of the height changes within one day occur in the steel structure.
During one year the concrete part of the foundation of the antenna will change its height according the temperature changes of summer- and winterseason.
A preliminary conclusion of our measurements is:
- maximum of the daily changes of height (during one 24h-session) is about 0.7mm; up to now we did measure a maximum of 0.5mm in the spring.

- the annually changes of the height will be about 3mm; during the period in spring, where we got a relative dense set of measurements, we measured height changes of 1.71mm.
- Height changes of antennas can be modelled with a relative small set of temperature sensors. The location of the temperaturesensors has to be chosen carefully. A comparison of measured and calculated measurement (calibration) should be done.
- Height changes of antennas should be taken into account of highprecision baseline measurements. The longer the baseline the more height changes show up in baseline changes. In diagrams showing baseline length versus time (years) we always can observe annual cycles; a part of these systematic effects should be removed by including height measurements in antennas.

A final statement is, that Wettzell has now 2 Water Vapor Radiometers; one of it will run permanently at the Fundamentalstation in Wettzell. Our first practical experience at Wettzell with the WVR is, that it needs a lot of maintenance. Obviously the WVR suffers a lot due to our weather conditions with rain, snow and ice. The unit operating in the Mediterranean Sea performed better .

Radioastronomy at the NASA Madrid Deep Space Communications Complex

A. Rius[1,2], A. Alberdi[1,3], J.A. Perea[4]
[1]LAEFF, INTA, Spain
[3]IAA/CSIC, Granada, Spain
[2]IEEC/CSIC, Barcelona, Spain
[4]MDSCC, Madrid, Spain
(e-mail: rius@laeff.esa.es, alberdi@laeff.esa.es, japerea@oort.mdscc.nasa.gov)

1 Introduction

The purpose of this report is to summarize the radioastronomical activities which have been performed during the year 1995, using the facilities provided by the **NASA Madrid Deep Space Communications Complex (MDSCC)**. The projects performed at the MDSCC required the unique resources available at the DSN: **large antennas, precise and accurate clocks, low noise receivers and high sensitivity** ... and its geographical location (in the case of interferometry observations).

We note that the reported activities have been performed in a specific environment: **a NASA spacecraft tracking station.** The positive action of many individuals at JPL and at the MDSCC/INTA have been necessary for the successful accomplishment of this work. We hope that our activities have also contributed to improve the primary activities of the DSN: **tracking spacecrafts.**

More details on the radioastronomical activities can be obtained from the different authors, and in the Technical Reports included in the Web-page of the MDSCC

URL Address: (http://www.laeff.esa.es/~alberdi/mdscc.html).

Presented at the 11th Working Meeting on European VLBI for Geodesy and Astrometry, Onsala, Sweden, 1996

2 The Radio Astronomy Program in the DSN

It is composed of the following segments:

- **Applied Radio Astronomy** in direct support of the DSN.

- **Support of the NASA** Office of Space Sciences and Applications (OSSA).

- **Host Country Observations.**

- **Radio Astronomical Observations which require the unique capabilities of the DSN.** The proposals must be submitted to the Program Committees of the VLBA (Very Long Baseline Array) and of the EVN (European VLBI Network) .

3 Experiments performed at the NDSCC During 1995

Geodesy Experiments:

- **Europe 1** - February 1st.
- **RDXTL 1** - March 13th.
- **Europe 2** - April 12th.
- **Europe 3** - June 8th.
- **GTRF 4** - August 14th.
- **Europe 4** - August 31st.
- **GTRF 9** - October 2nd.
- **Europe 5** - November 9th.
- **GTRF 7** - November 16th.
- **Europe 6** - December 6th.

Astronomy Experiments:

- **EA006A Radio Stars** - Alef - February 9th - X-Band.
- **EA006B Radio Stars** - Alef - February 10th - X-Band.

- **GM21B SN1993J** - Marcaide - February 11th - S-Band.
- **GR010 SN1993J** - Bartel/Rupen - February 12th - X-Band.
- **MAH13** - Space VLBI Pre-Launch Survey - Feb. 26th - L-Band.
- **MAH14** - Space VLBI Pre-Launch Survey - March 16th - K-Band.
- **MAH15** - Space VLBI Pre-Launch Survey - April 30th - K-Band.
- **JPLST Radio Stars** - Guirado - September 3rd - X-Band.
- **MAH16** - Space VLBI Pre-Launch - September 24th - K-Band.
- **GM25 SN1993J** - Marcaide - September 30th - S-Band.
- **MAH17** - Space VLBI Pre-Launch - November 4th - L-Band.
- **GR012S SN1993J** - Bartel/Rupen - December 18th - X-Band.

- **Multiple non-VLBI radioastronomical observing sessions.**

4 Scientific Objectives and Results

The scientific objectives included:

- **Study of the angular expansion of SN1993J.** A sequence of images from VLBI (DSS63 and DSS14 were essential part of the array due to their very high sensitivity) shows that the young radio supernova SN1993J is expanding with circular symmetry. A scenario in which freely expanding supernova ejecta shock mostly isotropic circumstellar material is strongly favoured.

- **Study of the parsec-scale relativistic jets** associated with quasars and Active Galactic nuclei. DSS63 has taken part in dual polarization VLBI experiments at X-band.

- **VLBI differential astrometry.** High precision VLBI differential astrometry observations have permitted to i) study the stability of the cores of the compact radio sources and ii) determine absolute motions of the VLBI components with precisions better than a tenth of a milliarcsecond.

- **Single-dish monitoring** of variable radiostars and galactic plane variable radio sources. The 70 metre antenna (DSS63) has been used to monitor the flux density of variable radiostars (as X-ray binaries, flare stars). Several campaigns were performed coordinated with X-ray, millimetre and sub-millimetre observations at other observatories.

- **VSOP Pre-launch survey**.6 experiments have been performed in order to determine which H_2O masers (at 22 GHz) and which OH masers (at 1.6 GHz) could be detected with VSOP.

- **Applications of VLBI to Geodynamics.** The antennas DSS63 and DSS65 have participated in the VLBI Geodesy campaigns.

- **Applications of GPS ("Global Positioning System")** observations to the study of the ionosphere and its effects on the proper calibration of the radioastronomical observations. During the period 22nd to 26th April 1996, a local network of seven GPS receivers was implemented around the complex with the purpose of gathering data to compare estimates of the water vapor content obtained with VLBI, GPS and WVR.

5 Problems with the Antenna DSS65

• In cooperation with the Goddard group, we have started the implementation of a model describing the **vertical displacements of the DSS65 VLBI reference point**. The model is based on the actual response of the runner under the load of the moving antenna. This model has been developped by J.M. Urech (MDSCC).

• Some mechanical problems at the DSS65 as well as a desire to obtain more precise and accurate pointing models, prompted us to produce **a new model to describe the pointing errors of the DSS65**. The new models have provided a significative agreement with the measurements. This work has been performed to contribute to the efficient use of the DSS65 in their

regular activities, which include DOSE, Europe CDP and Host Country Observations.

6 Publications in Refereed Journals in 1995

1. Alberdi, A., Krichbaum, T.P., Marcaide, J.M., Witzel, A., Zensus, J.A., Graham, D.A., Standke, K., Greve, A., Grewing, M., Schalinski, C.J., Booth, R.S., Baath, L.B., Colomer, F., Rogers, A.E.E., Doeleman, S. 1995, "The high frequency compact radio structure of the peculiar quasar 4C 39.25", Astronomy & Astrophysics, submitted

2. Guirado, J.C., Marcaide, J.M., Alberdi, A., Elósegui, P., Ratner, M.I., Shapiro, I.I., Kilger, R., Mantovani, F., Rius, A., Ros, E., Trigilio, C., Venturi, T., Whitney, A.R. 1995, "Absolute Internal Proper Motion in 4C 39.25", Astronomical Journal 110, 2586-2596

3. Lara, L., Marcaide, J.M., Alberdi, A., Guirado, J.C. 1995, "VLBI differential astrometry at large angular separation: 3C 395 - 3C 382", Astronomy & Astrophysics, in press

4. Marcaide, J.M., Alberdi, A., Ros, E., Diamond, P., Schmidt, B., Shapiro, I.I., Baath, L., de Bruyn, G., Elósegui, P., Guirado, J.C., Davis, R.J., Jones, D.L., Krichbaum, T., Mantovani, F., Preston, R.A., Ratner, M.I., Rius, A., Rogers, A.E.E., Schilizzi, R.T., Trigilio, C., Whitney, A.R., Witzel, A., Zensus, J.A. 1995, "Discovery of Shell-like Radio-Structure in SN1993J", Nature 373, 44-45

5. Marcaide, J.M., Alberdi, A., Ros, E., Diamond, P., Shapiro, I.I., Guirado, J.C., Jones, D.L., Krichbaum, T., Mantovani, F., Preston, R.A., Rius, A., Schilizzi, R.T., Trigilio, C., Whitney, A.R., Witzel, A. 1995, "Expansion of SN 1993J", Science 270, 1475-1478

6. Standke, K.J., Quirrenbach, A., Krichbaum, T.P., Witzel, A., Otterbein, K., Alef, W., Eckart, A., Alberdi, A., Marcaide, J.M., Ros, E., Lesch, H., Steffen, W., Kraus, A., Zensus, J.A. 1995, "The Intraday Variable Quasar 0917+624: VLBI and X-Ray Observations", Astronomy & Astrophysics, in press, February 1996 Issue

7. Paredes, J.M., Marti, J., Peracaula, M., Garcia-Sanchez, J., Estalella, R. 1995, "Single dish monitoring of galactic plane variable radio sources", Astronomy and Astrophysics, submitted

8. Rius, A., Juan, J.M., Hernandez-Pajares, M., Madrigal, A. 1995, "Measuring geocentric radial coordinates with a non-fiducial GPS network", Bulletin Géodésique 69, 320-328

Conference Proceedings

9. Alberdi, A. 1995, "The Centre of the Milky Way", in "The Formation of the Milky Way", ed. E. Alfaro and A.J. Delgado, Cambridge University Press, p. 224-230

10. Alberdi, A., Gómez, J.L., Guirado, J.C., Lara, L., Marcaide, J.M. 1995, "Aberration of light and time delay effects in Parsec-scale Relativistic Jets", in "Proceedings of the 2nd EVN/JIVE Symposium", ed. A. Kus, R.T. Schilizzi, K.M. Borkowski, L.I. Gurvits, p. 99-104

11. Alberdi, A., Perea, J.A., Rius, A. 1995, "Radioastronomy at the NASA Madrid Deep Space Communications Complex", in "XIth Working Meeting on European VLBI for Geodesy and Astrometry", ed. R. Lanotte & G. Bianco, p. 22-26

12. Guirado, J.C, Alberdi, A., Marcaide, J.M. 1995, "Absolute Internal Proper Motion in 4C 39.25", in "XIth Working Meeting on European VLBI for Geodesy and Astrometry", ed. R. Lanotte & G. Bianco, p. 181-187

13. Lara, L., Alberdi, A. 1995, "Velocity and Orientation of Accelerating Components in Relativistic Jets", in "Extragalactic Radio Sources", ed. R. Fanti and C. Fanti, Kluwer Academic Publishers (Dordrecht, The Netherlands), in press

14. Marcaide, J.M., Alberdi, A., Ros, E., Diamond, P., Shapiro, I.I., Guirado, J.C., Jones, D.L., Krichbaum, T., Mantovani, F., Preston, R.A., Rius, A., Schilizzi, R.T., Trigilio, C., Whitney, A.R., Witzel, A. 1995, "Spectral-Index Map and Rate of Expansion of SN 1993J", in "Radio Emission

from the Stars and the Sun", ed. A.R. Taylor & J.M. Paredes, Astronomical Society of the Pacific Conference Series, in press

15. Hernández-Pajares, M., Rius, A., Juan, J.M., Madrigal, A.M. 1995, "Study of the global electron content using GPS", in "European Geophysical Society Meeting", Hamburg, in press.

16. Juan, J.M., Rius, A., M.Hernández-Pajares, M. 1995, "Obtaining precise orbits with a non-fiducial method", in "European Geophysical Society Meeting", Hamburg, in press.

17. Rius, A., Juan, J.M., Hernández-Pajares, M., Sardón, E., Alberdi, A. 1995, "GPS as a tool for estimating the ionospheric delay on the VLBI observables", in "XIth Working Meeting on European VLBI for Geodesy and Astrometry", ed. R. Lanotte & G. Bianco, p. 141-147

18. Rius, A., Elgered, G., Johansson, J.M., Keihm, S., Zarraoa, N. 1995, "Tropospheric Delays Estimated from VLBI, WVR and GPS. A Comparative Study", in "XIth Working Meeting on European VLBI for Geodesy and Astrometry", ed. R. Lanotte & G. Bianco, p. 134-140

19. Tsutsumi, T., Peracaula, M., Taylor, A.R. 1995, "Centimeter to Submillimeter Observations of Four Radio-Emittting X-ray Binaries", in "Radio Emission from the Stars and the Sun", ed. A.R. Taylor & J.M. Paredes, Astronomical Society of the Pacific Conference Series, Vol. 93, p. 258, in press

20. Zarraoa, N., Juan, J.M., Rius, A. 1995, "Analysis of the European geodetic experiments with a Free Network concept", in "XIth Working Meeting on European VLBI for Geodesy and Astrometry", ed. R. Lanotte & G. Bianco, p. 87-90

7 Instrumentation

(See the 'Radio Astronomy and the Deep Space Network' reports generated yearly by the JPL Telecommunications and Data Acquisition Science Office, M/S 303-401, Pasadena, California 91109, for details on the available instrumentation).

a) Front End Areas

Telescopes	DSS63				DSS65	
Diameter	70 m				34 m	
Bands	L	S	X	K	S	X
Efficiency	.6	.7	.7	.4	.6	.7
System T(K)	35	20	20	60	55	21/40
Surface RMS (mm)	6-7				5	

b) Time and Frequency

2 Redundant Hydrogen MASERS.

c) Recording Terminals

1 Mark III A DAT (with two recorders)
It is controlled through the Linux-based Field System FS9 (GSFC)
and also the Bonn MkIII VLBI PC-Field System.

d) Other equipment

- SNR-8 ROGUE GPS Receiver.
- Pressure, humidity and temperature sensors integrated in the system.
- Water Vapour Radiometre: Method to estimate the wet delay.

e) Software

The permanent availability of the Mark III data acquisition terminal at the MDSCC and the need of improving existing observational capabilities, not specifically oriented towards the astronomy, prompted us to develop a set of programs, generically called RA-Tools, which, together with the Linux-based Field System FS9, allowed the host country community to use efficiently the NASA resources for radioastronomical observations.

Since the beginning of 1995, the new automatic procedure *"DR2DSN"* has been tested and used to produce the antenna predicts for VLBI experiments (extension -prd-). *DR2DSN* introduces a cross-scan in azimuth and another one in elevation in the predict file if there is enough time available between two consecutive scans, which permits to check the pointing before a VLBI scan. We are also using *DR2DSN* to generate simultaneously a command-file (extension -smc-) which controls the radiometre via PC. This command file *.smc is very useful since it permits i) to check the pointing for a given experiment, ii) to monitor the variation of the antenna temperature for a given experiment, iii) to make automatic flux density measurements (very useful for monitoring projects), iv) to obtain the gain curves of the antenna (DSS63 or DSS65) at different frequencies, between other possibilities. Different observing sessions have been performed with the help of the procedure *DR2DSN*, and the results are very succesful. The *'DR2DSN'* software is available via anonymous ftp from *dsnra.jpl.nasa.gov*.

8 Future Plans and Hopes

- **Upgrade to MkIV**: Middle of 1997 in Australia and Madrid.
  End of 1996 in Goldstone.

- **K-band HEMT Receiver**: 18-26.5 GHz Modules.
  + a second down-converter chain in the MMS:
  2 polsns or 2 spectral lines simultaneously!

- **22 GHz Tunable Maser**: End 1997

- **Remote Monitoring** DSN-Radioastronomy antenna and Recorder:
  End of 1996.

- **Space-VLBI Co-observing**: 4 experiments per week.
  The new 12m antenna for telemetry is already working.

- **Digital Spectrometre**:
  1024 channels correlator, with a bandwidth ~10 MHz.

1.6 GHz Receiver: OH Masers; 22 GHz: H_2O Masers

It is already in the process of characterization of the instrument.

		1612	**MHz**	**22**	**GHz**
Bandwidth (MHz)	Channel Spacing (Hz)	Velocity Range (Km/sec)	Velocity Resolution Km/sec	Velocity Range Km/sec	Velocity Resolution Km/sec
16	15.625	2978	5.82	218	0.426
8	7.813	1489	2.91	109	0.213
4	3.906	744	1.45	54.5	0.107
2	1.953	372	0.73	27.3	0.053
1	0.976	186	0.36	13.6	0.027
0.5	0.488	93	0.18	6.82	0.013
0.25	0.244	47	0.09	3.41	0.007

Status Report on Noto VLBI station

V. Tornatore[1,2], G. Tuccari[1], G. Nicotra[1], S. Buttaccio[1], C. Contavalle[1], C. Stanghellini[1]

(1) IRA-CNR Stazione Radioastronomica, Noto, Italy
(2) DIIAR Politecnico di Milano, Italy

Abstract. Some updates in data acquisition and timing systems of the station occurred in the last year. A description concerning the adoption of the GPS timing system and the performance of the cable delay calibration system is presented.
We summarize the carried out observative geodetic campaigns.
Developments in the project regarding the correction of source structure effects on geodetic VLBI experiments will also be discussed.

1. Instrumental developments during 1995-1996

The main features of the data acquisition and timing systems currently in use are presented in Figure 1.
The terminal is almost complete, it misses only two BBCs that will be delivered by Interferometrics this September.It's equipped also with the module "DELAY CAL", on loan by the Haystack Observatory.
The commonly employed PC based Field System (Goddard Space Flight Center standard) is the 9.0.8, but the version 9.1.3 has been also installed, it has been used only for VLBA observations and observative tests for the VSOP satellite.
The Digital Switch Board, upgrade of the Analog Switch Board, is under testing.
The GPS timing receiver 'TAC' (Totally Accurate Clock) has been introduced in the Time and Frequency Station, whose configuration is rapresented in Figure 1 too, since March '96.
Daily data of UT time from GPS have been collected since April '96. Some tests have been done in Socorro to evaluate the possibility of the so-called "blind Correlation".

Presented at the 11th Working Meeting on European VLBI for Geodesy and Astrometry, Onsala, Sweden, 1996

Data acquisition and timing systems

Fig. 1

- VLBA recorder *(Interferometrics)*
- VLBA data acquisition terminal with 12 BBC
- Digital switch board
- PC486 for field system *(Linux operating system)*
- FS 9.0.8 and 9.1.3
- Metereological equipment (Pressure, humidity and temperature sensors)
- Maser H-EFOS-5 and rubidium oscillators
- Loran-C and GPS timing receivers
- OSA-Clock

Time & Frequency standard configuration

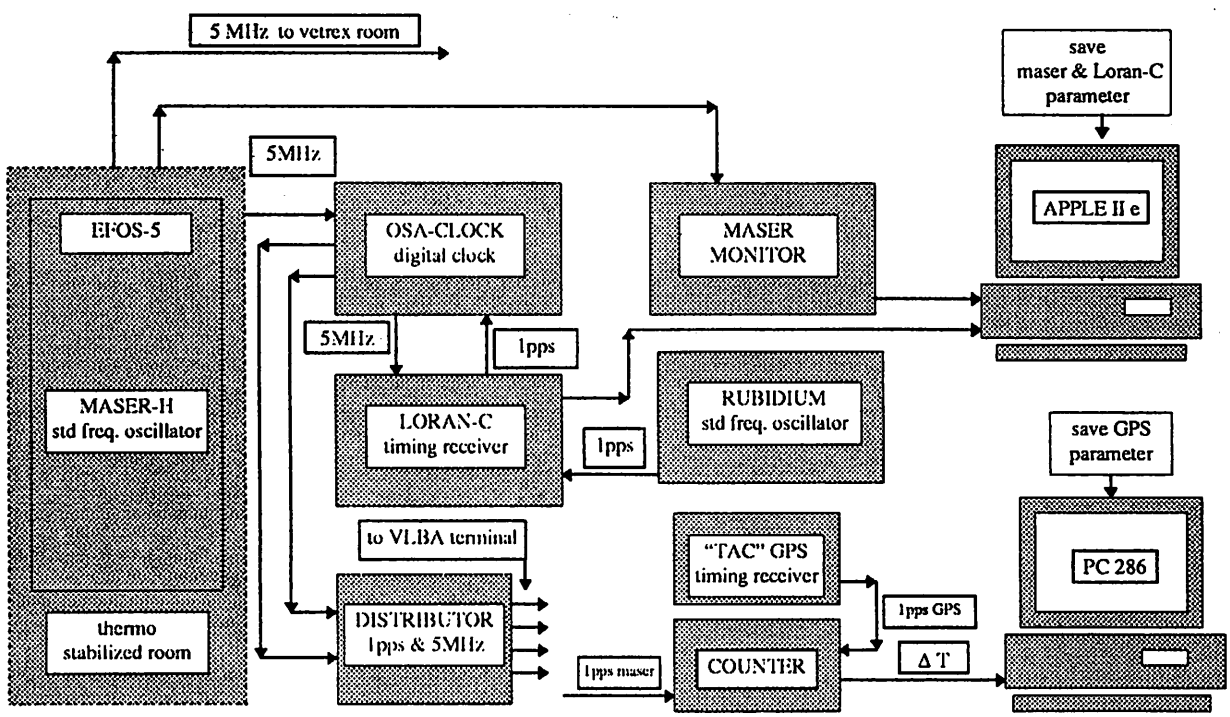

2. Preliminary results of "cable" measurements

Some measurements dedicated to the study of the stability of the cable calibration system have been carried out, due to the availability of the "ground unit" module.

The delay along a cable changes with the temperature and cable flexure. To evaluate the influence of the temperature itself, we recorded cable and temperature measurements for 24 hours every 10 minutes starting at about 19 UT while the antenna remained stationary in the stow position (AZ=206 EL=90 degree). Figure 2a and 2b show the daily behaviour of the two quantities.

Other measurements have been performed let the antenna moving in azimuth along the complete route of 520 degree in about 2 hours (during a temperature variation of about 1 degree around 25 C).

Figure 2c shows the cable measurements reported.

The variations of electrical cable lenght are bounded to the variations of the surface temperature, while are insensitive to the cable flexure.

Further measurements will be carried on to evaluate the dependence of the electrical cable lenght with the temperature.

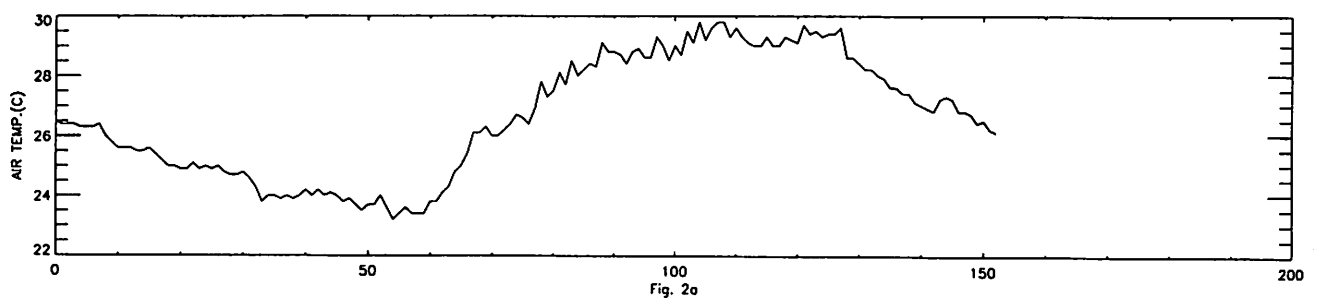

Fig. 2a

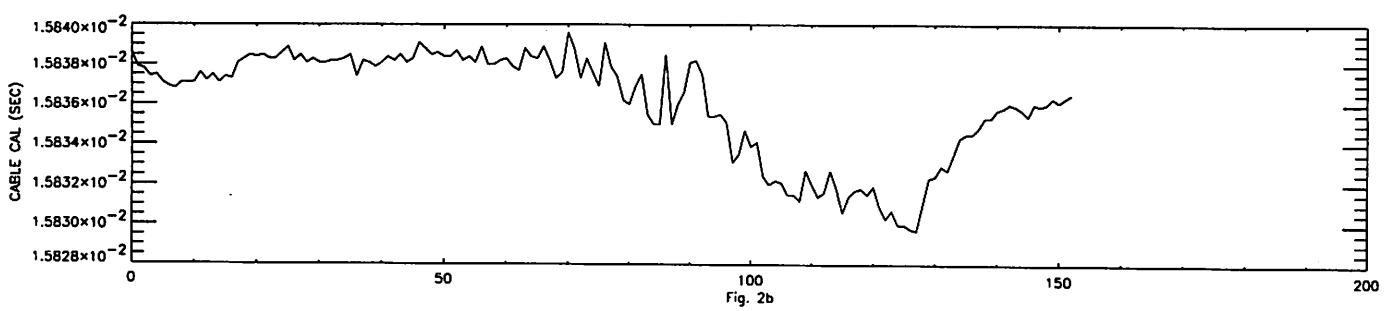

Fig. 2b

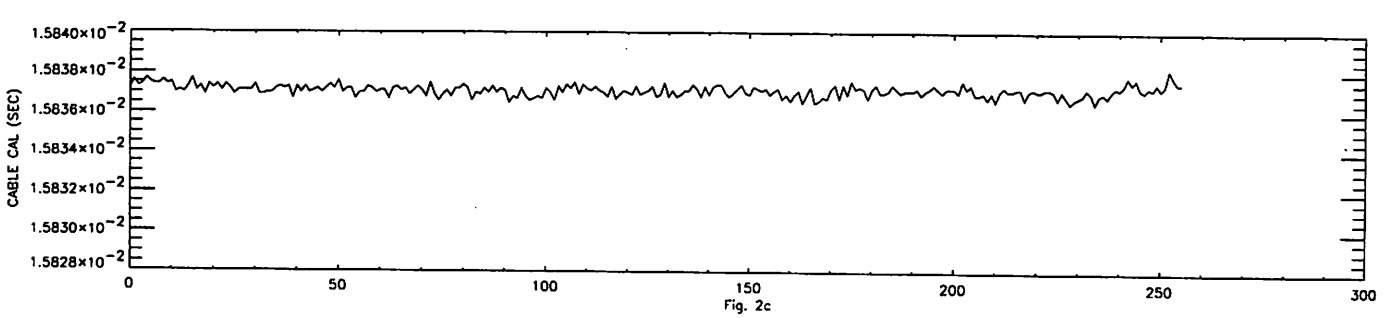

Fig. 2c

3. Interferences research

A true station to survey the interferences that disturb observations in the bands 92cm, 75cm, 21cm, 18cm and 13 cm has been developed at Noto. It consists of a movable antenna system, amplifiers for high and low bands, receivers and some accessories.
Table 1 and figure 3 summarize and schematize the characteristics of the system already operative.
The installation of a second movable antenna system that uses a parabolic one of 2 m (see Figure 4) is in progress to survey the bands of 6 cm, 3.6 cm and 2.5 cm.

Tab. 1

OPERATIVE

COVERED BANDS 92cm, 75cm, 21cm, 18cm, 13cm

MOVABLE ANTENNAS SYSTEM :

CREATE CLP 5130-2	log periodic antenna	105 - 1300 MHz	10 to 12 dBi	H-Pol.
CREATE CLP 5130-2	log periodic antenna	105 - 1300 MHz	10 to 12 dBi	V-Pol.
SAMA LPD-M3 s.02	log periodic antenna	1350 - 2350 MHz	13 dBi	H-Pol.
SAMA LPD-M3 s.02	log periodic antenna	1350 - 2350 MHz	13 dBi	V-Pol.

AMPLIFIERS :
HIGH BAND 1 (2350 to 1750 MHz)
H-V polarization selectable low noise RF amplifier Mini Circuits ZEL1724LN, +20 dB & ZHL1042J, +25 dB

HIGH BAND 2 (1750 to 1200 MHz)
H-V polarization selectable low noise RF amplifier Mini Circuits ZEL1217LN, +20 dB & ZHL1042J, +25 dB & TV Broadcaster filter -25dB

LOW BAND (105 - 1200 MHz)
H-V polarization selectable RF amplifier Mini Circuits ZFL1000H +28dB gain, FM Broadcaster filter -25dB

RECEIVERS :
ICOM IC-R9000 Communication receiver 100kHz - 2000MHz FM, FMw, AM, CW, FSK
Hewlett Packard HP8569B Spectrum Analizer 10MHz - 18GHz

ACCESSORIES:
Philips video monitor and video recorder
Hewlett Packard HP7470A plotter

Fig. 3

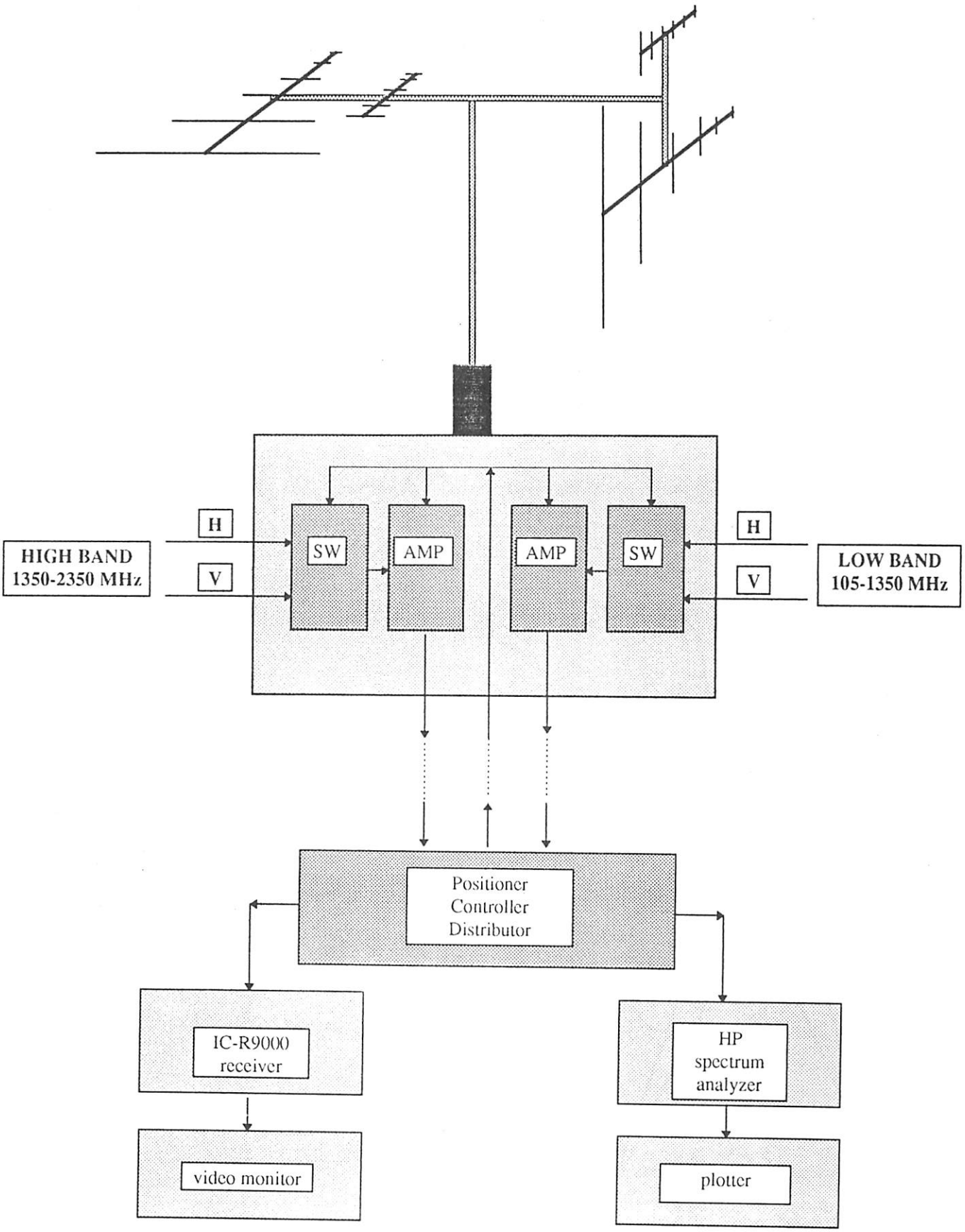
H
V
HIGH BAND
1350-2350 MHz
SW
AMP
AMP
SW
H
V
LOW BAND
105-1350 MHz
Positioner
Controller
Distributor
IC-R9000
receiver
video monitor
HP
spectrum
analyzer
plotter

Fig. 4

IN PROGRESS

COVERED BANDS 6cm, 3.6cm, 2.5cm

MOVABLE ANTENNA SYSTEM :

IRTE 200cm parabolic antenna, prime focus

EMME ESSE DSR3000 parabolic antenna positioner

YAESU G-2700SDX antenna rotator & controller

Self made log periodic antenna 3.5 - 8.5 Ghz, 10 dBi, developed in Noto

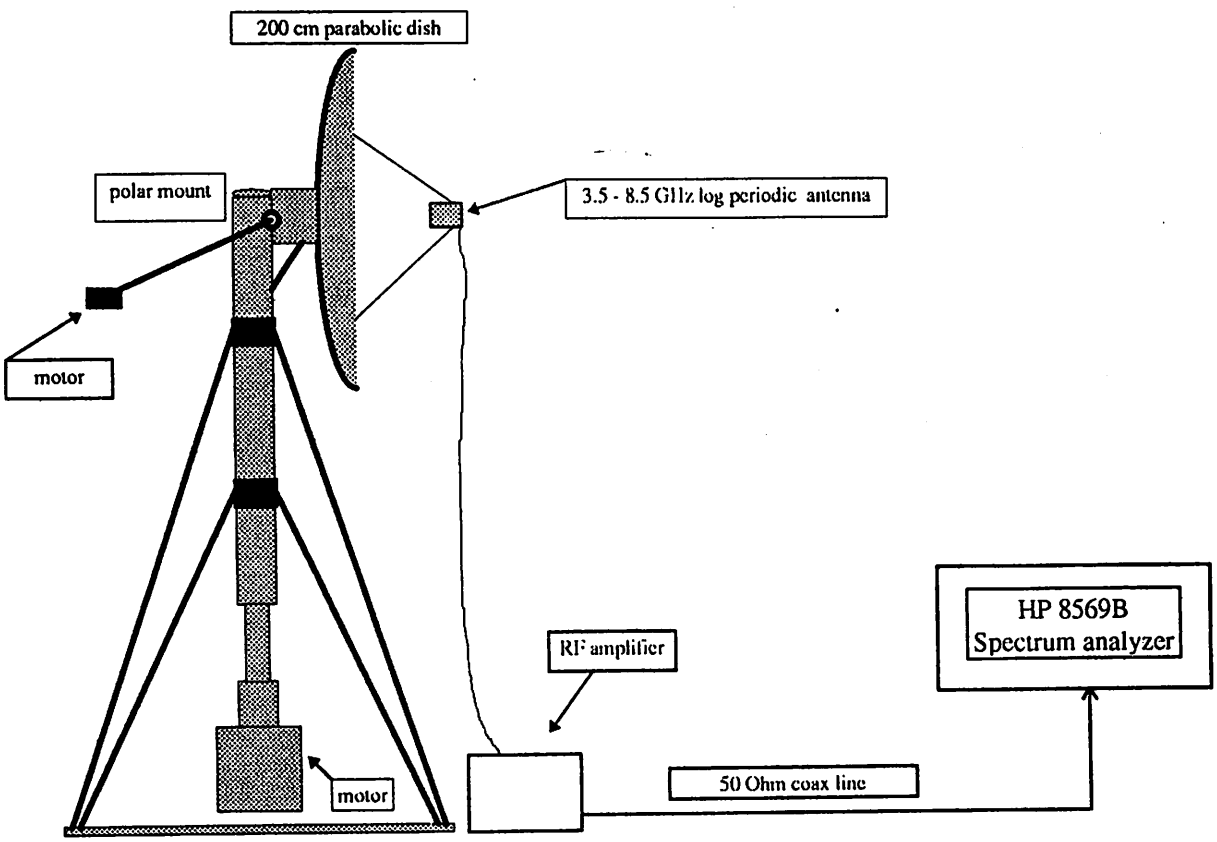

4. Geodynamical Observations

The observational activity performed in 1995 and first months of 1996 in the geodynamical field has been mainly devoted to VLBI campaigns. The station has taken part to the EUROPE experiments and to two new programs : the Global experiments (RDGTR3 and RDGTR5)
to evaluate Earth orientation parameters and the CRFexperiments whose purpose is to improve the determination of the celestial reference frame in the southern Hemisfere.
Dates and the participating stations in each experiment are indicated in Table 3
Noto is one of the 6 stations of the Italian GPS network (Noto-Matera-Cagliari-Medicina-Genova-Venezia) managed by ASI. The station is equipped with a Turbo Rogue receiver that acquires data in a permanently way since February 1995. Data are transferred on a daily basis to Matera where they are archived in the Geodetic Data Archive Facility (GeoDAF).
A campaign of GPS measurement has been effected for the SELF (SEa Level Fluctuations) project in July 1996.
The geodetic local network has been surveyed in June of last year by (ASI-Telespazio).

Tab. 3

VLBI

DATES			PROGRAMS	STATIONS
1995	FEB	01	EUROPE-1	Os-Md-Wz-Ma-Nt-Mt-Cr-Ny
	APR	12	EUROPE-2	Os-Md-Wz-Ma-Nt-Mt-Cr-Ny-Ef
	JUN	08	EUROPE-3	Os-Md-Wz-Ma-Nt-Mt-Cr-Ny-Yb
	JUL	24	RDGTR3	Nt-Kp-Ma-Fb-Yk-Hb-Kk-Ks-Ta-Sc
	SEP	18	RDGTR5	Nt-Wz-Nl-Fb-Ov-Hb-Kk-Ks-Ti-Ny-Ag
	NOV	09	EUROPE-5	Os-Md-Wz-Ma-Nt-Mt
	DEC	06	EUROPE-6	Os-Md-Wz-Ma-Nt-Mt-Ny-Ef
1996	FEB	07	EUROPE-1	Os-Md-Wz-Ma-Nt-Mt
	MAY	06	CRF-MSB-1	Nt-Bz-Hb-Ri
	JUN	01	EUROPE-3	Os-Wz-Ma-Nt-Mt

5. A research project

A project to perform observations of sources used in EUROPE experiments, in an astronomical way to obtain high resolution images in the S and X bands necessary to correct the effects of source structure on geodetic data has been developing in Noto.

Studies about the importance of these effects in geodesy and astrometry have been performed in these years (Britzen et al. 1993; Charlot P. 1990; and others). For high-precision geodetic VLBI analysis, with long term goal to include all the phenomena that may cause effects at 10 ps level, source structure effects must be accounted for. Software and algorithms have already been developed in this direction (Charlot P. 1990; Zeppenfeld G. 1991) : the determination of the source-structure effects and their proper correction in the analysis is possible but brightness distributions of the radio sources need to be well-known.

A research in the astronomical literature about the sample of 38 sources commonly observed during EUROPE experiments has been performed. We selected a subsample of 16 sources without any image in the S and X bands (see Table 3). Observing time has been granted in October to observe this subsumple with a network composed of EVN antennas (Effelsberg, Onsala, Noto, Jodrell Bank, Shangai, Urumqi, Simeiz) and some geodetic antennas Ny Alesund, Matera, Wettzell, Madrid.

The goal is to use these images to perform corrections on the data of the EUROPE5 '96 experiment that is scheduled at an almost "contemporary" epoc to the astronomical observations of radiosources, November 3. This would leave free of any variability in time of the source structure.

TAB.3 List of sources, positions and indicative flux densities at 2.3 GHz and 8.4 GHz

IAU NAME	RA (B1950)	DEC (B1950)	$S_{2.3}$ (Jy)	$S_{8.4}$ (Jy)
0048-097	00 48 09.98	-09 45 24.2	1.4	1.3
0059+581	00 59 43.50	+58 08 05.0	3.0	1.4
0119+041	01 19 21.39	+04 06 44.0	1.8	1.6
0336-019	03 36 58.95	-01 56 16.9	2.0	2.1
0457+024	04 57 15.54	+02 25 05.7	1.6	1.3
0528+134	05 28 06.76	+13 29 42.3	3.0	2.5
0804+499	08 04 58.40	+49 59 23.1	1.5	1.1
0955+476	09 55 08.53	+47 39 28.3	0.7	0.8
1044+719	10 44 49.74	+71 59 26.9	0.8	2.0
1219+044	12 19 49.20	+04 29 54.0	1.0	0.4
1357+769	13 57 42.12	+76 57 53.4	0.5	1.0
1606+106	16 06 23.40	+10 36 59.8	0.9	1.2
1638+398	16 38 48.17	+39 52 30.1	1.0	1.8
1726+455	17 26 01.20	+45 33 04.6	0.5	1.6
1958-179	19 58 04.61	-17 57 16.9	1.1	0.9
2121+053	21 21 14.80	+05 22 27.4	4.0	2.8

References

Ambrico F., Del Rosso D., Survey of the Noto Site, Nuova Telespazio s.p.a report for ASI.1995 Matera

Cenci A., G. Colucci, L. Garramone, GeoDAF, Geodetical Data Archive Facility, Manuale utente, Nuova Telespazio s.p.a report for ASI.1995 Matera

Britzen S., A.M. Gontier, A. Witzel, C. Schalinski, J. Campbell: Radio Source Structure and its influence on accuracy of Geodetic VLBI Analysis, Part 1.Proceedings of the 9th Working Meeting on European VLBI for Geodesy and Astrometry, Bad Neuenahr, FRG 1993, p. 157-166, Rep. ISSN 0343-7361, Bonn

Del Rosso D. Garramone L., Poggi M., Matera GPS Station report on the operational and performance evaluation activities from January to December 1995, Nuova Telespazio s.p.a report for ASI.1996, Matera

Charlot P., 1990, A..J. 99,1309

Tornatore V., The Radioastronomical Station of Noto Geodetic Status Report, Proceedings of the 10th Working Meeting on European VLBI for Geodesy and Astrometry, Matera, Italy 1995, p. 39-44, Eds. R. Lanotte and G. Bianco, Matera

Zeppenfeld G.: Source Structure Enhanced MKIII Data Analysis Software. Proceedings of the 8th Working Meeting on European VLBI for Geodesy and Astrometry, p. IV 16-21, Rep. MDTNO-R-9243 Delft, 1991

MATERA VLBI STATION: STATUS REPORT

G. Bianco
ASI - Centro di Geodesia Spaziale, Matera

D. Del Rosso, L. Garramone, G. Colucci
Nuova Telespazio S.p.A. - Centro di Geodesia Spaziale, Matera

1. INTRODUCTION

This report summarizes the present status of the operational VLBI activities at the Matera Space Geodesy Center (CGS).

More detailed information, including the 1995 VLBI Station Report, can be obtained on-line at this address: **http://geodaf.mt.asi.it/GDHTL/matera.html**

2. VLBI SYSTEM CHARACTERISTICS

The Matera VLBI system includes a 20 meter diameter antenna, designed and built in Italy by Selenia Spazio (now Alenia Spazio), a MARK-III D.A.T. built by Signatron Inc. (USA) (under contract with Telespazio) and a Time and Frequency system integrated by Politecnico di Torino (under contract with Telespazio).
Telespazio integrated the VLBI system developing also the interface software between the control system and the Antenna Control Unit.

Tab. 1 shows the declared technical characteristics of the MATERA VLBI antenna.

PARAMETERS RF IF RECEIVER SYSTEM PERFORMANCE	MEAS. UNIT	S - BAND	X - BAND
Instantaneous band at 2 dB	MHz	100	400
Working IF band	MHz	190÷330	100÷500
RF/IF gain	dB	70	70
Dynamics at 0.5 dB of compression	dBm	-70	-70
Gain stability (Temperature 20 °C)	dB/24h	±2	±2
Gain stability (Temperature 20 °C)	dB/1h	±0.1	±0.1
Image rejection	dB	30	30
Group delay in 2 MHz	ns	-1	-1
Input nominal level	dBm	-97	-90
Output nominal level	dBm	-27	-20
External temperature limit	°C	-10÷+40	-10÷+40
Wind velocity limit	Km/h	36÷50	36÷50
Differential thermal head in the structure lower than:	°C	5	5
Working RF band	GHz	2.2÷2.4	8.2÷8.6
Circular polarization		Right	Right
System noise temperature	°K	140	140

Tab. 1 Matera VLBI Antenna Technical Specifications

Presented at the 11th Working Meeting on European VLBI for Geodesy and Astrometry, Onsala, Sweden, 1996

The Time and Frequency System at Matera was designed in order to meet the requirements for both SLR and VLBI systems.

GENERAL CHARACTERISTICS.	• One H-MASER frequency standard; • Two CESIUM beam frequency standards; • One GPS time receiver; • Three independent time-scales; • Automated monitor and control system; • Absolute continuity of operations; • Environment-controlled room to host the frequency standards.
THECNICAL CHARACTERISTICS.	• frequency stability ($\Delta f/f$; t=1000 s) < 2E-15 (H-MASER) • spectral purity > 110 dB (1 Hz) • time stability ($\Delta t/t$; t>1 day) < 5E-13 (CESIUM) • synchronization (UTC) < 100 ns(GPS)

Tab. 2 Time and Frequency System: Characteristics

The Matera Time and Frequency system is composed of three frequency sources (two CESIUM beam an one H-MASER standards) and three independent clock chains. The EFOS-8 H-MASER from Oscilloquartz is used as frequency source for VLBI. This system, shows excellent performance in terms of stability (*$\Delta f/f$<2E-15; 1000<t<10000 s*), spectral purity (*>110 dB; 1 Hz*) and temperature sensitivity (*2E-14/°C*). The prime time scale is generated by a HP 5061B Cesium standard (a second Cesium standard is intended as back-up).
Synchronization to UTC is guaranteed by the use of a GPS receiver (FTS 8400).
In February the old computer HP 9000/310M that controlled the time system, was replaced by a DOS PC-286.
Absolute continuity of operations is guaranteed by the main power inverter. An additional battery back-up is dedicated to the frequency standards and other critical equipment.

3. VLBI Observations

The summary of the VLBI campaigns made from January to December '95, is reported in Tab. 3. During the 1995, Matera participated to 16 VLBI campaigns for a total of 238.5 hours of acquisitions. In particular Matera was involved in:

- 3 experiments coordinated by National Aeronautic and Space Administration (NASA)
- 5 experiments coordinated by Max Plank Institut Fuer Radioastronomie (MPIFR)
- 3 experiments coordinated by European VLBI Network (EVN) - Astronomical experiments
- 5 experiments coordinated by United States Naval Observatory (USNO) - Satellites experiments.

4. Main events at Matera during the first half of 1996

- In **April** the headstack of the VLBA recorder was replaced with a new one.
- In **May** the *Wide Band* upgrade of the system started. The new receiver (NASA standard) should be operative at the end of 1996, while the IF3 is now installed on MK-III rack.
- In **July** the elevation cable wrap was replaced with a new one. Also all the cables (including the signal cables) was replaced.

VLBI 1995 ACQUISITION SUMMARY

Experim.	Date	Dur.	Observ.	Tapes	Antenna	Power	Others	Time Lost	Degraded	Obs. Lost
RDGTR1	01/23/95	24	145	3		0.21		0.21		1
EUROP-1	02/01/95	24	193	3						
EA006A	02/09/95	12	196	5			0.37	0.37		7
EA006B	02/10/95	13	240	4		0.03	0.02	0.05	3	
ER1	02/12/95	13	235	4			0.17	0.17	4	
RDXTL1	03/13/95	24	200	3						1
EUROP-2	04/12/95	24	174	3			0.02	0.02	1	
EUROP-3	06/08/95	24	161	3			0.23	0.23		2
NVSAT24	09/20/95	1	18	1						
NVSAT26	09/27/95	1.4	17	1						
NVSAT27	09/28/95	2.1	24	1						
NVSAT28	09/19/95	2	23	1			0.11	0.11		2
NVSAT29	09/30/95	2	25	2			0.13	0.13		2
RDGTR6	11/07/95	24	154	3		1.60	0.10	1.70	1	15
EUROP-5	11/09/95	24	239	4			0.58	0.58		9
EUROP-6	12/06/95	24	256	3	0.82		0.55	1.37		17
16		**238.5**	**2300**	**44**	**0.82**	**1.84**	**2.28**	**4.94**	**9**	**56**
					16.6%	**37.3%**	**46.1%**	**100.0%**		

All Time Values are in decimal hours

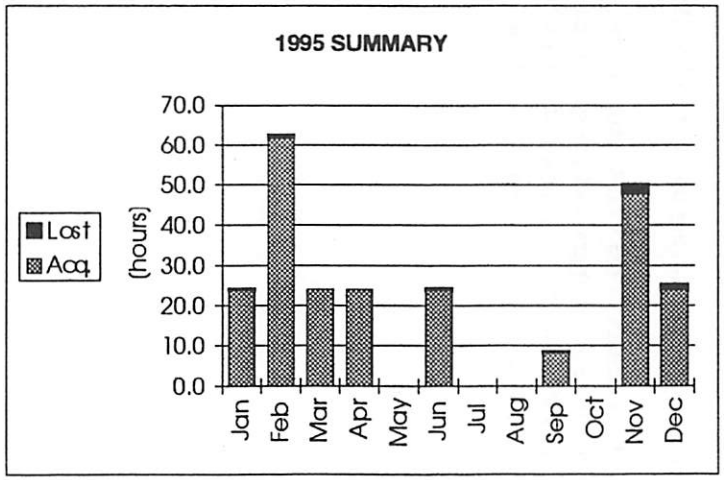

1995 SUMMARY

Month	Time Acq.	Time Lost	Sources Acq.	Sources Lost
Jan	24.0	0.2	145.0	1.0
Feb	62.0	0.6	864.0	7.0
Mar	24.0	0.0	200.0	1.0
Apr	24.0	0.0	174.0	0.0
May	0.0	0.0	0.0	0.0
Jun	24.0	0.2	161.0	2.0
Jul	0.0	0.0	0.0	0.0
Aug	0.0	0.0	0.0	0.0
Sep	8.5	0.2	107.0	4.0
Oct	0.0	0.0	0.0	0.0
Nov	48.0	2.3	393.0	24.0
Dec	24.0	1.4	256.0	17.0
	238.5	**4.9**	**2300**	**56**
		2.1%		**2.4%**

Year	Hours
1990(*)	126.0
1991	549.0
1992	873.0
1993	829.5
1994	928.0
1995	238.5
	3544.0

(*) Since May

Geodesy and VLBI in the Netherlands: A Status Report

Ronald Molendijk

In the past eight years the Netherlands did not participate in regular geodetic VLBI campaigns. One of the reasons has been the technical limitations of the WSRT for geodetic VLBI (i.e. S/X receiver capability). Now a lot of progress has been made in the upgrade of the WSRT and it is expected that Westerbork soon can take part in a geodetic VLBI campaign. Having in mind the importance of the vertical component for the Netherlands, much effort has been put in the connection of the Westerbork station to e.g. the national height network, the SLR/GPS site in Kootwijk, and some important Dutch tide gauges. The decision to review the activities of the Kootwijk Observatory for Satellite Geodesy and to shift these activities partially to Westerbork and the University of Technology in Delft opens up opportunities for a closer co-operation between the institutes involved. Within a few months the VLBI station Westerbork will also be equipped with a (new) absolute gravity platform, a permanent GPS receiver and a SLR platform.

Presented at the 11th Working Meeting on European VLBI for Geodesy and Astrometry, Onsala, Sweden, 1996

VLBI at Ny-Ålesund Space Geodetic Observatory
Station Report 1995-1996

Bjørn R. Pettersen

Geodetic Institute, Norwegian Mapping Authority, N-3500 Hønefoss, Norway
e-mail: bjornrp@gdiv.statkart.no

Abstract. The Ny-Ålesund VLBI facility continues to increase its participation in international geodetic networks. Forty-five observing sessions have been carried out between May 1995 and August 1996. Data are analysed by the Space Geodesy Group at the Geodetic Institute in Hønefoss, using the latest version of Occam. Observations since October 1994 show motions in accordance with existing plate tectonic models, but the time series is still too short for final conclusions to be made. A longer time series is available from GPS (since 1991) and compares well on relative scales. Eccentricity measurements to connect different instruments at the site to a common reference point still remains to be made. The VLBI recording equipment is currently being upgraded to Mark IV.

Observing Activities

The Ny-Ålesund Space Geodetic Observatory was inaugurated on August 16, 1995 by HM King Harald V, in the presence of Government representatives, members of the Norwegian Parliament, representatives of national, foreign and international science institutions, civil servants and administrators. Since the last Working Meeting on European VLBI, the observatory has participated in 45 VLBI observing sessions. Table 1 lists the details. A GPS rogue receiver continues to provide data to IGS, but will be replaced by a new turborogue in the near future.

Technical Upgrading

The VLBI recording equipment is being upgraded to Mark IV. Mechanical changes have been made to the magnetic tape station to accomodate thin tapes, and new filters have been installed into the video converters. A new formatter has been ordered for delivery in late September 1996, and the read/write electronics will be assembled and installed later this year. Decoder modifications and a new pcal-unit is awaiting delivery from Onsala Space Observatory. Software upgrading of the Field System to FS9.1 will take place this Fall.

A Prare unit was installed in late 1995. Following testing, it is now operational. A 12 channel Turborogue GPS receiver is connected to the existing IGS-rogue antenna and serves as a supplemental recorder. Upon completion of the testing program, it will operate with its own Dorne-Margolin antenna to replace the current IGS site.

An Earth-tide gravimeter has been installed and is currently being tested. It will go into continuous operation later this year. Plans also exist to install SAR-reflectors in Ny-Ålesund in 1996.

Presented at the 11th Working Meeting on European VLBI for Geodesy and Astrometry, Onsala, Sweden, 1996

Table 1: VLBI-observations from Ny-Ålesund

Date	Program
10 May 1995	CRF-N2
08 June 1995	EUROPE-3
14 June 1995	NAVEX-S6
27 June 1995	NEOS-A113
24 July 1995	GLOBAL TRF-3
31 July 1995	NAVEX-S7
15 Aug 1995	NEOS-A120
22 Aug 1995	NEOS-A121
23 Aug 1995	CONT-95A
24 Aug 1995	CONT-95B
25 Aug 1995	CONT-95C
26 Aug 1995	CONT-95D
27 Aug 1995	CONT-95E
28 Aug 1995	CONT-95F
29 Aug 1995	NEOS-A122
31 Aug 1995	EUROPE-4
18 Sep 1995	GLOBAL TRF-5
31 Oct 1995	NEOS-A131
09 Nov 1995	EUROPE-5
14 Nov 1995	NEOS-A133
06 Dec 1995	EUROPE-6
12 Dec 1995	NEOS-A137

Date	Program
09 Jan 1996	NEOS-A141
06 Feb 1996	NEOS-A145
22 Feb 1996	GOLDEN GLB-1
05 Mar 1996	NEOS-A149
13 Mar 1996	TRANS ASIA-1
19 Mar 1996	NEOS-A151
20 Mar 1996	GEO-VLBA-1
26 Mar 1996	NEOS-A152
16 Apr 1996	NEOS-A155
23 Apr 1996	GLOBAL TRF-10
24 Apr 1996	NAVEX-S9
25 Apr 1996	EUROPE-2
01 May 1996	NAVEX-S10
13 May 1996	GOLDEN GLB-2
28 May 1996	NEOS-A161
12 June 1996	EUROPE-3
14 June 1996	GEO-VLBA-2
20 June 1996	GOLDEN GLB-3
25 June 1996	NEOS-A165
09 July 1996	NEOS-A167
01 Aug 1996	GOLDEN GLB-4
14 Aug 1996	GEO-VLBA-3
20 Aug 1996	NEOS-A173

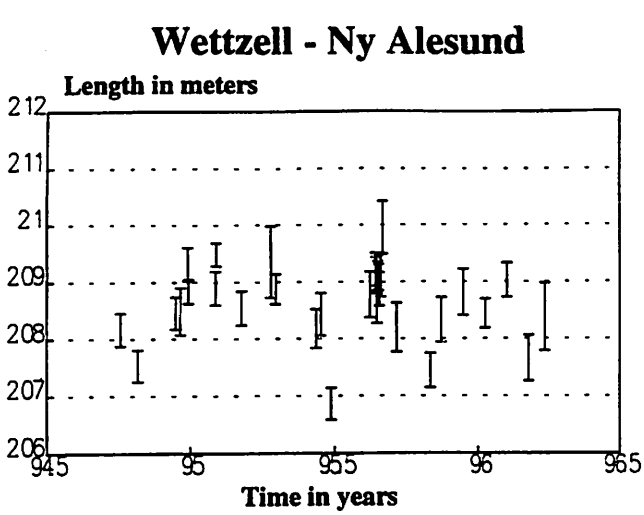

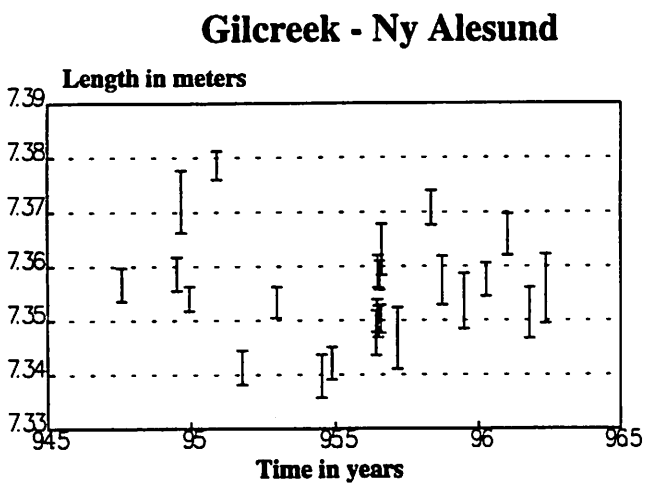

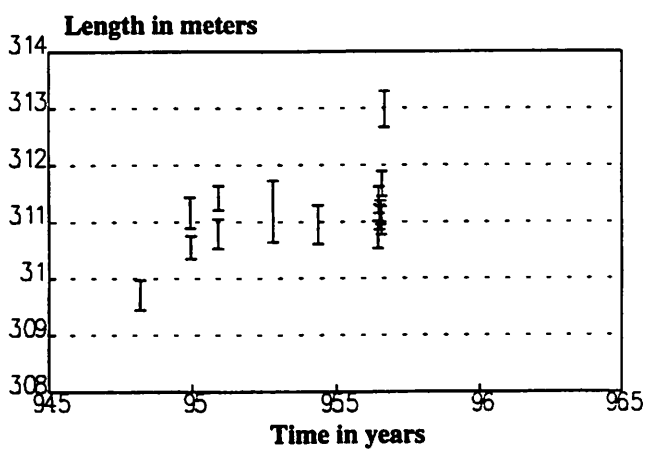

Figure 1. Baseline lengths between Ny Ålesund and three other VLBI stations

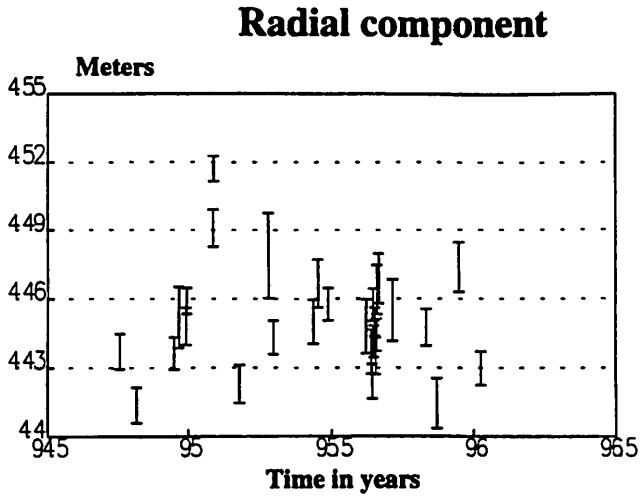

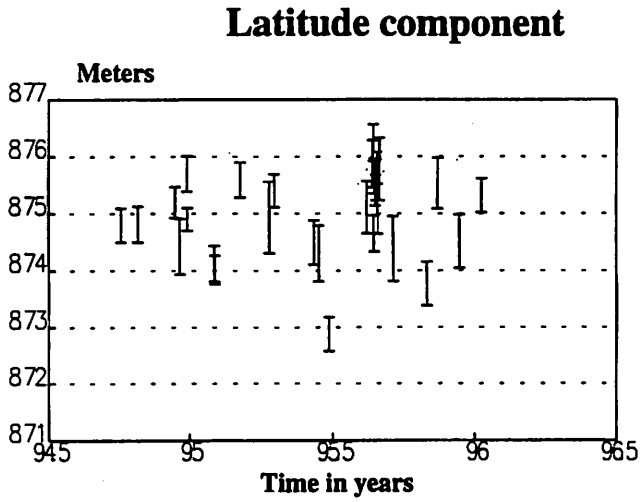

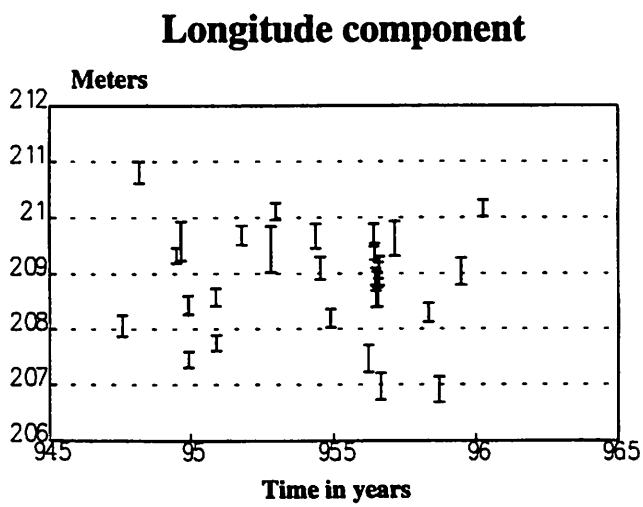

Figure 2. Local components estimated for Ny Ålesund

Table 2. Baseline lengths and velocities, with sigmas and RMS for epoch 1994.0

Baseline	Length (m)	Velocity (cm/year)	RMS (cm)
Ny-Ålesund - Wettzell	3283002.088 ± 0.005	-0.12 ± 0.30	0.6
Ny-Ålesund - Onsala (for 12 points)	2348793.105 ± 0.005	0.41 ± 0.33	0.3
Ny-Ålesund - Gilcreek	3909117.358 ± 0.008	-0.18 ± 0.53	1.0

Table 3. Ny-Ålesund velocity components, with sigmas and RMS for epoch 1994.0

Baseline	Length (m)	Velocity (cm/year)	RMS (cm)
Radial (for 27 points)	6357634.437 ± 0.012	0.50 ± 0.81	1.4
Latitude	8778248.745 ± 0.006	0.38 ± 0.39	0.7
Longitude	255372.086 ± 0.007	0.19 ± 0.49	0.9

Data Analysis

The first 18 months of VLBI data for Ny-Ålesund have been analysed with the OCCAM3.3 software (Titov et al. 1996). The time series includes 32 observing sessions between October 1994 and March 1996. Each session was analysed separately because the structure of the observing network changed from session to session. Wettzell was selected as the fixed reference station and the Earth orientation parameters from IERS Bulletin B fixed the orientation of the terrestrial reference frame. The celestial reference frame was defined by coordinates from ICRF92 with corrections from the IAU nutation model using IERS92 standards. The NNR NUVEL1 velocity field (Argus and Gordon 1991) was used to describe the tectonic displacements of all stations. A Kalman filter technique was employed where tropospheric corrections and clock offsets were treated as random walk stochastic processes.

The baseline lengths from Ny-Ålesund to Onsala and Wettzell, respectively, show no change with time, which indicates that Ny-Ålesund has no significant motion (<5 mm/year) relative to the Eurasian plate, at least in the North-South direction. The Ny-Ålesund to Gilcreek baseline shows a larger scatter, but there is no trend to indicate a velocity different from the NNR NUVEL1 model.

The time series for the vertical, latitude and longitude components of Ny-Ålesund may suffer from inexact definition of the terrestrial reference frame since the observing networks were not the same from session to session. The repeatability of the results are still acceptable, with rms values of 7 mm and 9 mm for horizontal components and 15 mm for the vertical. The derived velocity components do not contradict the GPS results by derived by Kristiansen et al. (1995) based on observations started in 1991.

References

Argus, D.F., Gordon, R.G., 1991, *No-net rotation model of current plate velocities incorporating plate motion model NUVEL1,* Geophys. Res. Lett. **18**, 2039-2042.

Kristiansen, O., Zarraoa, N., Pettersen, B.R., Engen, B., Hjelle, A., 1995, *Ny-Ålesund Space Geodetic Observatory: Geophysical Conditions and the First Geodetic Results,* presented at the XXI-th IUGG General Assembly, Boulder, July 1995.

Pettersen, B.R., 1995, *Space Geodesy from an Arctic Observatory,* Nordic Space Activities **3**, No. 1, p. 16.

Titov, O., Zarraoa, N., Pettersen, B.R., 1996, *Ny-Ålesund VLBI Station: First Year Analysis,* presented at the EGS General Assembly, Haag, March 1996.

Status Report of the TIGO-Project *

HAYO HASE, ARMIN BÖER,
WOLFGANG SCHLÜTER, REINER DASSING, PETER SPERBER
Institut für Angewandte Geodäsie
Fundamentalstation Wettzell
D-93444 Kötzting

RICHARD KILGER
Forschungseinrichtung Satellitengeodäsie
Fundamentalstation Wettzell
D-93444 Kötzting

Abstract

The Transportable Integrated Geodetic Observatory (TIGO) Project of the Institut für Angewandte Geodäsie is under completion at the Fundamental Station Wettzell. During 1995 and 1996 a platform for TIGO was built at Wettzell, the 6m radiotelescope has been assembled, the survey of the radiotelescope was performed, the S/X-receiver was installed, the NASA Mk4 PC-Field System adapted for radiotelescope control.

1 Introduction

"TIGO" is the abbreviation for 'Transportable Integrated Geodetic Observatory'. The concept of TIGO is based on the concept of a fundamental station for geodesy and geodynamics. It will serve as a measuring platform in spacetime in order to contribute to the celestial and terrestrial reference frames. All relevant space techniques as such as VLBI, SLR and GPS are included as well as gravity meter, seismograph, meteorological sensors. Communication infrastructure guarantees the connection to the data analysis centers [1].

The aspect of transportability is due to the desire to locate TIGO at remote sites preferably in southern hemisphere in order to densify the terrestrial reference frame [3]. TIGO is supposed to be setup for longer than annual periods abroad beginning in 1998.

2 Platform for TIGO

TIGO requires a prepared platform, in order to mount the radiotelescope on it and to setup the SLR-telescope. A platform was built at Wettzell in 1995 within 6 weeks. The specifications of the platform consists of:

Presented at the 11th Working Meeting on European VLBI for Geodesy and Astrometry, Onsala, Sweden, 1996

- concrete fundament ($10 \times 10 \times 1.5m^3$) for the radiotelescope containing a special steel construction to fix the radiotelescope,
- concrete fundament ($3.5 \times 3.5 \times 1.5m^3$) for the SLR module,
- concrete fundament to setup 5 TIGO containers,
- separated underground cable channels for either power or signal cables,
- grounding network to earth all instruments and containers,
- dehydration tubes.

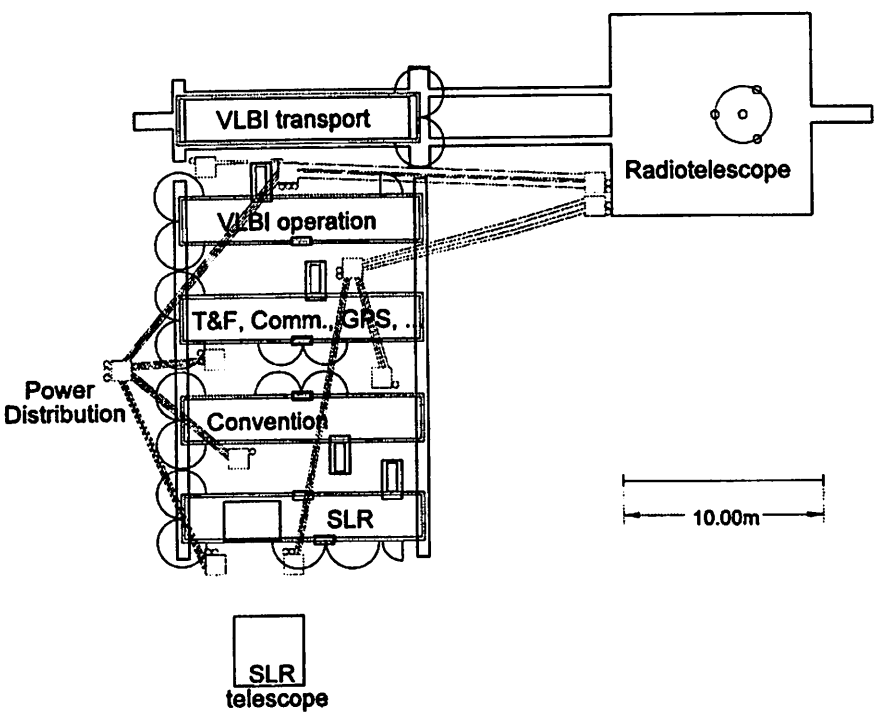

Figure 1: Schematic of the TIGO platform designed for Wettzell.

3 Setup of the TIGO-VLBI-Module

TIGO will serve as a fundamental station. Therefore all components are regarded as one unit. The VLBI-module is a part of TIGO, which consists basically of two containers:

Transport container contains the main structure of the $6m$-offset-radiotelescope during transportation.

Operation container consists of two rooms. The front room houses the control electronics for the radiotelescope, the VLBI Mk4 equipment and the back room is used for the transportation of the two sidepanels for the reflector.

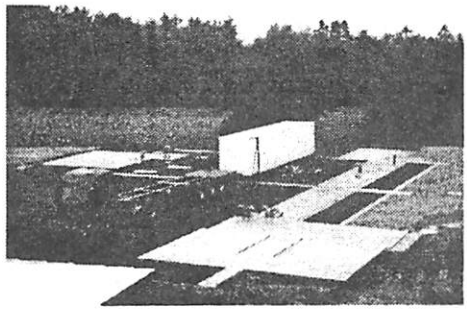

Figure 2: The TIGO platform at Wettzell.

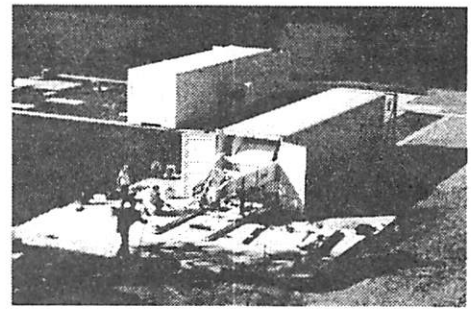

Figure 3: Pulling out the radiotelescope.

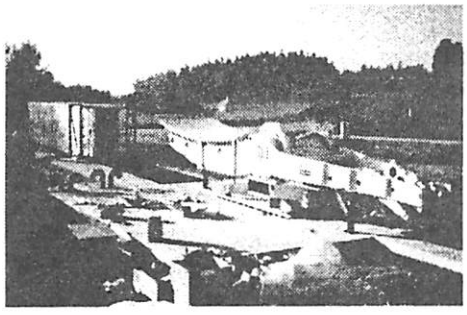

Figure 4: Shift back the transport container.

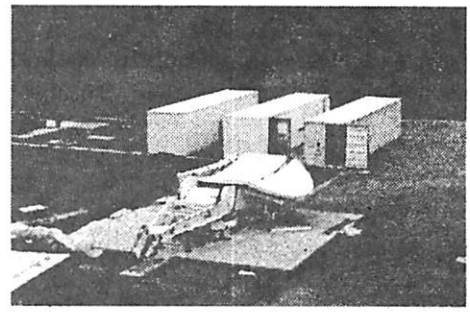

Figure 5: Mount the side panels.

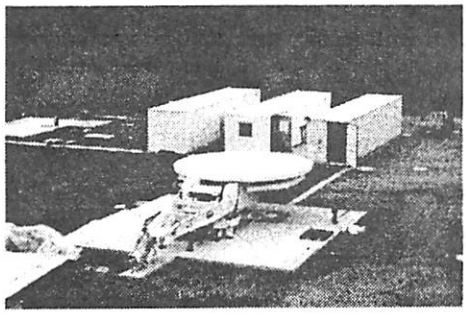

Figure 6: Side panels are mounted.

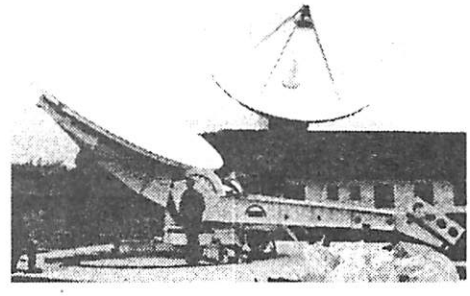

Figure 7: Move up the reflector.

All containers can be lifted from a truck trailer using mechanical lift tools.

The setup of the radiotelescope can be done by two experienced persons in less than a week and will be executed according to the following steps:

1. The transport container (weight: $25t$) will be setup close to the radiotelescope platform in order to keep distances for moving pieces as short as possible (Fig. 3).
2. The radiotelescope main part ($22t$) is slided out of the container on rails onto the platform. The radiotelescope will be fixed in the steel construction within the concrete (Fig. 3).
3. The transport container is shifted backwards to free the reflector (Fig. 4).
4. The operation container is setup to its destinated location (Fig. 2). The sidepanels of the reflector are taken out and are mounted to the main radiotelescope part (Fig. 5, 6).
5. The radiotelescope arm with the receiver is pulled out.
6. The cables between radiotelescope and operation container are connected.
7. The reflector is moved up to reach its operation position (Fig. 7), in which the receiver is in the focus. The reflector is fixed.
8. The final step is the horizontation of the radiotelescope.

4 Survey of the Radiotelescope

The survey was done for the final panel adjustment and to proof the meeting of the specifications. The results are presented in the following table:

Table 1: **Results of the survey of the TIGO 6m-offset-radiotelescope**

obliquity of azimuth axis (now compensated with dynamical horizontation)	3" @ 95-10-19 22" @ 96-05-03 due to consolidation of the fundament
excentricity of azimuth axis and reference bolt	0.1 mm (max.)
excentricity of azimuth and elevation axis	0.2 mm (max.)
perpendicularity of azimuth and elevation axis	13"
reflector surface RMS (normal)	0.09 mm @ 38° elevation 0.19 mm @ 0° elevation 0.16 mm @ 90° elevation
reproduction of reflector surface (unmount/mount sidepanels)	0.06 mm @ 38° elevation

Since the offset radiotelescope is unbalanced a preceding survey showed deformations depending on azimuth and elevation position. As a result of this survey the radiotelescope was equipped with two inclinometers which compensate the dehorizontation due to wind

and mass deformation in the azimuth part. The inclinometers are used for dynamical horizontation of the radiotelescope during operation.

The final results of the survey in Table 1 show that the TIGO radiotelescope will be a suitable geodetic tool for very long baseline interferometry. The accuracy of the intersection of the axis as geometrical reference point is within $1mm$.

5 S/X-Receiver

During July 1996 the NASA S/X cryogenic receiver was installed (Fig. 8). The performance of the receiving system is still under investigation, since a noise source at the powersupplies of the Wettzell Laser Ranging System (WLRS) (in $15m$ distance) was discovered. Since the delivery of the NASA Mk4 VLBI equipment is behind schedule some preliminary tests have been executed using the Mk3 equipment of the $20m$-radiotelescope at Wettzell. Very likely the noise of the powersupplies affected the performance tests. The test procedures to verify the specified efficiencies of better than 68% for X-band, respectively 64% for S-band are still going on.

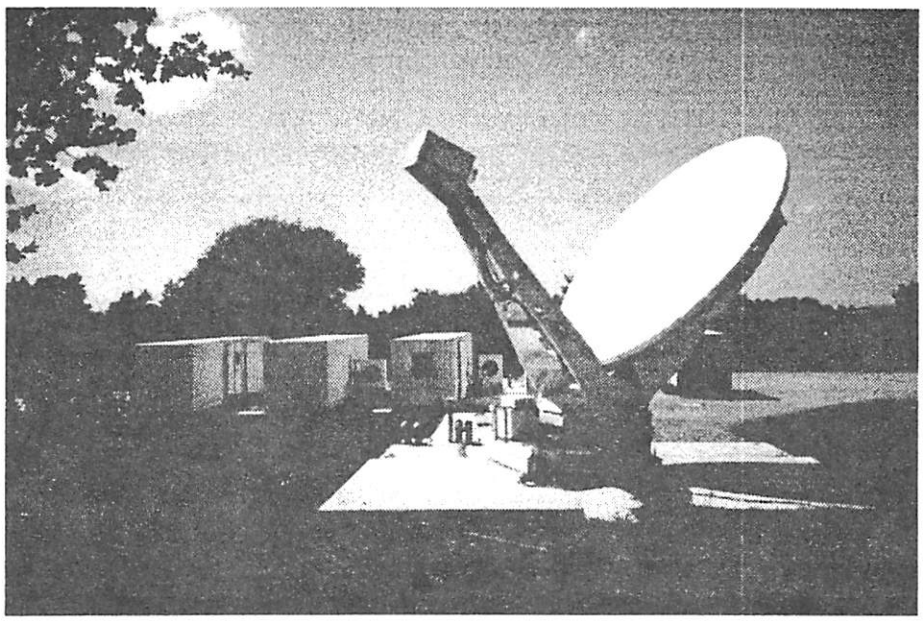

Figure 8: TIGO 6m-Offset-Radiotelescope with installed cryogenic S/X receiver in front of the TIGO operation containers.

6 Outlook

The TIGO VLBI-module becomes available for VLBI operations by the end of 1996 by using the existing Mk3 equipment of the $20m$-radiotelescope. As soon as NASA delivers TIGO's own Mk4 equipment Wettzell will have two VLBI telescopes operational, which

open a timely limited opportunity to make some experiences with cluster-to-cluster VLBI during 1997.

By the end of 1996 the delivery of the SLR-module to Wettzell is expected. During 1997 the integration of the basic module with different services as such as time and frequency, meteorology, communication etc. are necessary as well as extensive testing of the new fundamental station.

For the abroad use of TIGO it is necessary to define the prefered remote locations. Some considerations about possible locations can be found in [2], [4]. Contracts with a partner institution in the host country are of vital importance for TIGO in order to share the operation and achieving support for the required infrastructure.

References

[1] HASE, H.: **The Recent Status of the TIGO Project**, Proceedings of the 2nd EVN/JIVE Symposium Torun, October 21st, 1994

[2] HASE, H., SCHLÜTER, W., BÖER, A., DASSING, R., SPERBER, P., KILGER, R.: **Status of the TIGO Project**, Proceeding of the 4th Asia Pacific Telescope Workshop, December 4-7, 1995, CSIRO-ATNF, Sydney, (in print)

[3] IAG COMMISSION VIII - INTERNATIONAL COORDINATION OF SPACE TECHNIQUES FOR GEODESY AND GEODYNAMICS: **Status and Programme 1995-1999**, CSTG Bulletin No. 12, edited by Beutler, G., Drewes, H., Hornik, H., DGFI Abt. I, Munich, 1996

[4] SCHLÜTER, W., BÖER, A., DASSING, R., HASE, H., KILGER, R., SPERBER, P.: **Status of the TIGO Project**, Paper presented at IAG/CSTG working group on "IUGG Fundamental Reference and Calibration Network", Baltimore, May 20th, 1996

Geodetic Very-Long-Baseline Interferometry at the Onsala Space Observatory 1995–1996

G. Elgered
Onsala Space Observatory
Chalmers University of Technology
S–439 92 Onsala, Sweden

Abstract. We summarize the performed and planned geodesy VLBI activities at the Onsala Space Observatory for the period 1995–1996. A total of 26 experiments were carried out during 1995 and 15 experiments are planned for 1996. The VLBI data acquisition system has been partly upgraded to Mark-IV standards and the Field System software is since February 1996 running under the LINUX operating system. Development of a new S/X-band feed system resulting in an improved efficiency and dual polarizations has started and the status of this project is described. A measurement system for continuous monitoring of the height of the concrete foundation of the 20 m telescope is described briefly. The first two months of data show a clear correlation between temperature and height.

1. VLBI Observations

The Onsala 20 m antenna participates regularly in the experiments of the European network including the antennas at Noto, Matera, Medicina, Madrid, Wettzell, Crimea, Yebes, and Ny Ålesund. As usual also the Effelsberg antenna is included once per year. Six experiments were carried out during 1995; and another six experiments are planned for 1996. Other networks with Onsala participation have been a few "Global Terrestrial Reference Frame" (GTRF) experiments and the CONT–95 experiment. The latter consisting of six days of continuous geodesy VLBI in August 1995. A similar campaign, called CONT–96 V, involving the VLBA array in the US plus the Medicina and the Onsala stations in Europe, is planned for the beginning of November 1996.

2. Technical Developments During 1995–1996

The S- and X-band feed

An additional improvement of the sensitivity within the next couple of years is being investigated. A study aiming for new feed systems for all receivers used in the 20-m telescope is underway. The present feed uses a tertiary reflector for S-band which is equipped with a dichroic surface with a low transmission loss at X-band [*Jaldehag et al.*, 1993]. The planned new feed system consists of two feed reflectors for both the S- and the X-band. The principle of such a feed system is shown in Figure 1. The feed reflectors are illuminated by a dual-frequency-band horn. The horn will have aperture controlled beam widths in order to achieve the goal of a similar illumination of the subreflector (and hence also the primary reflector) at the two frequency bands. A prototype horn has been designed and manufactured (see Figure 2). Work is now going on to optimize the system for maximum efficiency. The plan is also to implement both the right and the left circular polarization at the two frequency bands.

Presented at the 11th Working Meeting on European VLBI for Geodesy and Astrometry, Onsala, Sweden, 1996

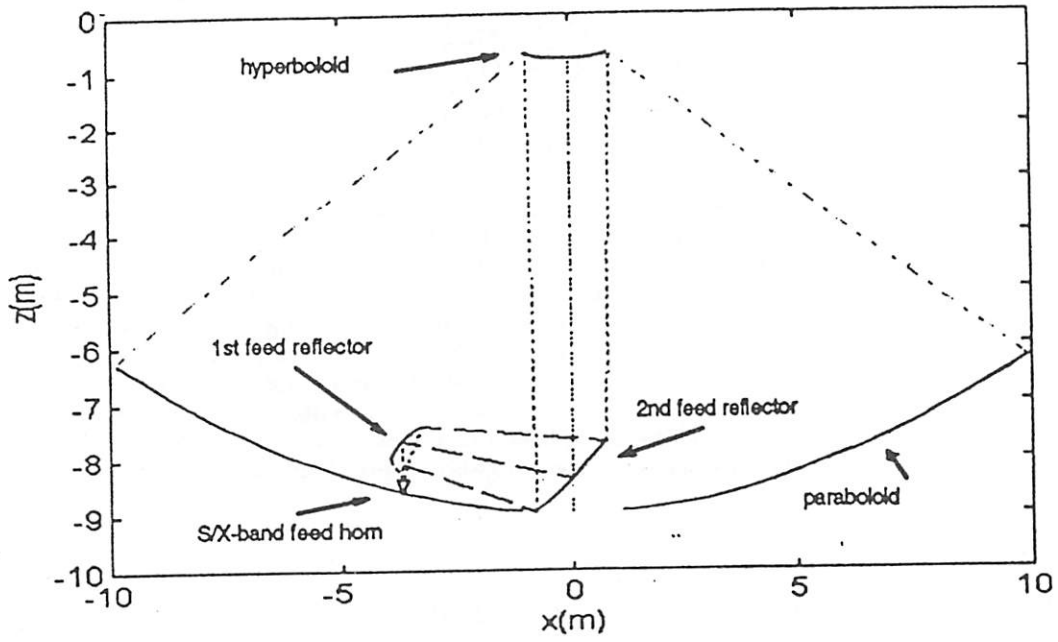

Figure 1. A possible feed horn and reflector geometry of the future S/X-band system in the 20 m telescope (from *Rubiñoz-López et al.* [1996]).

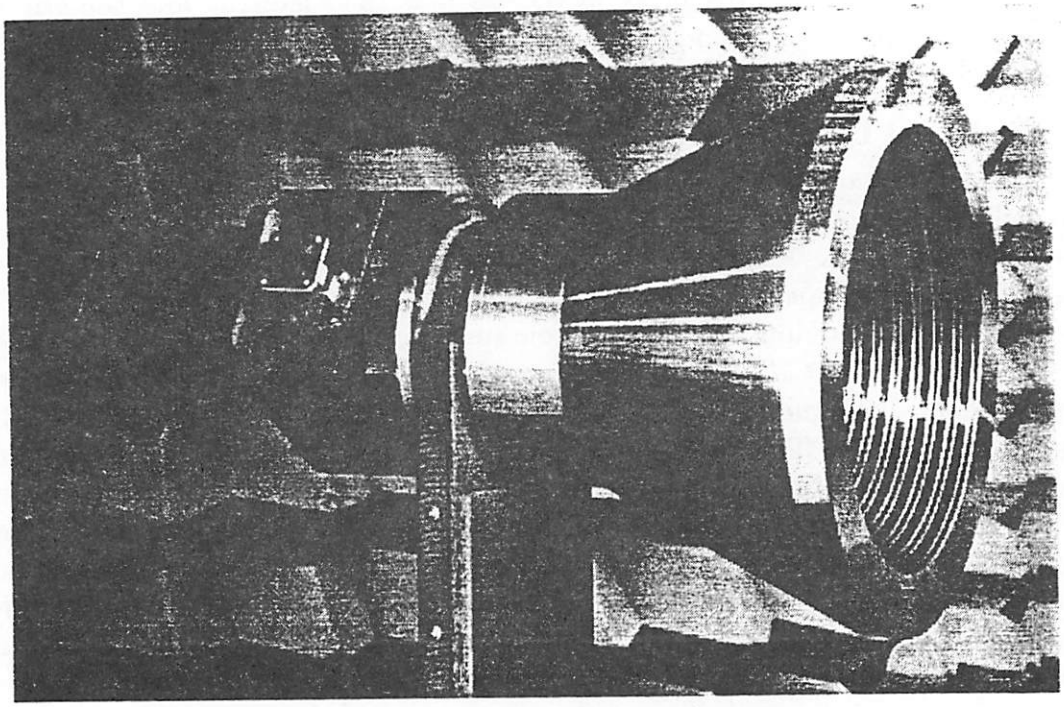

Figure 2. The prototype dual-frequency (S and X) feed horn (from *Flodin* [1995]).

Mark-IV upgrade
The upgrade to the Mark-IV system is carried out within the schedule of the Joint Institute for VLBI in Europe (JIVE). The video converters were upgraded in September 1995 and the mechanical part of the tape recorder upgrade was carried out in October 1995. The remaining part of the tape recorder upgrade and the Mark-IV formatter is planned to be installed in November–December 1996.

PC Field System
The only major change of the VLBI data acquisition system during the last year is that the Field System software is since February 1996 running under the LINUX operating system.

Station time monitoring
Station time was earlier monitored through the GPS Turbo-Rogue receiver used at the Onsala IGS site. Starting in September 1995 we have a continuous comparison between station time and GPS time using the "Totally Accurate Clock" (TAC). A PC data acquisition system reads and archives the time difference between the 1 pps signals from the station clock (driven by the H-maser EFOS–7) and the TAC every 30 seconds. Data are saved on hard disks for easy access but tape backups are also made regularly.

The station time was less accurate over the shorter time scales during the period from June 24 to September 7, 1996, when the H-maser was send for maintenance service. The station clock was then controlled by a Cesium frequency standard lend to us by the Swedish National Testing and Research Institute.

Measurements of the stability of the antenna tower
A PC-based system for monitoring of the temperature of the concrete tower of the 20-m antenna was described at last year's meeting in Matera [*Elgered and Carlsson*, 1995]. The temperature data logging started in December of 1994 and is continuously archived as 5 minute averages of the temperature measured at 20 locations in, on, and around, the foundation.

Starting in late June 1996 we are also measuring and archiving the vertical motions of the concrete tower. The measurement principle is shown in Figure 3. A reference point on the steel plate is brought down to the ground by using an invar rod. Using the fact that the temperature coefficient of invar is a magnitude smaller than that of concrete (and steel) it is possible to measure the vertical motion of the top of the tower relative to the ground. A detailed description of the system has been written by *Johansson et al.* [1996].

Figure 4 presents a summary of the data acquired from the end of June to the end of August 1996. The observed vertical motion of the invar rod is shown as a function of the arithmetic mean of the sixteen measured temperatures (see Figure 3). Assuming that this mean is a representative effective value of the concrete we can use these data to estimate the temperature coefficient of the concrete. Using the data in Figure 4 we obtain an observed average sensitivity of 0.082 mm·(°C)$^{-1}$. The temperature coefficient of the invar rod is specified to $1.5 \cdot 10^{-6}$ (°C)$^{-1}$. We can correct the observed motions for this expansion and a few other, less important, effects by increasing the observed motion with

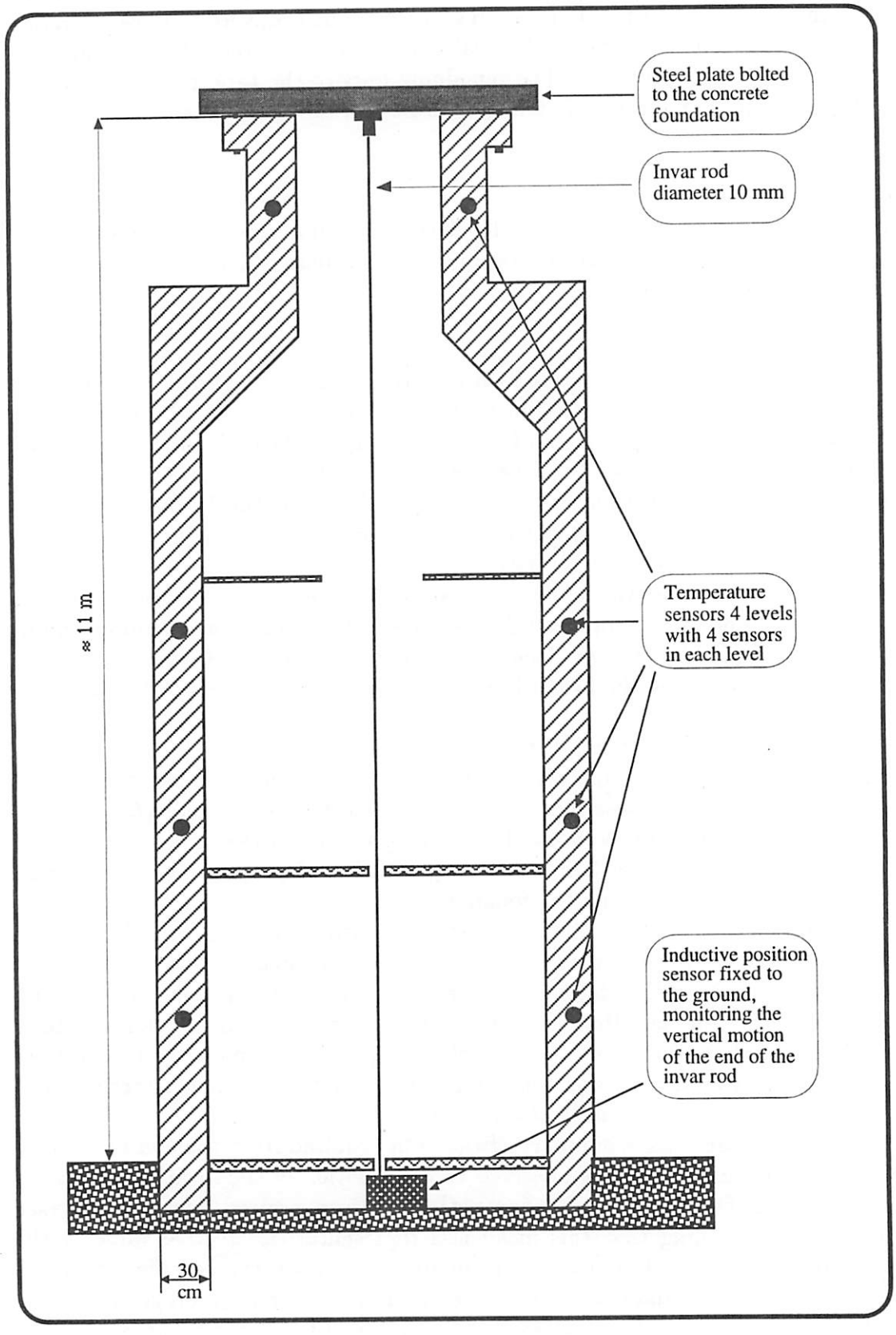

Figure 3. An overview of the monitoring of temperature and vertical movements of the concrete foundation of the 20 m antenna.

0.022 mm·(°C)$^{-1}$ in order to estimate the motion of the top of the foundation relative to the ground [*Johansson et al.*, 1996]. Assuming that the invar rod and the concrete is exposed to the same temperature variation we can make an experimental estimation of the temperature coefficient of the concrete foundation

$$\alpha_{exp} = \frac{(0.082 + 0.022) \cdot 10^{-3}}{11.3} = 0.009 \cdot 10^{-3} \quad [(°C)^{-1}]$$

This is slightly less than the expected value for dry concrete which is $12 \cdot 10^{-6}$ $(°C)^{-1}$. A possible explanation for the disagreement can simply be that the temperature sensors are not located correctly in order to yield a mean which is the effective temperature of the concrete. For example, there are no sensors located close to the ground where the temperature variations may be significantly smaller. Furthermore, the temperature of the invar rod is not presently measured but it is likely that these variations are larger than are the variations of the concrete. If such an effect is taken into account it would imply an increased value of the temperature coefficient. Another reason can be that the sensors are not well enough insulated from the outside air which would result in an observed temperature variation which is larger than that of the effective temperature of the concrete. An improved insulation of the sensors and monitoring of the invar rod temperature is being implemented right now and as more data become available the effect will probably be better understood.

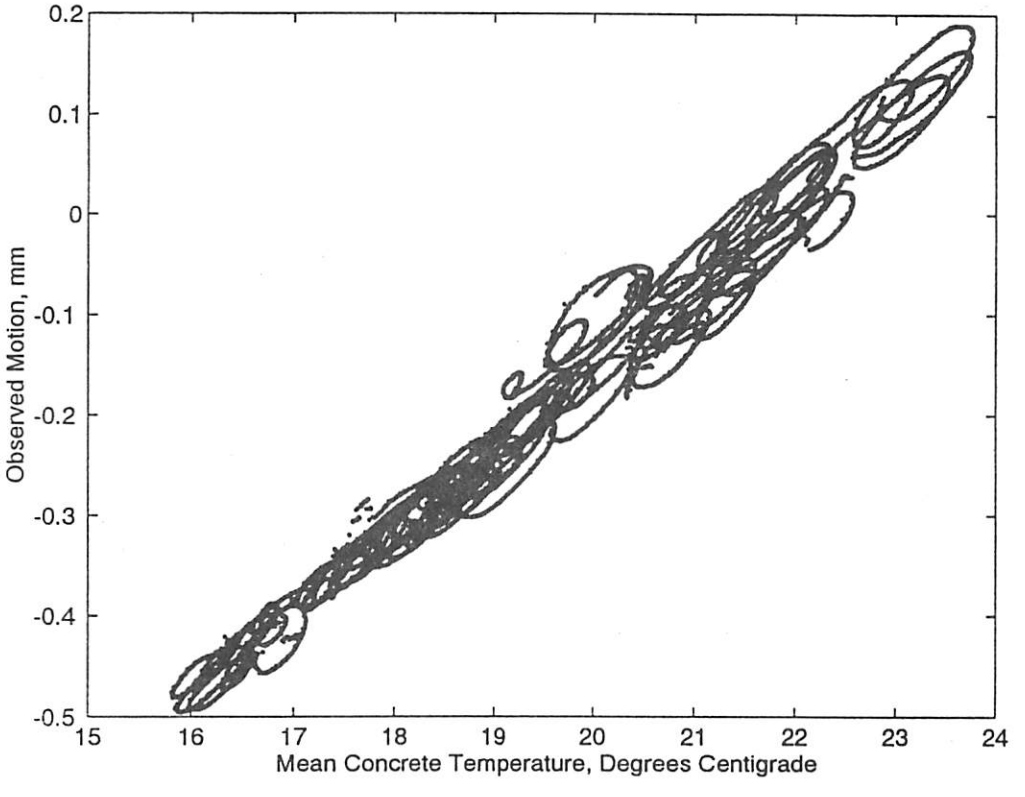

Figure 4. The data acquired so far of the vertical motion of the top of the foundation clearly show a strong correlation with the measured concrete temperature. The plotted data have not been corrected for any expansion of the invar rod (see text.)

The most important conclusion, however, is that the position measurements of the invar rod validates previous results based on temperature measurements only [*Elgered and Carlsson*, 1995; *Carlsson*, 1996]. The vertical motions of the concrete tower of the 20 m antenna can be modelled with sub-millimeter accuracy. Daily variations observed so far are much less than 1 mm. Given the present demonstrated accuracy of geodetic VLBI such an effect can be ignored. (See for example the results from the two week long CONT–94 experiment [*MacMillan*, 1995; *Carlsson et al.*, 1995].) An estimate of the maximum yearly variation is approximately 4 mm because the concrete temperature typically varies from -10°C for the coldest winter day to +30°C for the warmest day in summer. This remains to be verified by the measurements of the invar rod.

3. Other Activities Related to Geodetic VLBI

GPS applications

Onsala is a station in the "International GPS Service for Geodynamics (IGS)" meaning for example that a GPS receiver is operating at the site in a continuous mode. The first receiver was installed in December 1986. The present Turbo-Rogue receiver has been in operation since April 14, 1993.

GPS observations have been carried out on the observatory grounds during the summer of 1996 in order to monitor the local "footprint" around the VLBI antenna. The SWEPOS GPS network (established within Sweden together with the Swedish National Land Survey) is used to study the postglacial rebound in Fennoscandia [*Bifrost Project*, 1996]. It is of course also correct to view the entire SWEPOS network as a footprint which can be used to secure the VLBI reference point at the Onsala site through the densification and maintenance of a regional reference system based on the daily analysis of data from the GPS network.

Studies of the atmospheric propagation delay

The atmospheric influence on radio wave propagation delay has been studied using data from VLBI, the Global Positioning System (GPS), and microwave radiometry. The major applications being characterization of temporal and spatial variability of atmospheric water vapor and the validation of wet delay estimates using VLBI or GPS data. Results from this work are found in *Jarlemark and Carlsson*, [1996] and *Carlsson et al.* [1996] (both in this volume).

References

BIFROST Project (some 26 co-authors), GPS Measurements to Constrain Geodynamic Processes in Fennoscandia, *Eos Trans. AGU*, **77**, No. 35, 337–341, August 27, 1996.

Carlsson, T.R., Site Dependent Error Sources in Geodetic Very-Long-Baseline Interferometry, *Tech. Rept. No. 224L*, School of Electrical and Computer Engineering, Chalmers Univ. Tech., 1996.

Carlsson, R.T., G. Elgered, and J.M. Johansson, External wet tropospheric corrections in a two week long VLBI campaign, *Proc. 10th Working Meeting on European VLBI for Geodesy and Astrometry*, Eds. R. Lanotte and G. Bianco, Centro di Geodesia Spaziale, Matera, Italy, pp. 148–153, 1995.

Carlsson, T.R., G. Elgered, and J.M. Johansson, A Quality Assessment of the Wet Path Delay Estimated From GPS Data, *Proc. of the 11th Working Meeting on European VLBI for*

Geodesy and Astrometry, Research Report 177 (this volume), Ed. G. Elgered, Onsala Space Observatory, Chalmers University of Technology, 1996.

Elgered, G., and R.T. Carlsson, Temperature Stability of the Onsala 20-m Antenna and Its Impact on Geodetic VLBI, *Proc. 10th Working Meeting on European VLBI for Geodesy and Astrometry*, Eds. R. Lanotte and G. Bianco, Centro di Geodesia Spaziale, Matera, Italy, pp. 69–78, 1995.

Flodin, J., Design of an S/X Band Corrugated Horn Feeding the Onsala Radio Telescope via a Reflector System, *Master Thesis*, Department of Microwave Technology, Chalmers University of Technology, 1995.

Jaldehag, R.T.K., P.-S. Kildal, and B.O. Rönnäng, Dual Band Reflector Feed Systems for Classical Cassegrain Radio Telescopes, *IEEE Trans. Antennas Propagat.*, **AP-41**, 325–332, 1993.

Jarlemark, P.O.J., and T.R. Carlsson, Strategies For Spatial and Temporal Extrapolation and Interpolation of Wet Path Delay, *Proc. of the 11th Working Meeting on European VLBI for Geodesy and Astrometry, Research Report 177 (this volume)*, Ed. G. Elgered, Onsala Space Observatory, Chalmers University of Technology, 1996.

Johansson, L.-Å., F. Stodne, and S. Wolf, The PISA Project: Variations in the Height of the Foundation of the 20 Meter Radio Telescope, *Research Report 178*, Onsala Space Observatory, Chalmers University of Technology, 1996.

MacMillan, D.S., Atmospheric Gradients from Very-Long-Baseline Interferometry Observations, *Geophys. Res. Lett.*, **22**, 1041–1044, 1995.

Rubiños-López, J.Ó., P.-S. Kildal, J. Flodin, and G. Elgered, S/X-Band Beam Waveguide for the Onsala Radio Telescope, presented at IEEE International Symposium on Antennas and Propagation 1996, Baltimore, MD, Proceedings, July 21–26 1996.

A NEW S/X RECEIVER FOR NOTO ANTENNA

G. Tuccari[1], A. Orfei[2], V. Tornatore[1,3]

1. Istituto di Radiostronomia del CNR - Stazione di Noto
2. Istituto di Radiostronomia del CNR - Stazione di Medicina
3. DIIAR, Politecnico di Milano

Abstract

At present Noto station uses a not cooled S/X receiver for VLBI geodetic and astronomical observations. Its dimension and weight force a long job to mount it on the primary focus of the parabola.
To improve antenna flexibility in terms of frequency agility and to get better features a new cooled receiver will be built that will include the L (18 and 21 cm) and P (92 cm) bands. The receivers will be permanently placed on the primary focus and interchanged with the subreflector by installing the mechanical solution developed in Medicina.
This document presents the architectural project for such a receiver system, pointing out the new features we expect from its implementation.
In order to simplify the front-end receiver complexity and to optimize the signal transfer the possibility to adopt fiber optic technology is considered.

Presented at the 11th Working Meeting on European VLBI for Geodesy and Astrometry, Onsala, Sweden, 1996

1. Project for a multifrequency receiver.

This document presents the preliminary considerations regarding a new receiver to be used in the Noto antenna. The receiver will be placed in the primary focus in fixed position. A great improvement is expected in terms of antenna flexibility because a new system will be adopted as developed for the Medicina antenna. Such a system allows to move the subreflector in two positions: either in the antenna focus where it acts as secondary mirror or kept apart in order to leave in the focus the multifrequency receiver. As it was said this is in strong contrast with the present condition where either the subreflector or the receiver are placed in the primary focus of the parabola. The operation at present is performed manually and it involves for about 2 hours three people.

The receiver includes as much bands as possible considering the relatively small available space, that are: S/X, L (18 cm, 21 cm) and P (92 cm). The new system needs to have improved features with respect to the present condition. In the following tables a comparison between the present situation and the new goals is shown.

Present features

Band	Cooled	Hemt	Polarisation	Tsys (K)	Bandwidth (MHz)
P	Not	Yes	L & R	150/150	50
L	Not	Yes	L & R	70/70	80+80
S	Not	Not	R	150	160
X	Not	Not	R	130	400

New receiver features

Band	Cooled	Hemt	Polarisation	Tsys (K)	Bandwidth (MHz)
P	Not	Yes	L & R	<150/<150	50
L	Yes	Yes	L & R	<30/<30	80+80
S	Yes	Yes	L & R	<50	230
X	Yes	Yes	L & R	<50	800

Improvements regard the S/X bandwidth extension and the sensitivity for all the bands.

2. Architectural view.

Two schematic drawings show possible configurations for the multifrequency receiver. The difference between them regards the way to transfer the signals. In the more traditional version coaxial cables are used to transfer the intermediate frequency between the receiver placed in the primary focus and the antenna control room where the data acquisition rack is placed. The second schematic view shows the configuration to transfer the sky frequency directly to the control room. Such a solution uses single mode optical fibers and represent a not usual solution.

The feeds to be used are not yet chosen, but several possibility are under evaluation. Such feeds will be placed in the antenna focus using rotating or translating actuators. Restrictions are due to the available dimensions. The first schematic is self-explanatory and few points need to be described. Signals carrying left and right circular polarisation are injected in the cooled dewar where the hemt based front-end amplifiers operate at 20 K. After band limitation and amplification sky signals are down-converted making use of mixers and dedicated local oscillators. Three PLL are in general necessary if used at fixed frequency, but one fixed and one programmable can be adopted considering that only S and X band are simultaneously used. A matrix of coaxial switches is used to select the bands to be transferred to the data acquisition terminal. The possible configuration are SR/XR for geodetic observations, SL/SR, XL/XR,LL/LR,PL/PR for astronomic observations.

The second schematic drawing shows as the sky signals are directly transferred without any conversion.

The receiver itself is split in two sections, one operating in the prime focus, the second in the control room. This solution is made possible using a 10 GHz transceiver for optical fibers. Whether L band is used the two circular polarisation are injected in two identical transceivers, if S/X is selected both polarisation are injected for the two bands in the two transceivers. P band signals are transferred using traditional coaxial cables in both the circular polarisations.

The second solution presents the following advantages: the antenna section of the receiver is strongly simplified because no conversion is realised in that. On the other hand no local oscillator is needed for such a function. Less components mean more space available and great simplification in terms of maintenance. In the control room as local oscillators could also be used a commercial synthesiser with consequent system simplification.

The operative design for the multifrequency receiver is expected to start with the beginning of the next year and the final realisation to be completed before the end of 1998.

Bibliography

S. D. White, Hawaii S and X Receiver System, NRAO EDIR n.294, Green Bank, April 1994.

G. H. Tan, Report Feasibility Study Multi Frequency Front End, NFRA note 555, Dwingeloo, March 1990.

S. D. White, 20 Meter S/X Receiver, NRAO EDIR n.299, Green Bank, April 1995.

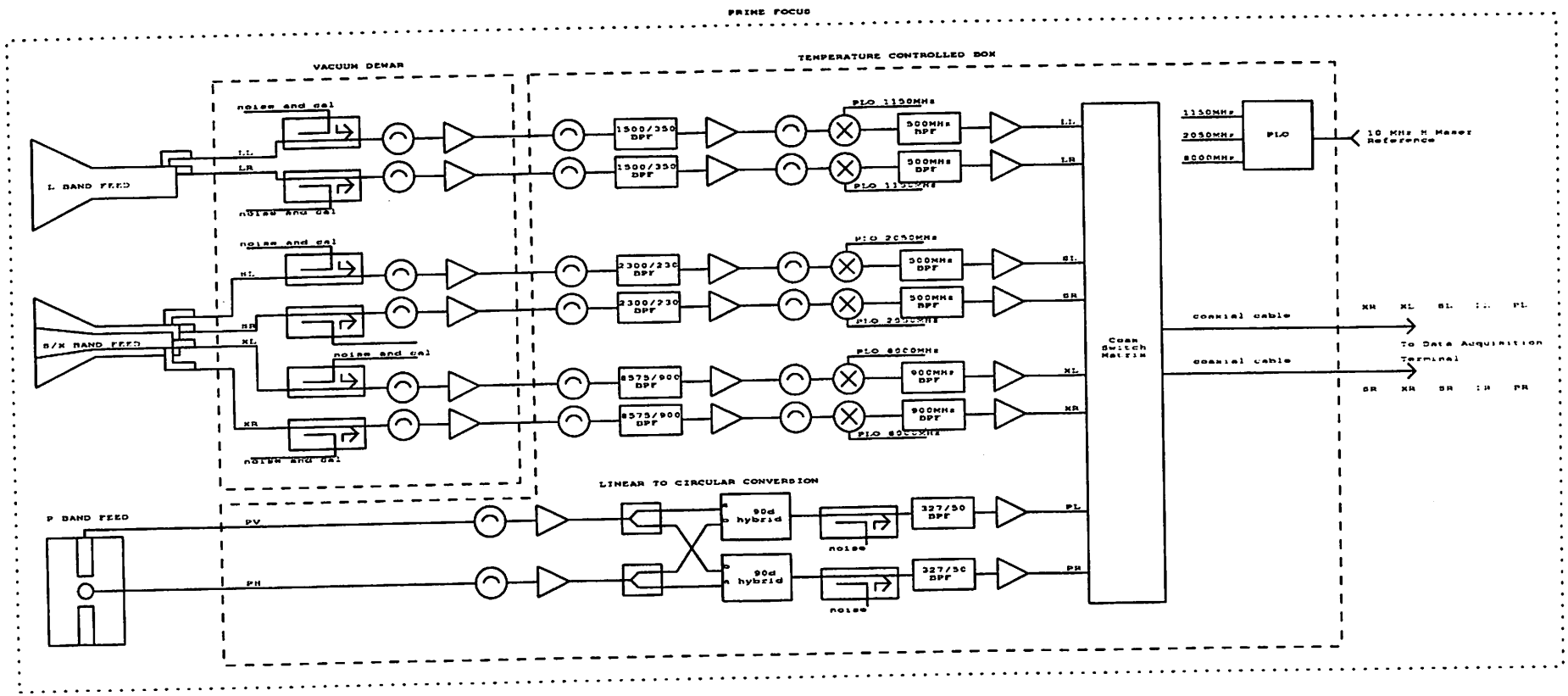

CNR	ISTITUTO DI RADIOASTRONOMIA Stazione di Noto	
	S/X/L/P Receiver Schematic View Coaxial Cable Link Option	
	Rev: 1.2	Drawn by: G. Tuccari — Date: July 28,1994

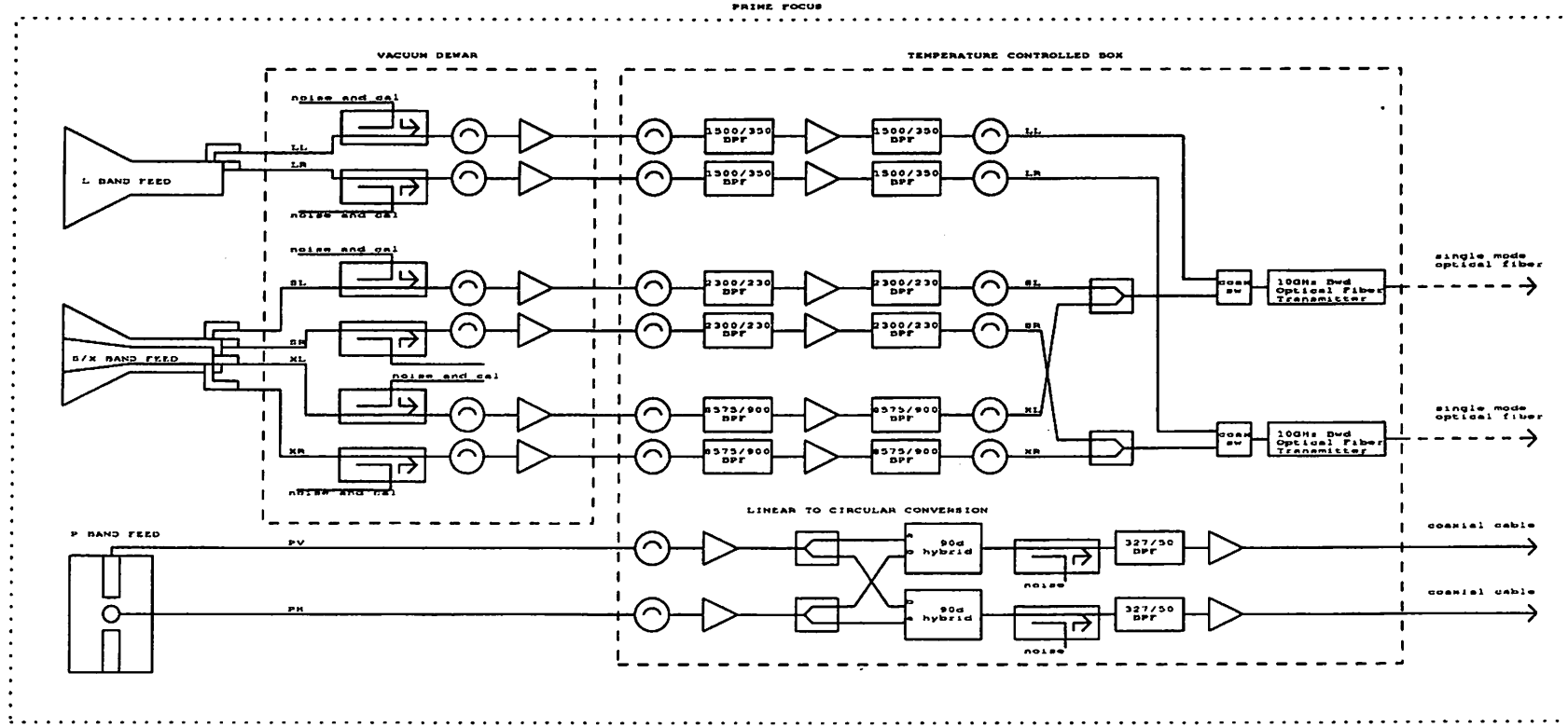

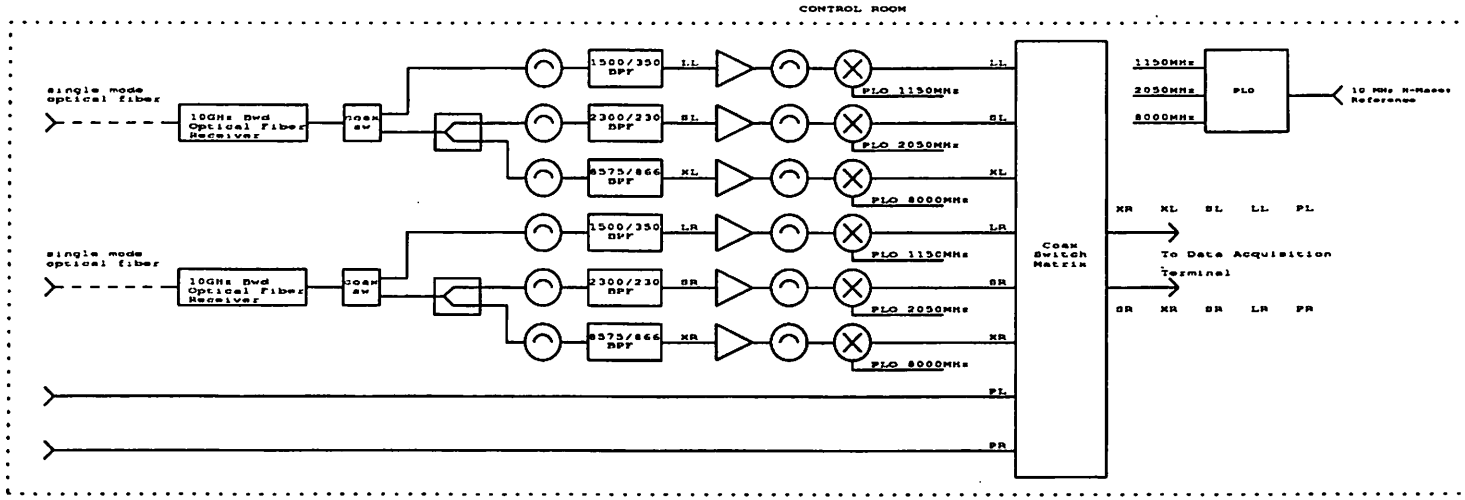

CNR	ISTITUTO DI RADIOASTRONOMIA Stazione di Noto
	S/X/L/P Receiver Schematic View Optical Fiber Link Option
	Rev: 0.2 Drawn by: Date: May 28,1997

Time Transfer with VLBI Better Than 1ns Accuracy *

HAYO HASE
Institut für Angewandte Geodäsie
Fundamentalstation Wettzell
D-93444 Kötzting

TAIZOH YOSHINO, SHIN'ICHI HAMA, HITOSHI KIUCHI,
AKIHIRO KANEKO, YUKIO TAKAHASHI
Communications Research Laboratory
Koganei, Tokyo

RICHARD KILGER
Forschungseinrichtung Satellitengeodäsie
Fundamentalstation Wettzell
D-93444 Kötzting

Abstract

The Very Long Baseline Interferometry (VLBI) is widely used in geodesy for the determination of Earth rotation parameters, station coordinates, baseline lengths all with respect to their rate. It is also possible to use VLBI for the absolute synchronization of the time standards at both ends of one baseline, if the instrumental delay of the antenna is known, which can be determined by using Short Baseline Interferometry (SBI). A Japanese-German project has the aim to demonstrate that accuracies better than $1ns$ for the intercontinental time transfer can be achieved with VLBI and SBI. For the maintenance of precise reference frames in space time accurate time transfers are indispensible.

1 Time Comparisons

National time keeping institutions have the task to distribute the time derived from atomic frequency standards as such as cesium clocks. The continued comparison of different time standards is performed by the Bureau International des Poids et Mesures (BIPM) in Paris [1],[2]. For the comparison of the time standards the globally available GPS-time which is refered to USNO cesium clocks is used as reference time. The accuracy of this time-transfer method is generally better than $200ns$ [4] and is at about $20ns$ (Wettzell-USNO) and about

*presented at 11th Working Meeting on European VLBI for Geodesy and Astrometry, Onsala, August 23-24, 1996

$5ns$ (Wettzell-PTB Braunschweig[1]) applying the common-view technique. If the selective availability (SA) [7] degrades the ephemeris, then the RMS for the time transfer is 3-4 times worse.

Besides the Time Transfer with GPS the first attempts of time comparison with VLBI have been carried out in 1977 [3]. An improved experiment was carried out in a Japanese-American cooperation in 1986/87 between Kashima and Richmond using a Zero Baseline Interferometry (ZBI) technique. The achieved accuracy was better than $1ns$ [5]. Currently a new attempt based on Short Baseline Interferometry is conducted between the $20m$ radiotelescope at Wettzell and the $11m$ antenna of the Keystone Project at Koganei in Tokyo.

For the establishment of a high accurate global reference frame in spacetime, the tie of local reference stations - defining individual local systems in spacetime - through a precise spacetime baseline vector is evident. The local clocks provides the local proper time scales, which are in general offset to each other and which differ in their rates due to being non-identical and due to the difference in the geopotential at the clock sites.

For the synchronization two different proper time scales τ needs to be reduced as if they were located on the geoid [8]. The reduced proper time τ^* at mean sea level is obtained by:

$$\frac{d\tau}{d\tau^*} \simeq 1 - \frac{(U - U_{geoid})}{c^2} \simeq (1 + \frac{gh}{c^2}) \quad (1)$$

where U is the geopotential, g is the gravitational acceleration, h is the height above geoid. Reduced proper times τ^* can be identified with TAI which is offset by a constant from TDT.

$$\mathrm{TDT} = \mathrm{TAI} + 32.184s = \tau^* + 32.184s \quad (2)$$

A time transfer needs to provide the offset and its rate of different proper times τ^*.

Very Long Baseline Interferometry technique is able to contribute the clock offsets and rates, if the instrumental delays of the radiotelescopes are well calibrated. Consequently it becomes possible to express a simultaneous "here-now" for the world-lines of both VLBI stations after the VLBI experiment. When real-time VLBI will become effective, a continous on-line determination of the offsets of the time standards will be possible.

2 Delays in VLBI

The primary observable in VLBI is the group delay τ and is equal to the correlated delay. It contains different delays:

1. τ_g, the geometrical delay due to the geometrical situation of the two antennas with respect to the radio source. The configuration of the interferometer is known apriori.
2. τ_p, the propagation delay due to the non-vacuum conditions in the atmosphere. The atmospheric conditions are modelled based on recorded meteorological data.

[1]The Physikalische Technische Bundesanstalt in Braunschweig is by law the responsible time keeping institution in Germany.

3. τ_c, the clock delay is the clock offset between the station clocks. The clock offset is known on μs-level apriori for the correlation.

4. τ_i, the instrumental delay which consists of

   (a) τ_{ant}, the antenna delay due to the multipath in the dish until the phasecal injection point, which depends on the antenna geometry and deformation,

   (b) τ_{srd}, the delay between the step recovery diode for the phasecal generation and the phasecal injection point, which is almost constant,

   (c) τ_{cab}, the delay due to cable-length between the front and back end, which is highly temperature dependent,

   is considered only as far as it concerns τ_{cab} in the data reduction.

It follows the VLBI observation equation expressed in terms of delays:

$$\tau = \tau_g + \tau_p + \tau_c + \tau_i \quad (3)$$

$$\tau_i = \tau_{ant} + \tau_{srd} + \tau_{cab} \quad (4)$$

Each VLBI system itself is affected by these different delay types and hence the interferometer of two systems is affected by the difference of those delays.

The VLBI observation equation (3) is a linear function. The VLBI software packages e.g. CALC/SOLVE, do not support a parameter for τ_i. Assuming that τ_{cab} is applied, the other two contributions of τ_i, namely τ_{srd} and τ_{ant} disappear in the estimated parameters for the clocks τ_c and for the atmosphere τ_p, without any effect on the baseline estimates.

For time transfer with VLBI we need to know τ_c without contributions from the instrumental delay. Therefore time transfer experiments with VLBI focus on the determination of the instrumental delay τ_i in the interferometer. From (3) follows the equation for the true clock offset determination:

$$\tau_c = \tau - \tau_g - \tau_p - \tau_i \quad (5)$$

The instrumental delay τ_i corresponds generally to the time delay due to the distance in time between the phasecal injection point and the geometrical reference point, which is usually the intersection of the telescope azimuth and elevation axis and hence the fixed point independent of the slewing of the antenna. τ_i includes therefore the multipath due to the reflections in the dish; (see fig. 1).

3 Determination of the Instrumental Delay τ_i

The instrumental delay at a single dish cannot be determined directly, since the wave propagation in the dish, in the feed and through the waveguides passing the phase calibration signal injection point until the step recovery diode as phasecal generator remains due to the lack of measure points indeterminable. Even if a different antenna design would allow such a measurement, the accuracy of it would be less than using a differential method. Therefore

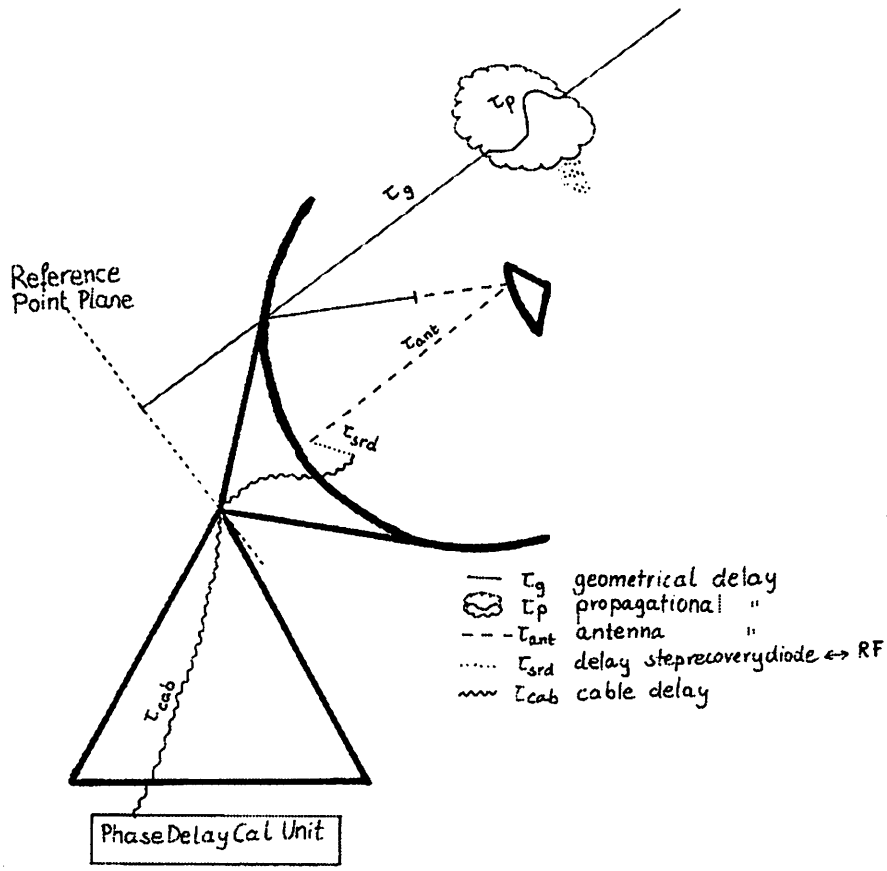

Figure 1: Delays due to propagation in the atmosphere, due to multipath, due to the distance step recovery diode - phasecal injection point and due to cablelength at a VLBI station.

the prefered method of the determination of the instrumental delay τ_i is a *double differential method* involving a transportable reference antenna.

The reference antenna can be mounted on the backside of the subreflector of the main antenna, which leads to the Zero Baseline Interferometry (ZBI) experiment [5]. Another possibility is to locate the reference antenna near by the main antenna and determine the short baseline vector between both geometrical reference point with a local survey. This vector can be transformed into a geometrical delay τ_g and applied to a Short Baseline Interferometry (SBI) experiment.

The time transfer experiment consists of three sub-experiments:

1. Determination of the instrumental delay between VLBI-antenna and the reference antenna at site 2, e.g. Wettzell, with a SBI experiment. From (3) follows (index ^{2r} denotes the differential delay between site 2 and the reference antenna)

$$\tau^{2r} = \tau_g^{2r} + \tau_p^{2r} + \tau_c^{2r} + \tau_i^{2r} \quad (6)$$

$$\tau^{2r} = \tau_g^{2r} + 0 + 0 + \tau_i^{2r} \quad (7)$$

$$\tau_i^{2r} = \tau^{2r} - \tau_g^{2r} \quad (8)$$

because the antennas refer to the same clock and the atmospheric conditions can be assumed to be identical. The geometrical delay is determined by the local survey, therefore only τ_i remains as unknown. It represents the differential instrumental delay between the main and the reference antenna.

2. Determination of the instrumental delay between VLBI-antenna and the reference antenna at site 1, e.g. Koganei, with a second SBI experiment. According to (3) and (6) follows:

$$\tau^{1r} = \tau_g^{1r} + \tau_p^{1r} + \tau_c^{1r} + \tau_i^{1r} \quad (9)$$

$$\tau^{1r} = \tau_g^{1r} + 0 + 0 + \tau_i^{1r} \quad (10)$$

$$\tau_i^{1r} = \tau^{1r} - \tau_g^{1r} \quad (11)$$

3. Applying the apriori derived instrumental delay from the previous SBI-experiments (8) and (11) which is for both main antennas:

$$\tau_i^{2r} = \tau_i^2 - \tau_i^r \quad (12)$$

$$\tau_i^{1r} = \tau_i^1 - \tau_i^r \quad (13)$$

$$\tau^{21} = (\tau_i^2 - \tau_i^r) - (\tau_i^1 - \tau_i^r) \quad (14)$$

$$= \tau_i^2 - \tau_i^1 \quad (15)$$

In a VLBI experiment between the station 1 and 2, e.g. Wettzell and Koganei, the in (14) determined instrumental delay between both antennas τ_i^{21} can be applied to (5). With accompanying careful measurements of cable lengths in the local time distribution system it is possible to determine the offset between both master clocks on a sub-nanosecond level.

4 Realization of SBI-Experiment at Wettzell

The Space Geodesy Section of CRL, Tokyo, provided the $1.2m$ reference antenna together with a complete K-4 VLBI terminal [6]. For compatibility reason an additional K-4 VLBI Input-Interface and a K-4 tape recorder (both Sony components) have been connected to the analog monitor outputs of the MkIII video converters of the $20m$ radiotelescope of Wettzell.

The short baseline between the main antenna and the reference antenna is about $25.20m$, hence the ionospheric and atmospheric disturbations are assumed to be identical for both antennas (see (7), (10)). Therefore the reference antenna needs only X-band capabilities and SBI-experiment is carried out accordingly.

According to fig. 4 the synchronization of both antennas is possible by using the same frequency standard. The K-4 system uses as reference frequency $10MHz$, the MkIII system uses $5MHz$. The $10MHz$ were derived from the $5MHz$ standard.

Another difference between an ordinary VLBI and a SBI experiment is, that in the latter the geometrical delay is almost zero. Therefore, undesired correlation of the two phasecal signals must be avoided. In order to prevent the correlation of the phasecal signal, the reference frequency of $10MHz$ in the K-4 system of the reference antenna is artificily offset by $-10Hz$ to $9.999990MHz$.

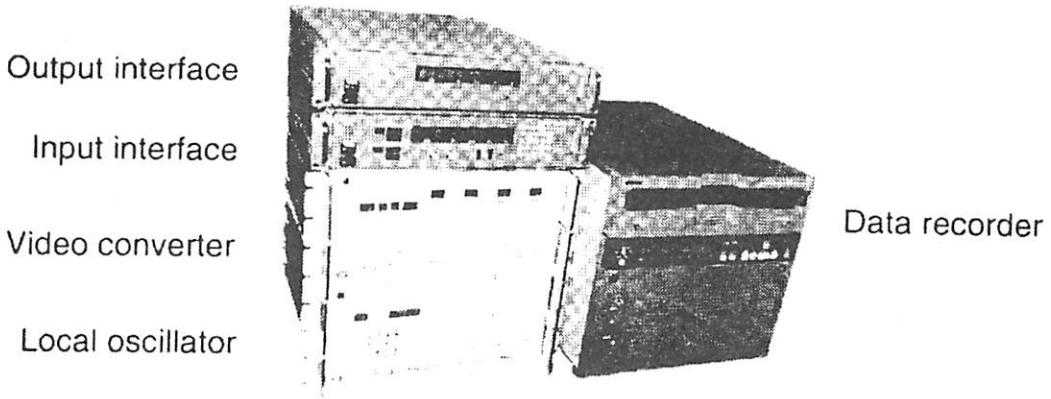

Figure 2: The complete K-4 system.

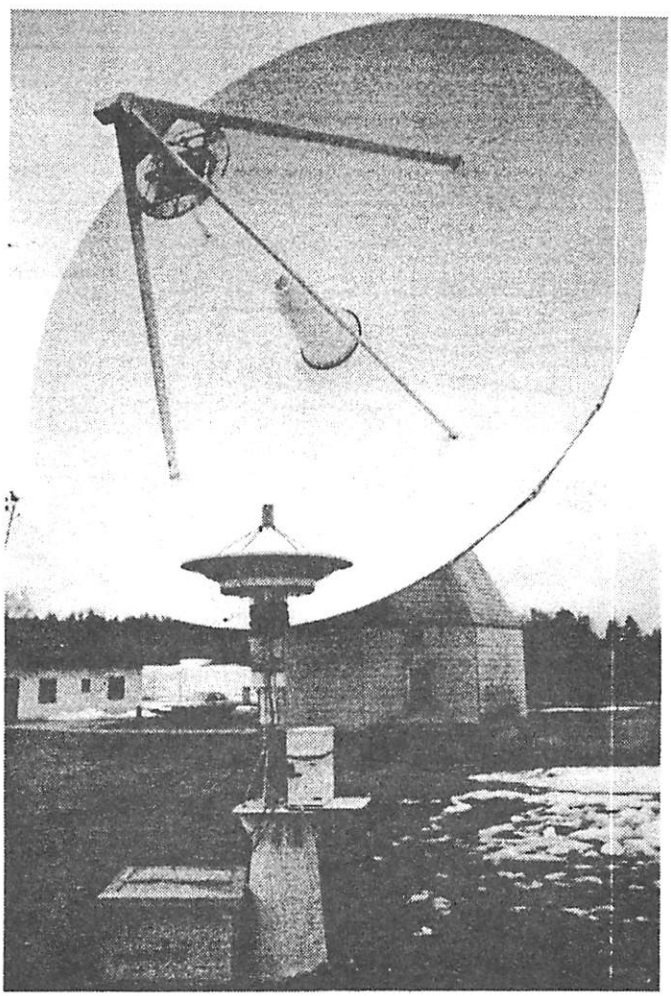

Figure 3: The 1.2m reference antenna and the 20m antenna for the SBI experiment at Wettzell.

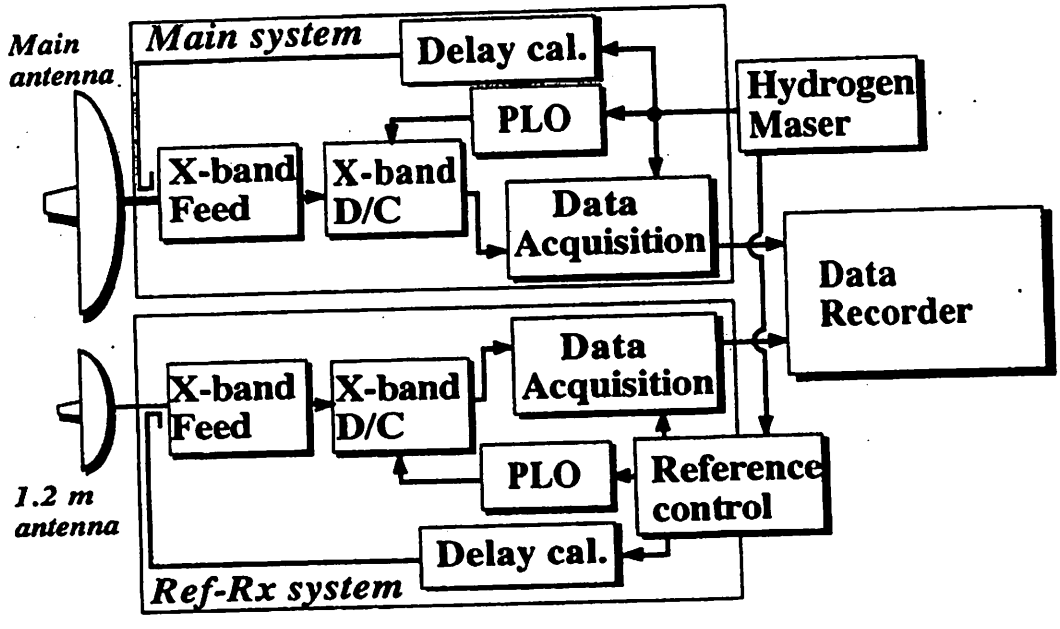

Figure 4: The block diagram of the SBI-experiment. Only X-band is needed. Both systems are using the same reference frequency standard. The data is recorded on two individual recorders.

5 Results

A test of step 1 has been carried out. The time transfer experiment will take place in the near future. Therefore we are so far restricted to the theory.

References

[1] BIPM, see:
`http://glen-ellyn.iit.edu/~clocks/clocks/bipm/bipmexp.html`

[2] BIPM-USNO, see:
`http://tycho.usno.navy.mil/bipm.html`

[3] CLARK, T.A., COUNSELMAN III, C.C., FORD, P.G., HANSON, L.B., HINTEREGGER, H.F., KLEPCZYNSKI, J., KNIGHT, C.A., ROBERTSON, D.S., ROGERS, A.E.E., RYAN, J.W., SHAPIRO, I.I., WHITNEY, A.R.: **Synchronization of Clocks by Very-Long-Baseline Interferometry**, IEEE Transactions on Instrumentation and Measurement, Vol. IM-28, No. 3, September 1979, pg. 184f.

[4] GPS Time Transfer, see:
`http://tycho.usno.navy.mil/gpstt.html`

[5] HAMA, S., KIUCHI, H., TAKAHASHI, Y., AMAGAI, J., YOSHINO, T., KAWAGUCHI, N., KLEPCZYNSKI W.J., MARTIN, J.O.: **Japan-U.S. Time Comparison Experiment for Realizing Better Than 1-ns Accuracy by Using a Radio Interferomentric Technique**, IEEE Transactions on Instrumentation and Measurement, Vol. 38, No. 2, April 1989, pg. 640f.

[6] KIUCHI, H., SUGIMOTO, Y., IMAE, M., KURIHARA, N., YOSHINO, T., TAKAHASHI, F., HAMA, S., TAKAHASHI, Y., TAKABA, H., IWATA, T., KOYAMA, Y., HANADO, Y., SEKIDO, M., NAKAJIMA, J., KONDO, T., AMAGAI, J., KANEKO, A.: **The Western Pacific Geodetics Project's Data Acquisition And Processing System**, Journal of the Communications Research Laboratory, Vol. 42, No. 1, March 1995, pp. 23-30

[7] Selective Availability, see:
`http://tycho.usno.navy.mil/gpsinfo.html#gpssa`

[8] SOFFEL, M.: **Relativity in Astrometry, Celestial Mechanics and Geodesy**, Springer, Berlin 1989

Yebes Phase Calibration Unit: Design, construction, performance and tests on thermal influence

I. López-Fernández

Centro Astronómico de Yebes, Observatorio Astronómico Nacional, Guadalajara, Spain

Abstract

We present a thermally controlled phase calibration unit (mainly based on Haystack '91 design) built for our S/X VLBI receiver. Series of measurements were taken to determine the importance of temperature control over this design. Some plots concerning the dependence of phase stability with temperature of the antenna unit, as well as the sensitivity of both antenna and ground units in cable measurements with temperature are presented.

1 Introduction

One of the very important elements of a Geo-VLBI system is the so called *phase-cal*, provided to measure any phase shifts in the receiver entire signal processing path (so calibrate the *instrumental delay*). The standard way to do this is to insert a calibration signal whose phase is precisely known at the front-end, before any electronics, and measure it at baseband. That signal is generated in the secondary focus cabin by the *antenna unit* from the 5 MHz reference of an H-maser. Another instrument (the *ground unit*) is needed in the control room to measure the extra delay of the cable that carries the reference to the antenna unit (AU).

Any disturbances in the phase of the calibration signal other than those due to the receiver itself will lead to inaccurate determination of the instrumental delay. Temperature changes are the main source of these phase instabilities. The ground unit (GU) accounts for the variations along the 5 MHz cable, but at stations without thermal control at the secondary focus, thermal influence on the AU could be very important.

This communication presents a new phase calibration AU built at the Yebes Observatory, with improved performance over the NASA unit we had on loan, and integrating a temperature control (TC) system. I will describe first the general principles of working and peculiarities of our system, giving some figures about its performance. Then I will focus on the TC, characterizing it, and discussing some interesting results we obtained on the depedence of the phase of the calibration signal the cable delay measurements with respect to the temperature of the AU (and the GU in the latter case).

2 Yebes unit design and electrical performance

Yebes AU is primarily based on the Haystack '91 design for Mark III terminals. In order to calibrate the group delay, it is essential to know the phase shifts at each BBC. This system

Presented at the 11th Working Meeting on European VLBI for Geodesy and Astrometry, Onsala, Sweden, 1996

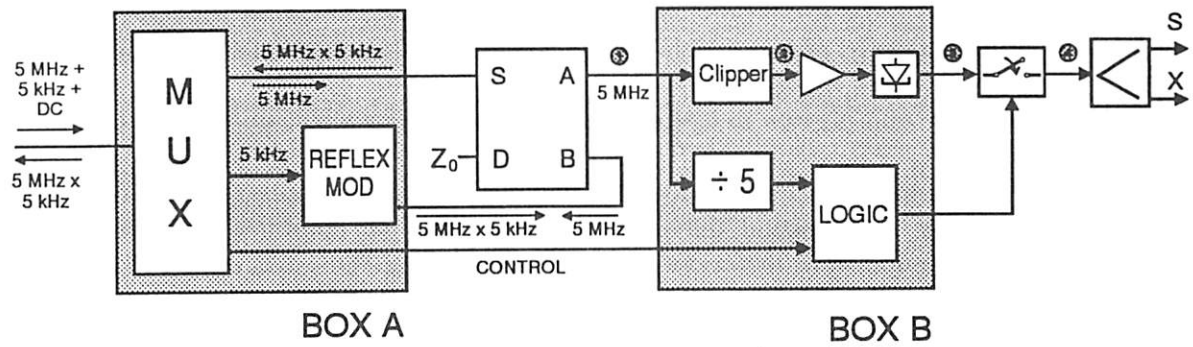

Figure 1: *Diagram of the signal path through the RF part of the* phase-cal. *All these elements are under thermal control. The sinusoidal wave (1) is clipped to a square wave (2) which after amplification produces sharp positive and negative pulses charging the tunnel diode (3). Only one positive pulse out of five pass through the switch (4). A power splitter divides the tones for each band.*

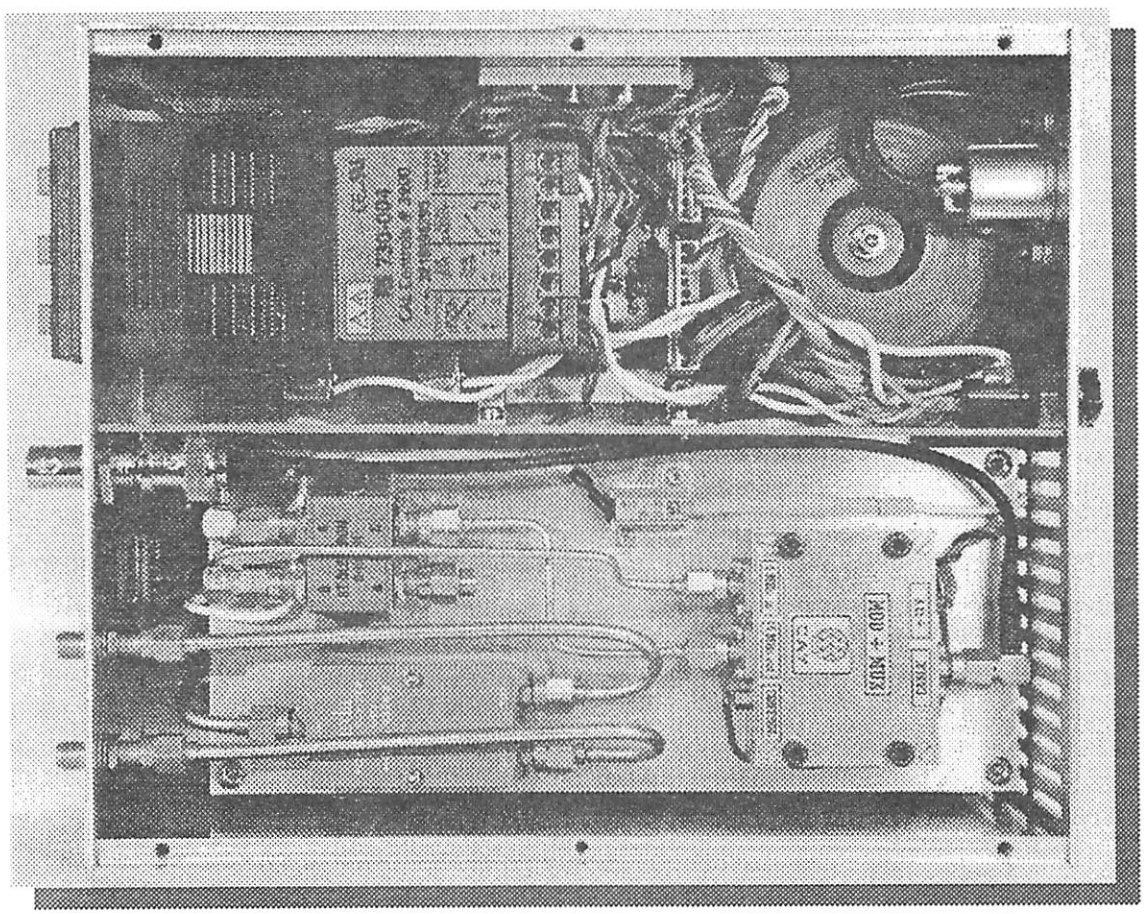

Figure 2: *Inside view of Yebes Phase calibration antenna unit. Note the aluminium plate in the lower half where the RF components are mounted (only one side visible).*

uses as calibration signal a sharp pulse wave with 1 μsec period generated by a tunnel diode, whose spectrum is a series of tones. Therefore, two tones will lie within every 2 MHz BBC band.

An outline of the unit is given in figure 1, while figure 2 shows a picture of the box without the top cover.

Three signals from the GU arrive added at the AU, where they are separeted by several filters (*multiplexor*): a DC signal that may disable the switch stopping pulse generation, the 5 MHz reference and a 5 kHz wave that is modulated by the 5 MHz (in the *reflection modulator*) and sent back to the GU where the cable delay is measured (the 5 kHz modulation avoid confusion with other reflections). These tasks are fulfilled by the elements in *box A*. An hybrid separates the modulated wave from the 5 MHz, that continues to the *pulse generator*, *box B*.

The signal flow through *box B* is explained in figure 1. The switch used to get one out of five pulses is different from the Haystack design one, and a power splitter providing *cal-signal* for both bands is also incorporated in the box.

Some figures about the *electrical* performance of the system are given in table 1. The determination of the pulse spectrum was made with a 45 °C setpoint, but no significant amplitude change was detected measuring at room temperature.

Pulse spectrum[1] (dBm)	S band (2.2 GHz)	-79.6
	X band (8.3 GHz)	-96.4
Spectral flatness (dB)	across bands[2]	0.7
	in 10 MHz	~0.0
5 kHz sidebands at 2.2 GHz (dBc)		-33.0

[1] Measurements include switch and power splitter

[2] Similar results at both S and X bands

Table 1: *Electrical performance*

The power delivered in X band has improved 9 dB over the NASA *phase-cal* we previously had. It should be mentioned that one parameter that most affected the power output is the length of the wire connecting the diode with the rest of the circuit. It must be kept as short as possible to ensure acceptable levels at high frequencies, where its inductance is very high.

The theoretical bandwith of the system is fixed by the pulse width τ, being $\frac{1}{\tau}$ the first null of the *sinc* function multiplying the pulse spectrum. Tipically $\tau = 25$ psec which yields $f_c = 40$ GHz. Our unit is further limited by the cutoff frequency of the switch, 18 GHz. Measurements at 16 GHz gave power levels of -104 dBm.

3 Temperature control description and characterization

Yebes *phase-cal* GU, being in the maser room, where the temperature varies less than ±1 °C, does not have any controller, but the AU as was previously mentioned, is provided with a buit in TC. A description of the way it is implemented follows.

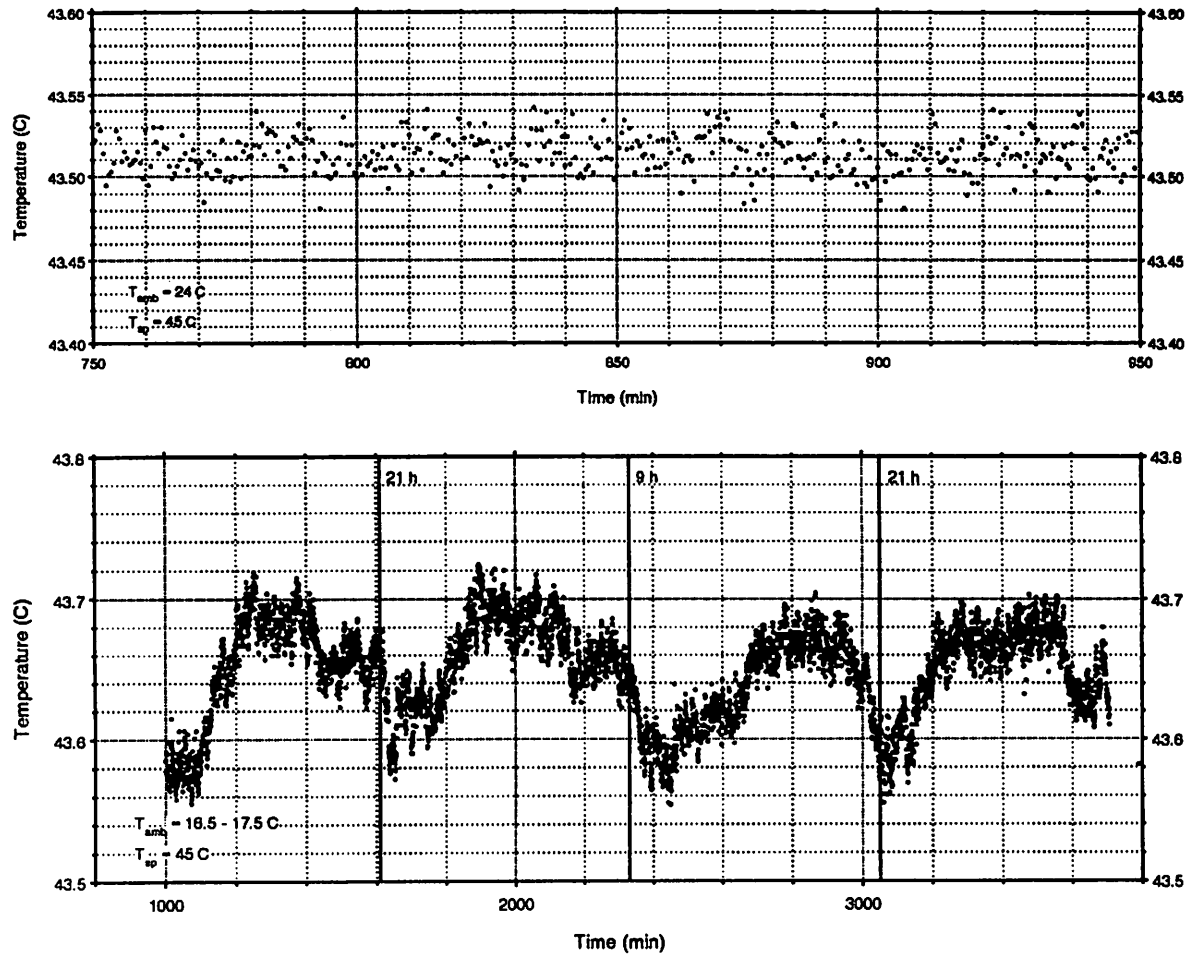

Figure 3: *Temperature regulation by the* phase-cal *TC. The top plot shows the short term regulation (0.0012 °C rms) and the bottom plot shows the long term regulation (0.04 °C rms).*

All elements in the signal path are mounted on both sides of a thick (1 cm) aluminium plate with the necessary thermal inertia (see lower half of figure 2). The plate is kept at 45 °C. It is thermally isolated from the rest of the box and the air flux from the fan that refrigerates the power sources and other elements is restricted to the other area of the box (upper half of figure 2) by a fiber glass panel. The cooling is needed to avoid having to raise too much the setpoint temperature of the controller in order to operate over the temperature of the box.

Several heater resistors are attached to the plate, as well as a PT100 sensor that reads the temperature. The resistors are turned on and off by a solid state relay (SSR), driven by a CAL 3200 autotune temperature controller (seen from above in the upper left of 2). This is a PID (*Proportional + Integral + Derivative*) device that actuates over a SSR with a working cycle that depends on the derivative of the temperature (input by the PT100) proportionally to the error, and also integrates the error function to correct any offsets. It atomatically tunes to any load, selecting several parameters which define its impulse response.

Series of measurements were taken to characterize the performance of the TC. Another PT100 sensor was fixed to the plate and read by a precision voltimeter connected to a computer via HPIB. It was found that the short term stability (mainly due to the working cycle noise) had an rms of 0.0012 °C, with peak to peak amplitudes of 0.06 °C, while the daily variations rms was 0.04 °C, 0.25 °C peak to peak (due to the resolution of the controller). Figure 3 shows two plots of short and long term readings respectively.

The TC response to sudden temperature changes of the order of 15 °C was also within these limits, as was checked putting the unit inside an oven and taking it out.

The noise spectrum was 1 over f like, disipating our worries about the incidence of the working cycle of the controller over the phase noise.

4 Study of TC effectiveness

4.1 Pulse phase stability

To quantify the phase fluctuation of the calibration signal with temperature and ascertain that a TC was justified, we devised the measuring system showed in figure 4.

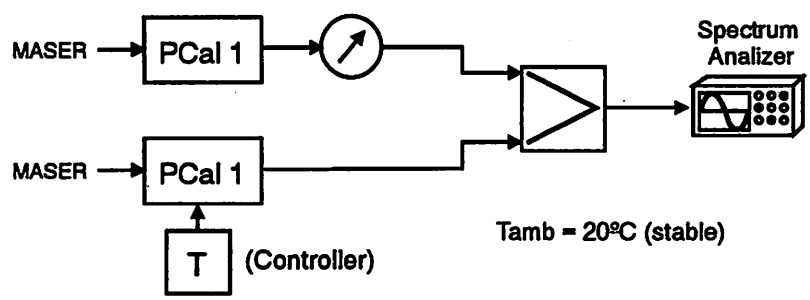

Figure 4: *Measuring system to calibrate the temperature sensitivity of the* phase-cal *signal.*

We used two *phase-cal* units fed by the same 5 MHz reference, one of them with the TC and the other with a variable phase shifter (NARDA 375) at its output. Both signals were combined (MiniCircuits ZAPD-1) and its sum was monitored with an spectrum analyzer. The analyzer would show a maximum at a 1 MHz harmonic when both units were in phase. Temperature variations in the first unit (selecting another setpoint on the TC) would eventually modify the pulse phase. The readout of the phase shifter after adjusting it to see a maximum in the analyzer will match the phase deviation induced by the temperature change.

Results at 20 °C room temperature, measuring the 5 GHz tone, and cycling the temperature of the controller from 20 °C to 40 °C and back were of 5 ps/°C. Using TC the influence is negligible, but without it, a 10 °C change during an experiment would yield 50 ps delay or 150° of phase at 8.3 GHz.

4.2 Cable delay measurements

A final set of measurements was carried out with the AU installed in its definitive location beside the IF unit at the secondary focus. It was aimed to test the proper working of the

cable measuring system and the significance of the temperature variations at the AU and GU.

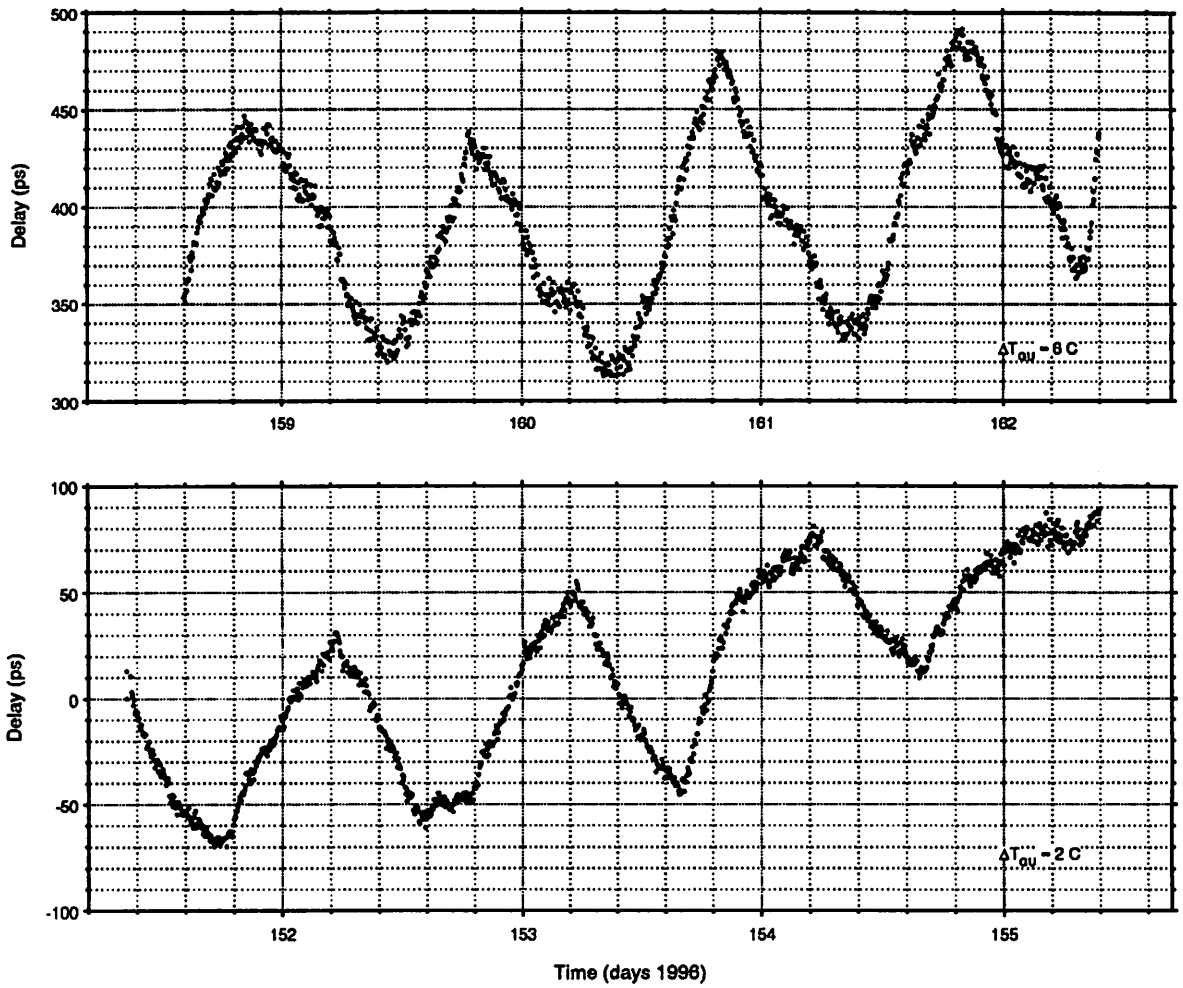

Figure 5: *Cable delay measurements. The bottom plot shows a tipical daily variation, with minima when the temperature is maximum. The GU was in the maser room. The top plot corresponds to the GU being in the control room without AC. Note the displacement of the minima due to the GU contribution to the delay.*

We should expect variations of the order of -100 ps for a 15 m RG-58 cable experiencing 10 °C increases. This was calculated measuring the delay of the reflections at 1 GHz of an RG-58 inside an oven with a network analyzer (yielded -0.7 ps/°C·m). Nevertheless, in our configuration, it was verified that the contributions from the AU and GU to the delay due to normal temperature changes was of same order as those from the cable.

Cable delay measurements were taken through the field system. Changing the setpoint of the AU, it was proved that the contribution to the delay from the AU was in the same direction as the cable one: it increased with temperature. The GU has a greater impact on the delay, and its sensitivity coefficent is in this case positive, as was checked changing the

temperature of the control room.

Cable delay data from several days with the GU in the maser room (±1 °C) and in the control room (±3 °C) are shown in figure 5. The GU positive delay sensitivity with temperature causes a displacement of the daily variation curve.

5 Conclusions

A compact *phase-cal* unit for geodetic VLBI with a built in temperature controller, designed and constructed at the Yebes Observatory has shown good electrical and thermal performance.

The sensitivity of the pulse phase to temperature was found to be 5 ps/°C, greater than expected, proving that a temperature control system is fully justified.

The elements of the cable calibration system are also sensitive to temperature, and without some kind of thermal regulation they could introduce errors in the cable delay measurements. The ground unit is specially critical, since its contribution is bigger and it increases the delay with temperature, conversly to the cable and the antenna unit.

Acknowledgement: The author would like to thank Dr. J. D. Gallego for his help, providing comments, suggestions and support during all phases of this project.

References

[] Alan E. E. Rogers, Manual for Mark III Phase and Group delay calibrator, Haystack Observatory, 1982.

[] Alan E. E. Roger, The New Delay Calibrator Antenna Unit, Haystack Observatory, 1988.

[] I. López Fernández *et al.*, Phase Calibrator: Antenna Unit, Technical Report 1996-4, Centro Astronómico de Yebes, 1996.

[] P. de Vicente *et al.*, Phase Calibrator: Control Unit, Technical Report 1995-10, Centro Astronómico de Yebes, 1995.

PROPAGATION DELAY FLUCTUATIONS IN THE EARTH TROPOSPHERE: RANDOM AND REGULAR COMPONENTS

A. A. Stotskii
Institute of Applied Astronomy, Russian Academy of Sciences
St.Petersburg, 197110, Russia, E-m: stotskii@isida.ipa.rssi.ru

The natural source of errors for the VLBI systems is the path delay fluctuations arising when radio waves pass through the Earth troposphere.

As the universal characteristic of the Earth troposphere related to path delay insuitability it is convenient to use the fluctuation of the path delay in zenith direction. To describe the statistical properties of these fluctuations the structure functions are used – temporal:

$$D_l(\tau) = \langle [l(t+\tau) - l(t)]^2 \rangle \qquad (1)$$

and spatial:

$$D_l(\rho) = \langle [l(\mathbf{r}+\boldsymbol{\rho}) - (\mathbf{r})]^2 \rangle , \qquad (2)$$

where l – path length in zenith direction, t – time, τ – time interval between observations, $\mathbf{r}$ – position coordinate of the point of observations, $\boldsymbol{\rho}$ – spatial separation between the points of observations. The angel brackets denote time or ensemble averaging.

Temporal and spatial structure functions of random fluctuations may be connected by using the principle of frozen turbulence:

$$D_l(\rho) = D_l(\tau v) , \qquad (3)$$

where v is the average velocity of irregularity motions.

Finding of the statistical theory of turbulence [1,2] and analysis of the observational data for the total path delay and separately for its wet and dry components [3-7] show that both the temporal random fluctuations and regular variations of the zenith path delay can be integrated in the unified model of the temporal structure function with the following regions:

(I) The power law of 5/3 – represents random fluctuations related to small-scale three-dimensional turbulence;

Presented at the 11th Working Meeting on European VLBI for Geodesy and Astrometry, Onsala, Sweden, 1996

(II) The power-law of 2/3 – represents random fluctuations related to large-scale two-dimensional turbulence;

(III) The region of the random fluctuations saturation and the regular variations with 1-year period.

So the unified temporal structure function may be written as:

$$D_t(\tau) = \begin{cases} C_{lt}^2 \tau^{5/3} & \tau < T_1 \\ C_{Lt}^2 \tau^{2/3} & T_1 < \tau < T_2 \\ C_s^2 + C_R^2 \sin^2(\pi\tau/T_y) & \tau > T_2 \end{cases} \qquad (4)$$

The estimations of this structure function parameters obtained on the base of observational data are as follows:

$C_{lt} = 5.4\times10^{-3}$ cm.s$^{-5/6}$, $C_{Lt} = 8\times10^{-2}$ cm.s$^{-1/3}$, $C_s = 5$ cm, $C_R = 8$ cm, $T_1 = 3.7$ min, $T_2 = 2.8$ days, $T_y = 1$ year.

The model of the structure function with these parameters and observational data are shown in Fig. 1.

It is important to note that the regular oscillations with 24-hourly period are not detected. The regular seasonal variations are connected only with wet component of the path delay. The dry component has only random fluctuations.

The spatial structure function of the random component of the spatial fluctuations in accordance with (3) has the same regions – (I), (II), (III) and the same shape in regions (I), (II) and in the begining of (III) as temporal one:

$$D_t(\rho) = \begin{cases} C_l^2 \rho^{5/3} & \rho < L_1 \\ C_L^2 \rho^{2/3} & L_1 < \rho < L_2 \\ C_s^2 & \rho > L_2 \end{cases} \qquad (5)$$

The regular component of the spatial structure function may be connected with the baselines latitude location and orientation. These effects must be especially noticeable in region (III) when ρ become comparable with the Earth radius. Unfortunately to-day it is not enough data to construct the regular component of the spatial structure function.

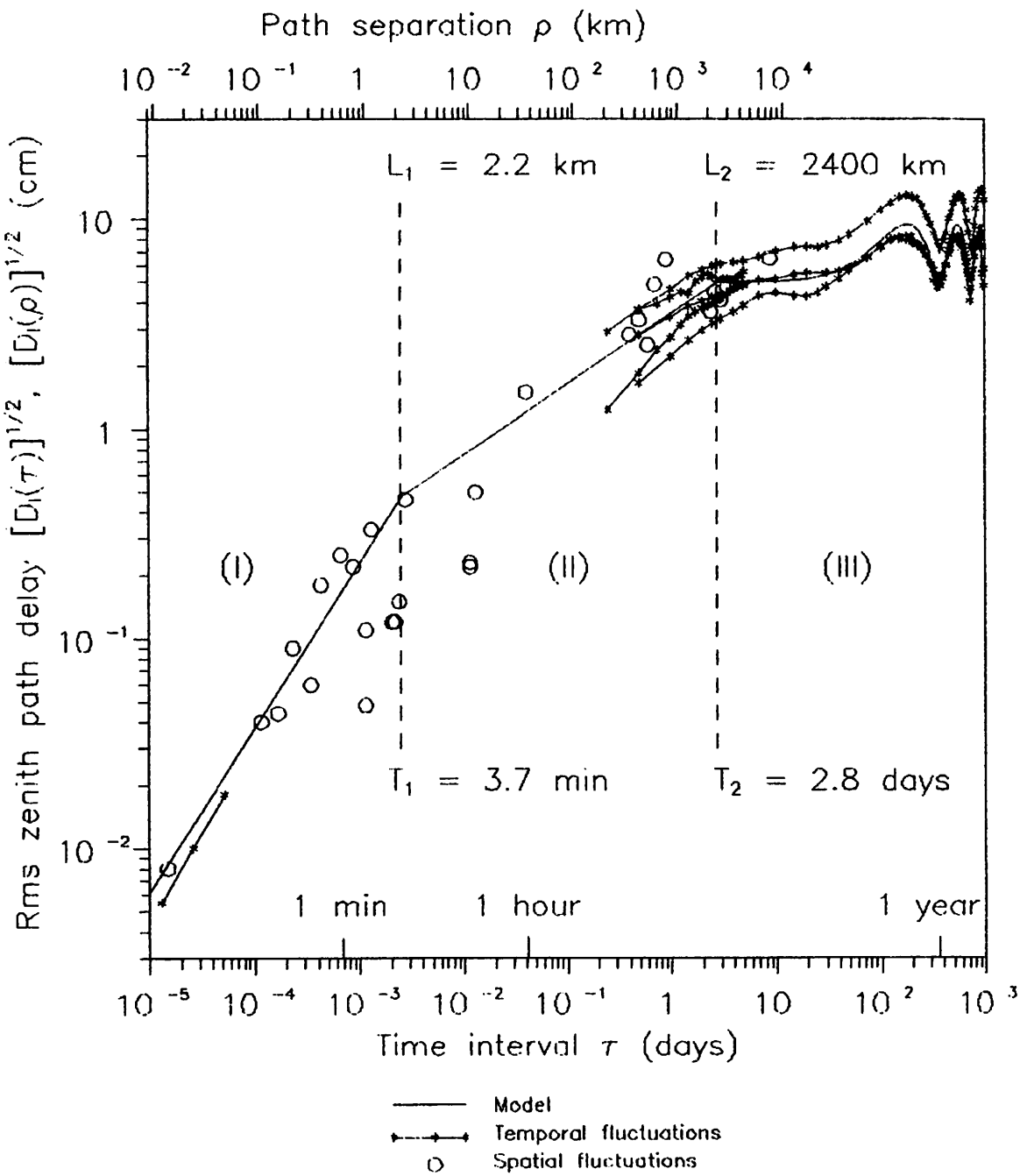

Fig. 1. The unified model of the structure function of the zenith pah delay in the Earth troposphere and observational data. For convenience there are shown the rms values = $[D(\tau)]^{1/2}$.

The estimations of the parameters of the structure function (5) which give agreement with the observational data are as follows:

$$C_l = 1.7\times10^{-5}\ \text{cm}^{1/6},\ C_{Lt} = 8\times10^{-3}\ \text{cm}^{2/3},\ C_s = 5\ \text{cm},$$
$$L_1 = 2.2\ \text{km},\ L_2 = 2400\ \text{km}.$$

The observational data of spatial fluctuations also presented in Fig. 1.

The spatial and the temporal data set on the same curve if one take in (3) the velocity v = 10 m/s. This defines the upper spatial scale on the unified structure function in Fig. 1 and gives the estimation of the v in the principle of frozen turbulence for the Earth troposphere. The same value of v was also defined in direct measurements when comparing the values of temporal and spatial fluctuations [4]. This value is consistent with the typical velocity of the air motions in synoptic processes.

Using the temporal structure function (4) it is possible to obtain the estimation of the rms velocity of the path delay variations as the functions of the observational time:

$$\nu_l(\tau) = \frac{\{<[I(t+\tau) - I(t)]^2>\}^{1/2}}{\tau} = \frac{[D_I(\tau)]^{1/2}}{\tau} =$$

$$= \begin{cases} C_{lt}\,\tau^{-1/6} & \tau < T_1 \\ C_{Lt}\,\tau^{-2/3} & T_1 < \tau < T_2 \\ [C_s^2 + C_R^2 \sin^2(\pi\tau/T_y)]^{1/2} / \tau & \tau > T_2 \end{cases} \qquad (6)$$

When processing the VLBI observations there is also used the another representation of this parameter – as the rms velocity of the time delay variations ν_t:

$$\nu_t(\tau) = \nu_l(\tau) / c\,, \qquad (7)$$

where c is the light velocity.

The dependencies (6) and (7) are presented in Fig. 2.

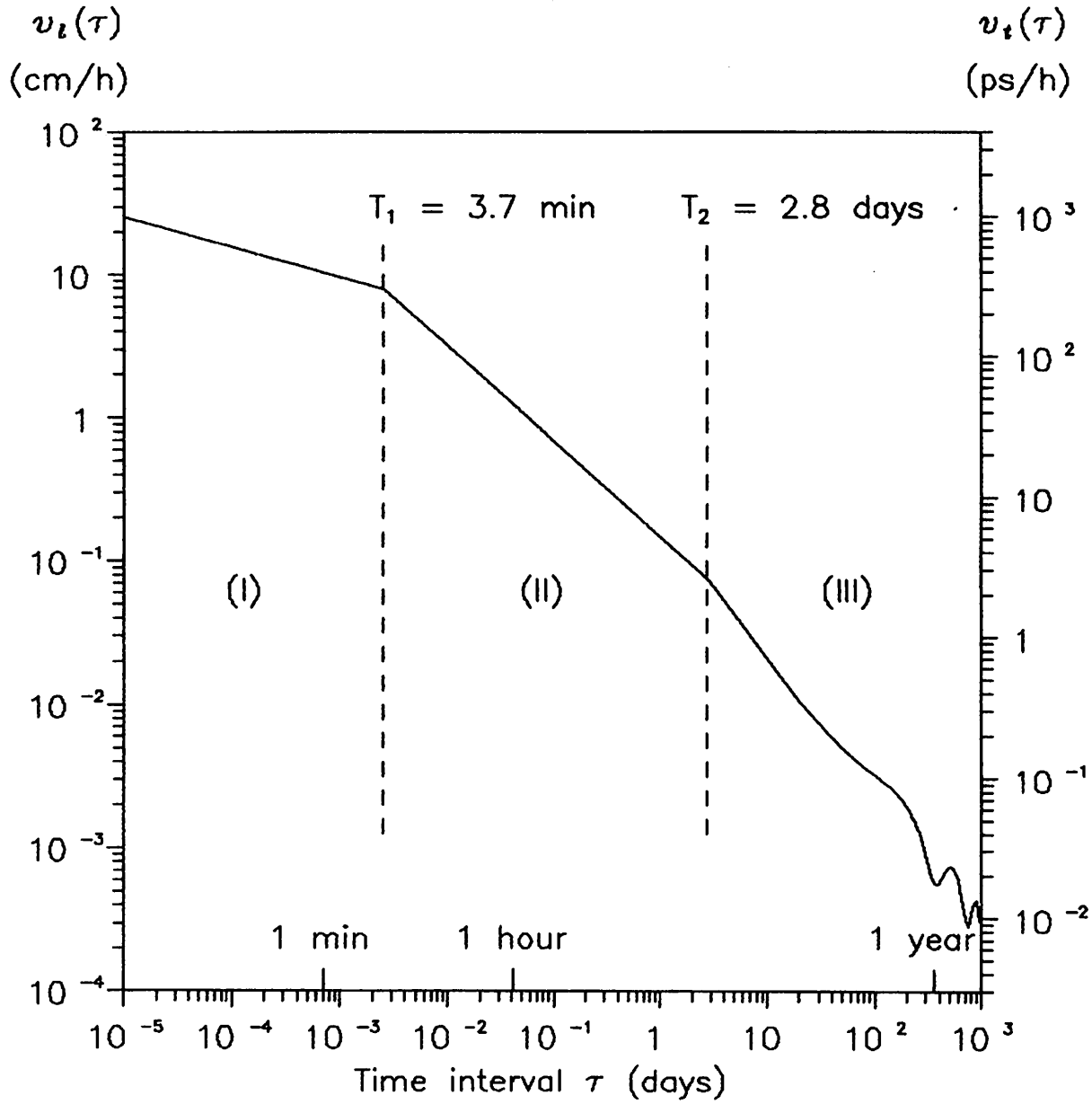

Fig. 2. Rms velocity of the path delay variations in the Earth troposphere. during the time interval τ.

References

1. V. I. Tatarskii. *Wave Propagation in a Turbulent Medium.* McGrow-Hill, New-York, 1964.
2. A. A. Stotskii. On Fluctuation Characteristic of Earth Troposphere. *Radiophis. and Quant. Electron.* **16**, 620-622, 1972.
3. A. A. Stotskii. Path Length Fluctuations through the Earth Troposphere: Turbulent Model an Data of Observations. In book: *Refraction of Transatmospheric Signals in Geodesy.* Pros. of the Symp. Ed. J. C. De Munck and T. A. Th. Spoelstra. Netherlands Geodetic Commission Publication on Geodesy. New Series, No 36, 179-182, 1992.
4. A. A. Stotskii and I. M. Stotskaya. Analysis of Tropospheric Pathlength Fluctuations Using Geostationary Satellite Observations. *Astronomical and Astrophysical Transactions*, 2, 327-339, 1992.
5. G. Elgered. Tropospheric Radio-Path Delay from Ground-Based Microwave Radiometry. In book: *Atmospheric Remote Sensing by Microwave Radiometry.* 215-258, Ed. M. A. Janssen. John Wiley & Sons, Inc. In press.
6. A. A. Stotskii and I. M. Stotskaya. Search of Correlation between Wet and Dry Components of Path Delay in the Troposphere. *Communication of the Institute of Applied Astronomy.* No 56, St.Petersburg, 1993.
7. A. A. Stotskii, K. G. Elgered and I. M. Stotskaya. Structure Analysis of Path Delay Variations in Neutral Atmosphere. *Astronomical and Astrophysical Transactions.* In press.

A Quality Assessment of the Wet Path-Delay Estimated from GPS Data

T. Ragne CARLSSON, Gunnar ELGERED, and Jan M. JOHANSSON

Onsala Space Observatory, Chalmers University of Technology, S-439 92 Onsala, Sweden

Abstract. We have investigated the possibility to use estimates of the excess path delay due to water vapor, the wet delay, from the Global Positioning System (GPS) as *a priori* information in geodetic Very-Long-Baseline Interferometry (VLBI), in the same way as Water Vapor Radiometer (WVR) data have been used before. We evaluate the quality of the GPS estimated wet delay, by comparison with WVR data at the Onsala Space Observatory and through studies of the GPS estimates at other European VLBI sites ,e.g., Matera, Madrid, Wettzell, and Ny Ålesund. We also identify bad periods in the GPS estimates, discuss error sources, and point out possible problems when using GPS data in the VLBI analysis.

1 Background

Aiming for better accuracy in geodetic Very-Long-Baseline Interferometry (VLBI) analysis the use of Water Vapor Radiometer (WVR) data as *a priori* information in the processing has been tried in several investigations [*Elgered et al.*, 1991; *Kuehn et al.*, 1991; *Elgered and Davis*, 1993; *Carlsson*, 1996]. These data have been used to correct for the excess path delay due to water vapor, the wet delay. The improvement on baseline reproducibility has however been limited, which can partly be derived from the lack of WVRs at other sites than the Onsala Space Observatory. Thus there is no baseline with corrections at both ends. One solution to this problem can be to use the wet delay estimated from Global Positioning System (GPS) data in the same way as WVR measurements have been used. GPS receivers are in contrast to WVRs available at most VLBI sites around the world, operating more or less continuously. Figure 1 shows a comparison between the different methods for three baselines from the NASA R&D experiment series. Each bar in the plot indicates the weighted root-mean-square (wrms) deviations from a linear fit to the data points, the reproducibility. There are four different bars for each baseline representing the standard solution, where we estimate the wet delay from the VLBI data, WVR solution where we have added WVR data at the Onsala site to correct for the wet delay, and GPS solution with Onsala GPS estimates added in the same way. The reason for having two bars showing the standard solution for each baseline is that the first is showing the result for the experiments were WVR data were available and the second one is showing the result where GPS data were available, typically 34 and 31 experiments respectively. The baselines are Onsala-Wettzell (919 km), Onsala-Fairbanks (6066 km), and Onsala-Fort Davis (7940 km). We can see a significantly improved reproducibility only in the shortest baseline. One reason for this result might be the large amount of data lost when using external measurements. In order to achieve the best reproducibility, when including GPS estimated wet delay in VLBI data processing, all observations below an elevation angle of 26 degrees are removed [*Carlsson*, 1996]. This angle is called the elevation cutoff angle. In the R&D network around 30% fewer observations are used with this setup than with the standard analysis setup using an elevation cutoff angle of 8 degrees. For the Onsala-Wettzell baselines there are still 130 observations in the solution, while there are only 60 for the Onsala-Fort Davis baseline.

Given these results using the R&D network the question arises: Could these results be improved for the Europe experiments? Some characteristics of the Europe experiments indicate that. The baselines are, with a few exceptions, much shorter compared to the R&D network. Hence we will not have the situation with long baselines and few common observations due to a high elevation cutoff angle. The Onsala-Wettzell baseline, the only baseline in the R&D network that is significantly improved in reproducibility, by using this method, is also part of the Europe network. The longer integration times and the slower antennas used in the European network result in a lower observation density. This will impair the possibility to solve for the atmosphere at each site, and consequently the processing might benefit from the use of external data.

If the use of wet delay estimates from GPS is going to improve the baseline reproducibility the most basic question is the quality of the estimates. In this paper we will investigate the quality of the wet delay estimated from GPS data for the Europe experiments carried out during the time period December 1993 to December 1995. This is done primarily by comparison with the Onsala WVR, but also through studies of the estimates at the other sites.

Presented at the 11th Working Meeting on European VLBI for Geodesy and Astrometry, Onsala, Sweden, 1996

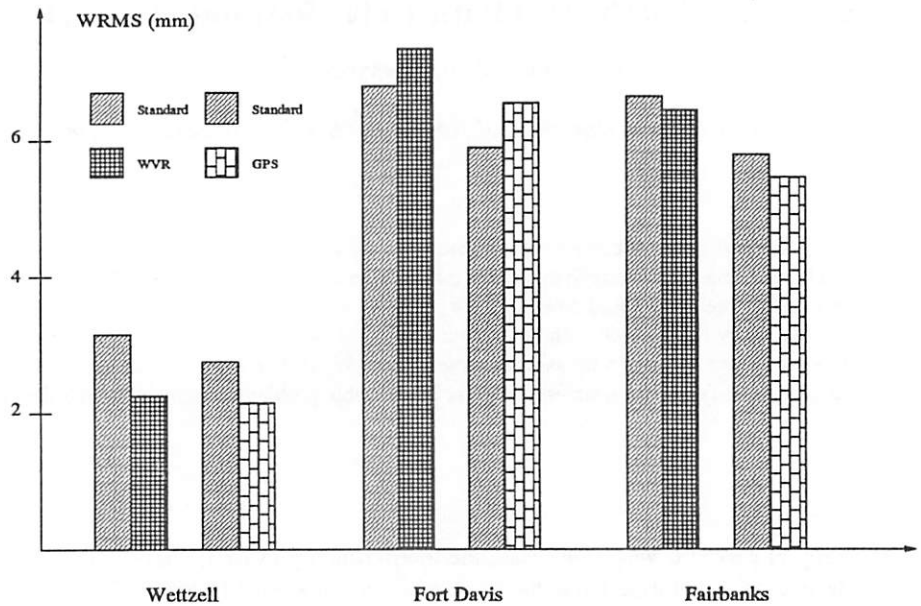

Figure 1: Baseline length wrms for the three baselines Onsala-Wettzell, Onsala-Fort Davis, and Onsala-Fairbanks. The four bars for each baseline represents the standard solution for the 38 experiments where WVR data were available, the corresponding WVR solution, the standard solution for the 31 experiments where GPS data were available, and the corresponding GPS solution (for the baseline Onsala-Fairbanks there are 37 and 30 experiments, respectively). (From Carlsson et al., in preparation).

2 Data set

GPS data from seven stations have been used, namely Medicina, Madrid, Matera, Noto, Ny Ålesund, Onsala, and Wettzell. All the data were analyzed with the GIPSY/OASIS software [*Webb and Zumberge*, 1993], using a Kalman filter technique to model the atmospheric delay as well as the drifts of the clocks in the satellites and on the ground. The residual tropospheric path-delay were, after removing *a priori* hydrostatic and wet values, estimated as random walk processes using the *Lanyi* [1984] mapping function. The elevation cutoff angle was 15 degrees. The wet delay was then determined from the residual delay using pressure readings, taken from the VLBI logfiles, at each sites. More information about the GPS data analysis can be found in, *e.g.*, *Bifrost project members* [1996]. For the quality evaluation of the GPS estimates we have used the Onsala WVR.

3 WVR comparison

Quality of measurements can be specified in a number of different ways. We therefore present a couple of different statistical measures of the comparison between the GPS estimates and the WVR measurements. One should also keep in mind when comparing two different techniques that it can be difficult to decide which one is the better of the two, when differences occurs. In the following comparison, since the WVR measurements are much more dense in time than are the GPS estimates the latter are used to calculate smoothed values to the epochs of the GPS estimates. For this purpose we used a gaussian window with a half width of 10 minutes.

Figure 2 shows the mean difference for each VLBI experiment, where both WVR and GPS data for Onsala have been available. Clear systematics is seen here where the WVR overestimates the wet delay compared to the GPS for all experiments except two. This tendency has been seen before at the Onsala site [*Carlsson*, 1996].

Figure 3 shows the rms difference between the GPS estimated wet delay and the WVR measurements. The filled part of the bars represents the unbiased rms, i.e., the rms when the mean difference is withdrawn. We can see that much of the total rms difference is due to the bias between the estimates. Since the experiments are conducted in different

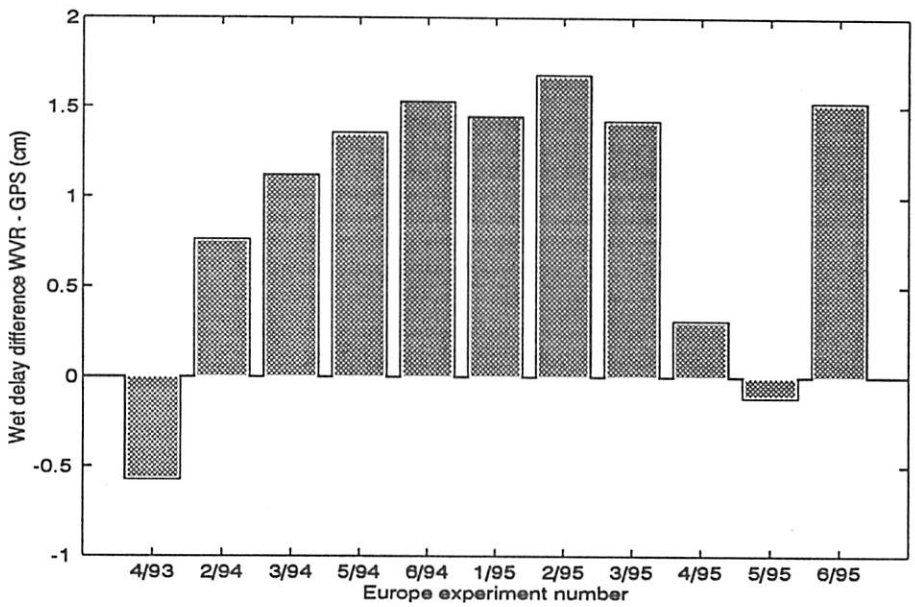

Figure 2: Mean difference between WVR measurements and the GPS estimates for each Europe VLBI experiment. Note that Onsala did not participate in the Europe 1/94 experiment, and that no WVR data exist for the Europe 4/94 experiment.

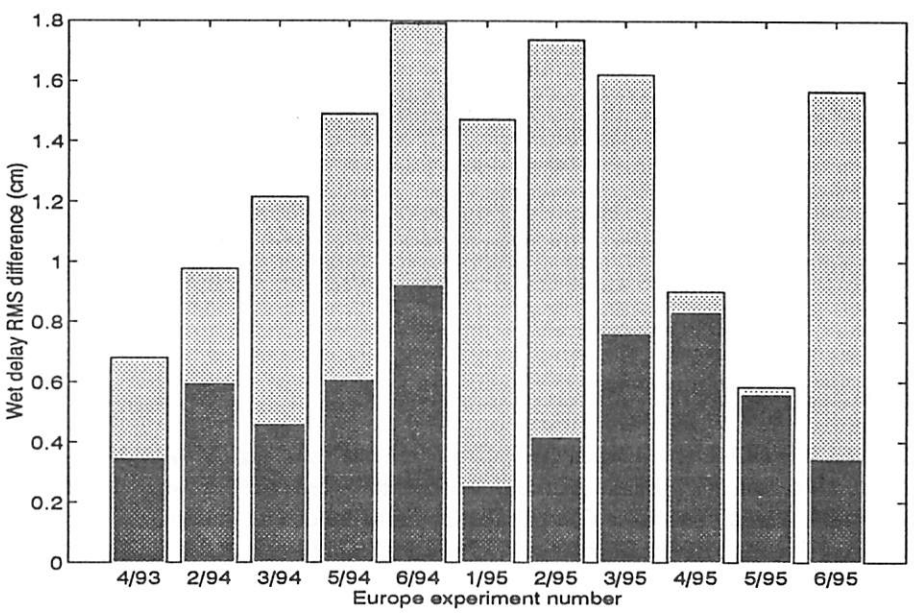

Figure 3: The rms difference between the WVR measurements and the GPS estimates for each Europe VLBI experiment. The darker part of the bars represents the rms difference obtained if the mean difference is removed, i.e., the standard deviation of the time series of differences, while the whole bars represents the total.

seasons, it can be interesting to study the rms difference in percent of the total delay. In Figure 4 we can see that the distribution is somewhat different, where the winter experiments, with very low wet delay, distinguish from the other.

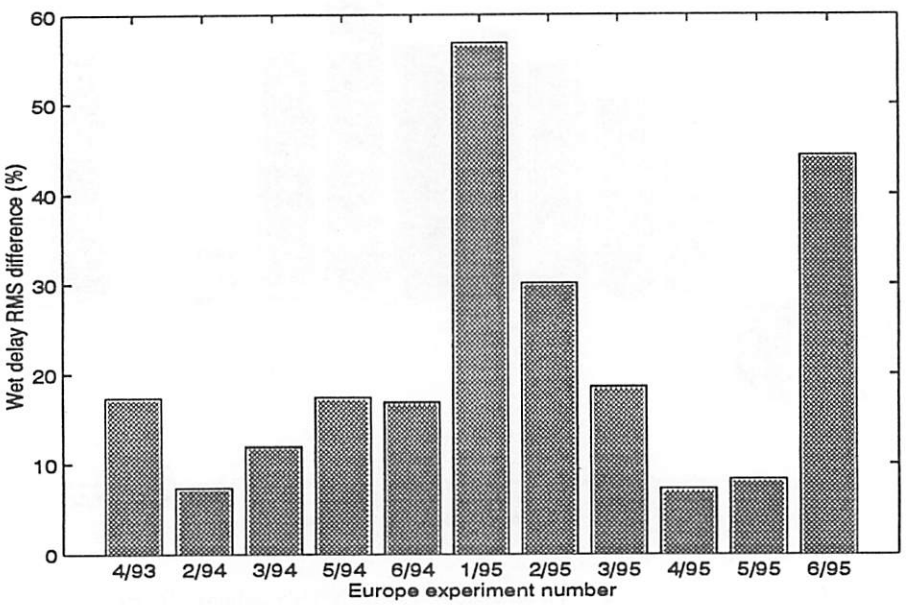

Figure 4: The rms difference between GPS estimates and the WVR measurements for each Europe VLBI experiment in percent of the GPS estimate.

Another measure used to study how well the variations in two different time series agree is the experimental linear correlation coefficient, defined as [*Bevington*, 1969]

$$r = \frac{N\Sigma x_i y_i - \Sigma x_i \Sigma y_i}{\sqrt{[N\Sigma {x_i}^2 - (\Sigma x_i)^2] \cdot [N\Sigma {y_i}^2 - (\Sigma y_i)^2]}} \tag{1}$$

where N is the number of measurements. This quantity can be viewed as the sample covariance matrix divided by the square root of the sample variances of each of the two processes. The value of r ranges from 0 to ± 1 for no correlation and complete correlation respectively. Figure 5 shows the correlation coefficient between the estimates for the experiments available.

4 Overall quality evaluation

For the other VLBI sites it is difficult to make an evaluation of the quality, using the GPS data alone. We can however for these estimates identify when something has clearly failed, and we can study the statistics from the different sites. Table 1 shows the participating stations in the Europe experiments together with their mean and rms values for the GPS estimates during the experiments between December 1993 and December 1995. A dash means that no GPS or pressure data have been available. We note a mean value of the wet delay at Ny Ålesund of −0.5 cm. This is of course physically impossible, but can very well be a result of a bias of the order of 1 cm, as seen at the Onsala site. We should however consider that the formal one-sigma errors are in the order of 0.5 cm.

In Figure 6 we can see an example of what sometimes occurs in the GPS estimates. This is the estimated wet delay at the Madrid site during the Europe 2 experiment 1995, where we can see a jump of about 2 cm in the estimate at 00.00 UTC. This is a difference in level between two estimates made independently from the two calendar days, telling us at least one of the estimates is biased.

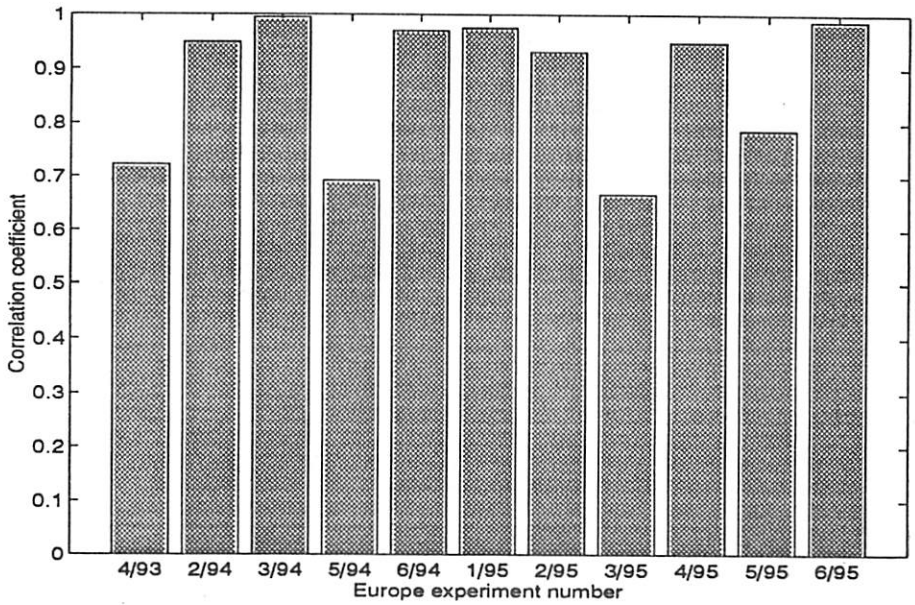

Figure 5: Correlation coefficient for the WVR and the GPS time series of the estimates of the wet delay for the experiments available.

Table 1: Participating stations in the Europe experiments with their mean and RMS values for the GPS estimates during experiments between December 1993 and December 1995. All values are in cm.

Exp	Medicina		Madrid		Matera		Noto		Ny Ålesund		Onsala		Wettzell	
	mean	RMS	mean	RMS	mean	RMS	mean	RMS	mean	RMS	mean	RMS	mean	RMS
93-4	-	-	6.7	0.8	6.4	2.6	-	-	-	-	3.9	0.5	4.6	0.4
94-1	-	-	-	-	6.7	0.6	-	-	-	-	-	-	4.8	0.6
94-2	-	-	9.2	1.6	7.7	1.2	-	-	-	-	13.3	1.9	8.6	1.0
94-3	-	-	7.3	0.9	15.9	2.0	-	-	-	-	10.2	4.0	17.6	1.9
94-4	-	-	8.5	0.9	-	-	-	-	-	-	11.1	2.2	17.7	1.8
94-5	-	-	-	-	-	-	-	-	-	-	8.5	0.5	5.9	0.5
94-6	-	-	7.2	4.0	9.6	0.7	-	-	-	-	10.6	2.2	9.5	2.7
95-1	-	-	5.3	0.7	4.2	0.9	-	-	-0.5	0.5	2.0	1.1	4.4	1.7
95-2	-	-	6.6	1.8	-	-	-	-	4.2	1.2	5.8	1.2	4.2	1.1
95-3	-	-	12.2	0.7	10.1	0.7	-	-	3.9	0.6	8.7	0.9	12.2	2.4
95-4	-	-	9.1	1.1	-	-	-	-	4.7	0.7	12.3	2.6	11.9	1.1
95-5	-	-	12.2	0.6	-	-	-	-	-	-	7.1	0.9	6.1	0.6
95-6	7.6	0.9	6.8	1.0	-	-	5.1	2.1	-	-	3.5	2.2	2.6	1.3

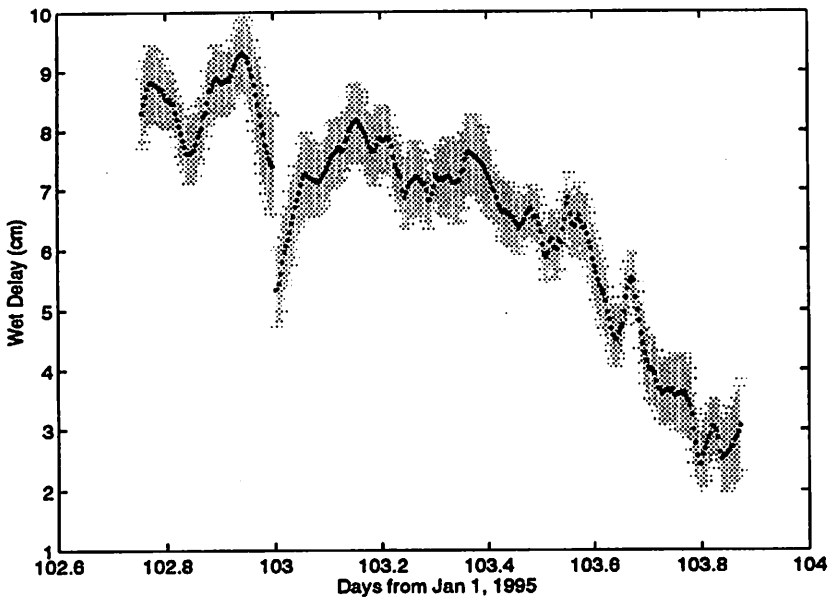

Figure 6: The GPS estimated wet delay with one-sigma formal error bars at the Madrid site during the Europe 2 experiment 1995. This is two GPS estimates made independently from two different calendar days, days number 102, and 103. We can see that there is a difference in level between the estimates, resulting in a discontinuity in the composite estimate.

5 Error sources

In the following we present some of the error sources that might affect the GPS estimates presented here, namely atmospheric gradients, signal scattering, Kalman filter parameters, and mapping function. When processing GPS data our models assume a horizontally stratified atmosphere. An azimuthal asymmetry in the atmosphere will, since it is unmodeled, have an effect on other estimates. These gradients can be of the size of some mm and the effect will probably be more on the wet delay than on the positions estimates, due to the similarities in elevation dependence. A detailed study of gradients determined from a WVR has been conducted by *Davis et al.* [1993]. Signal scattering problems have been investigated by, e.g., *Elósegui et al.* [1995] and *Jaldehag et al.* [1996], and shown to have an effect on the cm level on the vertical position estimate. This will consequently affect also the atmospheric propagation delay estimate. In the solution procedure the wet delay is assumed to vary according to a random walk process with a certain variance rate. This parameter is set to the same value at all sites. The actual size of the fluctuations of the wet delay can however vary significantly between different places. Too low or too high values for this chosen variance rate might introduce errors in the wet delay estimate. Tests with site dependent variance rate values for parameter estimation in VLBI have been conducted by *Herring et al.* [1990]. Finally the mapping function used, *Lanyi* [1984], is not a perfect scaling of the zenith delay to the specific elevation angle. This could also affect the wet delay estimates.

6 Conclusions

With the aim to use GPS estimated wet delay in the VLBI analysis we face mainly two problems. Since an error in the atmospheric zenith delay results in an error of about twice that size in the vertical position estimate, when external atmospheric corrections are used, [*Herring*, 1986], we are very sensitive to errors in the GPS estimates. The bias seen when comparing the GPS estimates with WVR data is therefore a major problem when trying to improve VLBI baseline reproducibility using GPS data.

Today VLBI experiments typically have many observations are at a fairly low elevation, i.e., below 20 degrees. This feature has been included in order to improve the quality of the wet delay estimates by being properly separated from

the vertical position estimate. When we use external corrections we do not not solve for any atmospheric parameters. Accordingly we do not need the low elevation observations. They are instead removed, since we benefit from a higher elevation cutoff angle when using external calibration [*Carlsson*, 1996]. However this implies that about 30% of the observations are discarded as mentioned earlier. The better solution would be to have an observing schedule with no low elevation observations. This is of course in contradiction to the method to estimate wet delay from VLBI data, where low elevation observations are a necessity. Therefore, given a certain network the schedule cannot be optimized for the two methods simultaneously. A choice has to be made depending on how sure we can be about having external data available for the processing.

References

Bevington, P. R., "Data reduction and error analysis for the physical sciences", *McGraw-Hill book company*, 1969.

BIFROST project members: R. A. Bennett, T. R. Carlsson, T. M. Carlsson, R. Chen, J. L. Davis, M. Ekman, G. Elgered, P. Elósegui, G. Hedling, R. T. K. Jaldehag, P. O. J. Jarlemark, J. M. Johansson, B. Jonsson, J. Kakkuri, H. Koivula, G. A. Milne, J. X. Mitrovica, B. I. Nilsson, M. Ollikainen, M. Poutanen, R. N. Pysklywec, B. O. Rönnäng, H-G. Scherneck, I. I. Shapiro, and M. Vermeer, GPS Measurements to Constrain Geodynamic Processes in Fennoscandia, *EOS, Transactions, American Geophysical Union, 35*, 1996.

Carlsson, T. R., "Site Dependent Error Sources in in Geodetic Very-Long-Baseline Interferometry", *Tech. Rept. 224L*, School of Electrical and Computer Engineering, Chalmers University of Technology, 1996.

Carlsson, T. R., G. Elgered, J. M. Johansson, Wet Path-Delay Corrections in Geodetic Very-Long-Baseline Interferometry, in preparation.

Davis, J. L., G. Elgered, A. E. Niell, and C. E. Kuehn, "Ground-based measurement of gradients in the "wet" radio refractivity of air", *Radio Sci.,28*, 1003-1018, 1993.

Elgered, G., J. L. Davis, T. A. Herring, and I. I. Shapiro, "Geodesy by Radio Interferometry: Water Vapor Radiometry for Estimation of the Wet Delay", *J. Geophys. Res., 96*, 6541-6555, 1991.

Elgered, G., and J. L. Davis, "Microwave Radiometry for Correction of Atmospheric Path-Length Variations in VLBI: Recent Results." *Proc. of the 9th Working Meeting on European VLBI for Geodesy and Astrometry*, ed. J. Campbell and A. Nothnagel, Bad Neuenahr, 98-108, 1993.

Elósegui, P., J. L. Davis, R. T. K. Jaldehag, J. M. Johansson, A. E. Niell, and I. I. Shapiro, Geodesy Using the Global Positioning System: The Effects of Signal Scattering on Estimates of Site Position, *J. Geophys. Res., 100*, 9921-9934, 1995.

Herring, T. A., Precision of Vertical Position Estimates From Very Long Baseline Interferometry, *J. Geophys. Res., 91*, 9177-9182, 1986.

Herring, T. A., J. L. Davis, and I. I. Shapiro, Geodesy by Radio Interferometry: The Application of Kalman Filtering to Analysis of Very Long Baseline Interferometry Data, *J. Geophys. Res., 95*, 561-581, 1990.

Jaldehag, R. T. K., J. M. Johansson, P. Elósegui, J. L. Davis, A. E. Niell, B. O. Rönnäng, and I. I. Shapiro, Geodesy Using the Swedish Permanent GPS Network: Effects of Signal Scattering on Estimates of Relative Site Positions, *J. Geophys. Res., 101*, 17814-17860, 1996.

Kuehn, C. E., W. E. Himwich, T. A. Clark, and C. Ma, An Evaluation of Water Vapor Radiometer Data for Calibration of the Wet Path Delay in VLBI Experiments, *Radio Sci.*, 26, 1381-1391, 1991.

Lanyi, G., "Tropospheric delay affecting radio interferometry" *TDA Progress Report 42-78* ,152-159, Jet Propul. Lab., Pasadena, Calif., 1984.

Webb, F. H. and J. F. Zumberge, An Introduction to the GIPSY/OASIS-II, *JPL Publ. D-11088*, Jet Propulsion Laboratory, Pasadena, California, 1993.

Measurement of Water Vapor by GPS, WVR, and Radiosonde

A.E. Niell[1], A.J. Coster[2], F.S. Solheim[3], V.B. Mendes[4], P.C. Toor[4] R.B. Langley[4] C.A. Ruggles[2]
[1]MIT Haystack Observatory, Westford, MA 01886
[2]MIT Lincoln Laboratory, Lexington, MA 02173
[3]Radiometrics Corp., Boulder, CO 80301
[4]University of New Brunswick,
Fredericton, NB, Canada E3B 5A3

ABSTRACT

During the CONT95 VLBI campaign, measurements of the atmosphere delay due to water vapor were made at Haystack Observatory using radiosondes, GPS, and a water vapor radiometer (WVR). The goals were to evaluate the accuracy with which precipitable water in the atmosphere could be measured with GPS and to investigate the distribution of water vapor, both spatial and temporal, around the Westford VLBI antenna during CONT95. Initial analysis of the GPS, radiosonde, and WVR data reveals that the comparison is limited by systematic errors in each of the instruments. These errors reach 40 mm of zenith wet delay for the radiosondes, 15 mm for the GPS, and 6 mm for the WVR. Such large errors within each technique must be reduced before accuracies of 1 mm of precipitable water vapor (~6 mm of zenith wet delay)) can be claimed.

OBSERVATIONS

In the last two weeks of August, 1995, measurements of water vapor delay in the atmosphere were made with eleven GPS systems distributed over a region within ~25 km of Haystack Observatory. Radiosondes were launched twice daily from the parking lot near the Haystack telescope, and a microwave water vapor radiometer was operated continuously on a tower approximately 625 m away.

Three of the GPS sites were within 1 km of each other at the Observatory, one near the WVR (MHR0), the second next to the Westford VLBI telescope (WES2), and the third 500 m further south (WFRD). All three were AOA 8-channel TurboRogue receivers attached to Dorne-Margolin antennas with choke rings. Four other TurboRogue systems occupied sites five to 25 km from the Observatory.

Two of the systems consisted of an Ashtech Z-12 receiver connected to the Ashtech version of the Dorne-Margolin with choke ring antenna; these were "protected" with the radome obtained from Ashtech. Two other Ashtech Z-12 receivers were used, but the associated antenna was in each case a Model 700718B antenna. One of these, FIRE, was mounted atop a fire tower 5 km west of the Observatory.

The WVR was a Radiometrics Corp. Model 1100™ dual frequency radiometer. The retrieval coefficients were calculated from VIZ radiosonde data from the NWS sites at Albany, NY (ALB), Chatham, MA (CHH), and Portland, ME (PWM). Data for the months of 1995 June-August, up to the time observations began at Haystack, were used.

Vaisala RS-80 radiosondes were launched from Haystack Observatory at 1200 and 2300 UT on all days and additionally at 1800 UT on some days. Winds were not measured. The raw data were captured at one second intervals, and the temperature and pressure were checked with independent measurements. For comparison, additional radiosonde data were obtained from the three nearest National Weather Service sites, approximately 150 km from Haystack uniformly spaced in azimuth.

Barometric pressure was measured at seven sites. Paroscientific Digi-quartz™ barometers were used at AEN0 and SGJ0 and were used to calibrate the other barometers. Comparison of the measurements at the seven sites showed that, during this two week period, the pressure at any site could be calculated from another with an accuracy of 0.1 mb based on the height difference, resulting in negligible error in the calculation of the apriori hydrostatic zenith delay.

RESULTS

Water Vapor Radiometer

The zenith wet delays (ZWD) measured by the WVR for the comparison period, 1995 August 18 through September 1, are shown in Figure 1.

Presented at the 11th Working Meeting on European VLBI for Geodesy and Astrometry, Onsala, Sweden, 1996

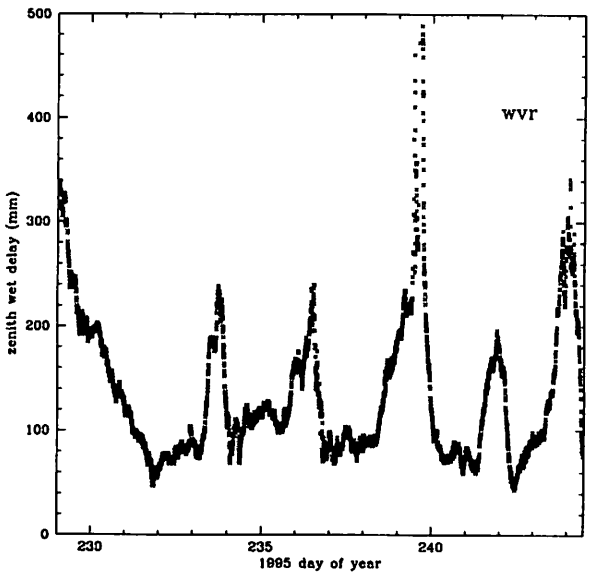

Figure 1. Zenith wet delay (mm) as measured by WVR at Haystack Observatory.

GPS data were acquired for day of year (DOY) 230 through 244. Unfortunately this was during a period of drought, but the range of daily variation of ZWD was not abnormally low. The rain on DOY 239, which is indicated by the extremely high values of ZWD, was light and serves to emphasize the limitation of the WVR in rainy conditions. For the purpose of evaluating different techniques for measuring water vapor, the dry conditions were fortunate since the WVR estimates of ZWD are not useful in the presence of rain or other conditions that cause liquid water to be present in the optics of the radiometer.

. The expected uncertainty in the WVR measurements ranges from 6 mm at ~100 mm of ZWD to 20 mm at ~300 mm (Elgered et al, 1993; Solheim, 1996 (private communication)). Determination of the retrieval coefficients from the NWS radiosonde data may introduce an additional error in the comparison because of the differences in radiosonde results noted in the next section. A test by P. Jarlemark (1996, private communication) indicates that this may be as large as 6 mm of ZWD for a total ZWD of 200 mm.

Radiosonde

Vaisala radiosondes were used because they were readily available near the Observatory and because they were also being used by another group at Lincoln Laboratory, the site of one of the GPS systems. However, this choice proved fortuitous in pointing out the discrepancy in measurements between sondes of different manufacturers in addition to differences that are documented for high and low relative humidities (Wade and Schwartz, 1993; Wade 1994). The ZWDs calculated by raytracing the radiosonde profiles for Haystack and for the NWS sites are shown in Figure 2.

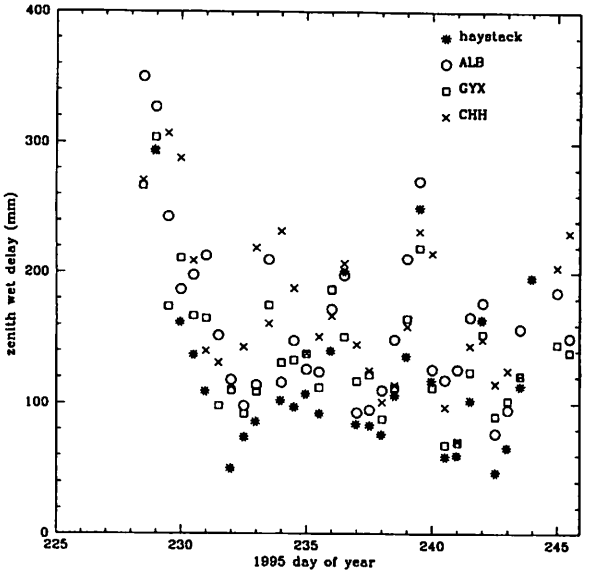

Figure 2. Zenith wet delay for radiosondes launched nearly simultaneously at four sites. Vaisala RS-80 sondes were used at Haystack Observatory VIZ sondes were launched and analyzed by the NWS at ALB, CHH, and GYX.

The Vaisala ZWD values appear systematically low with respect to the NWS results for ZWDs less than 200 mm. The differences averaged over the entire observation period are given in Table 1. In the third column the zenith wet delay differences have been converted to precipitable water vapor differences using a factor of ~1/6.15.

Table 1. The average and standard deviation of the zenith wet delays calculated from the NWS VIZ sondes relative to the Vaisala RS-80 sondes launched at Haystack Observatory.

	ZWD difference (mm)	PWV difference (mm)
ALB-HST	39 (26)	6 (4)
CHH-HST	50 (44)	8 (7)
GYX-HST	21 (26)	3 (4)

In the United States the primary source of radiosonde data is the National Weather Service (NWS). In recent years the principal sonde used by the NWS has been manufactured by VIZ Corporation. Because of linearity problems with the sensor, combined with errors in the treatment of the data by the NWS (Wade, 1994), the reported relative humidity does not go below ~15%. For the comparisons reported here only the data above the boundary layer are affected by this problem and thus the contribution to the difference in ZWD is negligible. Of more concern is the difference seen in the relative humidity mid-range. Fortunately on August 25 at 1200 UT (DOY 237.5) the same model of Vaisala sonde was launched at Lincoln Laboratory, ~25 km from Haystack, simultaneously with the Haystack and NWS sondes. The relative humidity as a function of pressure for the five sondes is shown in Figure 3.

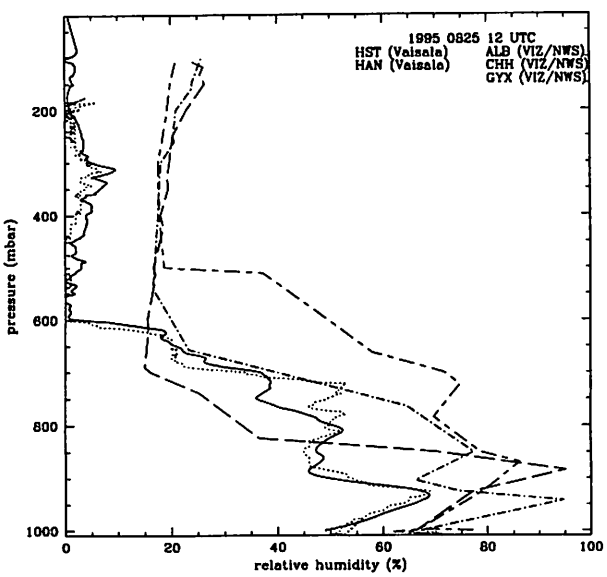

Figure 3. The relative humidity - pressure relation for radiosondes launched 1995 August 25 1200 UT (DOY 237.5) for the three NWS sites (VIZ sondes) nearest Haystack Observatory and for Vaisala sondes launched at Haystack Observatory and at Lincoln Laboratory, ~25 km away. HST (solid) and HAN (dots) are Vaisala RS-80 sondes from Haystack Observatory and Lincoln Laboratory, respectively. ALB (long dash), CHH (dot-dash) and GYX (- --) are VIZ sondes launched and analyzed by the NWS

In addition to the failure of the NWS/VIZ sondes to report the very low relative humidity (RH) above 600 mb level, there is a difference of about 20% through the boundary layer. This is not likely to be a local phenomena since the NWS sondes are uniformly spaced around the Haystack/LL sites, and the two Vaisala sites are separated by almost 20% of the distance to the NWS sites. Wade (1996, private communication) reports that there is evidence that the Vaisala sondes report RH ~4% low in mid- to high RH conditions, but the discrepancy observed here is much larger. England, Schmidlin, and Johansson (1993) flew Vaisala, VIZ and AIR sondes attached to the same balloon. They observed a larger difference (25% - 30%) at low humidity (above ~8000 m altitude), but a difference of only ~10% relative humidity above 80%.

Although radiosondes are considered the standard of accuracy of PWV measurements by the NWS, the large systematic differences between sonde results must be included in the uncertainty of the accuracy of measurements of ZWD.

GPS

Two types of GPS antenna were used, but perhaps more importantly, the antennas were mounted in significantly different environments, including tripod on a flat roof, tripod on the peaked roof of a wood house, steel tower, small pole over metal roof, and concrete pillar with metal support (FLINN monument). An important result from this measurement campaign is illustrated in Figure 4 which shows the dependence of the estimated height of four of the antennas on the minimum elevation of data included in the solution. These results were obtained using point-positioning with the GIPSY-OASIS II software. The ionosphere-corrected phases observables were used, and receiver clock, site position, and troposphere zenith wet delay were estimated. The zenith hydrostatic delay was calculated from the pressure at each site and mapped to the line-of-sight using NMFH (Niell, 1996). NMFW was used for the ZWD partials.

If the estimated height is not independent of the minimum elevation, an unknown bias will affect all solutions because of the changing satellite coverage with time (Elósegui et al, 1995). Similarly, the estimated ZWD will be affected temporally as changes occur in the minimum elevation of the satellites in view during the (effective) sample interval of the atmosphere estimate.

FIRE used an Ashtech 700718B antenna which was mounted above a flat metal roof; the other 7018B was located atop a 13 m amateur radio tower and suffered the same elevation dependence at all elevations (within 1.5 times the formal height uncertainty of ~3 mm at 5° and 14 mm at 30°), suggesting that the extreme elevation dependence (200 mm total height change) is dominated by the antenna and not by the mount. Of more serious concern are the different elevation dependencies exhibited by the Dorne-Margolin choke-ring antennas. The three illustrated in Figure 4 represent three types of mounting.

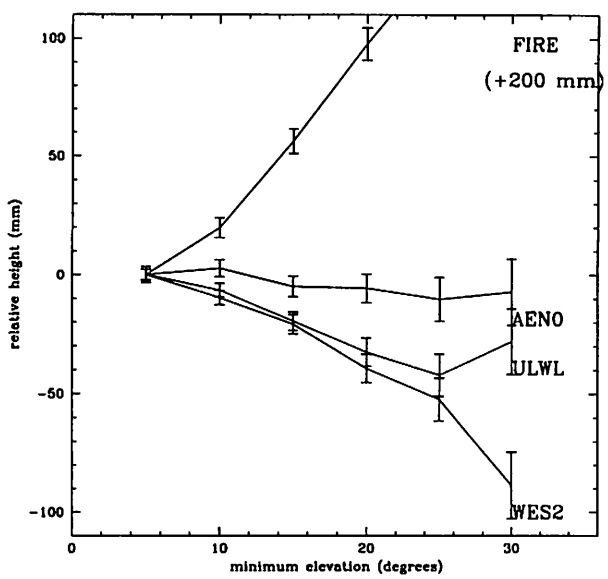

Figure 4. The dependence of estimated antenna height on minimum elevation of included data for four sites. FIRE is an Ashtech 7018B, and the other three are Dorne-Margolin antennas with choke rings. AEN0 and WES2 are manufactured by AOA. ULWL is manufactured by Ashtech and was covered by the radome available from Ashtech.

WES2 is attached to a metal supporting beam located on the top of a 10 m steel tower. AEN0 has a standard tripod/tribrach mount, but it was installed on the peak of the roof of a wood house. ULWL was also mounted on a standard tripod/tribrach but on a flat, rock-covered roof; in addition this antenna was covered by the radome available from Ashtech for the choke-ring antenna, which also has an effect on the height as a function of elevation (Niell et al, 1996). Elósegui et al (1995) demonstrated that the immediate environment of the antenna can have a significant effect on the estimated position and ZWD, and this is evident in Figure 4. The change in ZWD is approximately -0.4 times the change in height. Thus for any period during which the minimum visible satellite elevation was at least 30°, the zenith wet delay at WES2 would differ from that estimated with satellites visible to 5° by as much as 35 mm. This can be seen in Figure 5 in which the ZWD estimates for 5° have been subtracted from the 15° estimates for site WES2 for DOY 236. The average difference in ZWD between the two elevation cutoffs represents a bias of over 1 mm of PWV, and there are changes in difference of over 6 mm of PWV in less than an hour. By contrast, for AEN0, which exhibited the least change in height with change in elevation cutoff, the mean difference in ZWD for 15°-5° minimum elevation was 1.9 mm with a standard deviation of only 3.9 mm. This supports the contention that reducing the elevation dependence will improve the repeatability.

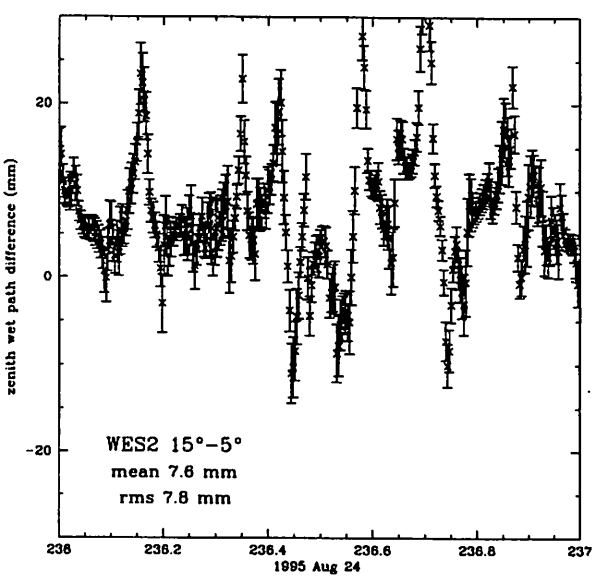

Figure 5. The difference in ZWD estimates for site WES2 between 15° and 5° minimum elevation solutions for DOY 236.

Although not shown, sites with similar mounts are found to have elevation dependencies that are similar. Thus it might be possible to find an environment, such as for AEN0, that would minimize the elevation dependence of the estimated parameters.

The precision of GPS measurement of ZWD can be evaluated by comparing results from MHR0, WES2, and WFRD, despite the differences in their supporting structures, since the elevation dependence

of the ZWD estimates is very close. The three sites are separated by a maximum of ~1 km and should have very similar amounts of ZWD. The average and standard deviation of the differences between these sites are given in Table 2. The biases and standard deviations between the sites are less than ~1 mm of PWV.

Table 2. The average and standard deviation of the differences in zenith wet delay estimates between the GPS antennas at MHR0, WES2, and WFRD using data down to 5° elevation

	Avg ZWD diff (mm)	Std.dev (mm).
WES2-MHR0	4.4	6.2
WFRD-WES2	1.2	4.8
WFRD-MHR0	5.5	6.8

COMPARISON OF TECHNIQUES

The averages of the difference in ZWD over the fifteen common days of observations with the radiosondes, the WVR, and GPS data from MHR0 are given in Table 3 .

Table 3. The average and standard deviation of the differences in zenith wet delay estimates between water vapor radiometer (WVR), the GPS antenna at MHR0 using data down to 5° elevation, and Vaisala RS-80 radiosondes (RS) launched at Haystack Observatory.

	Avg ZWD diff (mm)	Std.dev (mm).
WVR - GPS	6	9
GPS - RS	12	14
WVR - RS	18	13

In terms of PWV, the WVR registered ~1 mm higher on average than the GPS measurements, and the GPS was ~2 mm higher than the radiosondes. The WVR-GPS difference is well within the predicted uncertainties of the WVR and the unknown bias of the GPS results, and the radiosondes do not differ significantly more than the differences observed between the Haystack and NWS sondes.

As seen in Figure 1, however, expressing the differences as a bias does not address the question of linearity. The Vaisala sondes differ systematically with respect to the NWS VIZ sondes as a function of the total wet delay. A similar problem between the WVR and GPS results can be seen in Figure 6 in which the ZWD estimates agree near 0 and 24 hours but differ near the middle of the day by ~20 mm.

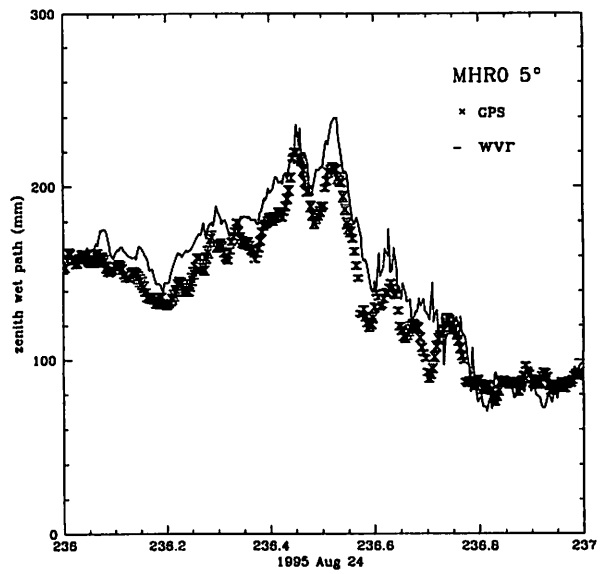

Figure 6. Zenith wet delay measured by WVR and by GPS at MHR0. The sites are separated by ~200 m horizontally and 6 m vertically. The minimum elevation for the GPS estimates is 5°.

DISCUSSION

Biases of measured PWV greater than 1 mm have been demonstrated for both the radiosondes (Vaisala compared to VIZ) and GPS (for different minimum elevation cutoffs). Comparison of different WVRs in side-by-side tests (Kuehn et al, 1993; Elgered et al, 1993) indicate that the level of agreement is no better than ~1 mm of PWV. Thus there does not appear to be any technique that can claim to measure PWV to better than 1 mm.

Duan et al (1996), in a 14 day campaign to compare WVRs and GPS, find biases of ~0.1 mm of PWV with RMS differences of ~1.2 mm. A minimum elevation of 15° was used in the GPS analysis. Given the results demonstrated above, however, such good agreement must be considered fortuitous.

Acknowledgement: We would like to thank Miranda Chin, Jim Davis, Tom Herring, Jan Johansson, Bob King, Gerry Mader, Pratap Misra, and Mike Pratt for the loan of GPS receivers; Tom Caudill, Artie Jackson, and Frank Colby for meteorological data and discussions; and Karl Buchmann for assistance with data acquisition and analysis. A.E.N. was supported by NASA grants NAS5-32353 and NAG5-1906. A.J.C. and C.A.R. were supported by a grant from the Lincoln Laboratory A.C.C. Committee.

REFERENCES

Duan, J., et al, GPS Meteorology: Direct Estimation of the Absolute Value of Precipitable Water, J. Appl. Meteor., 35, 830-838, 1996

Elgered, G., J.L.Davis, T.A.Herring, and I.I.Shapiro, Geodesy by radio interferometry: Water Vapor Radiometry for estimation of the wet delay, J. Geophys. Res., 96, 6541-6555, 1993.

Elósegui, P., J.L. Davis, R.T.K. Jaldehag, J.M. Johansson, A.E. Niell, and I.I. Shapiro, Geodesy Using the Global Positioning System: The Effects of Signal Scattering on Estimates of Site Position, J. Geophys. Res., 100, 9921-9934, 1995.

England, M.N., F.J. Schmidlin, and J.M. Johansson, Atmospheric Moisture Measurements: A Microwave Radiometer - Radiosonde Comparison, IEEE Trans. Geosci. Remote Sensing, 31, 389-398, 1993

Kuehn, C.E., G. Elgered, J.M. Johansson, T.A. Clark, and B.O. Ronnang, A Microwave Radiometer Comparison and Its Implication for the Accuracy of Wet Delays, in Contributions of Space Geodesy to Geodynamics: Technology, Vol. 25, David E. Smith and Donald L. Turcotte, eds., 1993.

Niell, A. E., R. W. King, S. C. McClusky, and T. A. Herring, Radome effects on GPS height measurements with choke-ring antennas, Trans. Amer. Geophys. Un., May, 1996.

Niell, A.E., "Global mapping functions for the atmosphere delay at radio wavelengths", J. Geophys. Res., 101, 3227-3246, 1996.

Wade, C.G., and B. Schwartz, Radiosonde humidity observations near saturation, 8th Symposium on Meteorological Observations and Instrumentation, 44-49, Am. Met. Soc., Anaheim, CA, Jan 17-22, 1993

Wade, C.G., An evaluation of problems affecting the measurement of low relative humidity on the United States radiosonde, J. Atmos. Oceanic Technol., 11, 687-700, 1994

Strategies for Spatial and Temporal Extrapolation and Interpolation of Wet Path Delay

Per O. J. JARLEMARK and T. Ragne CARLSSON

Onsala Space Observatory, Chalmers University of Technology, S-439 92 Onsala, Sweden

Abstract. The excess path delay due to the atmospheric water vapor, the wet delay, can be derived from water vapor radiometer (WVR) measurements. These measurements are not always in the directions of the VLBI sources, and need for methods to extrapolate and interpolate wet delay measurements are therefore obvious. We present and evaluate three different wet delay estimation methods. Two methods, the gradient method and turbulence method, uses the directional information in the data, while the third method does not. The turbulence method yielded the smallest RMS estimation errors in all investigations performed. The sizes of the errors from this method and the gradient method are, however, comparable when used for estimating the wet delay within and just outside the elevation range covered by the measurements. On the other hand, when the gradient method was used for estimating the wet delay at the elevation angle 23.6° from data acquired at and above the elevation angle 41.8° the RMS error was 5.5 mm, while the RMS error from the turbulence method was 2.9 mm. The algorithm used in the VLBI analysis software SOLVE to correct for the wet delay using external data is also evaluated. We found that it is easy to improve the performance of the existing algorithm when data from a WVR running in a sky scanning mode is used.

1 Introduction

The objectives of this study is to evaluate means of estimating the propagation delay due to the atmospheric water vapor, the "wet delay," at a specific time epoch in a specific direction from a set of measurements acquired in different directions at different times. This is of interest, *e.g.*, when external calibration of the wet delay in VLBI analysis is performed, since the external data is not always acquired in the direction of the radio source. A water vapor radiometer (WVR) is in general not able to measure the amount of water vapor at lower elevation angles than, say, 20° due to its large beam width. This complicates its use in VLBI sessions where numerous observations of sources at lower elevations are made. There can be other reasons why a WVR is not following the VLBI schedule. The WVR at the Onsala Space Observatory is continuously measuring in a multiplicity of directions within some minutes in order to get a good picture of the spatial variations in the wet delay. It is sometimes running in this scanning mode also under VLBI sessions.

We have studied two different estimation methods which use the directional information in the data. The first method searches for spatial gradients within the data [*Davis et al.*, 1993], and the second method is a statistical description which originates from turbulence theory [*Treuhaft and Lanyi*, 1987] yielding covariances between different wet delay values [*Davis*, 1993]. For comparison we have also used linear regression in time regardless of the direction in which data have been acquired. Using three different time series of WVR measurements we have investigated the ability of these methods to extrapolate the wet delay spatially, by which we mean estimate the wet delay at low elevation angles from high elevation data, and interpolate, *i.e.*, estimate the wet delay within the elevation range covered by the measurements.

The turbulence theory method can also be utilized in theoretical evaluations of different wet delay estimation schemes. Using this we have analyzed how well the wet delay values acquired at elevation angles at and above 23.6° can be extrapolated to elevations down to 6°. We have also calculated a theoretical performance of the selection principles used by the VLBI analysis software package SOLVE [*Ma et al.*, 1990] when external calibration of the wet delay is undertaken.

2 Estimation Methods

We will compare three different estimation methods for the wet delay. When using these methods we scale the wet delay values, ΔL, from any elevation angle ϵ, azimuth angle ϕ, and time t in order to get the equivalent zenith wet delay ΔL_z:

Presented at the 11th Working Meeting on European VLBI for Geodesy and Astrometry, Onsala, Sweden, 1996

$$\Delta L_z(\epsilon,\phi;t) \stackrel{\text{def}}{=} \frac{1}{m(\epsilon)}\Delta L(\epsilon,\phi;t) \tag{1}$$

where the mapping function, $m(\epsilon)$, is the average quotient between a wet delay measurement acquired at the elevation angle ϵ and one acquired in zenith. The equivalent zenith wet delay yields, loosely speaking, what the wet delay would have been in zenith if the measurement had been taken in a homogeneous atmosphere. In the following the wet delay is given as its equivalent zenith values if not otherwise stated.

2.1 The Gradient Method

Davis et al. [1993] has presented a model describing spatial and temporal variations in the zenith wet delay:

$$\Delta L_z(\epsilon,\phi;t) = \Delta L_z^\circ(t) + \cot\epsilon\,[1 - \chi_s \csc^2\epsilon]\cdot[G_n(t)\cos\phi + G_e(t)\sin\phi] \tag{2}$$

where ΔL_z° is the zenith wet delay for zero horizontal gradients, and G_n and G_e are the north and east components of what we will call the "wet-delay gradient." χ_s is the total refractivity at ground surface. We have used the value 300 ppm for χ_s in the following. This model can be derived from the assumption that the "wet refractivity," the refractivity component due to water vapor, has a constant horizontal gradient at each height.

When we use (2) for interpolation and extrapolation we solve for the three parameters ΔL_z°, G_n and G_e from a set of WVR measurements. Normally we allow for a linear change with time in the three parameters, thus giving us a total of six parameters. These parameters can then be used for calculating a wet delay estimate in any direction using (2).

2.2 The Turbulence Method

According to a turbulence theory model the wet refractivity χ_w at a position $\mathbf{r}$ and a position $\mathbf{r} + \mathbf{R}$ differs according to the law

$$< [\chi_w(\mathbf{r}+\mathbf{R}) - \chi_w(\mathbf{r})]^2 >= C_\chi^2 \cdot R^{2/3} \tag{3}$$

where <> indicates expectation values, C_χ is a constant and $R = |\mathbf{R}|$ [*Treuhaft and Lanyi*, 1987]. Together with the assumption that the spatial turbulent structure is passing a site with a constant speed, thus creating variations in time, one can calculate the covariances between the wet delay values in different directions at different time epochs in a manner presented by *Davis* [1993]. We used the same model parameters as *Davis* [1993] with the modification that instead of assuming a certain wind speed and direction we averaged the covariances resulting from twelve different wind vectors with directions separated 30°, all with a speed of 8 m/s.

Using the turbulence theory we can determine the covariance matrix, $C_{m,m}$, between all measured wet delay values during a specified time interval, and the covariance matrix, $C_{m,e}$, between the measured values and the estimated. From these covariances we can form good estimates as linear combinations of the measured wet delay values $\Delta L_z(\epsilon_i,\phi_i;t_i)$

$$\widehat{\Delta L_z}(\epsilon,\phi;t) = \sum_i a_i \cdot \Delta L_z(\epsilon_i,\phi_i;t_i) \tag{4}$$

where a_i are the weights of the wet delay values. A Best Linear Unbiased Estimator (BLUE) of the wet delay can be deduced [*Kay*, 1993]. It is the optimal linear combination according to (4) in the sense that the mean square difference between the estimated and the true wet delay is minimized under the condition that the sum of the weights a_i is 1 (we have no *a priori* information telling us that the estimated wet delay should be larger or smaller than the wet delay in any other direction). The optimal weights written in vector form $\mathbf{a}_{BLUE}$ become as follows

$$\mathbf{a}_{BLUE} = C_{m,m}^{-1}\cdot C_{m,e} + \frac{(1 - C_{m,e}^T \cdot C_{m,m}^{-1}\cdot \mathbf{s})\cdot C_{m,m}^{-1}\cdot \mathbf{s}}{\mathbf{s}^T \cdot C_{m,m}^{-1}\cdot \mathbf{s}} \tag{5}$$

where $\mathbf{s}$ is a vector of ones with the same length as $\mathbf{a}_{BLUE}$.

2.3 Linear Regression in Time

We have also made least squares fit of the zenith wet delay data to a straight line in time, over a specified time interval, regardless of the direction in which data were acquired. This linear model was then used for estimating the wet delay at other time epochs in any direction.

3 Method Evaluation

In order to evaluate the methods described above we used three data sets from the Onsala WVR acquired in January, May and September 1994. Figure 1 shows the three time series. A measurement procedure according to Figure 2 was used. It starts with a 360° azimuthal scan where the elevation angle is 30°. Then follows four "tip-curves," elevation scans starting at an elevation angle of 23.6° going over zenith and ending at the elevation 23.6° in the opposite azimuthal direction. This procedure, consisting of 64 measurements, takes 10 minutes and is repeated continuously.

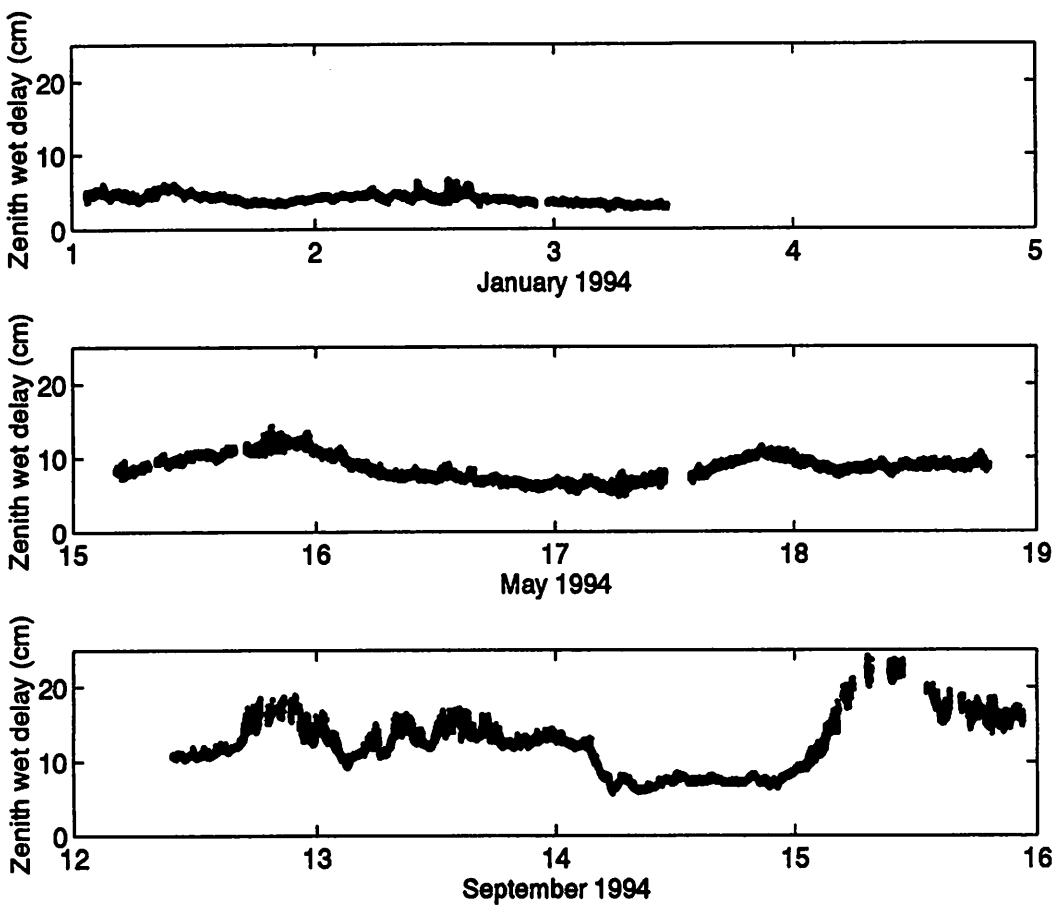

Figure 1: The three data sets of wet delay measurement utilizing the Onsala WVR which are analyzed in this paper.

We investigated the performance of the methods when used for spatial extrapolation. Two cases was tested: A) estimating the wet delay values at the elevation angle 23.6° from data acquired at the elevation 30° and above, and B) estimating the wet delay values at the elevation angle 23.6° from data acquired at the elevation 41.8° and above. In both cases we took all the measurements acquired at the elevation angle of 23.6° in the three data sets. For each of these measurement we estimated the wet delay in the current direction at the current time epoch from the appropriate

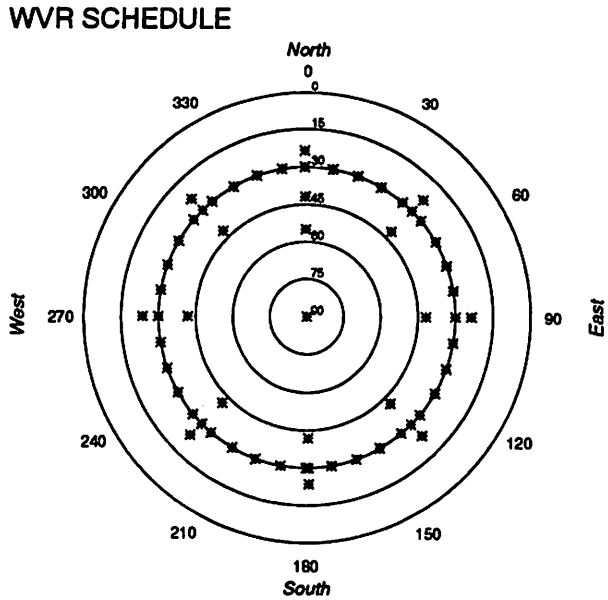

Figure 2: A polar plot describing the WVR measurement procedure used for the data sets in this paper. It starts with a measurement every 10° in azimuth at an elevation angle of 30°. Then follows four elevation scans each starting at the elevation 23.6° in one azimuthal direction, going over zenith, and ending at the elevation 23.6° in the opposite azimuthal direction.

measurements in a ±10 minute window around the current time epoch. The ability of the methods to interpolate data was also investigated. Again two cases was tested: C) estimating the wet delay values at the elevation angle 30° from data acquired at any elevation angle, and D) estimating the wet delay values at the elevation angle 41.8° from data acquired at any elevation angle. We took all the measurement acquired at the elevation angle of interest (30° and 41.8°) in the three data sets. For each of these measurements we estimated a corresponding wet delay value using the data in a ±10 minute window around the current measurement. The RMS errors of the estimates yielded by the three estimation methods was calculated for all four cases.

If we assume that the turbulence theory model is a correct statistical description of the wet delay variations, we can use this model for calculating theoretical RMS errors of the estimates. This can be done for the BLUE estimates and, since the estimates according to the gradient method and the linear regression in time both can be written as linear combinations of the measurements as in (4), the theoretical RMS errors of their estimates can also be calculated using the covariances mentioned above.

The RMS difference between the estimates and the measurements are plotted as the filled bars in Figure 3. It is seen that the turbulence method (BLUE) yield the smallest RMS errors in all four cases. The gradient method yield relatively small errors when used for interpolation (case C and D) and "short extrapolation" (case A). In the "long extrapolation" from elevations at and above 41.8° to 23.6° (case B) the errors yielded by the gradient method are significantly larger than the errors resulting from the other two estimation methods, a result which we will discuss below.

We have plotted the theoretically calculated RMS as the unfilled bars in Figure 3. Even though these bars in general differ slightly from the corresponding bars based on the measurements they present approximately the correct relative size of the errors of the three methods in all four plots.

4 Extrapolations to Low Elevation Angles

We have used the statistical description given by the turbulence theory model in order to calculate how well the three methods theoretically will estimate the wet delay at very low elevation angles. We assumed that we had measured with

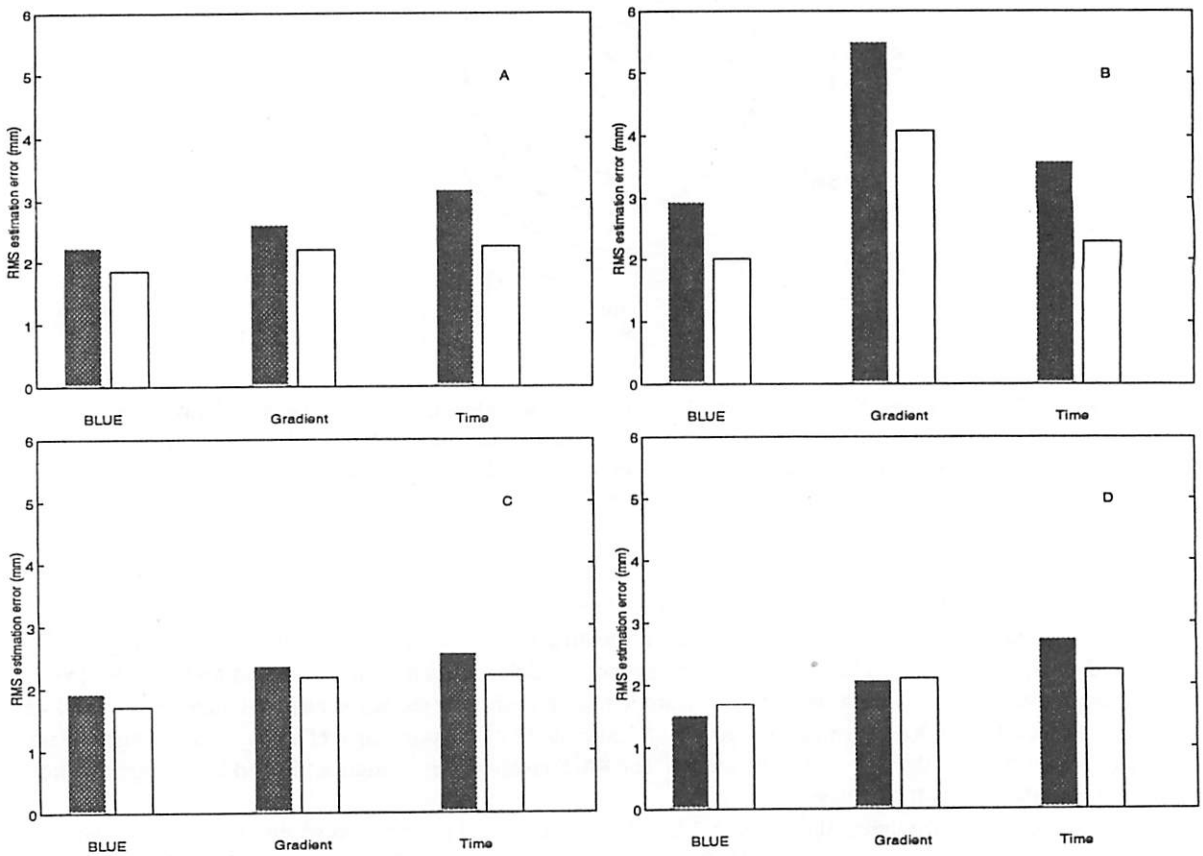

Figure 3: Evaluation of the RMS difference between the measured and estimated wet delays at some elevation angles are shown by the filled bars. In the upper left graph (A) all measurements with an elevation angle of 23.6° are compared with estimates based on the measurements acquired at elevation angles of 30° and more. The upper right graph (B) shows the RMS errors for the same data points ($\epsilon = 23.6°$) when estimated from measurements at elevation angles of 41.8° and more. The lower left graph (C) shows the errors for the points with ($\epsilon = 41.8°$) when estimated from all other data except for that particular measurement. The lower right graph (D) shows the errors for the points with ($\epsilon = 30°$) when estimated from all other data except for the actual measurement. The theoretically calculated RMS errors are shown by the unfilled bars.

the above described WVR procedure, and calculated the theoretical RMS error when estimating the wet delay having an azimuth angle of 180° and elevation in the range 6° to 23° at a time epoch when a new WVR cycle is starting. Data in a ± 10 minute window, *i.e.*, data from the cycle just starting and the previous one, were used in this calculation. The resulting errors are shown in Figure 4. Again we can see that the turbulence theory predicts that the estimates from the gradient method becomes worse than the linear regression in time at long extrapolations to low elevations.

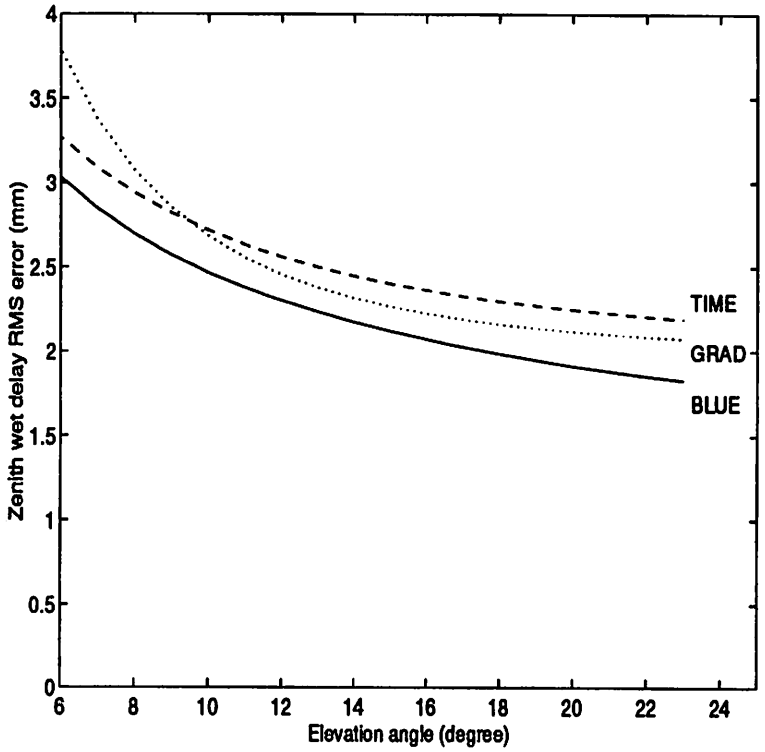

Figure 4: Theoretically calculated RMS errors when estimating the wet delay at elevation angles in the range 6° to 23° at an azimuth angle of 180°. Two ten minute cycles of WVR data acquired at elevation angles of 23.6° and higher was used for each estimation. The calculations are based on the assumption that a turbulence theory model gives a true statistical description of the variations. We used three different estimation methods: one from turbulence theory (BLUE), a gradient estimation procedure (GRAD), and linear regression in time (TIME).

5 The SOLVE Selection Principles

When external calibration of the wet delay is used in the SOLVE VLBI analysis software package [*Ma et al.*, 1990], a subroutine selects which wet delay measurement values to include for each radio source in the correction for the mean wet delay during the time interval of the observation. The wet delay measurements within the time of source observation are selected based on if they are acquired

- within 2° from the direction of the source
- within 7° from the direction of the source
- in zenith
- in any direction

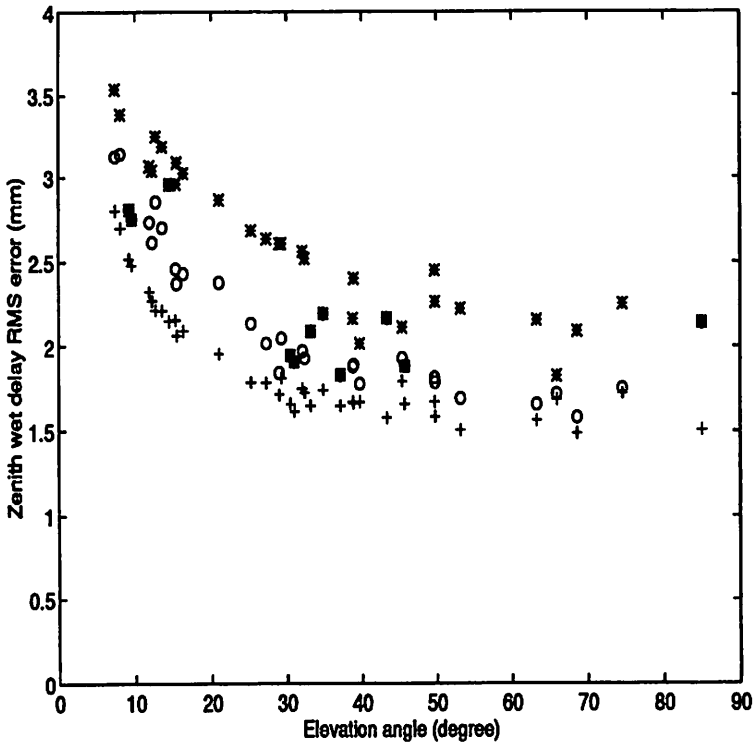

Figure 5: The theoretical RMS errors of the estimated mean wet delay in the direction of the radio sources plotted as functions of the elevation angle of the radio sources. We have used the schedule of the EUROP6-94 VLBI experiment in the calculations, and assumed that the WVR was running in a scanning mode. For clarity we show the errors for just every fifth source in the VLBI schedule. The mean wet delay estimates are from the turbulence method (plus signs), the present SOLVE selection principles (stars), and a modified version of the SOLVE selection principles (circles). The results from the two SOLVE versions coincides in many cases. The calculations are based on the assumption that a turbulence theory model gives a true statistical description of the variations.

Only the data belonging to the non-empty group with highest priority (highest position in this list) are used. The mean wet delay is estimated as the average of the measurements within this group. If no wet delay measurements have been conducted in the time of a VLBI observation the average of the wet delay measurements closest in time before and after the VLBI observation will be used.

We have studied how good the mean wet delay estimates from the algorithm above are when we use data from a WVR running with the procedure described in section 3. We used the schedule from the VLBI experiment EUROPE6 in 1994 and investigated which wet delay measurements SOLVE would have picked for each radio source. Again we used the statistical description from the turbulence theory model to calculate the RMS errors in the estimates of the mean wet delay. The resulting RMS errors yielded by SOLVE are plotted in Figure 5 as a function of the elevation angle of the radio sources. We have also plotted the resulting RMS errors if the optimal (BLUE) linear combination of the measurements were used. In many cases (73 out of 195) there are no measurements within 7° from the direction of the source, but a single measurement in zenith within the observation time. This measurement will then be selected, according to the list of priorities given above, even if the direction of the radio source is far from zenith. We seem to remember that the high priority of the zenith measurements is a remnant from earlier use of WVR data in SOLVE, where an average value of several WVR measurements from different directions was written as if it originated from the zenith direction. In order to find out how large influence these zenith measurements have on the RMS errors we took out this item from the priority list and just grouped the measurements according to the items 1,2 and 4 above. The RMS errors of the estimates yielded by SOLVE if the appropriate subroutine was modified in this way are also

plotted in Figure 5. The overall RMS zenith wet delay error for the optimal linear combination (BLUE) is 1.9 mm, for the present SOLVE estimates 2.6 mm, and for the modified SOLVE version 2.3 mm. We can probably reduce the RMS errors resulting from SOLVE further by tolerating larger angle differences than 2° and 7° in the two groups with highest priority. Few measurements are accepted with these limits, and the errors introduced by these pointing errors are relatively small. Another modification could be not to restrict the averaging of the measurements to just those in the group with highest priority if they are few.

6 Discussion and Conclusions

We have shown that an estimation method based on a turbulence theory model yields lower RMS errors compared to a method which estimates wet delay gradients modeling the wet delay in other directions. This was especially pronounced when the values at significantly lower elevation angles than the ones measured was estimated. The main reason for this is that water vapor is not well mixed with the other constituents of the atmosphere (which give rise to the hydrostatic, or "dry" delay). There are "blobs" of water vapor of any size, and what is estimated as a wet delay gradient from data in a limited range of elevation angles can be features with relatively small spatial extension. The use of the gradient method for extrapolation in this case give exaggerated variations at low elevations.

There are, however, occasions when the gradient description can be expected to perform better than it does in general, *e.g.*, at weather front passages. The model according to (4) might then not produce large enough deviations from the wet delay value in zenith at low elevations in the direction of the gradient. There are obvious front passages in the data set from September 1994. During these periods there are an increased number of time epochs where the gradient method performed better than the turbulence method for the short extrapolations. However also in these periods the turbulence method yielded a better overall performance. Thorough investigation involving wet delay measurements at lower elevation angles than 20° is needed in order to develop criteria of when the gradient method is to prefer.

The main obstacle with the turbulence theory method is that each covariance calculation involves a double integral and is thus relatively time consuming. In its present form we do not consider the method to be useful for "every-day" VLBI analysis, but merely for case studies like, *e.g.*, the evaluation of the algorithm used in SOLVE to add wet delay data to the data base. We are, however, convinced that simplified formulas yielding approximate values for the covariances can be constructed, thus making the computation time reasonable.

References

Davis, J. L., G. Elgered, A. E. Niell, and C. E. Kuehn, "Ground-based measurement of gradients in the "wet" radio refractivity of air", *Radio Sci., 28*, 1003-1018, 1993.

Davis, J. L., "The Effect of Turbulence on Atmospheric Gradient Parameters Estimated from Ground-based Radiometric and Space Geodetic Measurements", *Geophys Res. Lett., 21*, 2183-2186, 1993.

Kay, S. M., *Fundamentals of statistical signal processing: estimation theory*, Prentice Hall International Editions, 1993.

Ma, C., J. Sauber, L. Bell, T. Clark, D. Gordon, W. Himwich, and J. Ryan, " Measurements of horizontal motions in Alaska using very long baseline interferometry", *J. Geophys. Res., 95*, 21991-22011, 1990.

Treuhaft, R.N., G.E. Lanyi, "The effect of the dynamic wet troposphere on radio interferometric measurements", *Radio Sci., 22*, 251-265, 1987.

Update on European Geodetic VLBI Analyses at the Geodetic Institute of the University of Bonn

Axel Nothnagel

Geodetic Institute of the University of Bonn, Nussallee 17, D-53115 Bonn, Germany
E-mail: nothnagel@uni-bonn.de

Abstract. The European fixed station geodetic VLBI network has been producing baseline length and station displacement results for a number of years. In this paper we present the most recent results of these observations. The analysis contains all sessions of the EUROPE series from January 1990 to April 1996.

From the least squares adjustments where station coordinates are treated as arc parameters individual baseline length results are derived which show an unprecedented repeatability. The baseline length evolutions infered from these data have now stabilized at a satisfactory level and the investigations are focused on the repeatability of baseline components and the quality of individual sessions.

A second type of analyses which aims at the determination of station displacement vectors yields more uncertain results. Some logical discrepancies between the baseline length results and the displacement vectors give rise to suspicion concerning the stability of the latter type of least squares adjustments.

1. Introduction

On August 31, 1996 the three year funding of the EC Science Contract SC1*CT920829 to the European Geodetic VLBI members led by the Geodetic Institute of the University of Bonn has come to an end. In the last two years six sessions were scheduled and observed each year as was the target number of the project. Together with the sessions set up prior to the EC project the European Geodetic VLBI network has now observed 28 sessions which employed only observatories on the European continent in various configurations (see figure 1 in Sorgente, 1996, this issue).

At the Geodetic Institute the data was analysed in two different ways. In a first type of solution each experiment was analysed separately in a least squares adjustment estimating station coordinates for each station for the respective epoch except for one reference station. This type of solution permits a detailed analysis of the individual results as will be discussed in a later paragraph. In a second solution the data of all sessions is adjusted jointly estimating for each station the coordinates at a reference epoch and the time derivatives of these coordinates representing continuous station displacements.

The results have reached a high level of accuracy. However, before the final results can be published a number of details will have to be investigated. In the following paragraphs individual peculiarities in the results will be discussed. A detailed description of the data analysis can be found elsewhere (Nothnagel and Campbell, 1993). Only if a different approach has been chosen this will be mentioned at the appropriate item.

2. Discussion of Results

2.1 Baselines Wettzell - Apenin Peninsula

The observation history of the individual baselines is reflected in the plots of the baseline length results. So far the Noto - Wettzell baseline has been observed 19 times (Fig. 1). Until about mid 1994 the baseline length results show a fairly consistent evolution but a sudden baseline length increase of about 10 mm in mid 1994 disturbs the overall picture. Almost identical features are obvious on the Wettzell - Medicina (Fig. 2) and on the Wettzell - Matera baselines (Fig. 6) for the June and August 1994 sessions.

Presented at the 11th Working Meeting on European VLBI for Geodesy and Astrometry, Onsala, Sweden, 1996

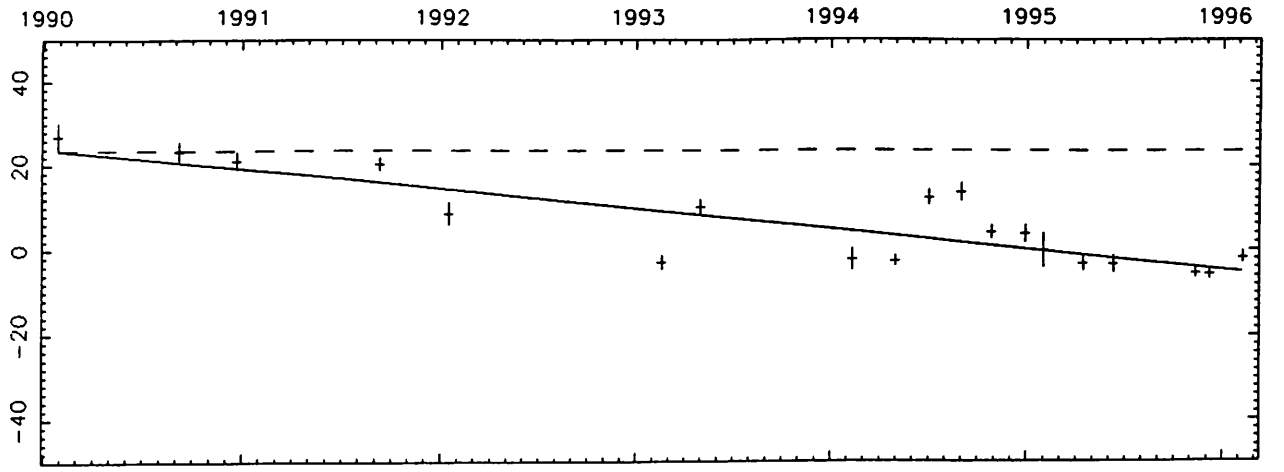

Fig. 1; Baseline Length: Wettzell - Noto, Observed Rate = -4.8 ± 0.8 mm/yr, WRMS = 5.4 mm

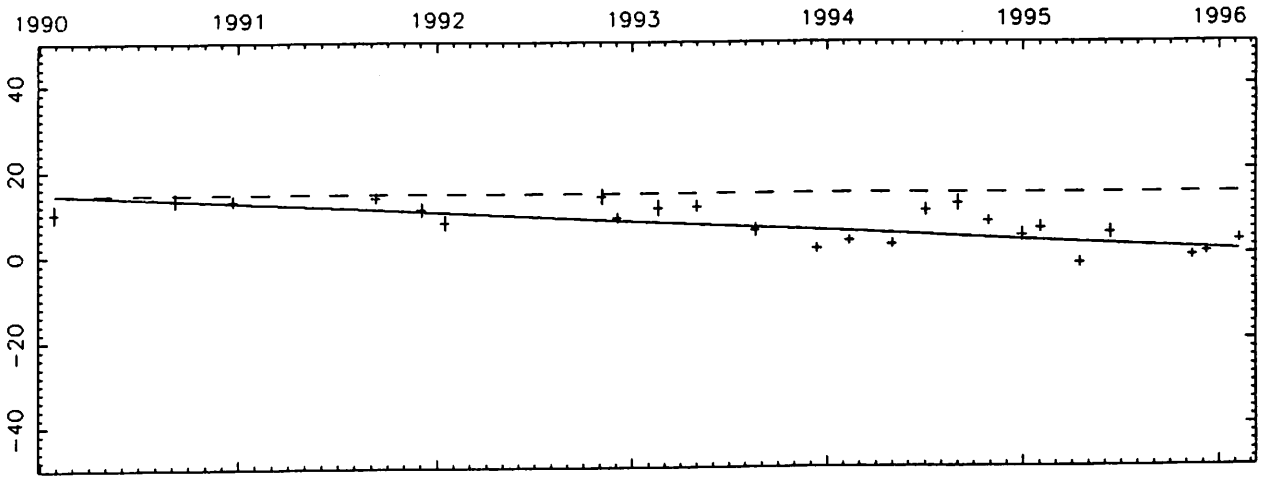

Fig. 2; Baseline Length: Wettzell - Medicina, Observed Rate = -2.3 ± 0.5 mm/yr, WRMS = 3.2 mm

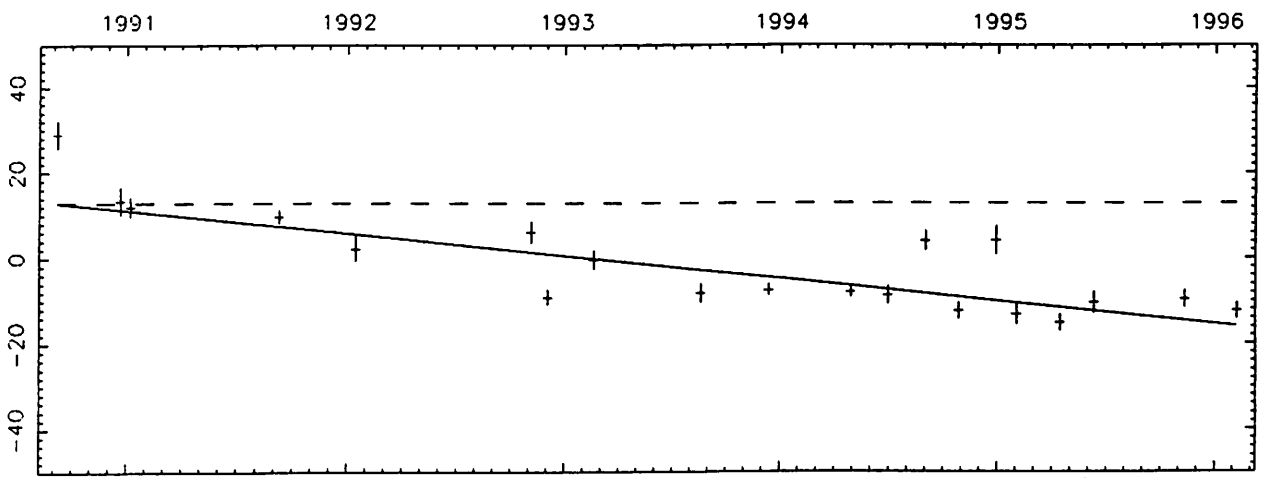

Fig. 3; Baseline Length: Onsala - Matera, Observed Rate = -5.3 ± 0.9 mm/yr, WRMS = 5.4 mm

It is, however, not a Wettzell problem since the Onsala - Noto baseline shows a similar feature though not as distinct. In contrast to this the Onsala - Matera results fit reasonably well for the June session but not for the December one which deviates by about 10 mm, similar to the August session (Fig. 3). Looking at the interlinking baselines one finds that both the Medicina - Matera and Medicina - Noto baselines show a very clean baseline evolution with a 2.7 and 2.8 mm RMS (Fig. 4 and 5). But again the Matera - Medicina baseline displays small deviations from the straight line fit for the August and December sessions.

The baselines perpendicular to the North - South axis formed by the Madrid telescope and the remaining stations also show increased lengths for the epochs mentioned above.

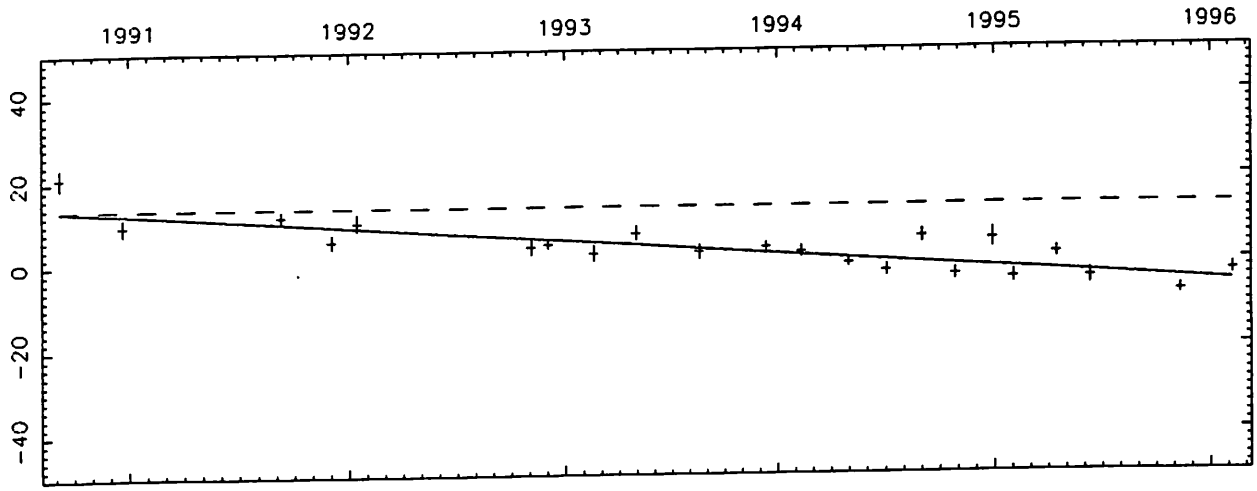

Fig. 4; Baseline Length: Medicina - Matera, Observed Rate = -3.4 ± 0.5 mm/yr, WRMS = 2.7 mm

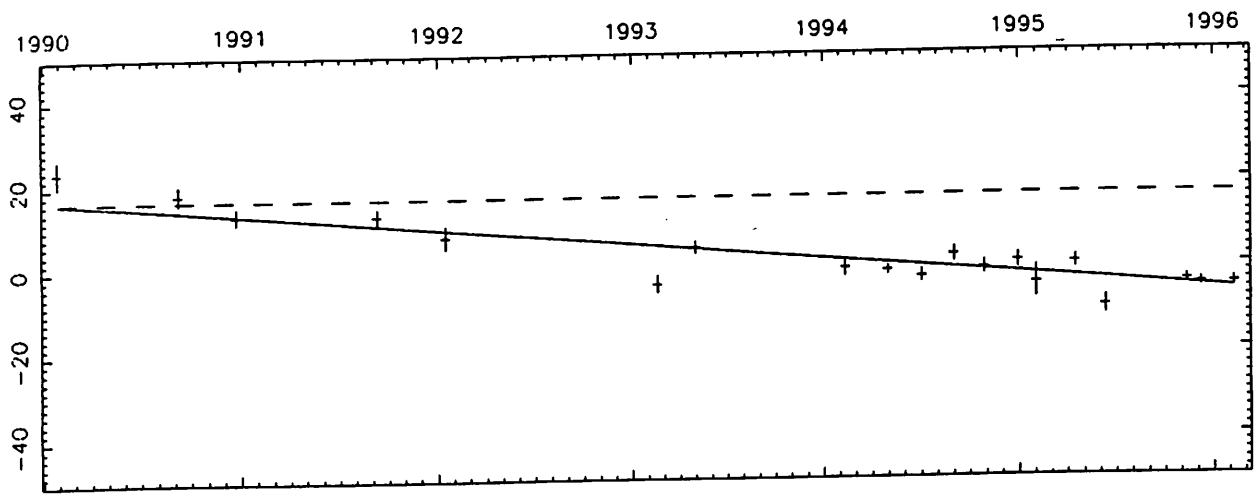

Fig. 5; Baseline Length: Medicina - Noto, Observed Rate = -3.7 ± 0.4 mm/yr, WRMS = 2.8 mm

In an attempt to find out about the reasons of these effects different parameterizations have been tested for the station clocks and tropospheres. While the standard Bonn parametrization aims at a minimal number of parameters the test computations regardlessly introduced new auto-constrained clock and wet tropsphere rate parameters for down to each 60 minute interval. As a result the repeatabilty improved only marginally still featuring the distinct excess lengths in 1994.

The key to the reason for the extended lengths may be found in the baseline height components in a length - transverse - vertical baseline oriented coordinated system (Ryan et al., 1993). In the figures of the baseline height components there are obvious abnormal deviations of some of the 1994 sessions from the general trend. The height variations are of the order of about 25 mm for the June and August 1994 sessions for a great number of baselines peaking at 50 mm on the Madrid - Noto baseline (Fig. 6).

The coherence of the deviations in the length and in the vertical component lead to the conclusion that the troposphere may not be modelled adequately for these sessions. However, one would expect that the troposphere affects the station height components rather than the baseline lengths,

a question which still has to be investigated.

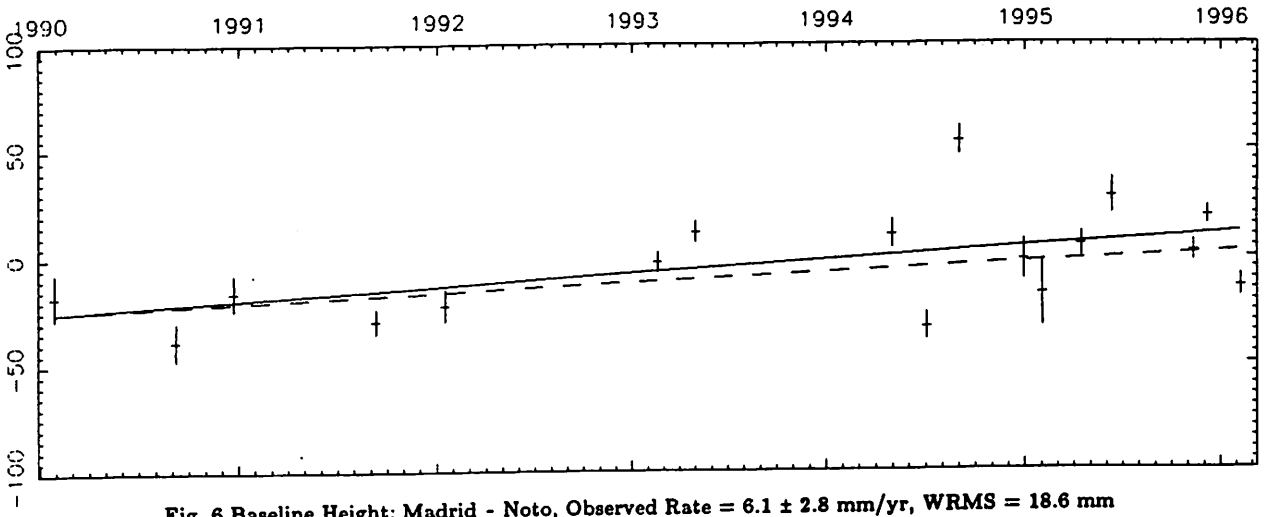

Fig. 6 Baseline Height: Madrid - Noto, Observed Rate = 6.1 ± 2.8 mm/yr, WRMS = 18.6 mm
NUVEL1 Model rate due to definition of origin (Ryan et al., 1993) = 4.6 mm/yr

In order to assess the external accuracy of the VLBI results a comparison has been made with GPS results provided by the Bern GPS group (Brockmann, pers. communication). Figure 7 depicts the results of both series for the Wettzell - Matera baseline with a small offset for better distinction which also represents the excentricities at the observatories. The VLBI data so far produces a baseline rate of -4.3±0.7 mm/year with an RMS of 4.9 mm while the GPS results yield -3.6±0.25 mm/year with an RMS of 2.7 mm. Both results agree pretty well within their formal errors.

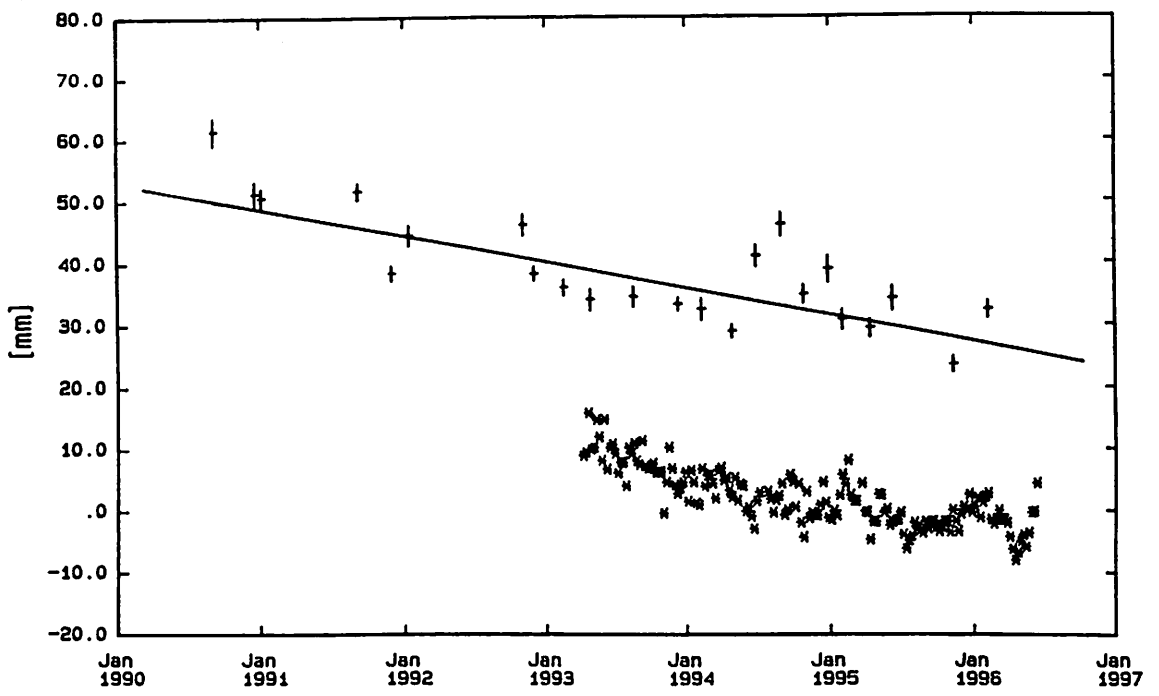

Fig. 7; Baseline Wettzell - Matera, Observed Rate (VLBI +) = -4.3 ± 0.7 mm/yr, WRMS = 4.9 mm
Observed Rate (GPS *) = -3.6 ± 0.25 mm/yr, WRMS = 2.7 mm

Another interesting aspect in the assessment of the quality of the results is the development of the baseline rates while more and more length observations are accumulated. Figures 8 and 9 show the individual rate results as a function of measurements used (solid lines). In addition, the weighted RMS for each of these solutions is displayed in parallel (+). While the rate results seem

to have settled down by early 1993 there is a sharp reduction in the baseline rates at exactly the epoch of the abnormal 1994 sessions with no trend to take up the earlier level. As a consequence the accuracies of the straight line fits as displayed by the RMS values reduce considerably with only a small trend to the better.

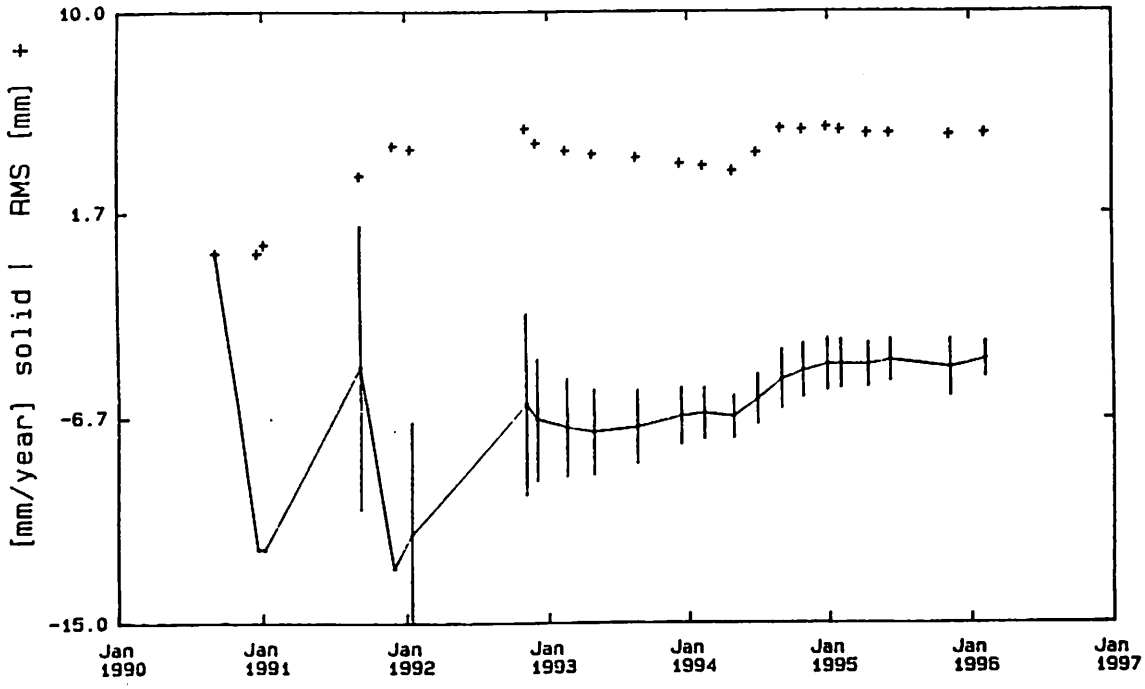

Fig. 8; Baseline Length: Wettzell - Matera, Baseline rate evolution with data up to respective epoch

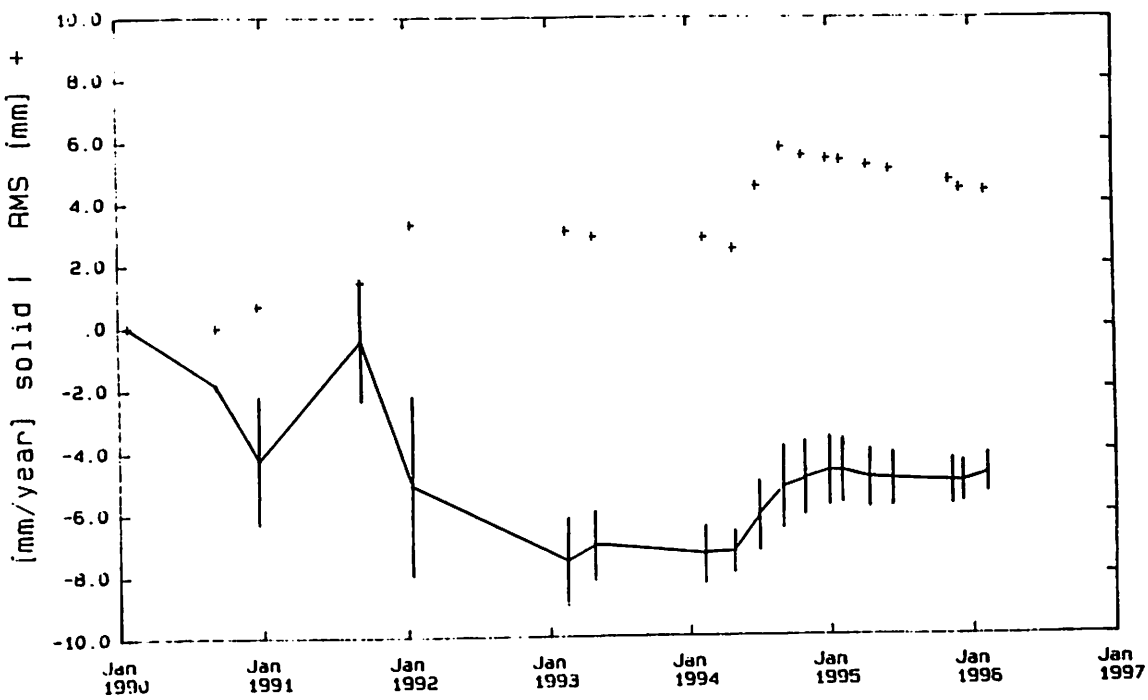

Fig. 9; Baseline Length: Wettzell - Noto, Baseline rate evolution with data up to respective epoch

2.2 Wettzell - Iberian Peninsula

The Madrid - Wettzell baseline length chronology shows a fairly smooth behaviour with a 3.9 mm weighted RMS (Fig. 10). The last 7 sessions display an enormous stability which stands in high contrast to the development of the height results at that time (Fig. 11). It seems that from

early 1994 the scatter in the height results increases continuously, a fact which is not discernible on the Matera - Madrid baseline.

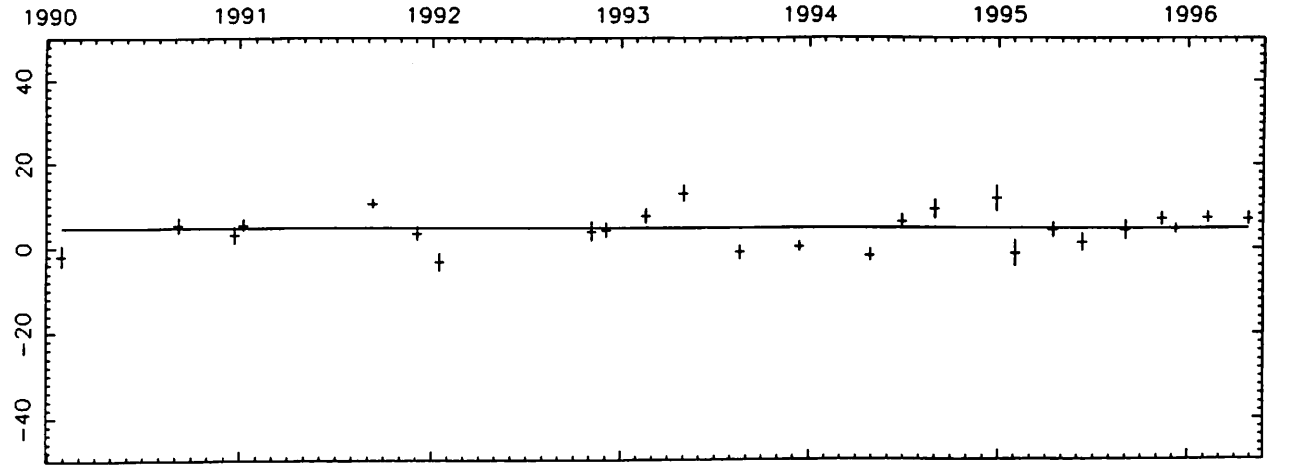

Fig. 10; Baseline Length: Wettzell - Madrid, Observed Rate = 0.0 ± 0.4 mm/yr, WRMS = 3.9 mm

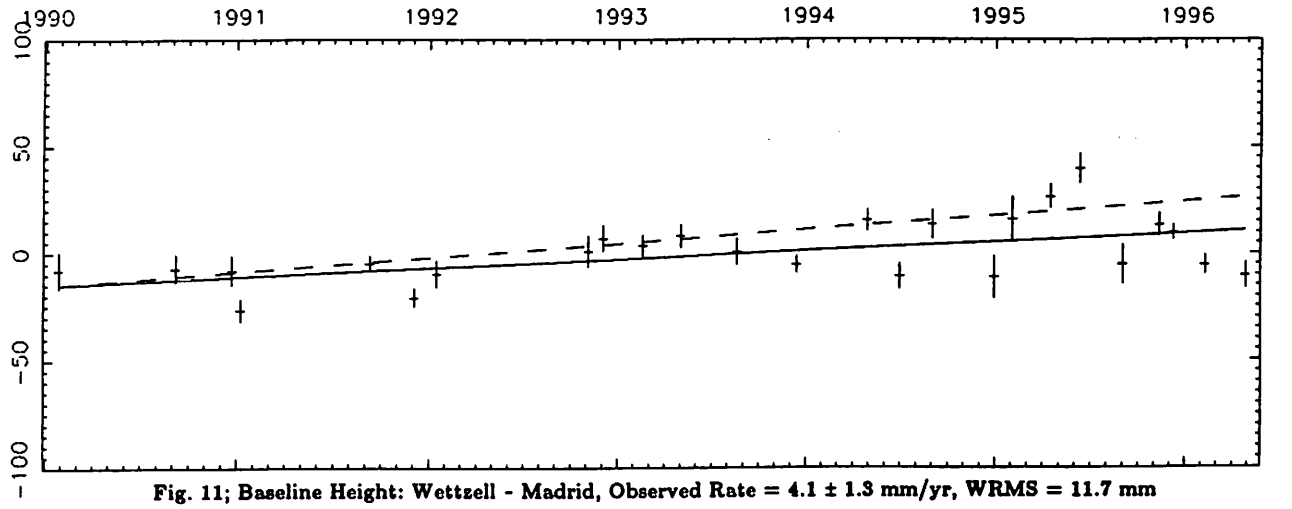

Fig. 11; Baseline Height: Wettzell - Madrid, Observed Rate = 4.1 ± 1.3 mm/yr, WRMS = 11.7 mm
NUVEL1 Model rate due to definition of origin (Ryan et al., 1993) = 6.6 mm/yr

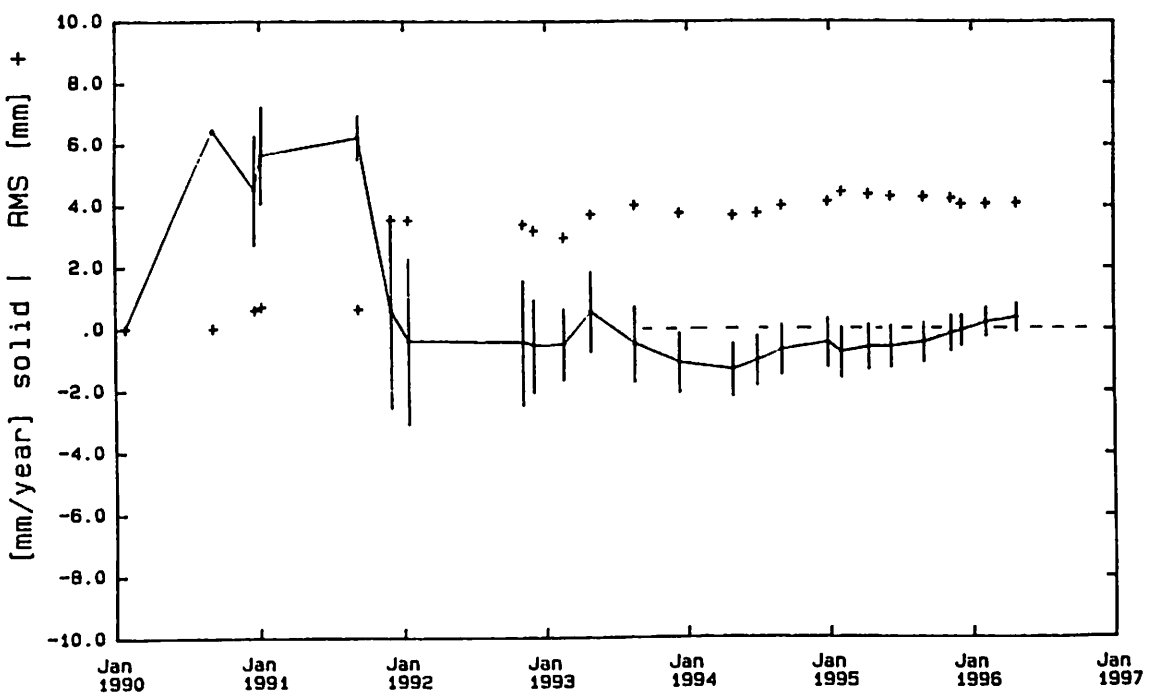

Fig. 12; Baseline Length: Wettzell - Madrid, Baseline rate evolution with data up to respective epoch

Comparing the Wettzell - Madrid baseline length residual plot with its rate development (Fig. 12) it appears that the 1994 sessions have not done any harm to the baseline rate. It seems that any additional session just changes the rate within the uncertainty of the previous values which must be considered as a strong indication that the Madrid station displacement in baseline direction is very small indeed.

Quite interesting is the fact that both the GPS and the VLBI baseline length results exhibit a slight rise in length at the end of the series analysed so far. We are very curious to see the further developments (Fig. 13).

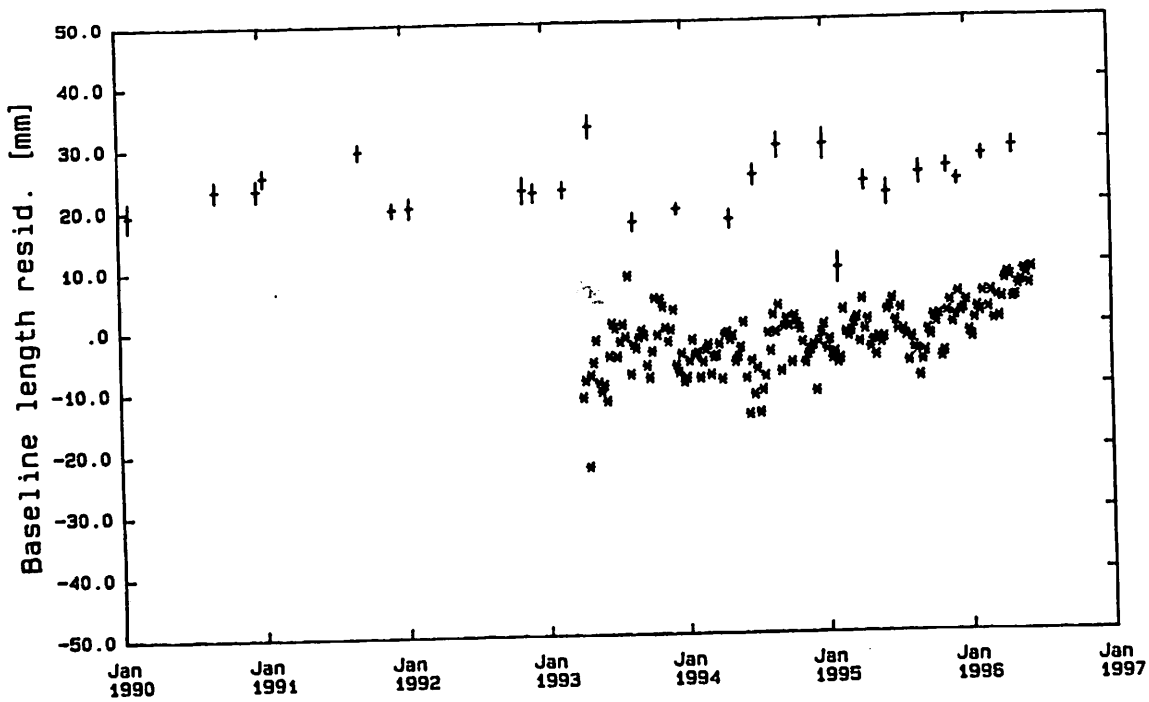

Fig. 13; Baseline Wettzell - Madrid, Observed Baseline Lengths (VLBI +, GPS *)

2.3 Wettzell - Onsala

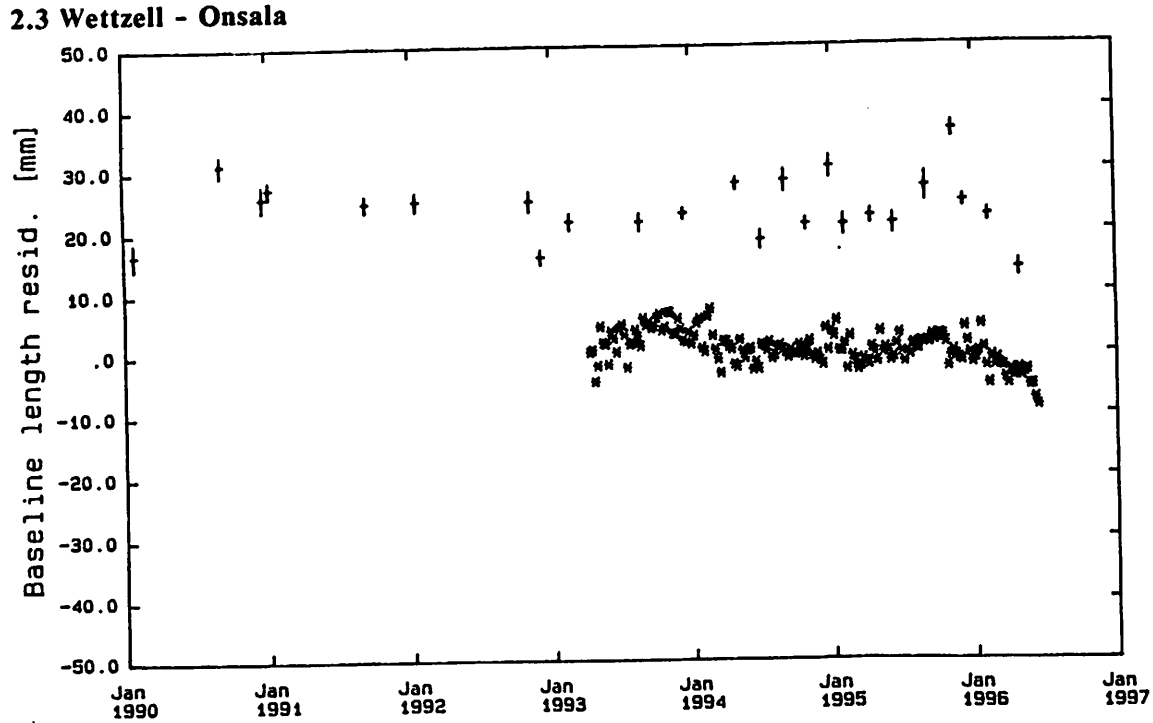

Fig. 14; Baseline Wettzell - Onsala, Observed Baseline Lengths (VLBI +, GPS *)

The Wettzell - Onsala baseline exhibits quite some scatter in the last part of the series. However, most interesting is the comparison with the GPS results in figure 14. Looking just at the last three VLBI sessions it seems that there is an odd decrease in the baseline length which goes in parallel to a decrease in the GPS results.

2.4 Wettzell - Ny Alesund

The Wettzell - Ny Alesund baseline was observed 8 times in the European geodetic VLBI network so far. The baseline length results demonstrate a very good repeatability would there not be one session in August 1995 which is off by 20 mm (Fig. 15). Similar features are present in the transverse and in the height component.

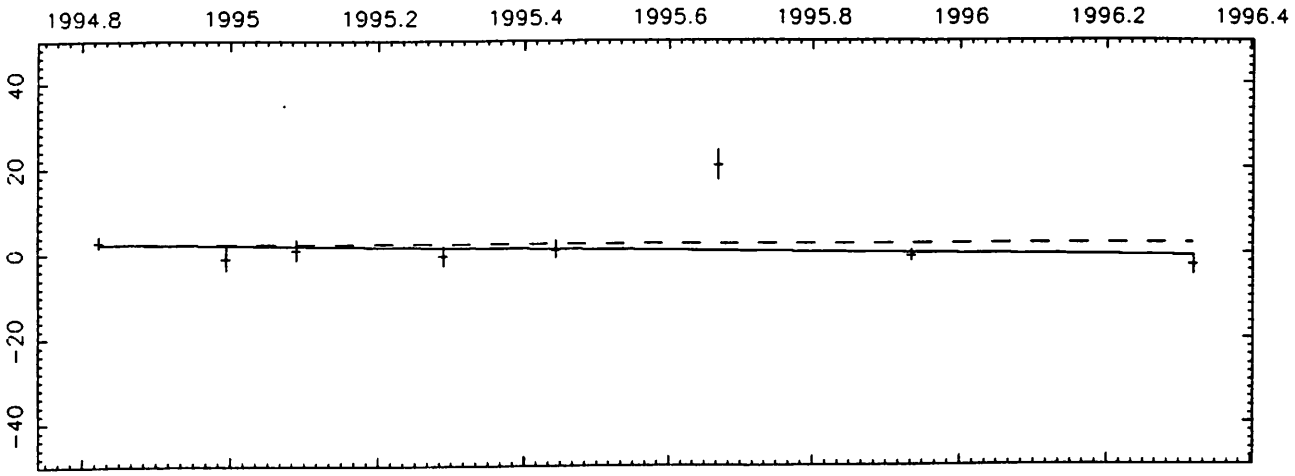

Fig. 15; Baseline Length: Wettzell - NyAlesund, Observed Rate = -2.0 ± 3.5 mm/yr, WRMS = 4.4 mm

Several investigations have been started to find out the reason(s) for this abnormal session. The most probable cause is to be found in the spatial distribution of observations. Figure 16a depicts the individual observations of this session in a stereographic projection of a baseline oriented coordinate system as seen from a fictitious interferometer mid point (Nothnagel and Campbell, 1991).

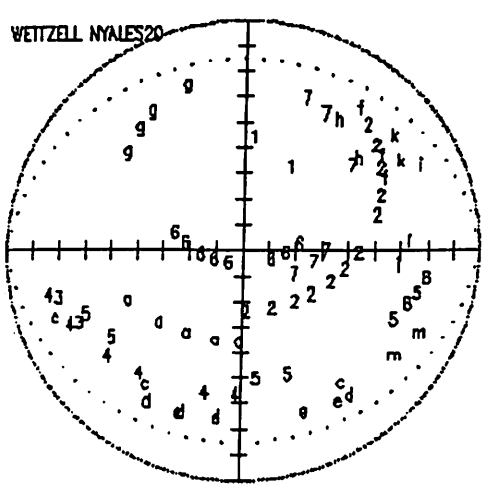

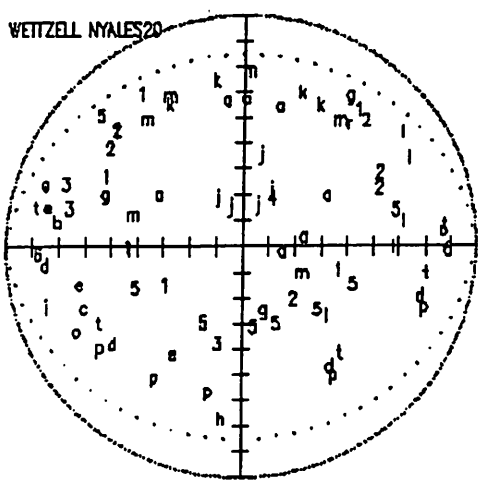

Fig. 16a: Session August 31, 1995;
Baseline Wettzell - NyAlesund: Distribution of Observations as seen from a ficitious interferometer mid point

Fig.16b: Session April 12, 1995

It is immediately obvious that there is a lack of observations in the 4th quadrant and that the observations are distributed in clumps. In sharp contrast to this is the distribution of the observations on this baseline for the previous sessions (Fig. 16b). Although the number of observations is fairly similar (76/81) the distribution looks more homogeneous in the latter. From this it can be expected that the estimation of the troposphere parameters has some deficiencies in the August session thus indeed causing the extraordinary behaviour of the results.

Since the distribution in figure 16 just displays the observations which are used in the least squares adjustment it still has to be investigated whether the observations were scheduled this way or whether technical problems lead to a loss of observations. In any case, a situation like this may be a good test bed for the determination of the troposphere via auxiliary GPS measurements.

2.5 Wettzell - Effelsberg

The Wettzell - Effelsberg and the Madrid - Effelsberg baselines are the most sensitive ones in the European network (Fig. 17 and 18). Although Effelsberg has participated only seven times so far the results are quite striking supporting the demand for high SNR observations which often exceed 100 on these baselines. With an RMS of 1.6 mm the 457 km Effelsberg - Wettzell baseline is the best one we have. The 1414 km Effelsberg - Madrid baseline is only slightly worse but with an RMS of 3.2 mm still extremely good. Even the transverse and vertical evolution display RMS values of only 3.7 and 6.8 mm (Fig. 19 and 20). In contrast the height evolution of the Effelsberg - Wettzell baseline is much more noisy (RMS 13.2 mm), a fact which still has to be investigated.

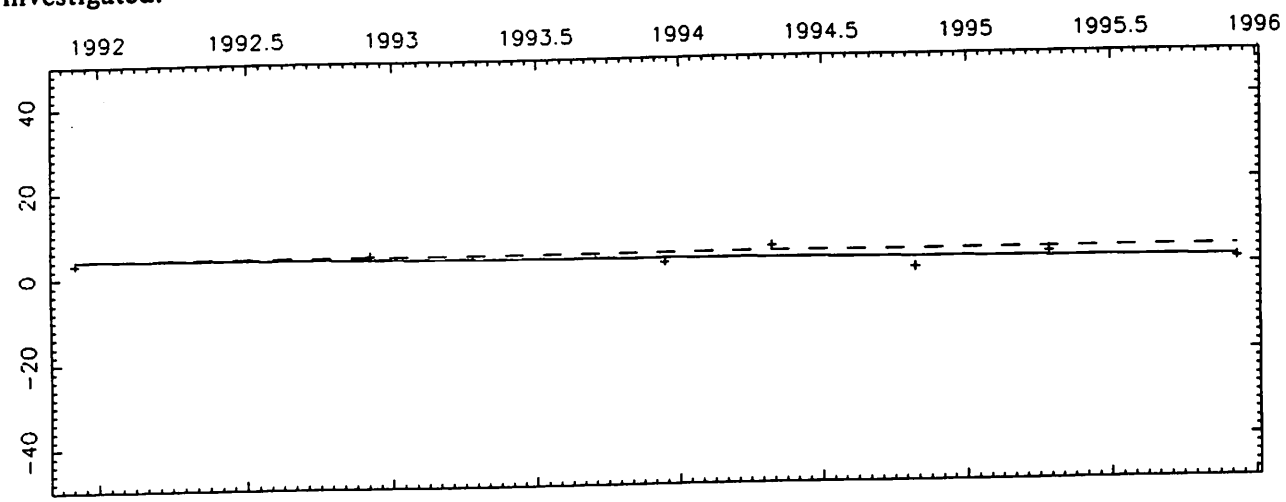

Fig. 17; Baseline Length: Wettzell - Effelsberg, Observed Rate = -0.6 ± 0.6 mm/yr, WRMS = 1.6 mm

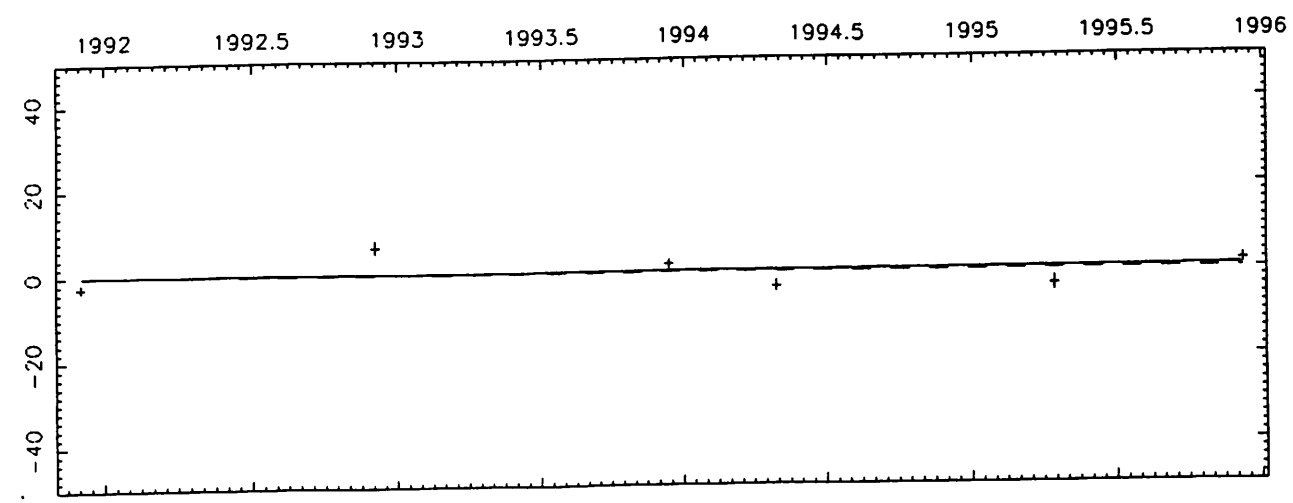

Fig. 18; Baseline Length: Madrid - Effelsberg, Observed Rate = -0.1 ± 1.2 mm/yr, WRMS = 3.2 mm

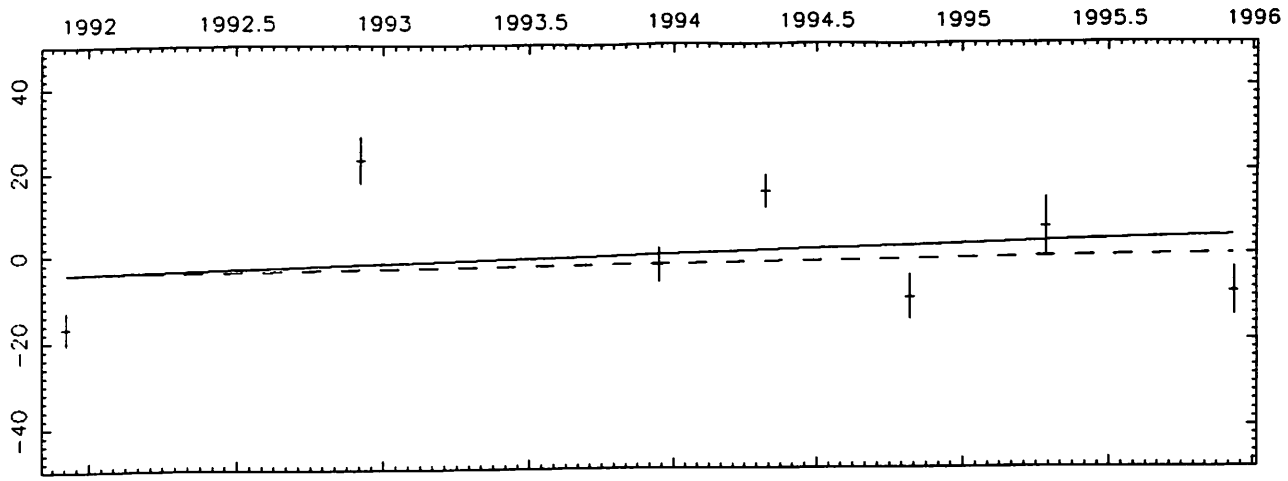

Fig. 19; Baseline Height: Effelsberg - Wettzell, Observed Rate = 2.2 ± 4.7 mm/yr, WRMS = 13.2 mm
NUVEL1 Model rate due to definition of origin (Ryan et al., 1993) = 1.0 mm/yr

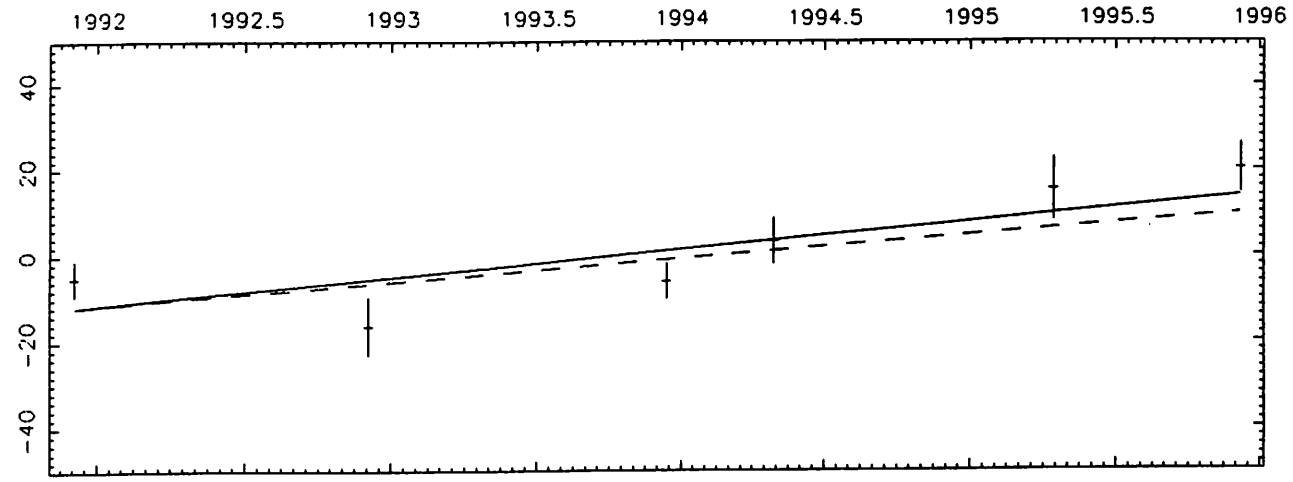

Fig. 20; Baseline Height: Madrid - Effelsberg, Observed Rate = 6.5 ± 2.5 mm/yr, WRMS = 6.8 mm
NUVEL1 Model rate due to definition of origin (Ryan et al., 1993) = 4.6 mm/yr

2.6 Results of the displacement vector solution

From the combined solution where station coordinates for a reference epoch and time derivatives of the components are estimated horizontal station displacement vectors can be infered. By now the European geodetic core network is stable enough to produce reliable displacement vectors without additional constraints. Only the station coordinates of Wettzell, their evolution according to the NUVEL-1A model (DeMets et al., 1994) and apriori Earth rotation parameters from the IERS Rapid Service (IERS, 1996) had to be fixed. The radio source positions which define the celestial reference frame were taken from a combined reference solution comprising a greater number of worldwide VLBI sessions (Nothnagel et al., 1996). Due to its unstable behaviour the station coordinates of Simeiz are treated as arc parameters in order not to introduce additional noise into the core network. The same is done for the Ny Alesund data which has too short a time base for a reliable displacement vector estimation.

Figure 21 displays the annual horizontal displacement vectors together with their error ellipses. While the Onsala and Madrid displacements are smaller than their one sigma error ellipses the Noto, Matera and Medicina data produced highly significant displacement vectors.

A little bit puzzling is the fact that there is such a significant vector estimated for Effelsberg of 1.2 mm/year in a south-easterly direction. This contradicts the arc parameter solution where the

Effelsberg - Wettzell baseline which closely represents this direction produces only a −0.6 ± 0.6 mm/year rate.

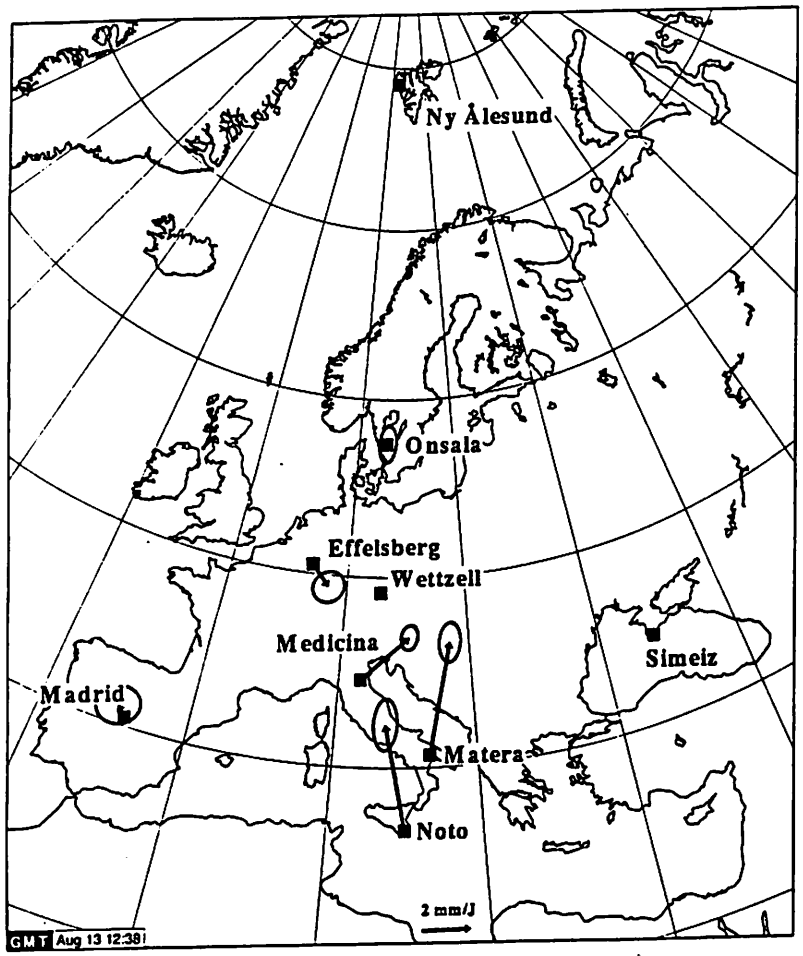

Fig. 21; Station displacement vectors with error ellipses

Conclusion

Over the last few years the European geodetic VLBI network has produced high quality results for both baseline evolution and station displacement vectors. These results have now stabilized and annual displacement vectors can be estimated without the introduction of additional constraints on the evolution of the terrestrial reference frame. However, there is still plenty of scope for refining the existing data which still contains excess measurement noise. Continuous comparisons of the VLBI results with GPS analyses may bear the possibility of detecting fine scale tectonic activities.

References

DeMets C., R.G. Gordon, D.F. Argus, S. Stein; Effect of Recent Revisions to the Geomagnetic Reversal Time Scale on Estimates of Current Plate Motions; GRL, Vol. 21, No. 20 p. 2191-2194; 1994

IERS, 1995 Annual Report; Observatoire de Paris, France, 1996

Nothnagel, A., J. Campbell; Polar Motion Observed by Daily VLBI Measurements; Proceedings of the AGU Chapman Conference on Geodetic VLBI: Monitoring Global Change; NOAA Technical Report NOS 137 NGS 49, p. 345 - 354, Washington D.C., 1991

Nothnagel, A., J. Campbell; European Baseline Rate Determinations with VLBI; Proceedings of the Nineth Working Meeting on European VLBI for Geodesy and Astrometry; Bad Neuenahr, FRG; Sept. 30 - Oct. 1, 1993; in Mitteilungen aus den Geodätischen Instituten der Rheinischen Friedrich-Wilhelms-Universität Bonn, Nr. 81, Bonn, 1993

Nothnagel, A., R. Haas, H. Seeger; International Radio Interferometric Surveying - South: Results of the first 100 sessions; Proceedings of the Eleventh Working Meeting on European VLBI for Geodesy and Astrometry, this issue; Onsala; 1996

Ryan, J.W.,C. Ma, D.S. Caprette; NASA Space Geodesy Program - GSFC Data Analysis - 1992, Final Report of the Crustal Dynamics Project VLBI Geodetic Results 1979-91; NASA Technical Memorandum 104572, Greenbelt, 1993

Sorgente, M.; Status Report on the Geodetic VLBI European Network; Proceedings of the Eleventh Working Meeting on European VLBI for Geodesy and Astrometry; Onsala Space Observatory, this issue; Onsala; 1996

Wessel, P., W.H.F. Smith; Free Software Helps Map and Display Data; EOS Trans. Amer. Geophys. U., Vol. 72, pp. 441, 445-446, 1991

A comprehensive and tentatively complete summary of oceanic effects in space geodetic baseline measurements

H-G Scherneck
Onsala Space Observatory, Chalmers University of Technology

Abstract

At the occasion of contributing yet another list of ocean loading coefficients that includes most of the active and a number of now historical space geodesy sites, this time using the Center of Space Research ocean tide model version 3.0 of Richard Eanes et al. the author intends to summarize in a wider scope how oceans affect geodetic baseline determinations. The list of effects ranges from

- stationary pressure gradients of a tidally decelerating ocean via
- secular changes of pressure loading on a postglacial earth,
- climatic and tidal oscillations affecting UT1 and Polar motion to
- the now well known tidal loading effects.

In spite of the uncontroversial claim that these effects in fact are at work, the closure in the chain of inference is still incomplete. For example a stationary pressure gradient in the Atlantic ocean alone that is compatible with the 2 ms/cy^2 tidal despinning of the earth–for which there is ample evidence–is equivalent to a meager 0.4 m surface slope across the ocean. We will have to live with indirect evidence for a long time.

1 Introduction

Ocean dynamics encompass a catalogue of phenomena which have an impact on precise geodetic measurements. The effects on observing stations that are attached to the solid mantle (as we hope) necessarily have an indirect nature. They can be characterized according to the nature of the processes, e.g. in categories of the nature of the forcing, atmospheric or gravitational. We can also discuss them in categories of time and space or in categories of mass or motion.

The geodetic aspects of the problem can be grouped in two categories, relating to either deformation or orientation of the earth, which has a deep meaning and logically following expressions in continuum mechanics. The notion of displacement $\mathbf{u} = \mathbf{x} - \mathbf{X}$ in a Lagrangian setting linear in terms of the *relative displacement vector*

$$d\mathbf{u} = \frac{\partial \mathbf{u}}{\partial X_j} dX_j \tag{1}$$

leads to a unique separation of deformation and rotation

$$\delta\mathbf{u} = \{\frac{1}{2}[\nabla\mathbf{u} + (\nabla\mathbf{u})^\mathsf{T})] + \frac{1}{2}[\nabla\mathbf{u} - (\nabla\mathbf{u})^\mathsf{T})]\}\delta\mathbf{X} \tag{2}$$

If higher orders of the Taylor series are required the stringence of the distinction can still be maintained using a decomposition of the deformation gradient in a symmetric part *(stretch tensor)* and an orthogonal part

$$\frac{\partial x_i}{\partial X_j} = R_{ik} S_{kj} \tag{3}$$

and associating rotation with the orthogonal part. However, the linear theory still suffices to separate *e.g.* nutations from diurnal tide displacement.

Presented at the 11th Working Meeting on European VLBI for Geodesy and Astrometry, Onsala, Sweden, 1996

2 Earth rotation

2.1 Matter and motion

The notion of the different roles of matter and motion in the case of atmospheric excitation of earth orientation parameters was a leading theme in *Barnes et al. [1983]*. In the case of the ocean, the arguments hold identically. The ocean plays a special, mediating role between the atmosphere on the one hand and the solid crust and mantle on the other, which in some aspects reminds of a clutch, in others of a fender.

The fender part is usually referred to as the Inverted Barometer (IB) response, an idealization of the ocean's yield under the load of the barometric pressure at its surface. What has usually been done in investigations on relations between atmospheric pressure and the solid earth's response in terms of deformation as well as perturbation of rotation and of the gravity field is to compute predictions alternately with the IB perfectly implemented, alternately neglecting the presence of the ocean *[e.g. Chao and Eanes, 1995]*, hoping to find that the truth would be close to either one of the alternatives.

2.2 Inverted Barometer

Several effects are neglected in the IB approximation. First, at short periods, the inertial terms become important. Second, the presence of pressure variations on a rotating earth correlates with a wind field which is largely geostrophic. Looking at the first item, how far into the short period range the ocean is able to achieve static equilibrium has always been a matter of debate. Most notably opinions collided on the question of the pole tide being in disequilibrium in certain predominantly shallow basins like the North Sea *[Wunsch, 1986]*. The arguments in favour of an equilibrium response hinge on the assumption that the barotropic modes of free ocean oscillations are the relevant modes, and that basin geometry confines them to diurnal and subdiurnal period domains. The arguments are relevant also to the inverse barometer discussion as surface pressure enters the equations of motion in an equivalent way as do the external tidal forcing field, including the perturbations of the centrifugal potential due to polar motion.

Discussing the second item, the wind field associated with cyclones and anticyclones generates currents in the ocean which in their turn induce surface elevation and thus deviations from an inverted barometer response, *cf Wunsch [1991], vanDam and Wahr [1993], Fu and Pihos [1994], Ponte [1994]*. The latter work shows that the IB assumption works well only below 10 days periods even in the open ocean, and that wind driven surface elevation becomes an important factor at periods shorter than three days.

Friction at the boundary layers are responsible for perturbations from perfect geostrophy between pressure and wind/current. The implication of nongeostrophic velocity fields in atmosphere and oceans are that they are effective in perturbing solid earth orientation whereas geostrophic fields have identically zero efficiency *[Barnes et al., 1983]*.

Discerning between matter and motion terms in the excitation of earth rotation variations thus means to concentrate on pressure (matter) and ageostrophic currents and wind.

2.3 Angular momentum forcing functions

In the forcing functions of *Barnes et al. [1983]* matter and motion terms can be identified also by spherical harmonic degree. However, a remark is at place dealing with the reference surface. Barnes et al. show explicitly the metric terms (appearing in the partial derivatives along curvilinear coordinates), noting that the advection terms and the pressure forces on the equatorial bulge together with the metric terms perfectly cancel each other. Since the earth's surface is close to a spheroid and close to being an equipotential surface, the matter and motion terms can be resolved on an ellipsoidal surface. Spherical harmonic analysis of the pressure and wind fields will assume this reference surface rather than a sphere, whence the compatible integration variable is pressure, dp.

As a side remark it is instructive to note the history of the particular form of the forcing functions that are now commonly used. In *Munk and MacDonald [1960]* the Euler-Liouville (E-L)

equations are given for the complex axis orientation vector

$$\begin{aligned} i\dot{\boldsymbol{\mu}}/\sigma + \boldsymbol{\mu} &= \boldsymbol{\psi} \\ i\dot{m}_3 &= \dot{\psi}_3 \\ \boldsymbol{\mu} \equiv m_1 + im_2 \qquad & \boldsymbol{\psi} \equiv \psi_1 + i\psi_2 \end{aligned} \tag{4}$$

$$\begin{aligned} \boldsymbol{\psi} &= [\Omega^2\Delta(I_{13} + iI_{23}) - i\Omega(\dot{I}_{13} + i\dot{I}_{23}) + \Omega(h_1 + ih_2) \\ &\quad -i\Omega(\dot{h}_1 + i\dot{h}_2) - i(L_1 + iL_2)]/\Omega^2(I_{33} - I_{11}) \\ &= [\Omega^2\Delta\mathbf{I} - i\Omega(\dot{\mathbf{I}}) + \Omega\mathbf{h} - i\dot{\mathbf{h}} - i\mathbf{L}]/\Omega^2(I_{33} - I_{11}) \\ \dot{\psi}_3 &= -(\dot{I}_{33} + \dot{h}_3/\Omega - L_3/\Omega)/C \end{aligned} \tag{5}$$

More convenient forms for the excitation terms were derived by *Barnes et al. [1983]*, also pointing out that the $\dot{\mathbf{I}}$ term in *Munk and MacDonald [1960]* was erroneously uncorrected for the solid earth yield under loading mass. The E-L equation turned out

$$i\dot{\boldsymbol{\mu}}/\sigma + \boldsymbol{\mu} = \tilde{\boldsymbol{\chi}} - (i/\Omega)\dot{\tilde{\boldsymbol{\chi}}} \tag{6}$$

with

$$\tilde{\boldsymbol{\chi}} = (\Omega\Delta\mathbf{I} + \mathbf{h})/\Omega^2(I_{33} - I_{11}) \tag{7}$$

However, $\boldsymbol{\mu}$ is the projection of the earth **rotation** vector on the equatorial plane, and this vector cannot be observed directly as pointed out by *Gross [1992]*. Solving for the earth orientation vector $\mathbf{p} = (X + iY)/a$ instead, where X and Y are the observed pole coordinates, the form turned out even simpler *[Gross, 1992]*,

$$\begin{aligned} i\dot{\mathbf{p}}/\sigma + \mathbf{p} &= \tilde{\boldsymbol{\chi}} \\ \dot{m}_3 &= -\dot{\tilde{\chi}}_3 \end{aligned} \tag{8}$$

The motion terms are related to angular momentum and thus to a vector spherical harmonic field of degree n=1 and toroidal shape,

$$\mathbf{u} = \sum_m U^{(T)}_{2,m}\hat{r} \times \nabla Y^m_1(\theta, \lambda), \; m = 0, 1 \tag{9}$$

whereas the matter terms are confined to degree n=2 relevant for the moments of inertia,

$$\begin{aligned} p_2 &= \sum_m \Pi_{2,m} Y^m_2(\theta, \lambda) \\ \Delta(C - \frac{1}{2}[A + B]) &= \frac{4\pi a^4}{5g} k'_{eff,2}\Pi_{20} \end{aligned} \tag{10}$$

Analoguous relations exist between the other SH orders and moments of inertia.

Reconciliation of observed short- and long-period ocean tide signatures in LOD and Polar Motion with existing ocean models has now a solid record of success. Remaining problems are confined to those thides that have accompanying or primary atmospheric terms (S_a, S_1, S_2) *[Chao et al., 1995], [Gross et al., 1996], [Sovers et al., 1993], [Brosche et al., 1989, 1991]*.

2.4 Load Love numbers

The matter-related forcing terms in the Euler-Lagrange equations include the effects of solid earth deformation under the pressure load. This effect is properly described by load Love numbers k'_2, however adjusted for a certain degree of decoupling of the fluid core; thus we employ an effective number $k' \equiv k'_{eff,2}$.

This applies to all matter (pressure) forcing terms (p) and discerns them from motion (wind or current) terms (w). Third, the resulting rotation perturbations (polar motion, l.o.d.) perturb the centrifugal potential, the effect of which is poperly described by free surface (tidal) Love number $K \equiv k_{eff,2}$. Equation 8 then reads

$$\begin{aligned} \frac{i}{\sigma_0}\dot{\mathbf{p}} + \mathbf{p} &= \frac{K_0(1 + k')}{K_0 - K}\boldsymbol{\chi}^{(\mathrm{p})} + \frac{K_0}{K_0 - K}\boldsymbol{\chi}^{(\mathrm{w})} \\ \dot{m}_3 &= -\frac{K_0 C}{K_0 C + 2K(C - A)}\left(k'\,\dot{\chi}^{(\mathrm{p})}_3 + \dot{\chi}^{(\mathrm{w})}_3\right) \end{aligned} \tag{11}$$

where $K_0 \equiv 3(C-A)G/\Omega^2 R^5$, untilded symbols are atmosphere (ocean) only, and all scaling quantities relate to standard earth parameters (*e.g.* $(C-A)/C$ dynamic flattening, σ_0 Chandler wobble frequency).

Of interest are here the frequency dependence of Love numbers, in particular the diurnal resonance and the decoupling factor ($k_{eff,2}/k_2$). The atmospheric pressure and wind terms have direct oceanic equivalences in bottom pressure and current, respectively.

The applicability of the Love number approach is justified as long as nonlinearity in the deformation equations of the solid Earth can be neglected, and—more importantly— spherical symmetry can be assumed; radially stratified, spheroidal earth models can still be handled if we accept the appearance of spherical harmonic coupling terms across degrees.

The Love number formulation is particularly suitable for frequency dependent phenomena. This may include visco-elastic modes of the earth's mantle as excited by *e.g.* the long-term loading and unloading processes in the succession of ice ages and interglacials. Resonating modes exist near the diurnal period as an effect of the fluid outer core and, possibly discernable also decoupled motion of the solid inner core, and in the seismic Free Oscillation band. More elusive and awaiting discovery by observations is the translational core mode triplet, the so-called Slichter modes. The ocean plays a noticeable, direct or mediating role in excitation of the resonance modes only at the free core nutation frequency, as oceanic tides near this frequency exist (K_1, P_1, Φ_1, Ψ_1, etc.), still the effect is more than one order of magnitude smaller than the leading resonance that is generated directly by the astronomical tide *[Wahr and Sasao, 1981].*

The viscous modes are more important and will be discussed in a separate chapter.

2.5 Space geodesy at subdiurnal resolution

In space geodesy subdiurnal variations can now uniquely be resolved in the records, much owing to observing campaigns that continue for several days or experiments that are regularly repeated. This contrasts the situation several years ago, when effective daily averaging in parameter estimation was intrinsic, when notably tidal variations were prone to aliasing and associated parameters had to be treated as representative for wide frequency bands—to be honest the entire band, from decades (the lifetime of VLBI) to minutes (the integration interval).

In the light of propositions for continuous monitoring, but also in the light of still increasing activities in permanent satellite station networks it might be worthwhile to spend some time of pondering on the capabilities of the methods on the one hand and objects of scientific curiosity and scrutiny that nature is offering us.

The ambition of a general review on this matter—geodynamic processes sensed by space geodesy—renders the question of the role of the ocean in space geodesy as somewhat narrow. Primarily the coupling between ocean and atmosphere with obvious linkages as well as more subtle ones, is a most active area of research, and emphasizing on the ocean could be likened to looking at trees instead of a forest. The role the atmosphere has must therefore be carefully acknowledged before this discussion is narrowed in on specific ocean processes. A view which is generally supported is that the exchange of atmospheric angular momentum engages the ocean to a considerable extent. The success of predicting polar motion and UT1 from the knowledge of atmospheric pressure and wind [*e.g. Dickey et al., 1994]* relates to the wind being an important factor, and that angular momentum must be conserved. At long periods, longer than 100 days, the presence of the ocean seams to be negligible *[Rosen and Salstein, 1990].*

The ocean can act as a transient storehouse of angular momentum only for a short time, since pressure gradients will build up within a few days that pass on the momentum to the solid earth via the resulting torque. Like in the discussion of the Inverted Barometer response, the barotropic modes of the ocean provide the key to the transition time; however, wind is more efficient than pressure to excite baroclinic modes, and discrepancies between surface elevation and sea bottom pressure may be prevailing in the process, and thus the momentum exchange may be delayed considerably, *cf* the discussion in *Eubanks [1993].*

An the high end of the frequency scale hydrodynamics become important as wavelength scale becomes shorter. A full understanding of tidal phenomena may be one of the most important aims. Particularly on the shelves ocean tides create the largest displacement and displacement rates of the sea surface among the hydrodynamic processes. Nonlinearity starts to become important. The hydrodynamic equations that describe the relations between the surface height perturbation ζ,

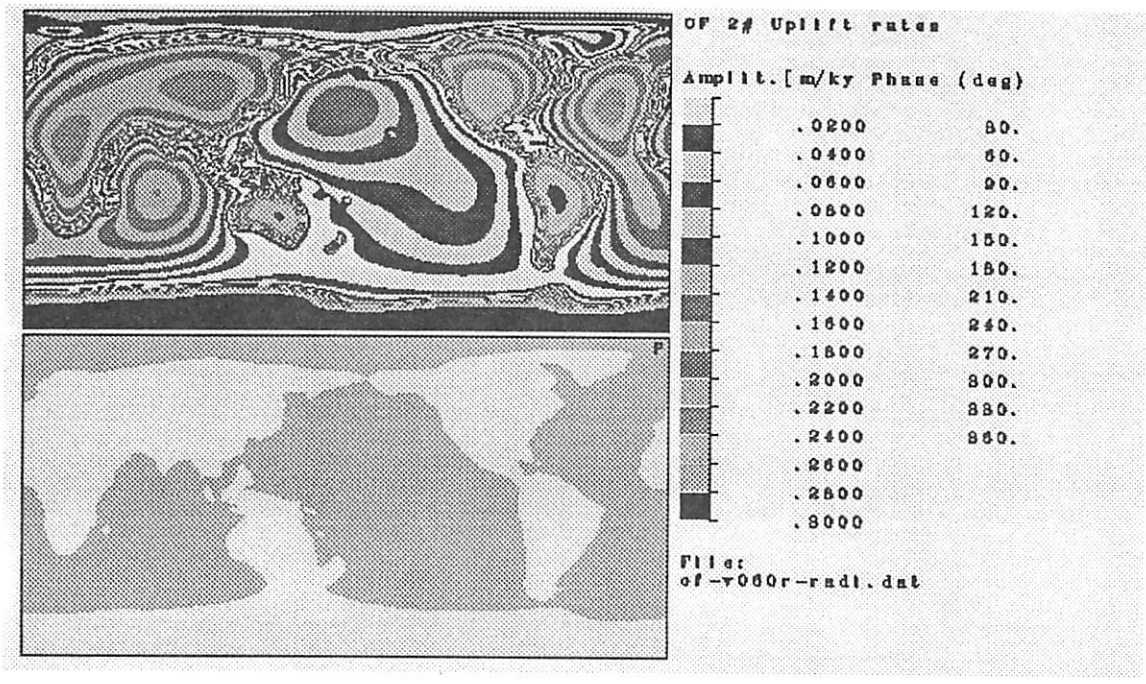

Figure 1: Radial displacement rates at present due to on=going filling of the ocean starting at 6 kyr b.p. at a rate of 1 m/kyr. This is approximately the actual rate. Maximum vertical uplift is found in the continents, a fact less surprising than the factual magnitude, 0.3–0.35 mm/yr

current $\mathbf{u}$ and forces,

$$\frac{\partial \mathbf{M}}{\partial t} + \mathbf{u} \cdot \nabla \mathbf{M} + 2\boldsymbol{\omega} \times \mathbf{M} = -gh\nabla(\zeta - \frac{\psi}{g} + \frac{p_b}{g\rho}) - F_b[\mathbf{u}] + F_s[\mathbf{w}] - A_h[\mathbf{M}] \tag{12}$$

including inertia, advection and Coriolis forces (terms 1,2 and 3 on the l.h.s) implied by the vertically integrated current $\mathbf{M}$, and driving potential, surface pressure gradient, bottom and surface boundary forces, and horizontal momentum diffusion (terms 2 to 5 on the r.h.s)

$$\frac{\partial \zeta}{\partial t} = -\nabla \cdot \mathbf{M} \tag{13}$$

Demanding continuity, supposing incompressibility

$$\mathbf{M} = \int_{-H}^{\zeta} \mathbf{u}\, dh, \qquad h = H + \zeta. \tag{14}$$

The hydrodynamic equations contain nonlinear terms in the advection part $\mathbf{u} \cdot \nabla \mathbf{M}$, due to bottom friction $F[\mathbf{M}]$, and due to the vertically integrated current to the elevated surface. All these terms are enhanced in shallow water.

The tide generating potential is partly external (sun, moon,...), moderated by the vertical and potential tide of the solid earth (incl. core); these sources can be combined using an effective slightly frequency-dependent factor $\gamma_n(\omega)\Psi_n^{(astr)} = (1 + k_n - h_n)\Psi_n^{(astr)}$ (n=2 usually), using the conventional Love numbers. However, the ocean tide perturbs ocean bottom displacement and gravity potential, which is a self-attraction and self-loading effect which requires a more elaborate, global convolution integral if the limitations of the *Accad and Pekeris [1978]* local factor approach are to be overcome.

Equation 12 applies to tides; I have also included atmospheric pressure forcing p_b which has the IB solution $g\rho\zeta = -p_b$ only as $t \to \infty$ and wind shear $F_s[\mathbf{w}] = 0$. The equation also shows the terms that exist in addition to the geostrophic balance $2\omega \times \mathbf{M} = -gh\nabla\zeta$. Equations for vorticity are usually more suitable to pick out wind driven modes, however.

2.6 Tidal friction

One consequence of nonlinearity are the generation of constant current, which on a planet without continents can be viewed as a material superrotation of the ocean with respect to the solid body.

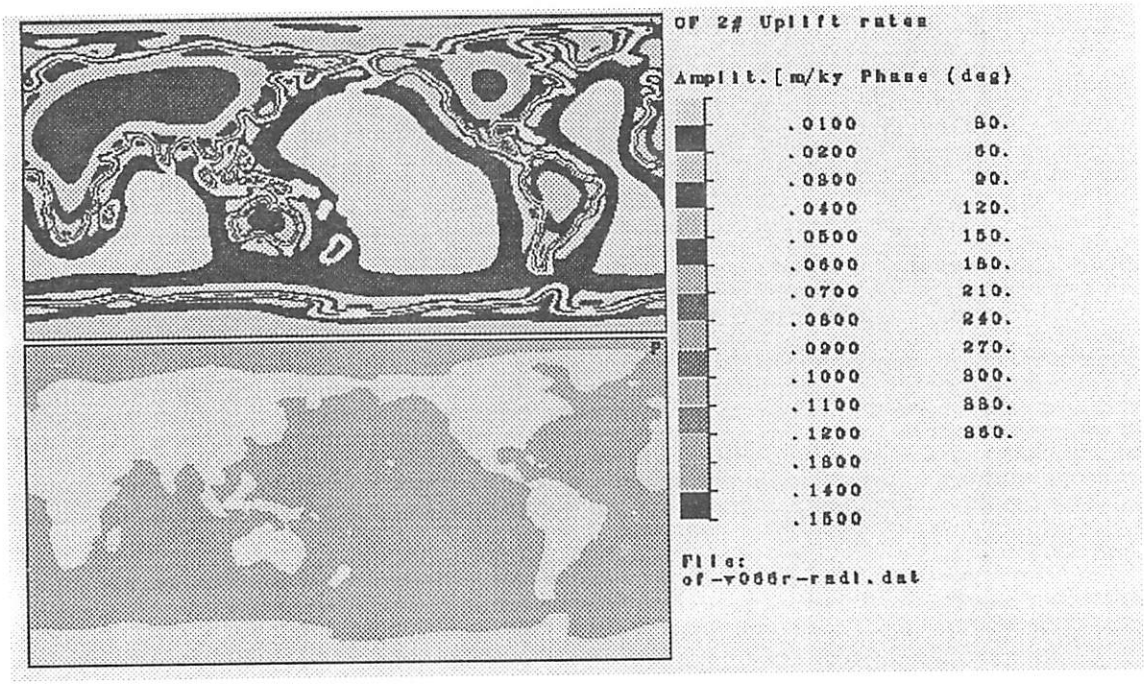

Figure 2: Radial displacement rates at present due to filling of the ocean between 12 kyr b.p. and 6 kyr b.p. at a rate of 1 m/kyr. The actual rate of change was about five times as high. Owing to the linearity of the process, the rates given in the legend can simply be multiplied with this factor. The top frame shows grey coded values for the amplitude of the rates. The lower frame shows "phase", *i.e.* the sign of the motion, being upward (dark grey) or downward (light grey).

Theoretically, the superrotation current is (1) compensated by north-south running coasts that bracket the ocean and thus allow uniform east-west surface slopes, and (2) limited by bottom friction where intervening continents are missing. On the earth the former process is highly efficient. In the two ocean basins, Atlantic and Pacific, *e.g.*, a surface elevation difference (east minus west) of 0.1 m along 10,000 km of north-south projected coastline pair generates a torque that decelerates earth rotation with 1 ms/cy^2.

Despite thorough analysis, however, it remains difficult to account for the most important sink of energy in the ocean tide *[Kagan and Sündermann, 1996]*.

2.7 The ocean and the postglacial water budget

Melting of the glaciers at the end of the pleistocene and continuing, although less vigorously, throughout the holocene implies redistribution of mass, from solid to liquid form, from continental locations into the oceans. As the ocean water is able to achieve gravitational equilibrium in the course of days, a self-adjusting process is initiated with each drop of water entering the world ocean, in which the ocean bottom and the earth's mantle is deformed and the ocean mass readjusts due to gravitational attraction until the mean ocean surface is in level.

Recent rates of change of sea level amounted to 1 m/kyr while average rates between 18 kyr b.p., the glacial maximum, and 6 kyr b.p., at the termination of the major glacial shields in Canada and Fennoscandia, were around 5 m/kyr. I have used the fluid limit of a visco-elastic loading Green's function for the potential,

$$\mathcal{G} = \frac{G}{a}\sum_n (1 + k'_{\infty n} - h'_{\infty n}) P_n(\cos\theta) \tag{15}$$

to derive a lower limit on the water load that is effective during the filling process. For the uplift rate response I used

$$\mathcal{G} = \mathcal{L}^{-1}\{\frac{G}{ga} s \sum_n h'_n(s) P_n(\cos\theta) \mathcal{L}\{R(t_0, t_1)\}\} \tag{16}$$

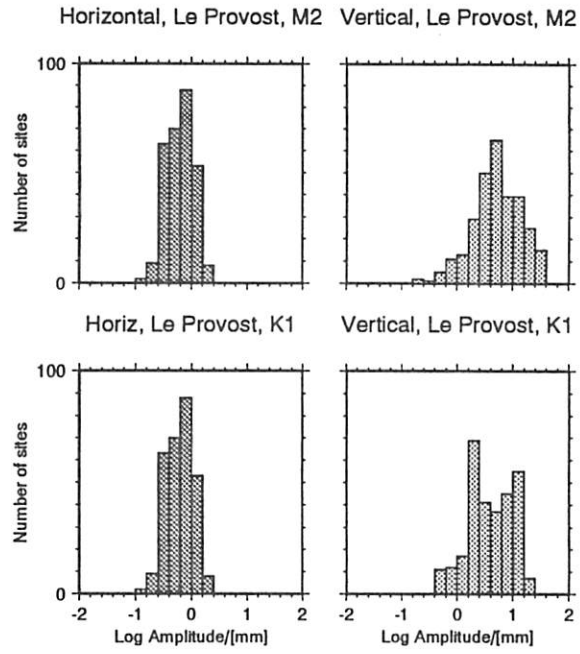

Figure 3: Histograms of the Ocean Loading Parameter file: Number of sites versus magnitude of displacements, using the ocean tide model of *Le Provost et al. [1994]*. Sites catalogue comprises all sites observing for the ITRF and IGS and many others of general and particular interest.

where $\mathcal{L}\{\}$ is the Laplace transform, s being the Laplace parameter, and $R(t_0, t_1)$ is a ramp function

$$R(t_0, t_1) = \begin{cases} 0, & t < t_0 \\ t, & t_0 \leq t \leq t_1 \\ t_1, & t_1 < t \end{cases}$$

The viscous Love numbers have been obtained using the program and earth model of Mitrovica [*e.g. Mitrovica and Peltier, 1991*]. The combined effect of filling the ocean during the two epochs at 5 and 1 m/kyr, respectively, induces present vertical motion of up to 0.8 mm/yr. A more sophisticated treatment of the effect would vary the upper mantle viscosity since in this particular loading problem the oceanic mantle is the primary yielding part, whereas the mantle viscosity profile that has been used in the calculation have been obtained from the continental problem of glacial unloading. Also the load history needs better resolution.

3 Ocean loading tides

Finally, I review in short recent additions to the IERS Standards 1992 *[McCarthy, 1992], [Scherneck, 1991]* on the subject of local site displacements due to ocean tide loading (OTL). The number of sites in the catalogue have been increased to roughly 300, which comprises also recently established GPS stations, primarily those in the IGS network. Many of these stations are near a coast. The recently established VLBI stations at Fortaleza and Ny Ålesund are also located in coastal regions. Fortaleza near the Brazil Atlantic coast where semidiurnal tide range is considerable, and Ny Ålesund on the Spetsbergen archipelago. Sites like these cause concern that ocean loading phenomena are carefully modelled.

3.1 Available data ses

Additions to the OTL catalogue also comprise totally new sets of coefficients adopting the new models that became available in the wake of TOPEX/POSEIDON (T/P) *[Le Provost et al., 1994], [Ma et al., 1994], [Egbert et al., 1994].* to mention three. The feasibility of satellite altimetry derived ocean tide models hinges on a few requirements, which in summary are (i) global coverage and (ii) frequency resolution.

Global coverage demands that important ocean areas are represented. This is an inherent problem in T/P since the satellite was confined to a ±66° latitude band. Also, shallow water areas and coastal zones imply modelling and data reduction problems and thus are not always represented *[Schrama and Ray, 1994]*.

The model of *Le Provost et al. [1994]* (LePr94) is a finite element numerical solution. It has been made available for the T/P mission, but does not draw from the altimetry data. One area which has important tides and is not represented in this model is the Bay of Fundy, otherwise the global coverage is satisfying.

The University of Texas model, Version 3 (CSR3), a high-resolution successor of Version 2 *Ma et al. [1994]*, does admit T/P data, starting from the LePr model as a basis. It has oceanic data also in some areas that are blanked out in LePr94, but does not always represent them realistically. Again, the Bay of Fundy is a problem; CSR3 shows amplitudes at decimeter level whereas the observed range is more like 10 m. Mediterranean tides appear realistic, though.

The *Egbert et al. [1994]* model from Oregon State University (OrSU) is the result of a sophisticated assimilation process of altimetry data into the hydrodynamic modelling equations. Thus, a good balance between observations and theoretical predictions can be obtained. For obvious reasons, the assimilation process cannot constrain the local tide over wide distance, whence the polar area cannot be resolved.

Frequency resolution is particularly elegant in CSR3 as this model is based on the orthotide method *Cartwright and Ray [1990]*, (originally *Groves and Reynolds [1975]*) which at each grid node states three coefficients to interpolate tide admittance in each of the diurnal and semidiurnal frequency bands. The instantaneous tide is then obtained by multiplying with the amplitude and argument factor of the partial tide in question.

However, all the recent models have the draw-back that they do not attempt to model long-period tides or, as in CSR3, settle the matter with an equilibrium approach.

3.2 Maps

In parallel with the traditional sets that are on a site-by-site basis, maps of ocean loading effects can be made available for random access, primarily suitable for sites in less difficult areas. The OTL information is retrieved from the maps using special but unsophisticated 2-D parabolical interpolation software. The special feature to emphasize is the storage efficient method the horizontal information is supplied. With the displacement Green's function

$$\hat{\alpha}\mathcal{G}^{(\mathbf{u})}(\theta) = \frac{G}{ga}\sum_n l'_n \frac{dP_n(\cos\theta)}{d\theta} \tag{17}$$

where $\hat{\alpha}$ is a unit vector along the azimuth from the load point to the field point and θ the subtended angle, the horizontal displacement vector $\mathbf{u}$ at a field point is obtained by point load convolution

$$\mathbf{u} = \int_{\mathcal{O}]]\dashv\backslash} \begin{pmatrix} \hat{e}\hat{e} \\ \hat{n}\hat{n} \end{pmatrix} \cdot \hat{\alpha}\mathcal{G}^{(\mathbf{u})}\, dm \tag{18}$$

However, the quantity

$$\Phi = \int_{\mathcal{O}]]\dashv\backslash} \mathcal{G}^{(\Phi)}\, dm \tag{19}$$

is both easier to compute and yields a scalar result, in effect a "displacement potential". It can be gridded in the same way as the vertical displacement. The local displacement is simply obtained by $\mathbf{u} = \nabla\Phi$, almost trivial to implement in the interpolation polynomial. The Green's function for this case is

$$\mathcal{G}^{(\Phi)}(\theta) = \frac{G}{g}\sum_n l'_n P_n(\cos\theta) \tag{20}$$

To test the usefulness of each of these new models I have computed a set of ocean loading predictions for the M_2 tide at a large set of gravimeter stations, using the Brussels catalogue *(Francis, pers.comm.), [Melchior 1994]*. Results compare well with those published recently in *Melchior and Francis [1996]* and *Llubes and Mazzega [1996]*, *cf* Fig. 4. The findings are that the *Schwiderski [1980]* (Schw) model is still a good competitor, and that none of the recent models mentioned above has serious draw-backs.

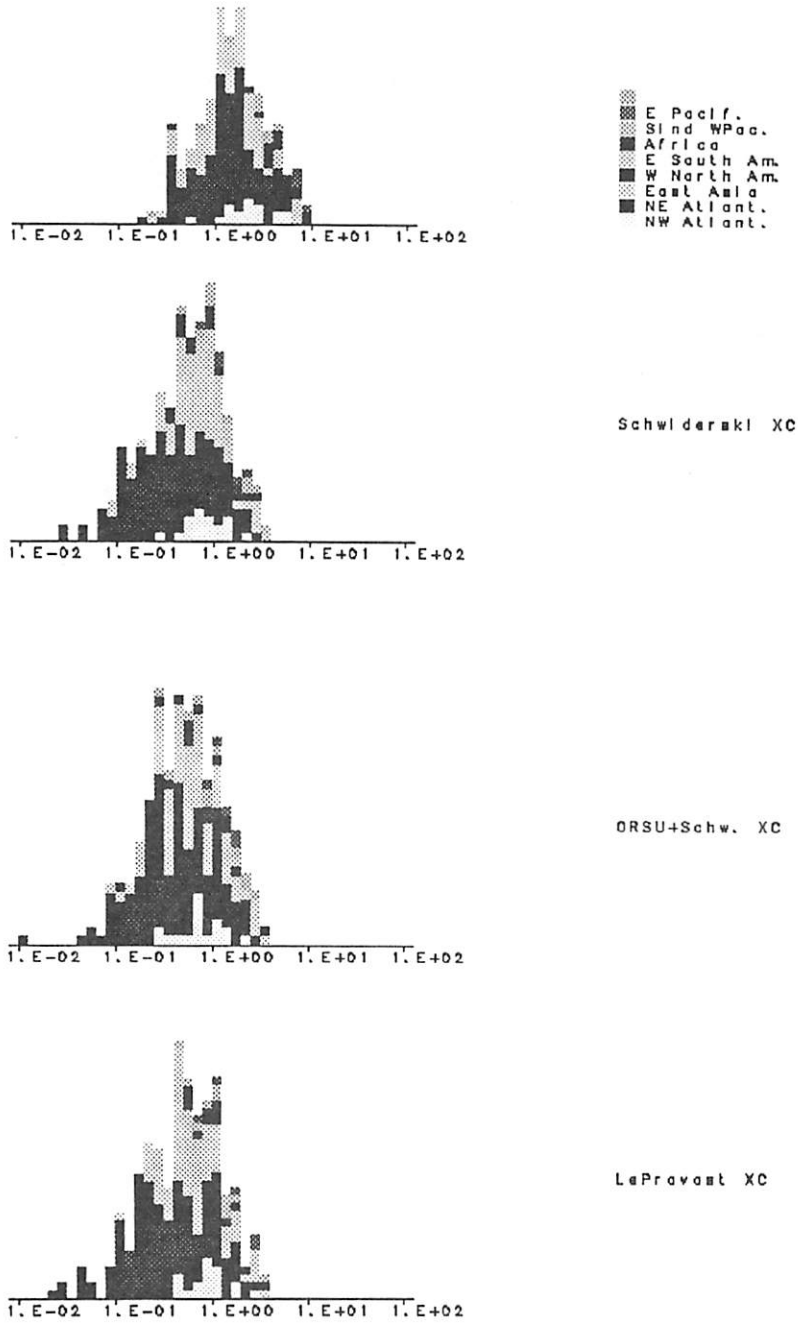

Figure 4: Histograms of ocean loading gravity residuals, M_2 tide, using the Brussels data base *[Melchior, 1994].* and three ocean tide models; Schw - *Schwiderski [1980],* OrSU+Schw - *Egbert et al. [1994]* with Schw supplemented in the Arctic Sea, LePr - *Le Provost et al. [1994].* In the topmost histogram no ocean loading corrections were applied. Abscissa values are in μgal = 10^{-8} m/s^2.

Thus, at present is appears viable to offer three solutions, based upon Schw, LePr94, and CSR3, adding long-period information always from Schw. The data can be downloaded from the ftp location

ftp://gere.oso.chalmers.se/pub/hgs/oload

Ocean loading tides are an oscillating process, having a tendency to be averaged out in mean site position estimates if observation time series are long enough and individual campaings are scheduled such that very low tidal beat periods are avoided—which is usually the case in 24 and 48 h experiments. The process is more important if solid earth tide parameters are to be estimated

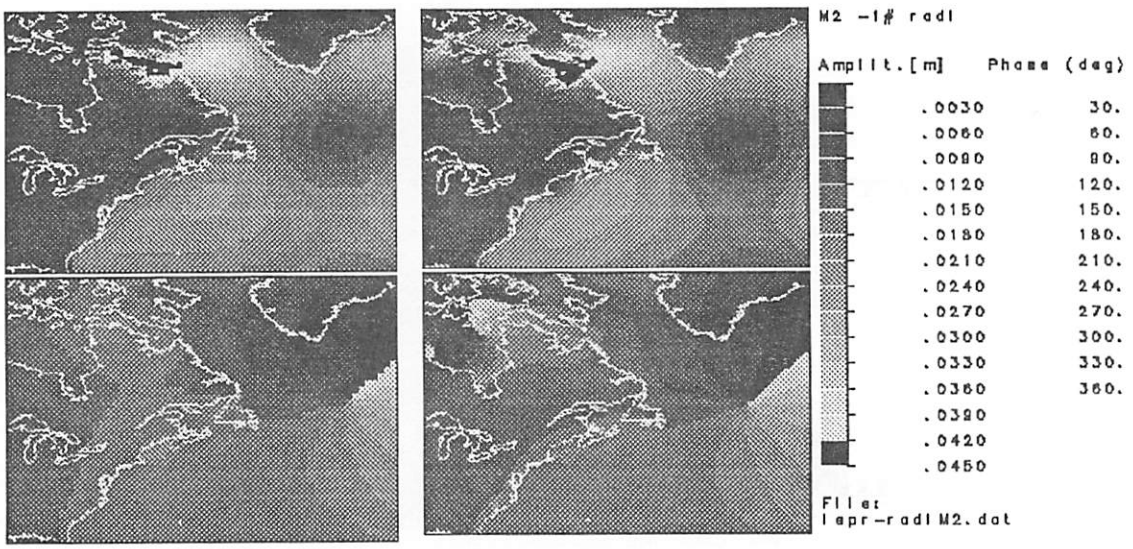

Figure 5: Ocean loading tide M_2 displacement maps, computed from Schwiderski (left column), Le Provost (right column), Amplitudes im metre (top row), Phases in degree (bottom row). Note discrepancy in the Bay of Fundy, a basin that is not represented in *Le Provost et al. [1994]*, extending into the neighbourhood of south-east Canada and New England, significant for the geodetic sites in Massachusetts.

since there is a perfect match between loading tide and astronomical tide frequencies. Thus, body tide Love numbers are likely to be systematically perturbed if OTL is unaccounted.

Figure 3 shows histograms of the magnitude of the M_2 loading tide in the set of sites of the OTL catalogue. Figure 5 shows maps of the M_2 radial displacement computed from Schw and LePr94, respectively, emphasizing the problems near the bay of Fundy which have bearing on the space geodetic stations *e.g.* in Massachusetts.

However, also an impact of ocean loading upon subdiurnal earth orientation parameters can be predicted. In the following I have analyzed the situation for three different VLBI networks, NEOS-A, IRIS-S, and CONT-96. Special concern was given to the fact that future VLBI operations for earth rotation will probably comprise many networks with each a small set of sites, but these network would relay their activities among each other to effectively achieve continuous monitoring. Networks with a small number of observatories, however, are susceptible to ocean loading, particularly earth orientation and deformation cannot fully be separated relying on the network geometry alone. Thus, ocean loading models may be crucial in pushing the precision limits in the future.

The largest loading tide effect is usually found in the vertical component. Since VLBI is a technique which is invariant for rigid translations of the baselines, constraining sites to the geocentre is no option. Thus, the full three-dimensional displacement vector folds into the earth orientation vector space. However, since horizontal ocean loading components have been applied in the past only in rare cases, and indirect control of the vertical movements is available to some degree using tidal gravimetry, I have distinguished two cases, one in which a vertical OTL model would work with perfect precision, and one in which the total OTL displacement is unmodelled, thus yielding the larger network orientation effects (*cf* Fig. 6).

Tidal movement of water masses in the ocean also comprise a very-long wavelength mode pertaining to spherical harmonic degree one, which means variations of the centre of gravity of the ocean with respect to the solid earth. Since the Joint centre of mass must be preserved, the Earth mantle and thus the geodetic observing sites perform counterbalancing translational motion. Since VLBI is translationally invariant but satellite methods are not, insight into these translational modes would come primarily from a comparison between colocated VLBI and satellite stations. Colocation would help to cancel the local ocean loading motion at each site. The accuracy of ocean tide models is most sensibly checked on local to regional scales, using tide gauges and satellite altimetry, respectively. The very-long wavelength modes are more difficult to retrieve. In

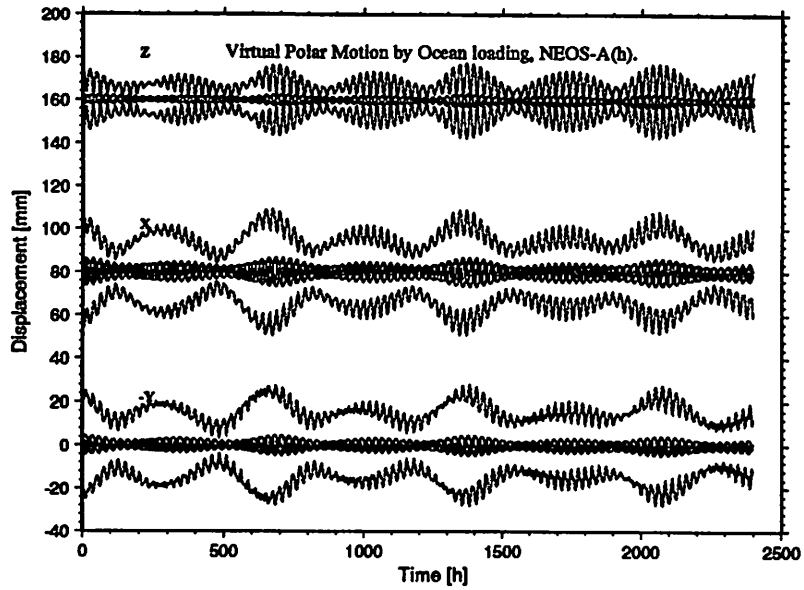

Figure 6: Ocean loading displacements in a small VLBI network like NEOS-A have a considerable rigid rotation mode. Thus, estimates of earth orientation parameters are affected. Shown are time series staring at Jan. 1, 1995 in units of millimetre at the earth's surface, pole offset (-Y and X) and orientation angle (Z). The innermost curves give the actual displacements assuming vertical ocean loading is reduced exactly but horizontal deformation is ignored. Also shown are the time series envelopes, which bracket the displacements tightly. The larger, outer envelopes show the virtual orientation effect when ocean loading tides are completely ignored. For readability the X, Y and Z components have been separated by adding 0, 80 and 160 mm.

The large impact of vertical displacement reflects VLBI's invariance to translation, which also implies that coordinate constraints to preserve the location of the geocentre cannot be imposed.

the light of this reservation, solid earth centre of mass movement predicted from ocean tide models might be much more erroneous than local site movement. The different ocean tide models lead to considerable disagreement as Fig. 7 demonstrates.

4 Summary

Future VLBI operations and joint solutions with the other space techniques will monitor earth rotation in an unbroken, very wide band of periods. The role of the ocean for earth rotation variations particularly at the high frequency end of the domain can be summarized as follows

- **Solid earth deformation**

Ocean loading tides, local site displacements	vertical	1–100 mm	
	horiz.	1–30 mm	
Ocean loading tides, small-network rotations	X,Y	1 mas	
	UT1	0.1 ms	
Loading effects due to non-IB ocean response	vertical	$\leq$ 10 mm	*[vanDam & Herring, 1994]*
Holocene water budget	vertical	$\leq$ 0.3 mm/yr	
Excitation of NDFW	v & h	$\leq$ 0.1 mm	*[Wahr & Sasao, 1981]*

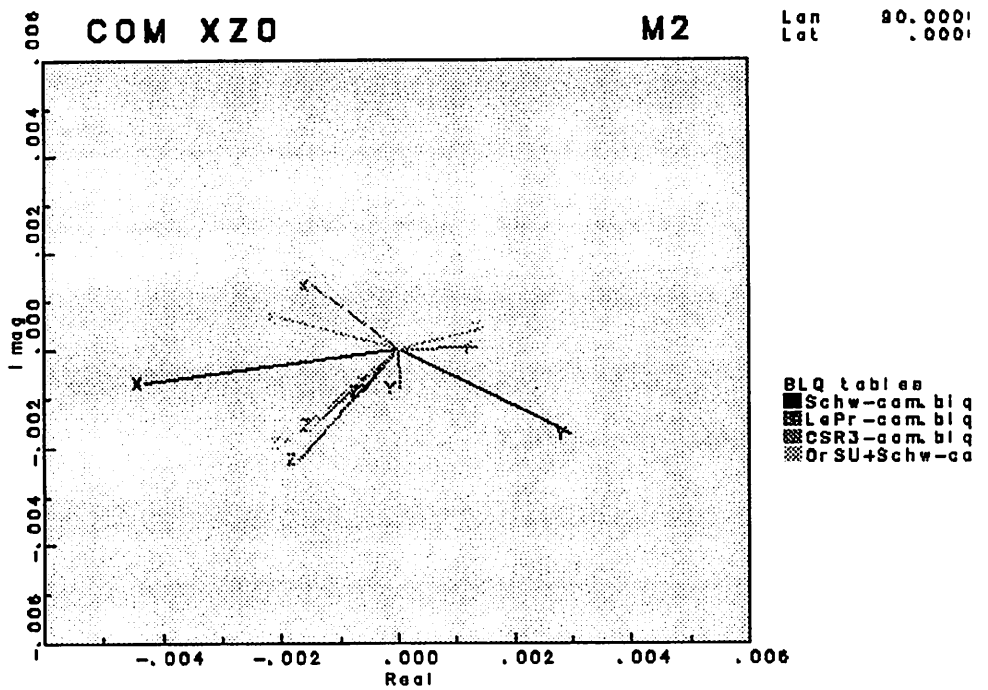

Figure 7: Centre of mass tide M_2 from the four different ocean models considered in the text. Movements are projected along geocentric XYZ-components. This is a phasor plot, meaning the real part is in phase with the tide at zero meridian, and the imaginary part is at a quadrature phase lag. Unit is metre.

- **Earth rotation**

Polar motion	K_1 (P_1)	10 (1) mas	
	other tides	0.1 mas	*[Gross, 1993]*
UT1	(sub-)diurnal	50 μs	
	long-period	1 ms	*[Gross, 1993]*
LOD	secular	2 ms/cy	
Holocene water budget		? (small)	
climate, weather		? (large)	

References

Accad, Y, and Pekeris, C. L., 1978. Solution of the tidal equations for the M2 and S2 tides in the world oceans from a knowledge of a tide potential alone, *Phil. Trans. R. Soc. London, Ser. A*, **290**, 235-266.

Barnes, R.T.H., Hide, R., White, A.A., Wilson, C.A., 1983. Atmospheric angular momentum fluctuations, length-of-day changes and polar motion. *Proc. R. Soc. London*, **A387**, 31-73.

Brosche, P., Seiler, U., Sündermann, J., and Wuensch, J., 1989. Periodic changes in Earth's rotation due to oceanic tides, *Astron. Astrophys.*, **220**, 318-320.

Brosche, P., Wuensch, J., Campbell, J., and Schuh, H., 1991. Ocean tide effects in Universal Time detected by VLBI, *Astron. Astrophys.*, **245**, 676-682.

Cartwright, D. E. and Ray, R. D., 1990. Oceanic tides from Geosat altimetry, *J. Geophys. Res.*, **95**, 3069-3090.

Chao, B.F., and Eanes, R., 1995. Global gravitational changes due to atmospheric mass redistribution as observed by the Lageos nodal residual, *Geophys. J. Int.*, **122**, 755–764.

Chao, B.F., Merriam, J.B., and Tamura, Y., 1995. Geophysical analysis of zonal tidal signals in length of day, *Geophys. J. Int.*, **122**, 765–775.

Dickey, J.O., Marcus, S.L., Hide, R., Eubanks, T.M. and Boggs, D.H., 1994. Angular momentum exchange among the solid Earth, atmosphere, and oceans: A case study of the 1982-1983 El Niño event, *J. Geophys. Res.*, **99**, 23,921–23,937.

Egbert, G. D., A. F. Bennett, and M. G. G. Foreman, 1994. TOPEX/POSEIDON tides estimated using a global inverse model, *JJ. Geophys. Res.*, **99**, 24,821–24,852.

Eubanks T M, 1993. Variations in the orientation of the Earth. In: Smith D E, Turcotte D L (eds), *Contributions of Space Geodesy to Geodynamics: Earth Dynamics*, pp 1–54. Crustal Dynamics Series, Vol 24, American Geophysical Union, Washington.

Fu, L. L., and G. Pihos, Determining the response of sea level to atmospheric pressure forcing using TOPEX/POSEIDON data, *J. Geophys. Res.*, **99**, 24,633–24,642, 1994.

Gross, R.S., 1992. Correspondence between theory and observations of polar motion, *Geophys. J. Int.*, **109**, 162-170.

Gross, R.S., 1993. The effect of ocean tides on the earth's rotation as predicted by the results of an ocean model, *Geophys. Res. Letters*, **20**, 293–296.

Gross, R.S., Hamdan, K.H., and Boggs, 1996. Evidence for excitation of polar motion by fortnightly ocean tide, *Geophys. Res. Letters*, **23**, 1809–1812.

Groves, G.W. and Reynolds, R.W., 1975. An orthogonalized convolution method of tide prediction. *J. Geophys. Res.*, **80**, 4131–4138.

Kagan, B. A. and Suendermann, J., 1996. Dissipation of tidal energy, paleotides, and evolution of the earth-moon system, in *Advances in Geophysics, Vol. 38*, pp.179–266, eds. Dmowska, R. & Saltzman, B., Academic Press, San Diego, 275pp.

Le Provost, C., M. L. Genco, F. Lyard, P. Vincent, and P. Canceil, 1994. Spectroscopy of the world ocean tides from a finite element hydrodynamical model, *J. Geophys. Res.*, **99**, 24,777–24,798.

Llubes, M, and Mazzega, P., 1996. The ocean tide gravimetric loading reconsidered, *Geophys. Res. Letters*, **23**, 1481–1484.

Ma, X.C., Shum, C.K., Eanes, R. and Tapley, B. D., 1994. Determination of ocean tides from the first year of TOPEX/POSEIDON altimeter measurements, *J. Geophys. Res.*, **99**, 24,809–24,820.

McCarthy, D.D. (ed.), 1992. *IERS Standards (1992)*. IERS Technical Note 13, Observatoire de Paris, 150 pp.

Melchior, P., 1994. A new data bank for tidal gravity measurements (DB92), *Phys. Earth Planet. Inter.*, **88**, 223–256.

Melchior, P. and Francis, O., 1996. Comparison of recent oceanic corange-cotidal maps with ground based tidal gravity measurements through the gravitational attraction and elastic loading due to the moving water masses, *Marine Geodesy*, in print.

Mitrovica, J. X. and Peltier, W. R., 1991. On postglacial geoid subsidence over the equatorial oceans, *J. Geophys. Res.*, **96**, 20,053-20,071.

Munk, W.H., and MacDonald, G.J.F., 1960. *The Rotation of the Earth*, Cambridge University Press, 323pp.

Ponte, R. M., 1994. Understanding the relation between wind- and pressure-driven sea level variability, *J. Geophys. Res.*, **99**, 8033–8039.

Rosen, R.D., and Salstein, D.A., 1990. Discrepancies in the earth-atmosphere angular momentum budget, *J. Geophys. Res.*, **95**, 265–279.

Scherneck, H.-G., 1991. A parametrized solid earth tide model and ocean tide loading effects for global geodetic baseline measurements, *Geophys. J. Int.*, **106**, 677-694.

Schrama, E.J.O., and Ray, R. D., 1994. A preliminary tidal analysis of TOPEX/POSEIDON altimetry, *J. Geophys. Res.*, **99**, 24,799–24,808.

Schwiderski, E. W., 1980. On charting global ocean tides, *Rev. Geophys. Space Phys.*, **18**, 243-268.

Sovers, O.J., Jacobs, C.S., and Gross, R.S., 1993. Measuring rapid ocean tidal earth orientation variations with Very Long Baseline Interferometry, *J. Geophys. Res.*, **98**, 19,959–19,971.

Wahr, J. M. and Sasao, T., 1981. A diurnal resonance in the ocean tide and in the earth's load response due to the resonant free 'core nutation', *Geophys. J. R. astr. Soc.*, **64**, 747-766.

Wunsch, C., 1986. Dynamics of the North Sea pole tide reconsidered, *Geophys. J. R. astr. Soc.*, **87**, 869–884.

Wunsch, C., 1991. Large-scale response of the ocean to atmospheric forcing at low frequencies, *J. Geophys. Res.*, **96**, 15,083–15,092.

vanDam, T. M., and Herring, T. A., 1994. Detection of atmospheric pressure loading using very long baseline interferometry measurements, *J. Geophys. Res.*, **99**, 4505-4517.

vanDam, T. M. and J. Wahr, 1993. The atmospheric load response of the ocean determined using Geosat altimeter data, *Geophys. J. Int.*, **113**, 1-16.

SPECTRAL ANALYSIS OF THE BASELENGTH TIME SERIES.

O. Titov[1], H. Yakovleva[2]

1. Institute of Applied Astronomy, Sanct-Petersburg, Russia
2. Sanct-Petersburg University, Department of Astronomy, Sanct-Petersburg, Russia

Introduction

In accordance with conventional model of tectonical plates motion NNR-NUVEL1 the variations of baselengths should be a straight lines [1]. But at the beginning of 90th some scientists found a seasonal signatures in a few baselines time series [2,3]. More recently the various deviations from linear dependence were discovered [4], but they have not been explained yet. The problem becomes complicated due to the facts that the detected seasonal variations are able to be arisen from incorrectness of some another natural effect modeling. For example, Niell [5] calculated that the seasonal variations into both horizontal and vertical components can be affected by incompleteness of mapping function simulation. Therefore one should be more careful during interpretation of the effect.

Interesting results on annual variations of the Earth surface were published at the papers about atmospheric pressure loading effect on VLBI station components displacement [6,7]. In spite of different approaches for modeling, the similar estimates of annual shift of vertical components (1-2 cm) were obtained. Therefore there is a reason to assert that the variations under study are arisen from seasonal moving of large air masses. Ma and McMillan [2] have made the same conclusion from analysis of VLBI data adjustment with different meaning of elevation angle cutting.

The second possible reason of seasonal effects is a snow loading. Recently it has been showed that snow cover with the height more than 30 cm and radius of 100 km around site of observations reduces quasi-geoid level up to 12 mm [10]. It seems the effect should be taken into account for VLBI stations at the middle- and high-latitudes.

As usual scientists pay more attention to high-frequency (~2 weeks) variations of atmospheric pressure and VLBI site components than to seasonal ones [8,9]. At the papers mentioned above spectral analysis has not been applied for baselength time series processing although some baselines have a few hundred of observations. Therefore up to now there is no an evidence that the period of seasonal signature is equal to 1 year.

Therefore they are seasonal variations of baselengths which are considered at the paper. Daily estimates of baselengths for time period from 1982 till 1995 have been taken from current publication of GSFC [11]. It is the most perfect and precise result of VLBI data adjustment since 1979. Therefore an application of spectral analysis will allow to catch signatures into range from some days to some years.

Results of analysis

We have chosen a set of 35 baselines which have long observational history or have been operating actively during last years (Table 1). The lengths range is from 500 km to

Presented at the 11th Working Meeting on European VLBI for Geodesy and Astrometry, Onsala, Sweden, 1996

11.000 km; the 17 VLBI stations are located on different continents as well as latitude zones. The choice allows to extract both regional and global natural phenomena.

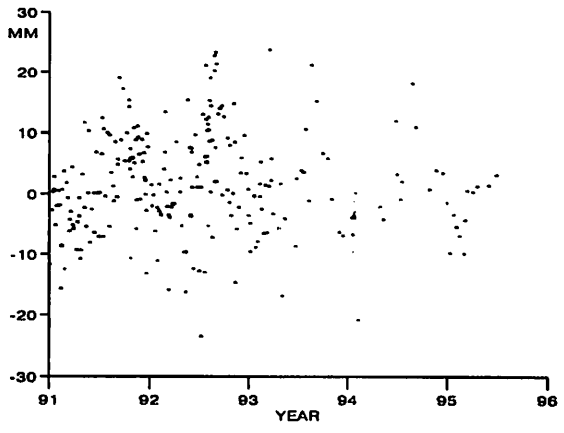

Fig.1a
Evolution of Westford - Wettzell baseline.
There are significant seasonal variations.

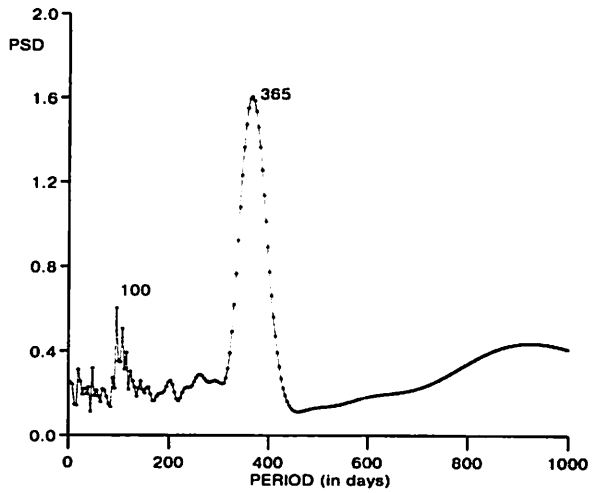

Fig.1b.
Spectrum of Westford - Wettzell baseline variations.
The largest harmonic is an annual one. There is no semiannual harmonic.

Spectral analysis using approach developed by Barning for uneven spaced time series showed that the annual signature is present at the almost all 35 time series. Fig.1a demonstrates Westford - Wettzell baseline evolution between 1990 and 1995. Corresponding power spectrum density is shown on Fig.1b. Obviously that the annual signature predominates. Moreover, there is small peak near period 100 days. In reality there are too close peaks with periods ~95 and ~107 days.

For a few baselines a meaningful semiannual signature has been discovered. Fig.2a demonstrates time variations of Gilcreek - Wettzell baseline, fig.2b - the corresponding power spectra density.

On the preliminary results foundation the following parametrical model for baselength time series approximations has been chosen.

$$l(t) = a + bt + c_1 \cos(\frac{2\pi}{P} t) + d_1 \sin(\frac{2\pi}{P} t) + c_2 \cos(\frac{4\pi}{P} t) + d_2 \sin(\frac{4\pi}{P} t) + w \qquad (1)$$

where l(t) is the mean of baselength; a, b - linear trend parameters; P - period of the Earth rotation on orbit; c_i, d_i - coefficients of the annual (i=1) and semiannual (i=2) signatures; w - random error.

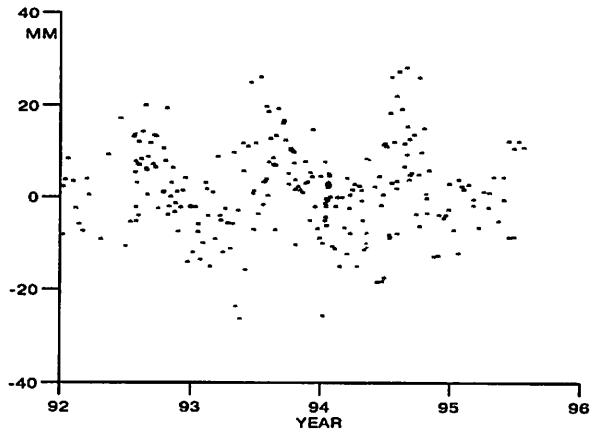

Fig.2a
Evolution of Gilcreek - Wettzell baseline.
There are significant seasonal variations, especially, during 1992-1995 years.

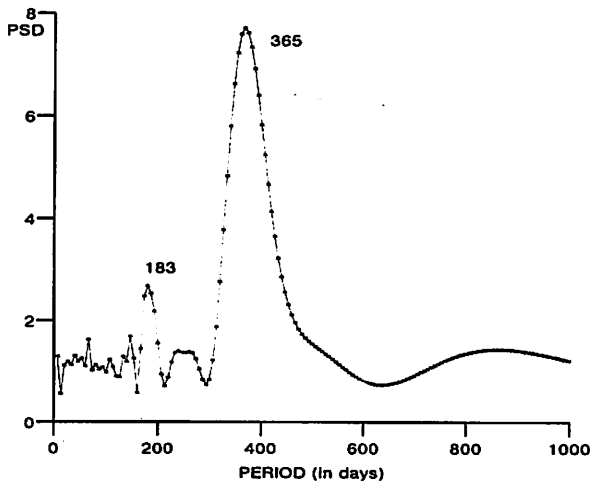

Fig. 2b
Spectrum of Gilcreek - Wettzell baseline variations.
There are both annual and semiannual harmonics.

In spite of the presence of some other signatures we have not included them into model (1), because their origination is unclear yet. They changes from baseline to baseline, therefore there is no possibility to suppose that the variations are global ones. Sometimes the signatures can be caused by local effects (for example, seasonal thermic deformation of antenna). A detailed special investigation needs being made for final identification.

No		Baseline	Length (km)	Number of points	Time span of observations
1	i	Wettzell - Medicina	522	38	04.04.87 - 09.06.95
2	c	Wettzel - Onsala	920	226	17.11.83 - 29.06.95
3	c	Wettzel - Matera	990	77	21.12.90 - 09.06.95
4	c	Richmond - Westford	2045	563	05.01.84 - 19.08.92
5	c	Richmond- HRAS085	2363	350	05.01.84 - 30.10.90
6	i	Westford - HRAS085	3135	375	04.01.85 - 17.06.89
7	c	Richmond- Mojave12	3595	221	05.01.84 - 11.08.92
8	i	Gilcreek - Mojave12	3816	284	08.07.84 - 01.09.92
9	i	Westford - Mojave12	3904	445	29.06.83 - 01.09.92
10	c	Gilcreek - Kokee	4728	146	09.09.93 - 26.07.95
11	c	Gilcreek - Kauai	4728	368	08.07.84 - 15.03.94
12	i	Gilcreek - NRAO85 3	5035	378	20.02.89 - 26.07.95
13	i	Gilcreek - Westford	5040	290	29.08.84 - 29.06.95
14	c	Gilcreek - Kashima	5427	152	30.07.84 - 25.07.95
15	c	Westford - Onsala	5601	212	18.03.82 - 29.06.95
16	i	Wettzell - Westford	5998	822	17.11.83 - 29.06.95
17	c	Fortleza - NRAO85 3	6074	115	07.07.93 - 19.07.95
18	c	Wettzell - Algopark	6155	51	02.07.90 - 15.06.95
19	i	Wettzell - NRAO85 3	6726	186	20.11.91 - 26.07.95
20	i	Wettzell - Gilcreek	6858	290	31.08.84 - 26.07.95
21	c	Kokee- NRAO85 3	7208	118	09.06.93 - 26.07.95
22	c	Kauai- NRAO85 3	7208	227	20.02.89 - 15.03.94
23	c	Wettzell - Fortleza	7215	123	22.04.93 - 19.07.95
24	c	Matera-NRAO85 3	7356	91	05.10.90 - 20.12.94
25	c	Wettzel - Richmond	7588	534	25.01.84 - 19.08.92
26	c	Gilcreek - Matera	7660	84	05.10.90 - 24.01.95
27	i	Wettzell - Hartrao	7832	98	10.01.86 - 18.07.95
28	i	Wettzell - HRAS085	8418	415	17.11.83 - 30.10.90
29	i	Wettzell - Mojave12	8589	266	31.08.84 - 01.09.92
30	i	Hartrao - Hobart26	9168	99	21.12.89 - 25.07.95
31	c	Gilcreek - Fortleza	9865	82	07.07.93 - 12.07.95
32	c	Wettzell - Kokee	10357	148	09.06.93 - 26.07.95
33	i	Westford - Hartrao	10659	85	10.01.86 - 04.04.95
34	i	Gilcreek - Hobart26	10953	78	27.09.89 - 25.07.95
35	c	Fortleza - Kokee	11064	100	14.07.93 - 19.07.95

Table 1. Information about baselines.
Sign 'i' means that the baseline contains inland sites only.
Sign 'c' means that one or both sites are close to ocean coast.

Baseline	Rate (mm/year)	Ampl. of annual signature (mm)	Phase of annual signature (degrees)	Ampl. of semiannual signature (mm)	Phase of semiannual signature (mm)
Wett - Med	-2.3 ± 0.3	1.0 ± 0.9	35 ± 53	2.7 ± 1.5	200 ± 17
Wett - Ons	-0.6 ± 0.1	0.7 ± 0.4	124 ± 30	0.3 ± 0.4	193 ± 65
Wett - Mat	-3.7 ± 0.4	2.8 ± 0.6	117 ± 13	1.3 ± 0.5	276 ± 25
Rich - West	-0.3 ± 0.1	0.7 ± 0.4	187 ± 32	0.9 ± 0.4	300 ± 25
Rich-HRAS	2.0 ± 0.3	1.0 ± 0.8	150 ± 42	0.5 ± 0.7	33 ± 86
West-HRAS	5.2 ± 0.3	3.1 ± 0.6	140 ± 11	1.2 ± 0.6	227 ± 28
Rich- Moj12	5.1 ± 0.6	2.2 ± 0.7	165 ± 20	0.5 ± 0.8	156 ± 79
Gilc - Moj12	-10.7 ± 0.2	3.1 ± 0.5	98 ± 10	2.6 ± 0.5	336 ± 11
West- Moj12	0.7 ± 0.2	3.4 ± 0.4	126 ± 8	0.7 ± 0.5	251 ± 37
Gilc - Kok	-43.9 ± 0.9	5.2 ± 0.7	99 ± 7	1.8 ± 0.8	287 ± 22
Gilc - Kau	-45.5 ± 0.2	4.1 ± 0.6	121 ± 8	1.3 ± 0.6	304 ±.25
Gilc-NRAO	-1.9 ± 0.3	4.9 ± 0.5	120 ± 6	2.2 ± 0.5	223 ± 15
Gilc - West	-0.3 ± 0.1	3.1 ± 0.4	136 ± 8	1.1 ± 0.4	243 ± 21
Gilc - Kash	1.7 ± 0.4	7.8 ± 1.4	129 ± 10	2.4 ± 1.3	289 ± 35
West - Ons	17.4 ± 0.2	6.5 ± 0.8	167 ± 7	0.6 ± 0.8	193 ± 77
Wett - West	17.4 ± 0.1	5.5 ± 0.4	119 ± 4	1.9 ± 0.4	205 ± 12
Fort-NRAO	4.6 ± 1.7	4.4 ± 1.3	132 ± 17	1.7 ± 1.2	96 ± 40
Wett - Alg	17.6 ± 1.5	10.5 ± 9.0	114 ± 33	6.0 ± 4.7	53 ± 44
Wett-NRAO	15.6 ± 0.8	7.4 ± 0.9	142 ± 7	1.4 ± 0.9	201 ± 38
Wett - Gilc	10.0 ± 0.4	5.4 ± 0.7	111 ± 7	3.4 ± 0.7	257 ± 11
Kok-NRAO	15.6 ± 1.6	6.3 ± 1.3	147 ± 12	1.4 ± 1.2	174 ± 53
Kau-NRAO	13.8 ± 0.9	6.3 ± 1.4	135 ± 12	1.0 ± 1.4	182 ± 80
Wettl - Fort	18.6 ± 2.2	5.1 ± 1.7	120 ± 17	0.9 ± 1.5	250 ± 101
Mat-NRAO	14.1 ± 1.5	11.9 ± 1.8	133 ± 9	2.9 ± 1.8	306 ± 36
Wettl - Rich	14.8 ± 0.3	3.6 ± 0.9	138 ± 15	1.4 ± 0.9	143 ± 37
Gilc - Mat	2.3 ± 1.6	9.2 ± 1.8	129 ± 12	3.2 ± 1.8	287 ± 31
Wett - Hart	-2.9 ± 0.8	3.0 ± 2.9	100 ± 48	3.7 ± 2.7	206 ± 41
Wett-HRAS	14.0 ± 0.7	7.9 ± 1.7	167 ± 11	0.9 ± 1.6	148 ± 99
Wett- Moj12	8.3 ± 0.6	7.4 ± 1.1	114 ± 8	1.0 ± 1.1	85 ± 62
Hart- Hob26	32.9 ± 2.7	13.1 ± 5.1	323 ± 23	2.4 ± 5.3	112 ± 125
Gilc - Fort	12.1 ± 3.3	9.7 ± 2.7	93 ± 14	3.7 ± 2.4	334 ± 37
Wett- Kokee	-20.0 ± 2.2	11.3 ± 1.8	113 ± 8	3.5 ± 1.8	267 ± 26
West - Hart	13.0 ± 1.5	9.3 ± 5.8	89 ± 31	7.8 ± 5.4	207 ± 38
Gilc - Hob26	-34.9 ± 1.9	8.4 ± 5.0	319 ± 35	16.4 ± 4.8	335 ± 17
Fort - Kokee	36.2 ± 4.1	8.5 ± 3.0	83 ± 19	3.3 ± 2.8	333 ± 49

Table 2.
Results of parametrical model (1) estimation.
Titles of sites cut down.

After parametrical model (1) adjustment we have obtained an estimates of the six parameters. Table 2 contains the linear trend coefficients as well as amplitudes and phases of annual and semiannual signatures with standard deviations. Fig.3 shows the relation 'baselength-annual amplitude signature' for all 35 baselines; and, separately, for baselines from both so-called 'inland' and one or two 'coast' stations in order to evaluate the ocean influence on the seasonal variations. Table 3 contains the parameters of their regressions. The coefficients are practically equal to each other therefore one can make the conclusion that the power of annual variations does not depend on location of VLBI station relatively to large mass of water.

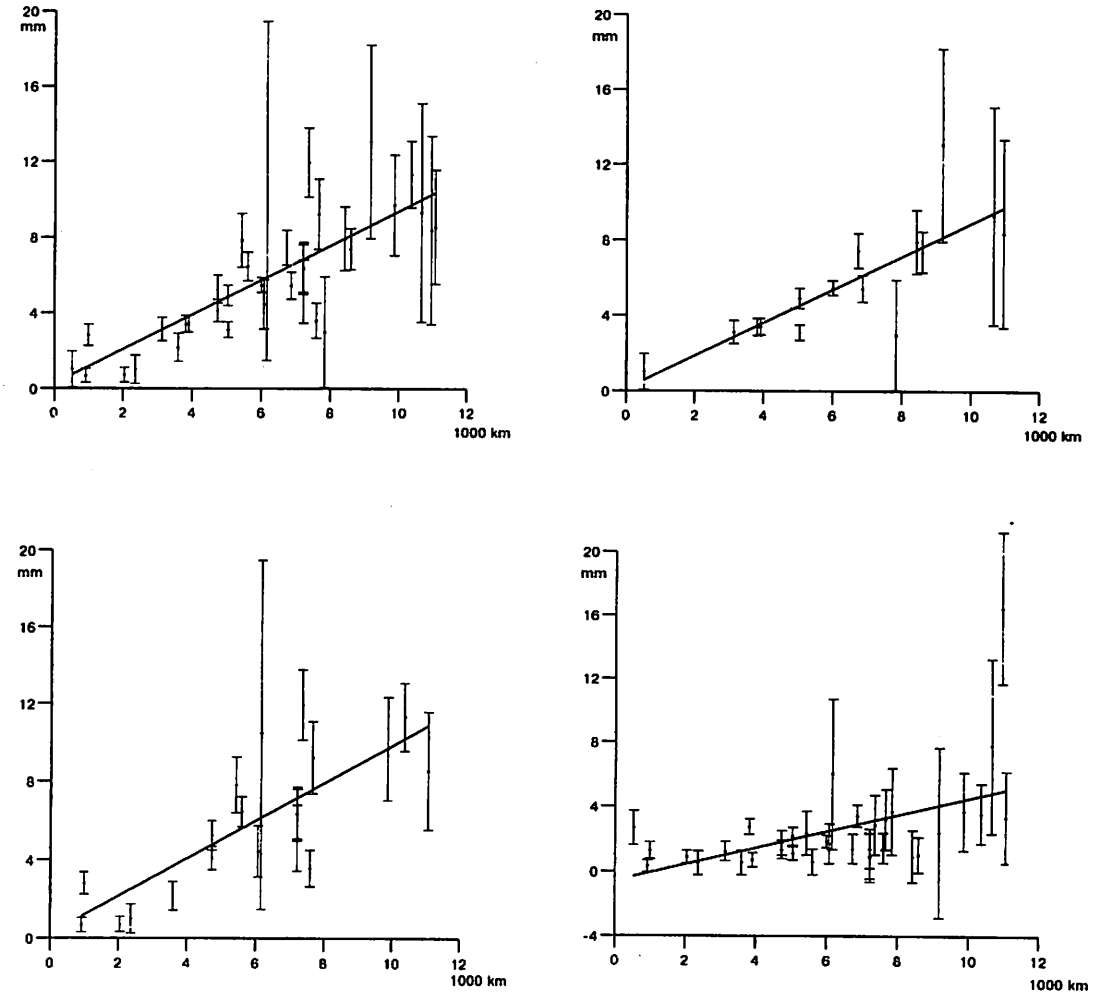

Fig.3.
The pictures baselenght versus amplitude of annual signature
for all 35 baselines (left, top), 15 baselines from inland sites only (right, top),
20 baselines with coast stations (left, bottom) and of semiannual signature
for 35 baselines (right, bottom). Error bars and linear trend are shown.

For semiannual signature there is no so obvious correlation between amplitude and baselength. Moreover, for 10 baselines from the set under study the amplitude estimates are not meaningful. Fig.3 (right, bottom) shows the plot 'baselength-semiannual signature amplitude' and last column of Table 3 contains regression coefficients. It seems that semiannual signature amplitude increases proportionally to baselenght too, but the

dependence is not so clear as for annual one. Probably, the effect is larger for high-latitude stations. For example, semiannual signatures are meaningful for all baselines with station Gilcreek (latitude 64°). For baseline Gilcreek - Hobart26 which has the largest latitude angular distance (106°) the effect exceeds 15 mm! The corresponding point is too far from linear trend on Fig.3.

Discussion.

Increasing of both seasonal signatures proportionally to baselength means that they are affected by variations of the site radial components. The similar conclusion has been made for high-frequency baselength variations as well [8,9]. But in contrariety to the latter, amplitudes of annual and semiannual signatures do not depended on distance from ocean coast. Therefore the inverted barometric effect (which reduces contribution of high-frequency atmospheric pressure variations to total load) has no influence on the seasonal effect. It is known that the high-frequency displacements of the Earth are arisen mostly from variations of atmospheric pressure on site and adjacent area (1000-2000 km) [8]. It means that the natural phenomena causing the seasonal effects is global one because it distorts the Earth surface on large area simultaneously.

The conclusion confirms by distribution of annual signature phases. Almost all of them (32 from 35) are at the range 80°-190°; 22 from them are at the range 110°-150°. Three baselines: Wettzell - Medicina, Gilcreek - Hobart26 and Hartrao - Hobart26 have an estimates of phases out of the span. First one is the shortest (522 km). It seems that the variations of radial component are not valuable on the short distance. In Table 2 the standard deviations of short baselines only slightly lesser than amplitudes of annual signature. Standard deviations of phases are large for short baselines, for Wettzell - Medicina baseline it reaches ±53°.

Coefficient	annual, 35 baselines	annual, 15 baselines ("inland")	annual 20 baselines ("coast")	semiannual, 35 baselines
c (mm)	-0.09 ± 0.40	0.15 ± 0.68	-0.17 ± 0.54	0.53 ± 0.20
k (mm/1000 km)	0.88 ± 0.09	0.83 ± 0.13	0.92 ± 0.14	0.21 ± 0.06

Table 3.
Results of linear trend A(b) = c + kb parameters estimation. A is the amplitude of annual or semiannual signature, b is the mean of baselength.

As to baselines with Hobart26 it is obvious that both of them have meanings of phase which are far from span of maximum concentration (110°-150°) on one half of period (180°). Making hypothesis that the Australian station is responsible for the baselengths variations on global scale, we should accept that radial component of the site variates in opposition to radial components of other sites. Therefore radial components for the Earth at all become the shortest at the 'winter-spring' (February-March in Northern hemisphere and August-September in Southern hemisphere) and the longest at the 'summer-autumn'

epoch. One should note that the epoch of minimum coincides with one of snow melting for both hemispheres.

Amplitudes of semiannual signature in Table 2 are lesser than for annual one usually. The phases do not concentrate to any special range. Therefore there are some doubts that the semiannual variations are directed by global process. Probably, seasonal effects are more powerful in high latitudes only; it follows from simulation using atmospheric observations [6]. For example, in Table 2 all estimates of semiannual signature amplitude are meaningful for baselines which contain the most north station Gilcreek (64°). We hope that the problem will be solved in future after improvement of data precision.

Conclusions.

Applying spectral analysis to set of 35 baselines we have found variations of their lengths with periods 1 and 0.5 year. Variations of VLBI site radial components are responsible for the effect because the amplitudes of the seasonal variations increase with baselength. The following expression introduce the slope 'baselength-annual signature amplitude'

$$A(b) = 0.09 + 0.88b \qquad (2)$$

The estimated coefficients of linear trend do not depend essentially on distance of individual station from ocean coast. Therefore inverted barometer effect is not likely to reduce the contribution of annual pressure variations to the station displacement. Moreover, the phase estimates concentrate to very narrow span (40°). Unlikely that the phase distribution is accident. These results indicate that annual signature is affected by any global natural process.

As to semiannual signature there is no so strong confidence that it is a global effect. However it is enough powerful for a few baselines, especially, which are located at the high latitudes. Below the relationship like (2) follows

$$A(b) = 0.53 + 0.21b \qquad (3)$$

To point out a reason of the seasonal variations into baselengths is difficult now. Annual signal could be arisen from a variety natural phenomena with period 1 year which are able to contribute into total loading effect. Fortunately, the discovering of semiannual signal indicates that any theoretical hypothesis should predict an occurrence of signal with period 0.5 year. It seems seasonal transferring of atmospheric mass is the most appropriate explanation of the effect. However, snow loading could make essential contribution to total load for stations at the middle and high latitudes as well.

References

1. D.F.Argus, R.G.Gordon, *No Net Rotation Model of Current Plate Velocities Incorporating Plate Motion Model NUVEL-1.* Geophys. Res. Let., 18, pp.2039-2042, 1991.
2. D.S.MacMillan, C.Ma, *Very Long Baseline Interferometry Atmospheric Modeling Improvement.* Journal of Geophys. Res., 99, pp. 637-651, 1994
3. T.A.Herring, D.Dong, *Current and future accuracy of Earth Orientation Measurements*, in Proc. of AGU Chapman Conference on Geodetic VLBI: Monitoring and Global Change, pp.306-324, 1991.
4. N.Zarraoa, *VLBI in the far North. A closer look.* in Proc of 10-th Meeting on VLBI for Geodesy and Astrometry, pp. 103-108.
5. A.E.Niell, *Vertical Change and Atmosphere Correction in VLBI, Current and future accuracy of Earth Orientation Measurements*, in Proc. of AGU Chapman Conference on Geodetic VLBI: Monitoring and Global Change, pp.147-158, 1991.
6. W.Rabbel, J.Zschau, *Static deformations and gravity changes at the earth's surface due to atmospheric loading*, J.Geophys., 80-99, 1985.
7. S.Manabe, T.Sato, S.Saki, K.Yokoyama, *Atmospheric loading effect on VLBI observations, Current and future accuracy of Earth Orientation Measurements*, in Proc. of AGU Chapman Conference on Geodetic VLBI: Monitoring and Global Change, pp.111-122, 1991.
8. T.M.vanDam, T.A.Herring, *Detection of atmospheric pressure loading using very long baseline interferometry*, Journal of Geophys.Res., 99, pp.4505-4517, 1994.
9. D.S.MacMillan, J.M.Gipson, *Atmospheric pressure loading parameters from very long baseline interferometry observations.* Journal of Geophys. Res., 99, pp. 18081-18087, 1994.
10. V.B.Bakushevich, P.D.Dvulit, *The influence of snow cover and underground water level on the determinations of the Earth rotation in Poltava*, in Proc. of Journees 1995, Earth Rotation, Reference Systems in Geodynamics and Solar System, Ed. by N.Capitaine, B.Kolaczek, S.Debarbat, p.172, 1995.
11. C.Ma, J.Ryan, *NASA Space Geodesy Program - GSFC, Data Analysis*, VLBI Geodetic Results, 1979 - 1995.5, Goddard Space Flight Center, Greenbelt, Maryland, 1995.

Determination of Height Changes in Regional GPS Networks

Barbara GÖRRES

Geodetic Institute of the University of Bonn, Nußallee 17, D-53115 Bonn, Germany
E-mail: goerres@uni-bonn.de

Abstract: At the University of Bonn an interdisciplinary geodynamics project has been initiated in 1991 to study the complex processes associated with the transport of matter between the atmosphere and the ground including its subsurface layers. The area under investigation is the Lower Rhenish Embayment, a zone both known for its present-day seismo-tectonic activity and its extensive brown coal mining. One section of the project is concerned with the determination of temporal changes in height by geodetic means, such as precise levelling and GPS.
While precise re-levellings have been carried out by the survey administrations at regular intervals since 1956, a series of annual GPS-campaigns covering 13 simultaneously observed points has been started in 1993. The size of the network is about 100 km.
In extensive tests it turned out that apart from taking into account tropospheric refraction and phase center variations it is important to extend the observation sessions to at least 24 hours and use low elevation observations in order to improve the accuracy (repeatability) of the height component. This is archieved even when standard models for the tropospheric refraction are used, on condition that tropospheric path delay parameters are estimated.
Extensive tests show that the best repeatabilities are obtained when using an elevation cutoff of about 10°.
At three points significant ground water induced height changes of up to 25 mm/year were detected. Comparison with levelling results for identical stations lead to good agreement.
The agreement in terms of wrms repeatability is at the level of ± 2 mm in the height component on distances of up to 100 km, which is superior to the levelling accuracy on distances longer than 10 km. The conclusion points to an increasing importance of GPS for height determinations in extended networks.

1 Introduction

The new Euro-VLBI-project is going to deal with the determination of heights in European dimensions. In particular concerning the handling of the tropospheric refraction it was already stated, that VLBI can benefit from GPS. What else can be carried over? How can experiences in regional networks contribute to improve european solutions? Especially the question about the "best" elevation cut-off has to be raised.

2 The GPS network HEIKO

The area under investigation is the Lower Rhenish Embayment (fig. 1), which is part of the West European Rift Belt. The region located north-west of Bonn and Cologne (detailed map see fig. 6) is known for its

Presented at the 11th Working Meeting on European VLBI for Geodesy and Astrometry, Onsala, Sweden, 1996

present-day tectonic activity (small earthquakes along the active faults) and its extensive brown coal mining, which causes ground-water descent down to some 100 m.

The geodetic part of the project is concerned with the determination of temporal changes in height by precise levelling and GPS.

The GPS network HEIKO (**H**öhen-änderungen in **E**ifel und **KO**elner Bucht = height changes in the Eifel and the Cologne embayment) covers this area and consists of 13 sites [GÖRRES 1996]. The size of the network is about 100 km with baselines between 4 and 50 km length. The maximum height difference in the net amounts to approximately 600 m.

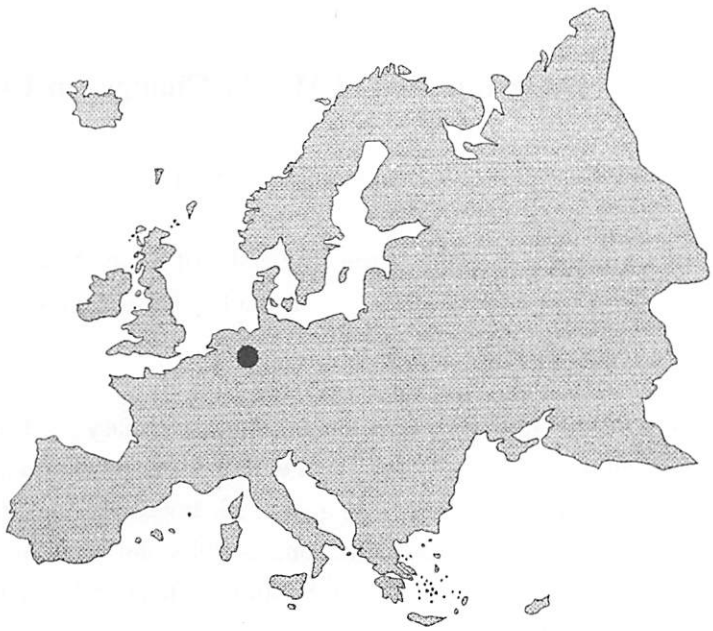

Fig.1: Location of the Lower Rhenish Embayment

Precise re-levellings have been carried out by the survey administrations at regular intervals since 1956. From these levellings we know that one can find ground-water induced height changes of up to 2.5 m within a span of time of 40 years [FRÖHLICH et al. 1986]. The levelling results give an excellent comparison standard for the estimated GPS heights.

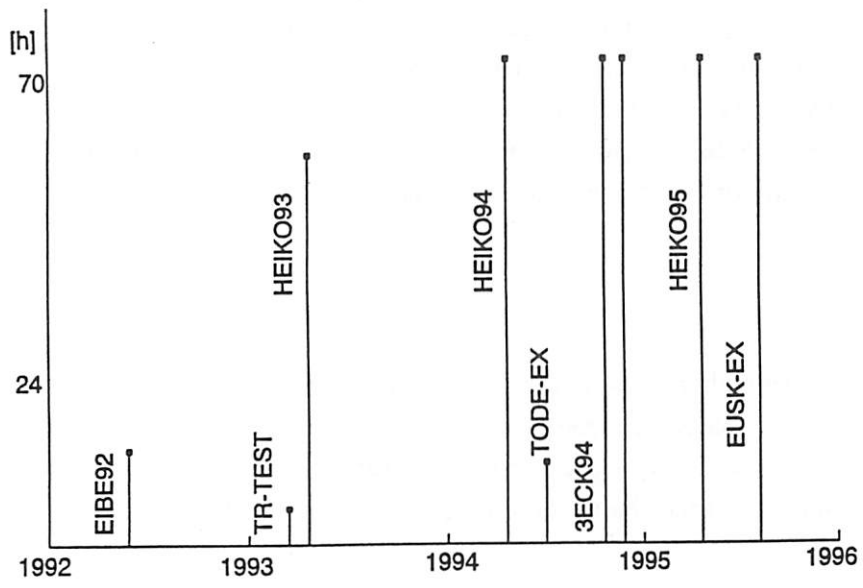

Fig.2: GPS campaigns in the network HEIKO from 1992 to 1995 (up component: length of observation time)

The series of annual GPS-campaigns (fig. 2) in the net has been started in 1993. The so-called HEIKO-campaigns are observed around the clock for 3 consecutive days. All points are observed simultaneously.

The first campaign in 1993 had to be carried out with a 'mix' of three different receiver/antenna types, i.e. Trimble SSE, Ashtech XII and Leica SR299, whereas the subsequent campaigns were observed only with

Trimble receivers (except one permanent station which is equipped with a TurboRogue). Moreover there are some extra measurements on selected points for special investigations.

3 Possibilities for the improvement of the height accuracy

The Global Positioning System provides the possibility to determine three dimensional coordinates with very high accuracy. Until now applications for monitoring of deformations of the earth surface have been focused on the horizontal components, because GPS yields them with higher accuracy.

The critical biases (tab. 1), which cause deviations in the height components, are the satellite geometry, phase center variations, multipath and above all the tropospheric refraction.

systematic errors		requirement for the elevation cut-off
satellites	satellite clocks	
	orbital errors	
	satellite geometry	0°
receiver and antenna	antenna height	
	phase center variation	calibration
	receiver clock	
signal propagation	ionospheric refraction	
	tropospheric refraction	?
	multipath	rather high
processing	ambiguities	

Tab.1: The critical biases for the height estimation are elevation dependend

The height accuracy can be improved either by advanced modelling or by selection of appropriate strategies. The main topic of our investigations is the development of strategies for the field measurements and the processing.

Of importance is, that all these mentioned problematic biases can be influenced by variation of elevation cut-off. Unfortunately the requirements particularly for the cut-off are not uniform but partly opposite.

- From the point of view of the geometric satellite-to-antenna relations the best ratio between height and horizonal components is received in round the clock-observation sessions with a cut-off of 0° [Santerre 1991]. (In any case the height result is by at least two times worse than the horizontal ones).
- Elevation dependend phase center variations enforce the precise calibration of all used antennas.

Above all they affect the height component. Because of the mix of different types of antenna in 1993 they have been estimated from field-measurements at the geodetic institute [BREUER et al. 1995]. All values from the calibration measurements were taken into account for the processing of the HEIKO data sets and improved the height accuracy significantly.

- Multipath cancels out in extended observation sessions and doesn't occur when a high cut-off is chosen or the points are situated in a surrounding void of reflections. That was considered when establishing the HEIKO network.

- For the tropospheric refraction the optimal procedure concerning observation duration and cut-off is not evident [more details see GÖRRES 1996]

The main question is: How can we come to a compromise concerning the choice of the cut-off? We look for a value right between the gain of additional important information when lowering the cut-off and the corruption of the results by roughly disturbed low-elevation data, which have been influenced by tropospheric refraction or multipath.

To focus on that item the processing results, where all the biases interact with each other, were analysed. All processings are done with the Bernese GPS Software.

Criterion for the quality of the estimated heights herein is not the height result itself but the repeatability of the heights. They show the height changes subsequently.

4 Cut-off tests

The cut-off tests were done with the results of two campaigns of the same 20 km baseline. The height results are given as a function of the variation of the cut-off between 2° and 25°.

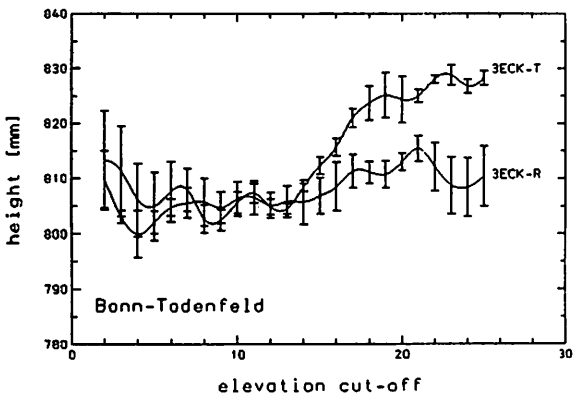

Fig.3a: short-term and long-term repeatability

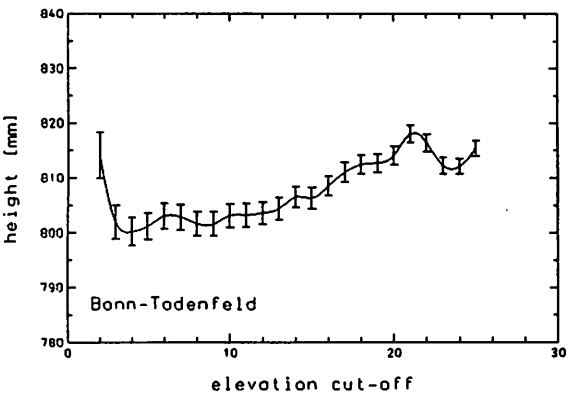

Fig.3b: formal errors of a single-day solution

In fig. 3a all heigh results are campaign results, which means that they consist of t12he mean of three 24 h observation sessions. In addition the standard deviation from the three daily solutions was estimated.

To make a comparison the second plot (fig. 3b) shows the results of a single-day together with the formal

errors given from the program adjustment. The impression found from that second plot are growing formal errors when lowering the cut-off. That is exactly the opposite as what is expexcted from the pure geometric understandings. The reason is probably increasing noise for low elevation signals.

Contradicting to the formal errors (fig. 3b) the repeatabilitis (fig. 3a) indicate the best results for lower elevation cut-offs.

The comparison of the different possibilities to estimate the height accuracy (formal errors, short-term and long-term repeatability) shows that even the daily repeatabilities within one campaign, which are in fact short-term repeatabilities, do not give a realistic value for the accuracy. A reliable accuracy can be given only by comparing the result of several campaigns as long-term repeatabilities.

From that contrast the best agreement of the height results evidently come out for a cut-off of about 10°.

The final confirmation of the cut-off was taken from the comparison of all results estimated from the same 20 km test baseline as before (fig. 4). The height difference amounts to approximately 300 m. The measurements were performed during all seasons and with different receiver and antenna types (even antenna combinations are included).

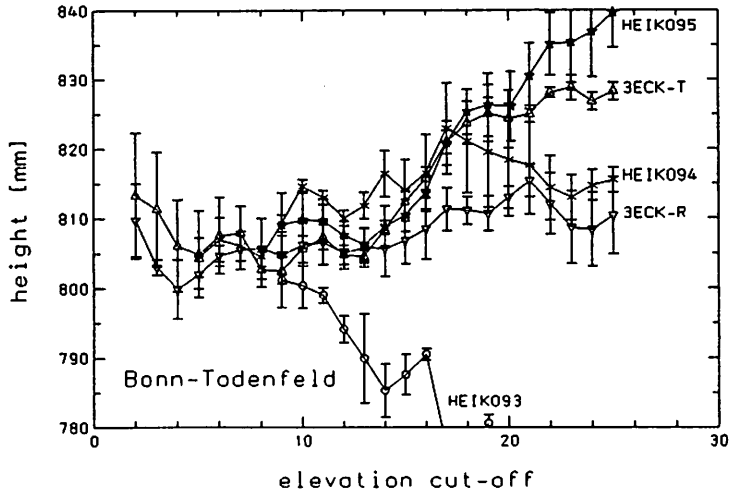

Fig. 4: Cut-off test with all campaign results for a 20 km baseline

Again the best agreement of the height results is to be within the region of approximately 10°, wheras the difference reaches up to 10 cm when using a cut-off of 25°. We see the consequence of the bad geometric situation for high cut-offs. It gives an impression of the variations which can occur only by changig the elevation cut-off in the processing routine. It is known that normaly 15° or even 20° is used in GPS processing.

To sum up all cut-off tests, which were done in GÖRRES [1996] the best repeatabilities are allways obtained when using an elevation cutoff of about 10°.

5 Estimated heights and height changes

The main topics of the used strategies for the field measurements and the processing of the HEIKO data are shown in tab. 2a and 2b:

site selection	surrounding void of reflections open visibility down to 10°
equipment	uniform antenna types
observations	session length: 24 h campaign duration: minimum of 3 sessions all points simultaneously
meteorological data	not necessary

Tab. 2a: Strategies for the field measurements

orbits	precise IGS-orbits
antenna phase-centers	elevation dependend phase center variations (or uniform antenna types)
ionospheric refraction	ionosphere free linear combination L_3
tropospheric refraction	a priori: Saastamoinen estimation of tropospheric parameters
ambiguities	solve to integers
elevation cut-off	about 10°

Tab. 2b: Processing strategies

It can be pointed out that apart from a careful selection of the points and taking into account the phase center variations it is important to extend the observation sessions to at least 24 hours and to use low elevation observations in order to improve the accuracy of the height component.

This is archieved even when a standard model (as Saastamoinen) is used for the tropospheric refraction, on condition that tropospheric path delay parameters are estimated. Additional solutions using recorded meteorological data did not improve the results.

The height results of the HEIKO network which were performed using this concept are given in the sample of plots in fig. 5 for each point. The coordinates of one point were kept fixed to the same numbers in all cases.

After fitting a straight line the rates (blue numbers) give significant height changes of up to -25 mm/year at three points. The average standard deviation of the rate is 2.4 mm/year. The agreement in terms of WRMS repeatability between all campaigns is at the level of ± 2 mm.

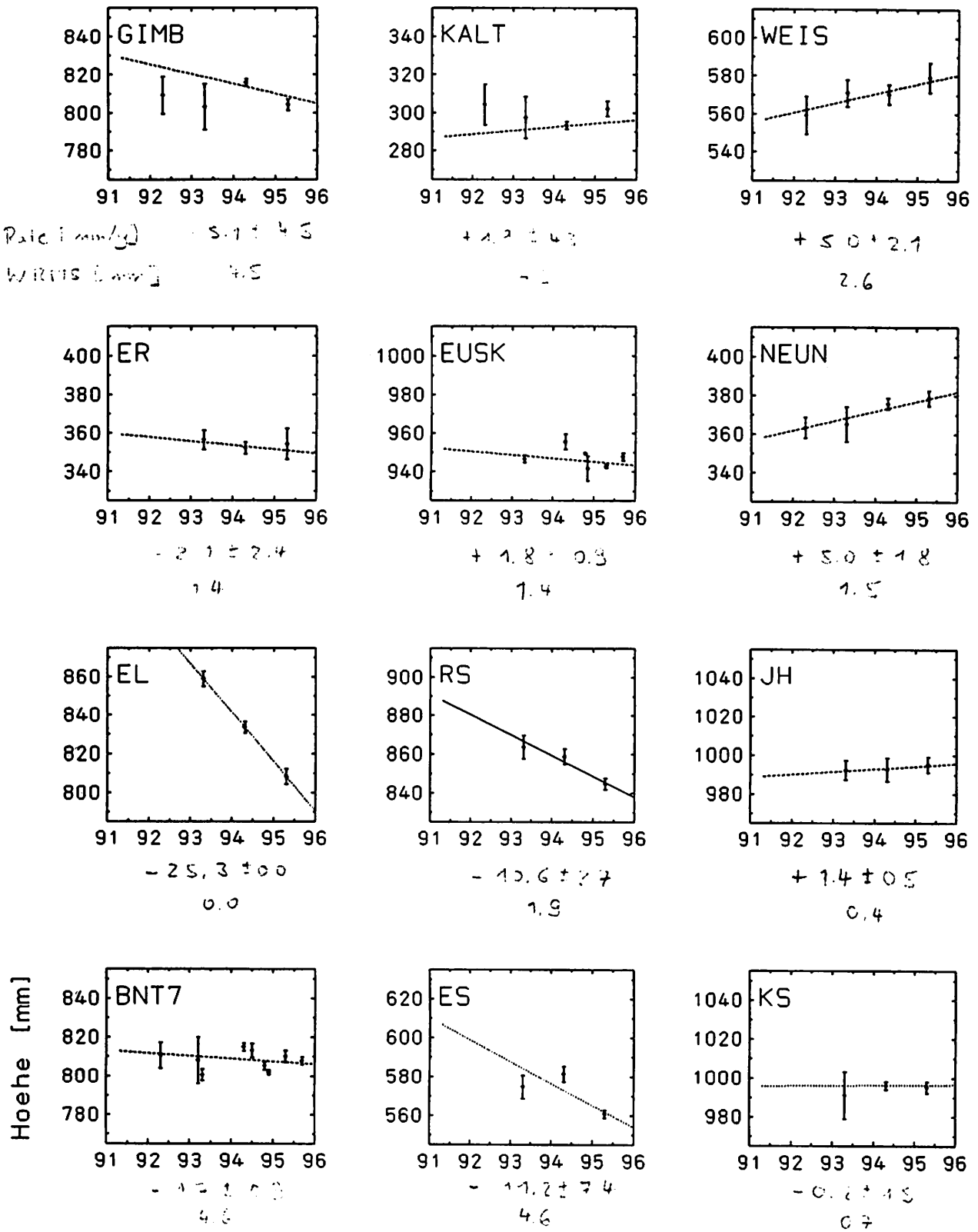

Fig. 5: Height results in the network HEIKO including rate and WRMS for each point

From fig. 6 it can be seen, that all points, which show a decrease in height, are located in the vicinity of the minings and the height changes are ground water induced.

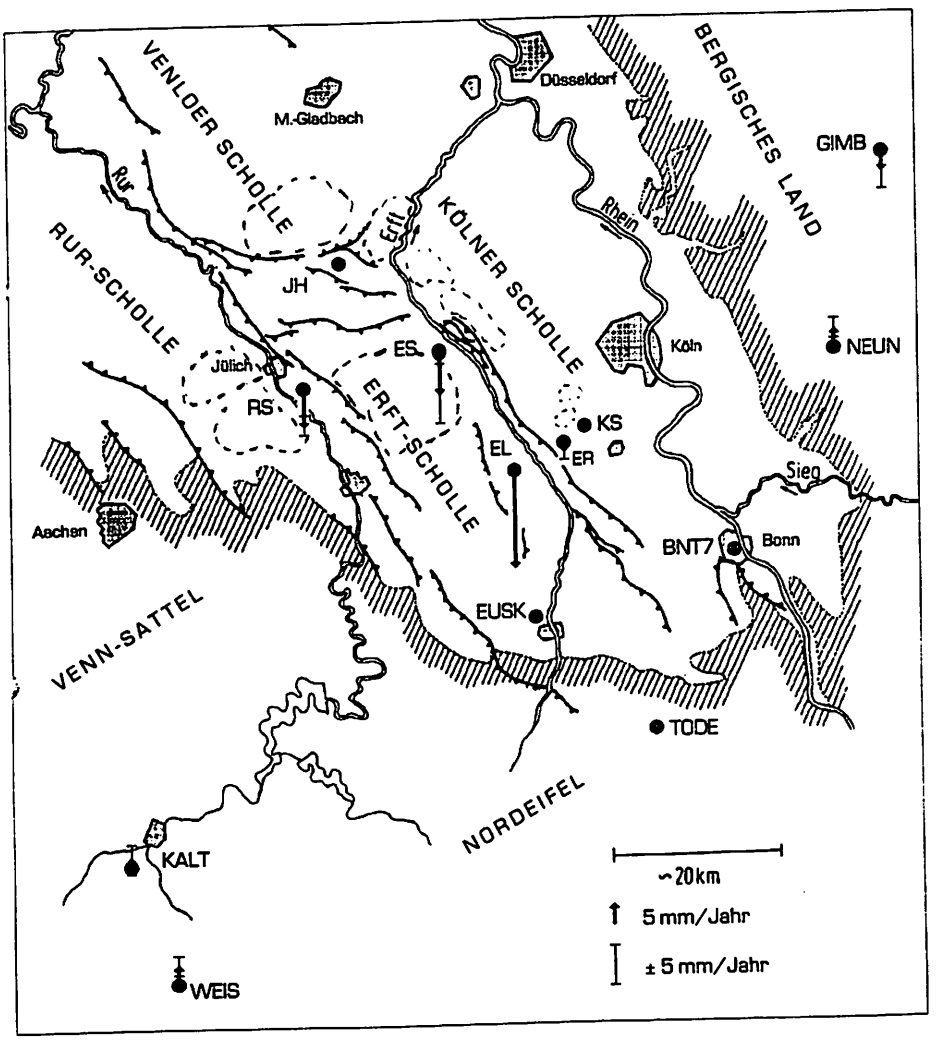

Fig. 6: estimated rate of height changes in the HEIKO GPS network from 1992 to 1995

6 Comparison of height changes from GPS and levelling

A good agreement in the quantities can be seen by comparison with the levelling results for 6 identical stations (fig. 7). Three stable and three descending points are determinable with both methods uniquely [LVermA]. No system tranformations of heights between GPS ellipsoidal heights and orthometric heights were applied, because only temporal height differences are checked. This is of course valid only under the condition of constant reference systems, e.g. that gravity changes may be neglected.

$$H_{ell}(t_i) - H_{ell}(t_j) \approx h_{orth}(t_i) - h_{orth}(t_j)$$

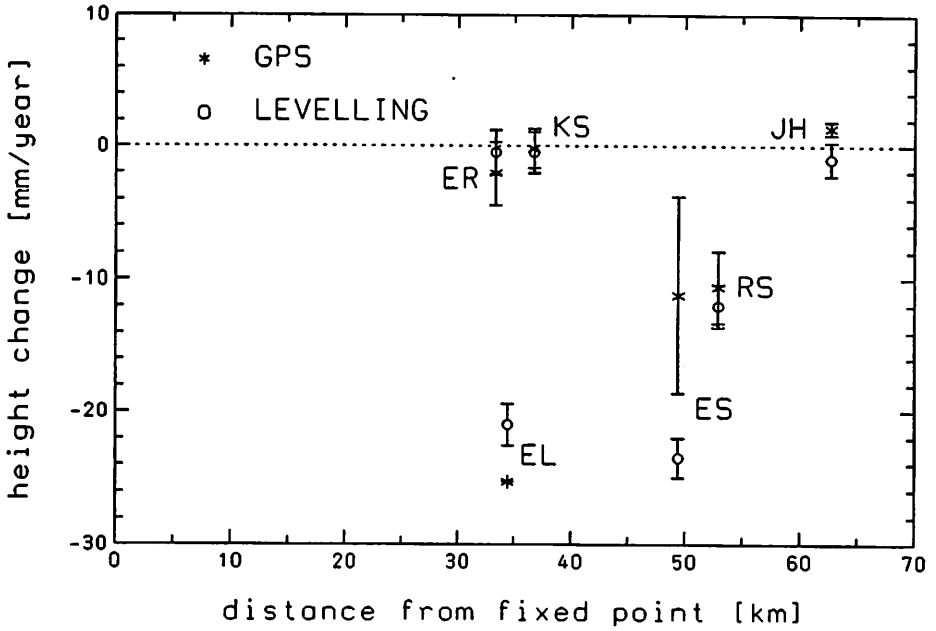

Fig. 7: Height changes from GPS and levelling from 1993 to 1995

A comparison of the estimated accuracies (fig. 8) shows that the GPS accuracy is superior to the levelling accuracy on distances longer than 10 km. The WRMS was used for GPS and the theoretical curve for precise levellings. The reason for the relatively bad levelling results for the long distances is the incremental progess which leads to excellent results only on short distances. The GPS accuracy doesn't depend on the baseline length up to 100 km.

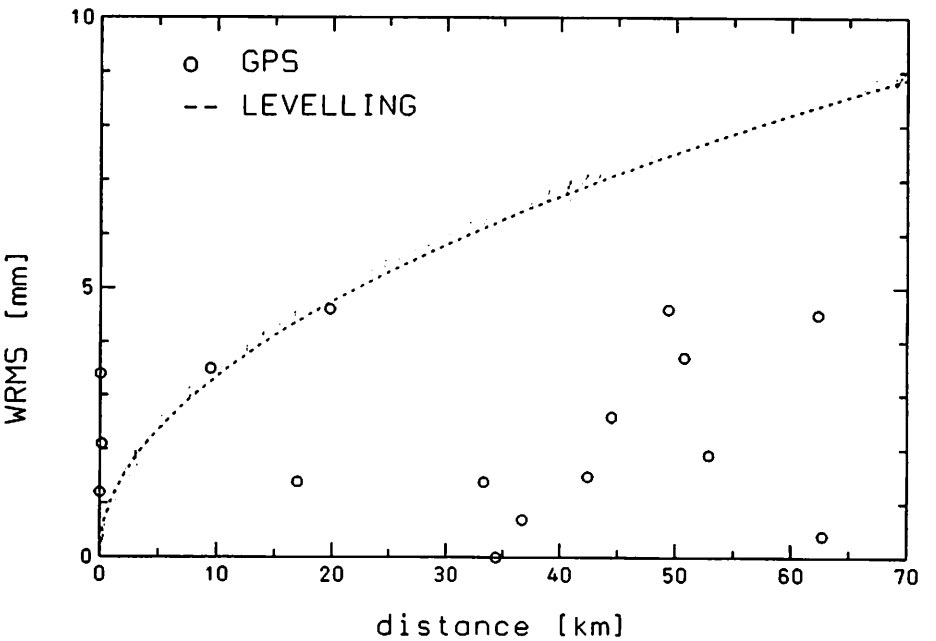

Fig. 8: Comparison of the accuracies
(GPS: WRMS, levelling: m_0 = 1.06mm/$\sqrt{km}$)

7 Conclusions and outlook

The conclusion points to an increasing importance of GPS for height determinations in extended networks.

In the European net the GPS results can be checked by comparing them to the VLBI results. This is in particular important to further valuations of the variations of heights as a function of the cut-off.
Only these comparisons will permit the examination of the absolute values of the heights.

Subsequently further augmentation of the accuracy are possible by improving the models of tropospheric refraction.

As a result we see a high potential for the estimation not only for the horizontal but also for the height component with GPS - on the condition that well-defined suitable strategies for the measurements and the processings are used- as shown by the investigations in the net HEIKO.

8 References

Breuer, B., J. Campbell, B. Görres, J. Hawig, R. Wohlleben: *Kalibrierung von GPS-Antennen für hochgenaue geodätische Anwendungen*, Zeitschrift für Satellitengestützte Positionierung, Navigation und Kommunikation, 49-59, 1995

Fröhlich, H., G. Müller: *Leitnivellements und regionale Deformationsanalyse in Nordrhein-Westfalen*, Vermessungswesen und Raumordnung 58/1, 1-19, 1986

Görres, B: *Bestimmung von Höhenänderungen in regionalen Netzen mit dem Global Positioning System*, DGK Reihe C Nr. 461, Verlag des Instituts für Angewandte Geodäsie, Frankfurt 1996 (in press)

Landesvermessungsamt Nordrhein-Westfalen (LVermA NW): *Ergebnisse der Leitnivellements 1993 und 1995*, (personal communication)

Santerre, R.: *Impact of GPS satellite sky distribution*, manuscripta geodetica 16. 28-53, 1991

Service of VLBI data analysis at the Institute of Applied Astronomy

PETROV L.
Institute of Applied Astronomy, Sanct-Petersburg, Russia

Summary:

Data analysis of geodetic VLBI experiments at the Institute of Applied Astronomy is at the present a routine operation and addressed towards 3 directions: the analysis of selected regional programs, rapid service of the Earth orientation parameters determination and obtaining global solutions of world wide VLBI network. Databases are being acquired from GSFC and from USNO analysis centers. Further analysis: calculation of the theoretical time delays and delay rates, group delay ambiguity resolution, parameter estimation, editing and reweighting are being carried out by means of the software system VORIN developed at the IAA, on a VAX6340 computer. Continuous series of the Earth orientation parameters, series of the positions of some stations produced in local mode are presented.

1 Introduction

Activities in the field of VLBI data analysis at the Institute of Applied Astronomy started in 1989 in the framework of the project QUASAR. The objectives of the activities were

— developing independent data analysis system. We believe that the best way to master the art of VLBI is to create own software.

— investigation of the procedure of data analysis.

— analysis of VLBI data for the purposes of hardware performance monitoring.

— scientific analysis of VLBI measurements for manifold astronomical and geodetic applications.

Software system VORIN was developed for these purposes [1]. After a long period of thorough testing we started to analyse VLBI data on a regular basis from the beginning of 1996.

Data analysis of geodetic VLBI experiments at the Institute of Applied Astronomy is at the present a routine operation and addressed towards the following directions:

- the analysis of selected regional programs;
- rapid service of the Earth orientation parameters determination;
- obtaining global solutions using observations of the world wide VLBI network.

In this paper we will first describe data analysis procedure, then present some results of the analysis.

Presented at the 11th Working Meeting on European VLBI for Geodesy and Astrometry, Onsala, Sweden, 1996

2 Data analysis procedure

Databases with measured group time delays and delay rates are being acquired from GSFC and from USNO via ftp. It is assumed that a primary data analysis of raw correlator output producing the values of group time delays and delay rates has been done by correlator personnel. This stage of the data processing is not implemented in the presented data analysis system. Further analysis is carried out by the software system VORIN [2], [3]. The analysis includes the following steps:

- **Reduction of the observations.** Theoretical time delays and delay rates are calculated in this step as well as their partial derivatives. A great deal of options in theoretical model is supported. Models adopted by IERS in Standards 1989, 1992 and IERS Conventions 1996 can be used as well. We strive for gathering a full collection of various published models of the effects affected on delay at one-picosecond level.

- **Crude estimation.** It includes determination of the preliminary values of clocks drift and shift for each station except fiducial one, group delay ambiguity resolving and detection of strong outliers. Special algorithm for crude estimation in automatic mode was implemented.

- **Accurate estimation.** The following parameters can be estimated: coordinates of the stations, source positions, Love numbers, Earth orientation parameters: UT1, angular velocity of the Earth Ω, pole coordinates X_p, Y_p, nutation offsets $\Delta\psi$, $\Delta\varepsilon$, tropospheric delay in zenith direction and clock functions for each station. Zenith tropospheric delay and clock function can be modelled by N–segmented linear spline.

  Parameters can be estimated in two modes: local mode when one session is included in analysis and global mode when observations collected in a set of sessions are analysed simultaneously. Weighted LSQ method is used. The equations of the equalities of the rates of change of the troposphere path delay in zenith direction on adjacent intervals with weights 1/(50 psec/hr) usually are added to the system of equations. Analogous equations for the clock function with weights $1/(7.5 \cdot 10^{-14})$ are added as well.

  Due to the the fact that not all observations depends on the whole set of the parameters normal matrix appeared to be considerably sparse. Moreover, it has a regular structure. Normal matrix which we produce in the local mode is a double bordered block-threediagonal. Normal matrix which we produce in the global mode is a double bordered block-diagonal, but its diagonal blocks are in turn double bordered block-threediagonal matrixes. Special fast algorithms are implemented for solving LSQ problems for such kind of matrixes. The solution strictly coincides with solution produced by straightforward way but it is calculated by several orders faster.

  For each session and for each baseline an additive corrections to the weights obtained on the base of signal to noise ratio are calculated. After applying these corrections to the raw weights the ratio of the weighted sum of the post-fit residuals to the estimates of their mathematical expectation becomes close to 1.

  When parameters are estimated in local mode several iterations are done usually. Each step of the iteration includes calculating normal matrix, solving the normal system, detecting outliers, expelling them out, calculating additive corrections to weights. Weights and outliers are stored and can be used further for global solution.

Software VORIN runs under Open VMS operating system and includes

- utilities for preparing auxiliary files: a priori Earth orientation series, catalogues of station coordinates, source coordinates, source maps (when available), ocean loading amplitudes and phases, planet ephemerides and other files.
- procedures to handle special database of VLBI observations. Software supports reading files with observations in original GSFC database format or in NGS format. Data are extracted from input files, transformed into an internal format and stored in a compressed form.
- procedures of reduction of VLBI observations, crude and accurate estimation. Special language KPOT is implemented for describing the job for parameter estimation. It provides sufficient flexibility in choice of the mode of the work and the objects of estimation.
- utilities for extraction of results of the estimation from the database, their transformation and representation.
- advanced set of testing routines.

Special attention has been paid to developing tools supporting data analysis in automatic mode on the base of specified configuration files. In the adopted approach an operator should not manage analysis, but only inspect the results of analysis produced in batch mode and correct configuration files if necessary. Nevertheless, utilities for analysis in interactive mode are implemented also. Our experience shows that processing at least 90% analysed sessions yield reasonably good results without human interference.

3 Presentation of the results

Weekly VLBI observations under the program NEOS-A are being analysed regularly. Databases with observations are being acquired from USNO in automatic mode. In operational solution the Earth orientation parameters: UT1, angular velocity of the Earth Ω, pole coordinates X_p, Y_p, nutation offsets $\Delta\psi$, $\Delta\varepsilon$, topocentric coordinates of some stations, the positions of poor determined sources as well as a number of nuisance parameters are estimated. The theoretical model is similar to the model proposed in IERS Standard 92 [4], except the following points:

— station displacements due to the solid tides of the 2-nd order were calculated using the complete expression of Wahr [5]. Radial displacements due to the lunar tide of the 3-rd order were also taken into account. Permanent tide was not removed from the calculated tidal displacements.

— diurnal and semidiurnal tidal variations in the polar motion and UT1 calculated according to the expansion GSFC 94 R 01 [6] were added to the interpolated a priori pole coordinates and UT1.

— vertical displacements of the stations due to the atmospheric loading were calculated using the regression coefficients obtained by Manabe [7].

We calculate atmospheric delay using the Saastamoinen expression for the dry delay in zenith direction and the mtt dry mapping function [8].

Operational solutions are being issued during 24 hours after appearing the databases. The results of the operational solutions are being published in monthly IERS Bulletin B.

Global solutions have also been obtained. The aim of the global solutions is to construct celestial and terrestrial reference systems as well as the station velocities field. On the basis of the global solutions a list of stations and sources is produced whose positions are estimated in operational solutions.

When coordinates of all stations, sources and the Earth orientation parameters are estimated the global matrix of equations has incomplete rank. To overcome this difficulty identifiability restrictions technique is used [9]. Strict conditions requiring that the new celestial system does not have rotation with respect to the a priori system and that the new terrestrial system does not have translation, rotation, translational velocity, rotational velocity with respect to the a priori system were imposed.

In global solution IAA 96 R05 all NEOS-A VLBI sessions from NEOS-A-1 (05-MAY-93) till NEOS-A-170 (30-JUL-96) were analysed. Coordinates and velocities of 10 stations and positions of 81 sources were estimated. A raw solution were obtained at the first step under no-net-rotation, no-net-translation conditions. The final celestial and terrestrial reference systems, the field of velocities and the EOP series were produced from the raw systems and the raw EOP series by applying to them additional translation and rotation. Parameters of the transformation were determined from the following boundary conditions: 1) position and velocity of the station WETZZELL should coincide with the values defined in ITRF-93 catalogue; 2) the right ascension of the source 2145+067 should coincide with the value defined in ICRF-93 catalogue; 3) the pole coordinates, UT1 and the nutation offsets to the IAU 1980 nutation theory at the moment MJD 49770.2519 should coincide with the values obtained by cubic spline interpolation of the EOP C04 series; 4) the angular velocity of the terrestrial reference system should coincide with the net angular velocity calculated under assumption that all stations whose velocities we estimated would move according to the NNR-NUVEL1A [10] velocity field. Obtained catalogues as well as the series of the Earth orientation parameters are available via anonymous ftp at `ftp://isida.ipa.rssi.ru/pub/EOS/VLBI`

In total 154 213 group delays from 170 sessions were included in analysis. W.r.m.s. of postfit residuals for the solution was 38.8 psec.

W.r.m.s. of postfit residuals for each session are shown in the plot 1. A series of corrections of the nutation in longitude to the IAU 1980 values is shown in the figure 2 and the plot of differences IAA 96 R05 and smoothed series IERS C04 for Y pole coordinate is depicted in the figure 3. Table 1 contains statistics of the systematic differences of EOP series IAA 96 R05 and IERS C04 for the period 1993.34–1996.59

Table 1:

Parameter	shift	drift (1/yr)	r.m.s.
UT1 (msec)	0.035	0.008	**0.018**
X_p (mas)	0.37	0.09	**0.25**
Y_p (mas)	−0.33	0.03	**0.21**
$\Delta\psi$ (mas)	−0.12	0.01	**0.27**
$\Delta\epsilon$ (mas)	0.01	−0.01	**0.11**

Figure 1: w.r.m.s of post fit residuals for sessions (psec)

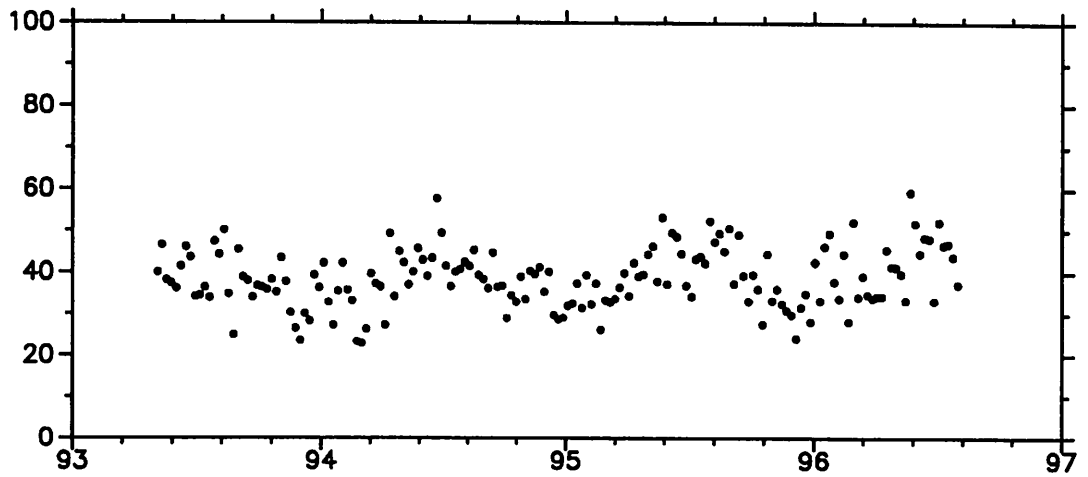

Figure 2: Corrections of the nutation in longitude to the IAU 1980 (mas)

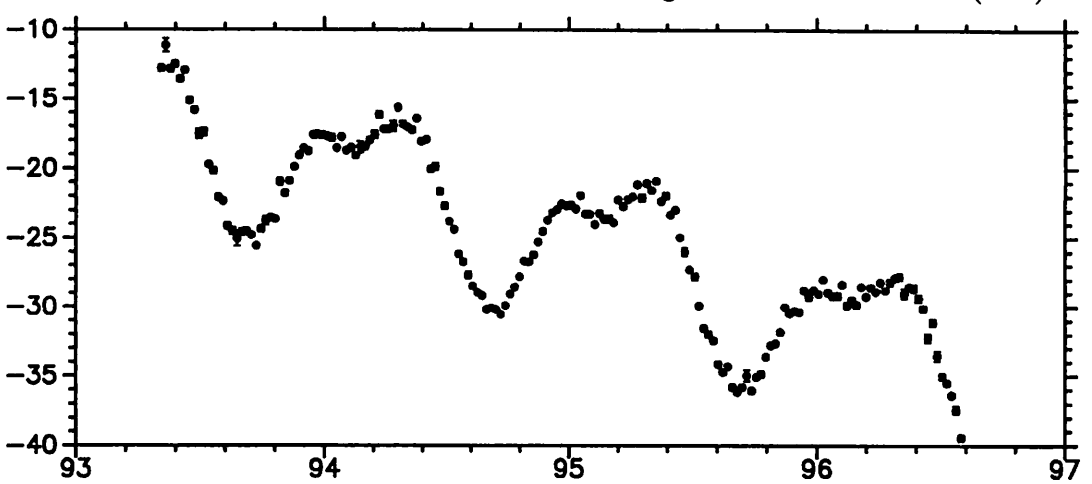

Figure 3: Diff. IAA 96 R05 and IERS C04 series for Y pole coordinate (mas)

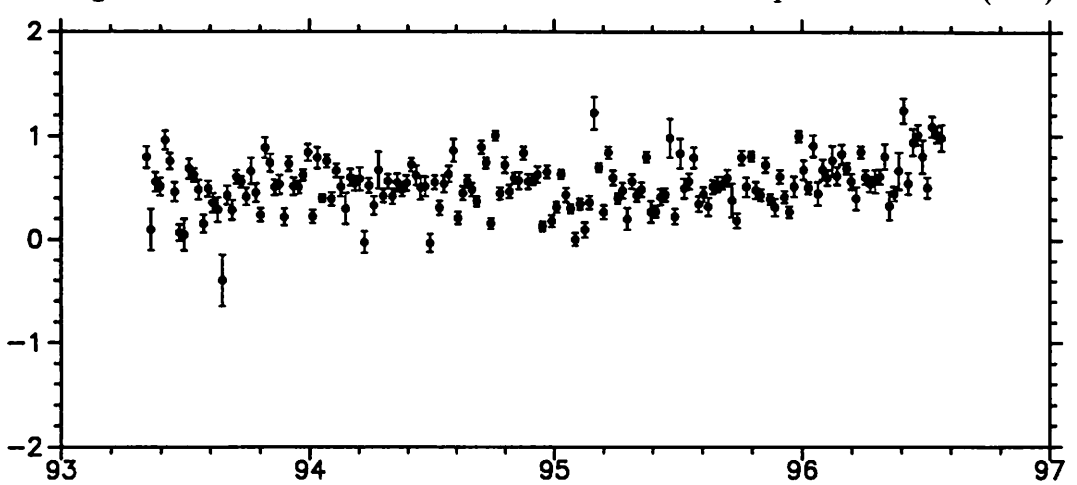

Figures 4–6 show the evolution of the topocentric positions of some stations which recently began to participate in geodynamical VLBI observations obtained from operational solutions. Table 2 presents corrections for vertical, east and north components to the a priori position on the epoch of the first session and correction to velocities produced from the series of coordinates with respect to the values predicted by NNR-NUVEL1A model. A priori coordinates of these stations were taken from the catalogue GLB979f [6]. Last column contains weighted standard deviation from linear fit. These series were obtained from the analysis of the observations under the NEOS-A program and the regional VLBI experiments where station CRIMEA participated.

Table 2:

Station	N sessions	time span (years)	Comp	Position (mm)	Velocity (mm/yr)	dev. (mm)
NYALES	20	94.76–96.52	V	1.0 ± 4.5	-5.2 ± 4.0	8.7
NYALES	20	94.76–96.52	E	1.1 ± 1.1	0.0 ± 1.1	2.3
NYALES	20	94.76–96.52	N	0.9 ± 2.1	0.1 ± 1.9	4.2
NRAO20	41	95.10–96.54	V	8.3 ± 3.9	-3.1 ± 4.3	8.9
NRAO20	41	95.10–96.54	E	-1.0 ± 1.8	-1.0 ± 2.0	4.1
NRAO20	41	95.10–96.54	N	2.6 ± 1.8	1.5 ± 2.0	4.5
MIAMI20	10	95.45–96.33	V	3 ± 16	20 ± 27	16.7
MIAMI20	10	95.45–96.33	E	-16.5 ± 4.8	21.0 ± 9.1	5.3
MIAMI20	10	95.45–96.33	N	5.7 ± 5.5	-14 ± 10	5.7
CRIMEA	10	94.48–96.31	V	10 ± 24	-13 ± 36	48.7
CRIMEA	10	94.48–96.31	E	17.7 ± 2.0	-6.0 ± 3.1	4.1
CRIMEA	10	94.48–96.31	N	-4.6 ± 1.5	-6.8 ± 2.5	3.0

Figure 4: Evolution of the topocentric position station Ny Alesund (cm)

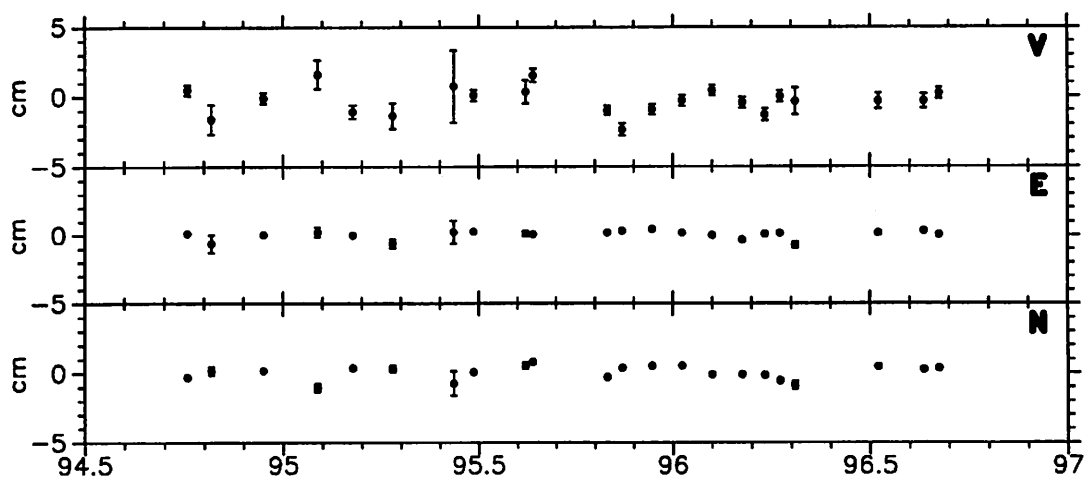

Figure 5: Evolution of the topocentric position station NRAO20 (cm)

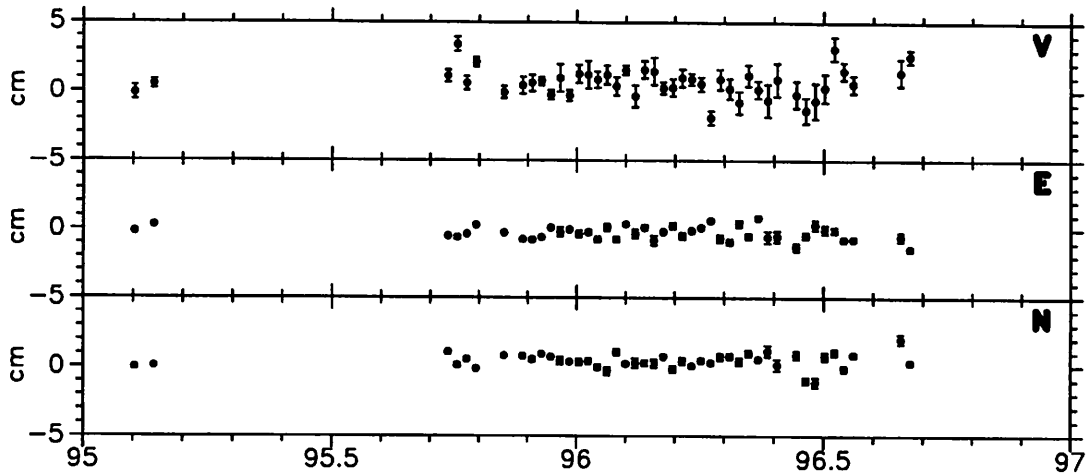

Figure 6: Evolution of the topocentric position station Crimea (cm)

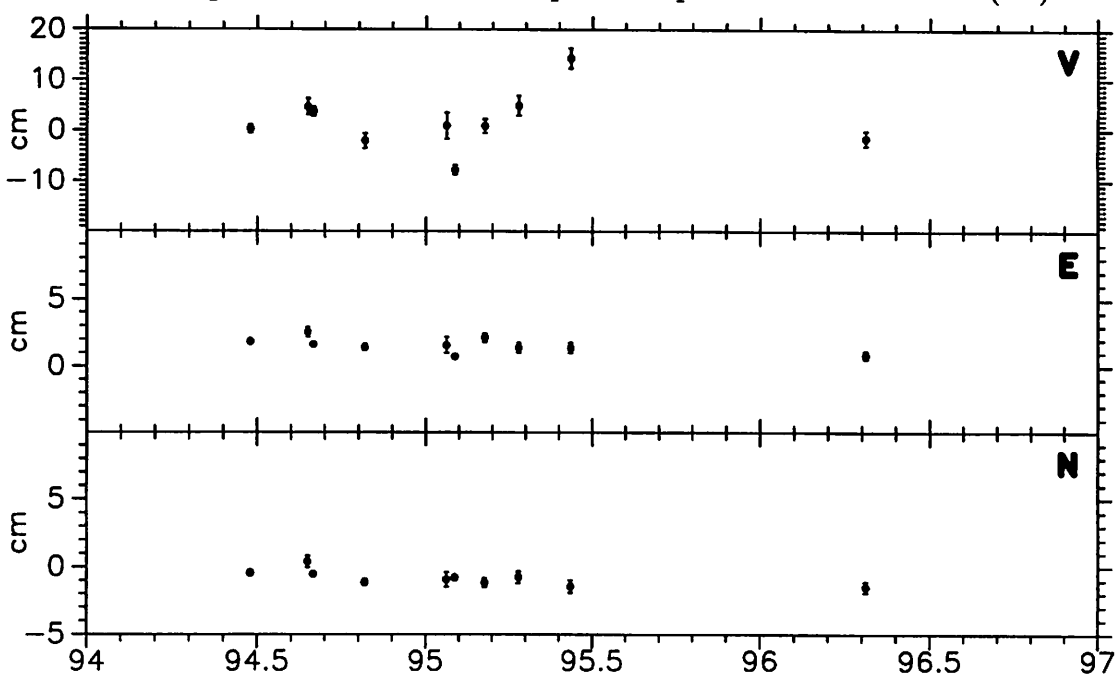

Starting from May of 1996 daily VLBI observations carried out under the program NEOS Intensive are being analysed in operational mode. During VLBI intensive experiments 4–5 sources are observed at a single east-west baseline during 2 hours. Shift and drift of the reference clock of a baseline, tropospheric delay in zenith direction for both stations and correction to UT1 were estimated in analysis of these data. Pole coordinates were set to the values from IERS Bulletin A and nutation angles were calculated using VKSNRE95.1 expansion [11]. Series IAA 96 R06 contains UT1 determined from NEOS Intensives for the period 96.04–96.57 . Figure 7 shows the plot of the differences IAA 96 R06 and smoothed IERS C04 for UT1. Standard deviation from IERS C04 series after subtracting linear trend is 28 μsec.

Figure 7: differences IAA 96 R06 and IERS C04 for UT1 (μsec)

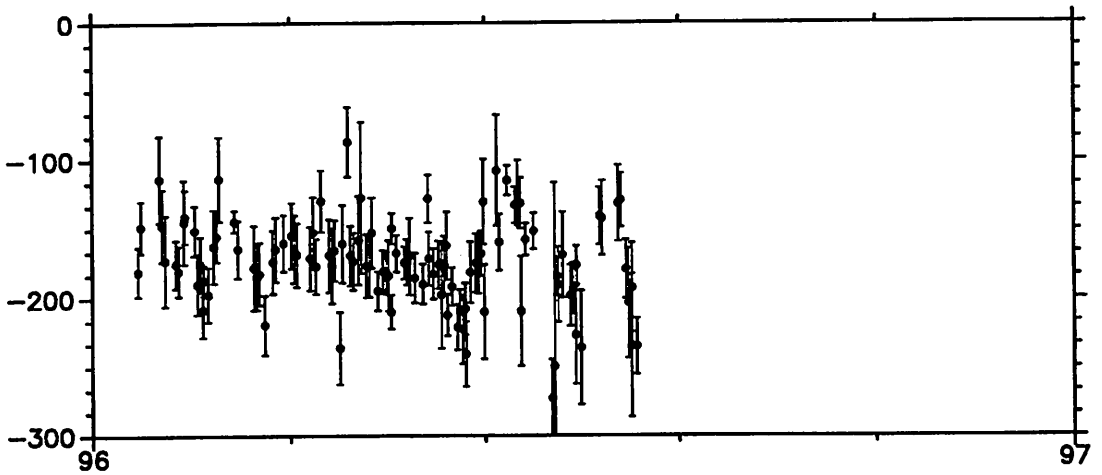

4 Conclusion

Results of the service of VLBI data analysis of the Institute of Applied Astronomy demonstrate the capacity to determine the Earth orientation parameters in operative mode with external accuracy not worse than 0.2 mas. The series of estimated topocentric coordinates of 4 new stations permit us to conclude that

— the repeatability of horizontal coordinates of the stations are 3–5 mm. This quantity appears to reflect real accuracy of the observations.

— Vertical repeatability of the position of stations NYALES and NRAO20 is excellent. Their horizontal velocities coincide with the values predicted by NNR-NUVEL1A model within their formal errors (1–2 mm/yr).

— Vertical repeatability of the position of stations CRIMEA and MIAMI20 is poor. The reason of bad vertical performance is not clear now. The departure estimated horizontal velocities from NNR-NUVEL1A model is detected for both stations on the 2σ level. It is difficult to judge now whether these discrepancies are real since too few data were analysed.

5 Plans for the future

In the next phase of these activities we plan

— to extend operational solutions on sessions conducted under other programs.

— to obtain global solutions using full set of geodynamical VLBI observations.

— to start producing monthly updates of terrestrial and celestial reference systems.

6 Acknowledgments

VLBI data used in this work have been provided by GSFC and USNO. I am indebted to Jim Ryan and Marshal Eubanks for granting access to the data and for useful discussion. I would like to thank A. Voinov for help in network programming.

References

[1] Petrov L. Software VORIN for secondary data analysis of geodetic VLBI observations. In *The sixth General Assembly of Wegener, St. Petersburg, June 20th — June 24th*, Pearlman J., P. Wilson, eds, pp. 51–56. Smithsonian Astrophysics Observatory, 1994.

[2] Petrov L. Secondary data analysis of geodetic VLBI observaion. I-II. Model of the reductions. Messages of IAA $\mathcal{N}$ 74–75, Institute of Applied Astronomy, St. Petersburg, p. 117, (in Russian), 1995.

[3] Petrov L. Secondary data analysis of geodetic VLBI observaion. Parameter estimation. Messages of IAA $\mathcal{N}$ 76, Institute of Applied Astronomy, St. Petersburg, p. 47, (in Russian), 1995.

[4] MacCarthy D.D. (ed.). IERS Standards. IERS Technical Note $\mathcal{N}$ 13, Observatoire de Paris, July 1992.

[5] Wahr J.M. Body tides on an elliptical, elastic, rotating and oceanless Earth. *Geophysical Journal of Rojal Astronomical Society*, **64**(3), pp. 677–703, 1981.

[6] Ma C., J.W. Ryan, D. Gordon. Site positions and velocities, source positions, and Earth orientation parameters, from the NASA space geodesy program GSFC: solution GLB979f. *IERS Technical Note*, $\mathcal{N}$ 19, pp. R13–R20, September 1995.

[7] Manabe S., T. Sato, S. Sakai, K. Yokoyama. Atmospheric loading effects of VLBI observations. In *Proceedings of the AGU Chapman Conference on Geodetic VLBI: Monitoring Global Change*, NOAA Technical Report NOS 137, NGS 49, pp. 111–122. Washington, D.C., 1991.

[8] Herring T.A. Modeling atmospheric delay in analysis of spase geodetic data. In *Proceedings of the Symposium on Refraction of Transatmospheric Signals in Geodesy, Netherland Geodetic Commission, Delft, Netherlands, Publications on Geodesy, N36*, De Munk J.C., T.A. Spoelstra, eds, pp. 157–164, 1992.

[9] Scheffe G. *Dispersion analysis.* N.Y., 1977.

[10] De Mets C., R.G. Gordon, D.F. Argus, S. Stein. Effect of recent revisions to the geomagnetic reversal time scale on estimates of current plate motions. *Geophysical Research Letters*, **21** (20), pp. 2191–2194, 1994.

[11] Souchay J., M. Fessel, C. Ma. Precise modeling of nutation and VLBI observations. *Astronomy and Astrophysics Supplements*, **116**, p. 473, 1996.

Determination of Tidal Parameters from VLBI Data

Rüdiger Haas
Geodätisches Institut der Universität Bonn (GIUB)
Nußallee 17, 53115 Bonn, Germany, (haas@uni-bonn.de)

Harald Schuh
Deutsches Geodätisches Forschungsinstitut (DGFI), Abt. I
Marstallplatz 8, 80539 München, Germany, (schuh@dgfi.badw-muenchen.de)

Johannes Wünsch
Astronomische Institute der Universität Bonn (AIUB)
Auf dem Hügel 71, 53121 Bonn, Germany, (wuensch@astro.uni-bonn.de)

Abstract We determined second degree and third degree Love and Shida numbers of the solid Earth tide model from VLBI data. The results for the different parts of the tidal spectrum (long-period, diurnal, semi-diurnal) are slightly different and a clear resonance in the tidal deformation can be seen around the Free Core Nutation [FCN]. In a more general approach complex Love and Shida numbers are used. This corresponds to a phase lag of the tidal deformation due to anelasticity of the Earth. Imaginary parts of the Love numbers h_{21} and l_{21} were solved for the strongest semidiurnal and diurnal tides. Finally the complex eigenfrequency of the FCN resonance was determined, with a FCN period of 430 $\pm$ 22 days in the celestial reference frame and a quality factor Q of 1400 ($1000 < Q < 2100$). This direct determination of Q based on tidal deformations measured by VLBI agrees rather well with superconducting gravimeter measurements but disagrees with former analyses of VLBI nutation data.

1 Introduction

A recent point of interest in geodesy is the investigation of high-frequency, i.e. diurnal and subdiurnal, tidal phenomena as for instance the solid Earth tides. Theoretical models for the solid Earth tides predict a frequency dependence of the tidal deformation in the diurnal frequency band which is expressed by frequency dependent second degree Love and Shida numbers h_{21} and l_{21}. Due to anelastic dispersion in the Earth's mantle the tidal deformation lags behind the tide generating potential. This can be expressed by complex Love and Shida numbers. In our paper we present Love and Shida numbers for individual tides and also parameters which describe the resonance of the tidal deformation in the diurnal frequency band. All those parameters were determined directly within a VLBI solution. This was done for the case of an elastic Earth and also by solving for imaginary parts of the Love and Shida numbers, corresponding to an anelastic Earth. The VLBI measurements permit the determination of these parameters independently from other hypotheses using a direct estimation approach.

2 Theoretical solid Earth tide model

Each theoretical model of the solid Earth tides consists of two parts. The first part is the tide generating potential due to the gravitational attraction of the solar system bodies. The second part is the so-called Earth's transfer function, which describes the change of the Earth's shape as a response to variations of the tide generating potential. It is determined by the Love number h for the radial displacements, the Shida number l for the tangential displacements and the Love numer k for the free space potential induced by the tides.

Presented at the 11th Working Meeting on European VLBI for Geodesy and Astrometry, Onsala, Sweden, 1996

In the most trivial case of a non-rotating, spheroidal and elastic Earth the topocentric tidal displacement of a station with spheroidal coordinates (ϕ, λ, r) is described by equations (1) to (3) which contain constant Love and Shida numbers. In these equations Δ_U, Δ_E, Δ_N are the tidal displacements in topocentric Up, East and North direction, respectively. The tide generating potential is denoted by W, g is the gravity at the station considered and ϕ and λ are the latitude and longitude of the station.

$$\Delta_U = h \cdot \frac{W}{g} \tag{1}$$

$$\Delta_E = l \cdot \frac{\partial W}{\partial \lambda} \cdot \frac{1}{g \cdot \cos(\phi)} \tag{2}$$

$$\Delta_N = l \cdot \frac{\partial W}{\partial \phi} \cdot \frac{1}{g} \tag{3}$$

The relationship between the tide generating potential and the tidal displacements becomes more complicated if we consider the Earth's shape, its structure, its material properties and its rotation. The Love and Shida numbers are not constant values anymore but become frequency and latitude dependent. Due to the different direction of the rotation axis of the Earth's fluid core and the rotation axis of the Earth's mantle the Earth has a normal mode called the Free Core Nutation [FCN] with an eigenfrequency in the diurnal frequency band. This mode is resonantly excited by the second degree, first order tidal potential so that the solid Earth tides in that period range are strongly frequency dependent.

This can be expressed by frequency dependent Love and Shida numbers. WAHR [1981] determined transfer functions for an elliptical, rotating, elastic and oceanless Earth and gives the Love and Shida numbers for individual tides. Using a harmonic expansion of the tide generating potential equations (1) to (3) can be substituted by equations (4) to (6).

$$\Delta_U = \sum_{n=1}^{n_{max}} \sum_{m=0}^{n} \sum_{T} h_{nm}(\omega_T) \cdot \frac{W_{nmT}}{g} \tag{4}$$

$$\Delta_E = \sum_{n=1}^{n_{max}} \sum_{m=0}^{n} \sum_{T} l_{nm}(\omega_T) \cdot \frac{\partial W_{nmT}}{\partial \lambda} \cdot \frac{1}{g \cdot \cos(\phi)} \tag{5}$$

$$\Delta_N = \sum_{n=1}^{n_{max}} \sum_{m=0}^{n} \sum_{T} l_{nm}(\omega_T) \cdot \frac{\partial W_{nmT}}{\partial \phi} \cdot \frac{1}{g} \tag{6}$$

In equations (4) to (6) $h_{nm}(\omega_T)$ and $l_{nm}(\omega_T)$ are the Love and Shida number of a tide T of degree n and order m with frequency ω_T. Each tide T contributes by W_{nmT} to the total tide generating potential.

For the Love and Shida numbers of the second degree diurnal tides Wahr gives the resonance formulas (7) and (8). In these equations ω_T, ω_{O_1} and ω_{FCN} are the frequencies of each specific tide T, of the tide O_1 and of the FCN, respectively, and h_{RS} and l_{RS} are resonance strength factors.

$$h_{21}(\omega_T) = h_{21}(\omega_{O_1}) + h_{RS} \cdot \frac{\omega_T - \omega_{O_1}}{\omega_{FCN} - \omega_T} \tag{7}$$

$$l_{21}(\omega_T) = l_{21}(\omega_{O_1}) + l_{RS} \cdot \frac{\omega_T - \omega_{O_1}}{\omega_{FCN} - \omega_T} \tag{8}$$

In Wahr's model based on the seismic Earth model 1066A by Gilbert and Dziewonski the period of the FCN is 461 sidereal days in the celestial reference frame. Figure 1 shows Wahr's resonance model for the second degree Love and Shida number in the diurnal frequency band.

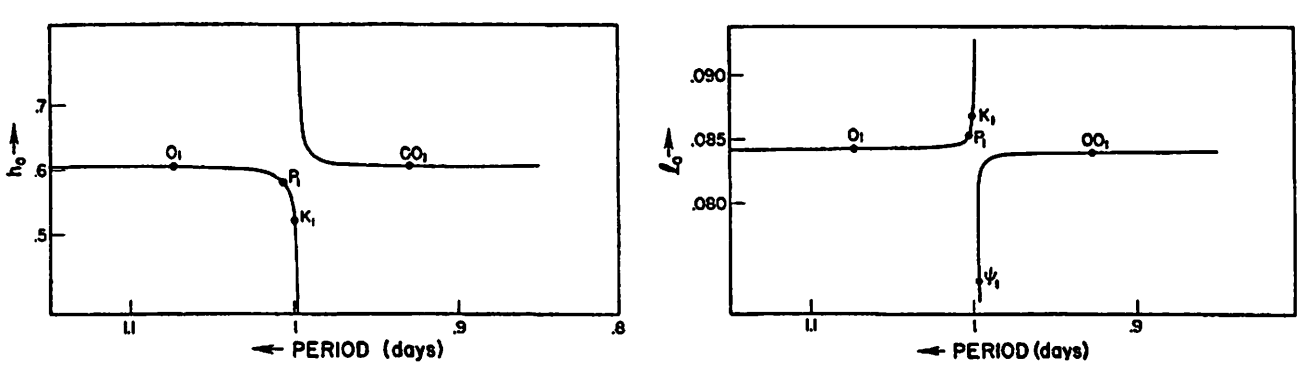

Figure 1: Frequency dependence of Love and Shida numbers for second degree diurnal tides, [WAHR, 1979]

Anelasticity of the Earth's mantle causes a lag of the tidal deformation with respect to the tide generating potential [e.g. WAHR AND BERGEN, 1986]. This can be described by complex transfer functions whose imaginary parts represent the out-of-phase tidal response (see figure 2). In this general approach the Love and Shida numbers in equations (4) to (6) have to substituted by complex Love and Shida numbers. The resonance parameters in equations (7) and (8) become complex quantities, too. A complex eigenfrequency of the FCN ($\omega_{FCN} = \Re(\omega_{FCN}) + i\Im(\omega_{FCN})$) allows to determine the so-called 'quality factor' Q, which describes the damping of the resonance. It can be calculated from the real and the imaginary part of the eigenfrequency ($Q = \Re(\omega_{FCN})/(2 \cdot \Im(\omega_{FCN}))$).

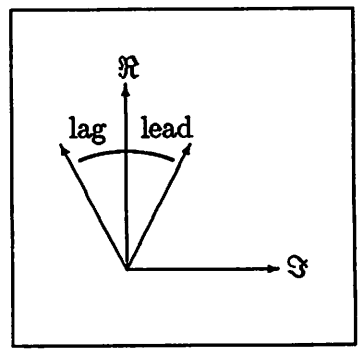

Figure 2.: Complex representation: $\Re$ is the real part (in-phase), $\Im$ is the imaginary part (out-of-phase)

3 Solid Earth tides in space geodetic data analysis

The present standard version of the CALC/SOLVE VLBI software follows the International Earth Rotation Service [IERS] Standards [MCCARTHY, 1992] that recommend a simplified version of Wahr's theoretical model for an elastic Earth which includes only second degree tides. The frequency dependence of the solid Earth tides due to the FCN resonance is only taken into account for the K_1-tide for the radial displacements. The tangential displacements are not corrected for frequency dependence.

There are several other tidal waves close to the FCN resonance for which the present IERS Standards do not include frequency dependent h_{21} and l_{21}. The analysis of space geodetic data requires high accuracies in the sub-millimeter range. In a recent paper [HAAS AND SCHUH, 1996] it was shown that the differences between a more complete frequency dependent solid Earth tide model (43 additional diurnal terms, radial and tangential) and the present IERS-model amount to ± 5 mm and cannot be neglected any more in present space geodetic data analysis.

New harmonic developments of the tide generating potential published by TAMURA [1987], HARTMANN AND WENZEL [1995], ROOSBEEK [1996] consider the contributions of the Moon and the Sun up to a degree higher than two. Indirect planetary effects and direct planetary effects are also accounted for. There are only very small differences for the tidal station displacements, namely less than ± 0.03 mm, depending on which of the present harmonic expansions of the tidal potential is chosen to account for the frequency dependence of the Love and Shida numbers. Small shifts in the FCN period, by one or two days, will only marginally influence the tidal station displacements.

The new IERS Conventions as follow-up paper of the IERS Standards have been published in July 1996 [MCCARTHY, 1996]. They contain a considerably improved model for the solid Earth tides and it is strongly recommended to implement this new theoretical model in VLBI as in any other space geodetic analysis software.

There is a variety of geodynamical and local geophysical effects in the diurnal and subdiurnal frequency bands. The most important ones are:

- high-frequency variations of the Earth rotation parameters
- ocean loading, i.e. the deformation of the Earth's crust due to oceanic tides and currents
- atmospheric loading, i.e. the deformation of the Earth's crust due to moving atmospheric pressure fields
- thermal deformations of the VLBI telescopes
- variations of the troposphere

All other diurnal and subdiurnal effects which are related to tides have been investigated and modeled consistently in a Ph.D. thesis by HAAS [1996]. It was shown that insufficient models for the solid

Earth deformation and for ocean tidal loading cause an apparent diurnal signal in the Earth rotation parameters determined by VLBI.

4 Estimation of Love and Shida numbers for individual tides

First we solved directly for frequency dependent Love and Shida numbers of individual tides from VLBI data. The harmonic expansion of the tide generating potential by TAMURA [1987] was used to calculate partial derivatives for the main diurnal tides which were entered in a least squares analysis with the CALC/SOLVE VLBI data analysis software package. Again, it should be mentioned that taking any other of the present tidal potential models yields almost identical results.

About 725,000 VLBI delay observables observed in different international VLBI networks from 1979 to 1996 (which is about 50 % of all geodetic VLBI data presently available) were combined for a so-called 'batch solution'. In a batch solution 'global parameters' which are common to all VLBI experiments as well as 'arc-parameters' which belong to individual VLBI experiments only are estimated together. Apart from minor differences, the models used in the CALC/SOLVE software package agree with those recommended by the IERS Standards [1992]. This includes corrections due to ocean tide loading computed according to SCHERNECK [1991].

4.1 Elastic Earth

If we consider the Earth being elastic equations (4) to (6) are used for the determination of Love and Shida numbers for individual tides from VLBI data. In a batch solution station positions and velocities, radio source positions, daily Earth orientation parameters (i.e. pole position x_p, y_p, Universal Time UT1 and nutation corrections $\delta\psi$, $\delta\epsilon$), clock and atmosphere parameters and additionally 12 discrete h_{21} and 12 discrete l_{21} for the main diurnal tides were estimated. The Love and Shida numbers of the tide S_1 were fixed to their theoretical values because the tide S_1 is a strong atmospherical tide as well.

Table 1: Estimates of frequency dependent Love and Shida numbers h_{21}, l_{21}

Tide	Doodson number	Love number h_{21}		Shida number l_{21}	
		Wahr	This paper	Wahr	This paper
Q_1	135.655	0.603	0.560 ± 0.012	0.084	0.074 ± 0.003
O_1	145.555	0.603	0.606 ± 0.002	0.084	0.082 ± 0.001
M_1	155.655	0.600	0.435 ± 0.030	0.084	0.069 ± 0.008
π_1	162.556	0.587	0.623 ± 0.090	0.085	0.108 ± 0.022
P_1	163.555	0.581	0.574 ± 0.005	0.085	0.085 ± 0.001
K_1	165.555	0.520	0.496 ± 0.002	0.087	0.086 ± 0.001
K_1'	165.565	0.514	0.458 ± 0.014	0.087	0.054 ± 0.005
ψ_1	166.554	0.937	-0.136 ± 0.228	0.074	-0.428 ± 0.056
ϕ_1	167.555	0.662	0.702 ± 0.121	0.082	0.094 ± 0.030
θ_1	173.655	0.612	0.934 ± 0.158	0.084	0.080 ± 0.039
J_1	175.455	0.611	0.538 ± 0.031	0.084	0.075 ± 0.008
OO_1	185.455	0.608	0.555 ± 0.054	0.084	0.074 ± 0.013

Table 1 gives the estimates for the discrete h_{21} and l_{21} and their scaled standard deviations in comparison to values published by WAHR [1981]. The standard deviations obtained from the least squares fit are scaled independently of the tidal frequencies and represent an inner accuracy, which is usually too optimistic by a factor 2-3. The correlation coefficients between the estimated tidal parameters were investigated, too. The maximum correlations are about 0.6 and they were obtained between Love and Shida numbers of the same tide. All other correlation coefficients are very small, i.e. less than 0.18, 72% of them ≤ 0.05.

In figures 3 and 4 the solid lines show the theoretical model of Wahr in the diurnal frequency band with an FCN period of 461 sidereal days. Love and Shida numbers estimated from VLBI are plotted by discrete points, and the error bars show the scaled standard deviations. The estimates of h_{21} and l_{21} of those tides with a strong tidal potential (e.g. Q_1, O_1, P_1, K_1) have small error bars and they lie close to the theoretical values. The tide M_1 is the only tide for which h_{21} shows a discrepancy from theory

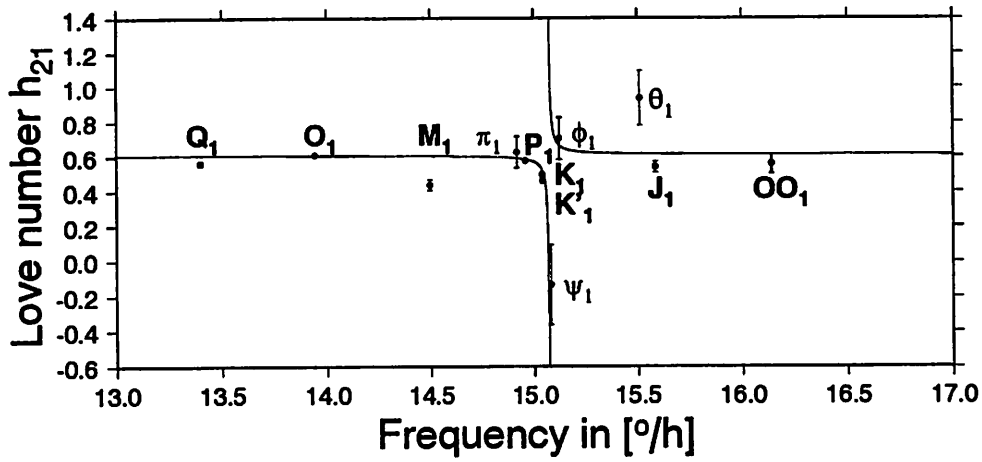

Figure 3: Estimates of frequency dependent Love numbers h_{21} and Wahr's theoretical model (solid line).

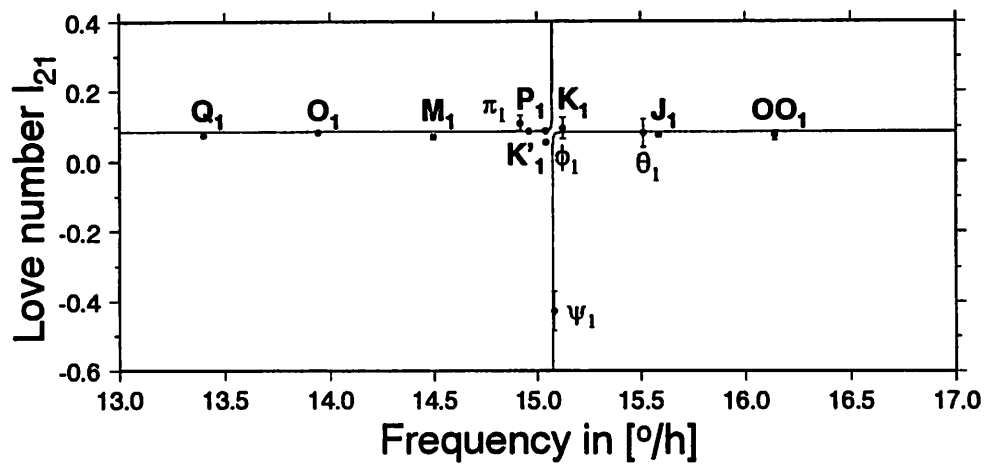

Figure 4: Estimates of frequency dependent Love numbers l_{21} and Wahr's theoretical model (solid line).

larger than three times the formal error. This confirms analyses of gravimetric data which usually show for M_1 differences between observations and theory [e.g. MELCHIOR ET AL., 1996] probably due to interactions between Earth tides and ocean tides. The results for h_{21} and l_{21} of tides with a weak tidal potential show larger discrepancies from the theoretical values but these discrepancies are always less than double the formal error. Anyway, this first attempt to determine h_{21} and l_{21} for individual diurnal tides directly from VLBI data is successful and shows a rather good agreement with Wahr's theoretical model. The resonance close to the FCN can be seen very clearly not only for the K_1 tide but also for the smaller terms nearby. It is notable that from VLBI data good estimates for the Shida number are obtained corresponding to tangential tidal displacements which are much smaller than the radial displacements.

4.2 Anelastic Earth

Based on the same VLBI data which were used in the previous chapter for determining real Love and Shida numbers, i.e. the elastic case, we solved now for real and imaginary components of the main diurnal and semidiurnal tides. Theoretical values of the real and imaginary parts due to anelasticity

are given in the new IERS Conventions for the main tides [McCarthy, 1996]. Our results are shown in the last columns of table 2 and 3 again with their scaled standard deviations and are compared with theoretical values taken from the IERS Conventions and with other empirical determinations published recently [Mitrovica et al., 1994, Ray et al., 1995].

Table 2: Theoretical values and estimates of frequency dependent and complex Love numbers h, real parts are denoted by $\Re$, imaginary parts by $\Im$

Tide	Theory		Mitrovica et al., 1994		Ray et al., 1995		This paper	
	$\Re$	$\Im$	$\Re$	$\Im$	$\Re$	$\Im$	$\Re$	$\Im$
Q_1	0.603	−0.002		-		-	0.559 ± 0.012	$+0.046 \pm 0.012$
O_1	0.603	−0.002	0.618 ± 0.007	-0.010 ± 0.007	0.594	-0.004 ± 0.013	0.612 ± 0.002	-0.017 ± 0.002
M_1	0.600	−0.002		-		-	0.422 ± 0.031	$+0.086 \pm 0.031$
π_1	0.588	−0.002		-		-	0.484 ± 0.093	$+0.098 \pm 0.093$
P_1	0.582	−0.002	0.56 ± 0.02	$+0.010 \pm 0.010$		-	0.567 ± 0.005	$+0.002 \pm 0.005$
K_1	0.523	−0.003	0.50 ± 0.01	-0.010 ± 0.009	0.512	-0.006 ± 0.012	0.512 ± 0.003	-0.003 ± 0.003
K_1'	0.518	−0.003	0.53 ± 0.06	-0.03 ± 0.060		-	0.429 ± 0.019	-0.156 ± 0.019
ψ_1	1.053	−0.002	0.8 ± 0.6	-0.6 ± 0.5		-	-0.277 ± 0.234	$+0.150 \pm 0.234$
ϕ_1	0.664	−0.002	0.5 ± 0.4	$+0.2 \pm 0.3$		-	0.764 ± 0.126	-0.583 ± 0.126
θ_1		-		-		-	0.705 ± 0.161	-0.321 ± 0.161
J_1		-		-		-	0.542 ± 0.031	$+0.036 \pm 0.031$
OO_1		-		-		-	0.495 ± 0.054	-0.034 ± 0.054
N_2	0.603	−0.002		-	0.626	$+0.015 \pm 0.044$	0.615 ± 0.006	$+0.034 \pm 0.006$
M_2	0.603	−0.002		-	0.613	-0.000 ± 0.007	0.600 ± 0.001	-0.002 ± 0.001
S_2	0.603	−0.002		-		-	0.592 ± 0.002	$+0.010 \pm 0.002$
K_2	0.603	−0.002		-		-	0.641 ± 0.010	-0.015 ± 0.010

Table 3: Theoretical values and estimates of frequency dependent and complex Love numbers l, real parts are denoted by $\Re$, imaginary parts by $\Im$

Tide	Theory		This paper	
	$\Re$	$\Im$	$\Re$	$\Im$
Q_1	0.085	−0.001	0.076±0.003	+0.016±0.003
O_1	0.085	−0.001	0.083±0.001	−0.001±0.001
M_1	0.085	−0.001	0.072±0.008	−0.033±0.008
π_1	0.085	−0.001	0.054±0.023	+0.008±0.023
P_1	0.086	−0.001	0.083±0.001	+0.001±0.001
K_1	0.087	−0.001	0.090±0.001	+0.002±0.001
K_1'	0.087	−0.001	0.060±0.006	−0.036±0.006
ψ_1	0.071	−0.001	−0.460±0.058	+0.234±0.059
ϕ_1	0.083	−0.001	0.081±0.031	−0.106±0.031
θ_1		-	0.047±0.040	−0.180±0.040
J_1		-	0.076±0.008	+0.003±0.008
OO_1		-	0.058±0.013	−0.014±0.013
N_2	0.085	−0.001	0.091±0.001	+0.011±0.001
M_2	0.085	−0.001	0.088±0.001	+0.007±0.001
S_2	0.085	−0.001	0.084±0.001	+0.008±0.001
N_2	0.085	−0.001	0.091±0.002	−0.011±0.002

Different from our direct solution the first reference [Mitrovica et al., 1994] chose an indirect approach via radial displacements determined by VLBI and the results of the second reference [Ray et al., 1995] are based on satellite altimetry and ocean tidal measurements. The approach described in this paper allows the direct determination of complex Love and Shida numbers and is more precise than any previous attempt. However, only some of our results for the imaginary parts are significantly different from zero. In the range of the FCN resonance large imaginary parts are obtained, which in

the case of h for two tides (K_1', ϕ_1) exceed their fourfold standard deviations. Further investigations have to follow, whether dissipation processes exist within the Earth which could cause larger phase lags than those predicted so far.

5 Estimation of resonance parameters for the tidal deformation

The next idea was to estimate the five parameters of a frequency dependent model for the diurnal tides, i.e. to solve for $h_{21}(\omega_{O_1})$, $l_{21}(\omega_{O_1})$, h_{RS}, l_{RS}, ω_{FCN} in equations (7) and (8). Again the harmonic expansion of the tide generating potential by Tamura was used to calculate partial deriatives. The same VLBI data as described in the previous section were used again to run batch solutions.

5.1 Elastic Earth

We started again with an elastic Earth. Those five resonance parameters mentioned above were solved for as well as h_{20}, l_{20} for the long-period part, h_{22}, l_{22} for the semidiurnal part of the second degree tidal spectrum and h_3, l_3 for the third degree part of the tidal spectrum. Equations (7) and (8) are not linear with respect to ω_{FCN} and therefore a sufficient number of iterations had to be carried out to obtain final results. Table 4 gives the results for the 11 parameters and their standard deviations after 12 iterations of the least squares fit.

Table 4: Estimates of resonance parameters in the diurnal frequency band and h_{20}, l_{20}, h_{22}, l_{22}, h_3 and l_3 compared with theoretical values published by WAHR [1981].

	VLBI analysis estimates, this paper			Wahr [1981]	
second degree, long periods					
h_{20}	0.559	±	0.012	0.606	[/]
l_{20}	0.094	±	0.003	0.0840	[/]
second degree, diurnal periods					
$h_{21}(\omega_{O_1})$	0.598	±	0.002	0.603	[/]
$l_{21}(\omega_{O_1})$	0.080	±	0.0005	0.0842	[/]
h_{RS}	−0.00162	±	0.00016	−0.00246	[/]
l_{RS}	0.00011	±	0.00003	0.0000781	[/]
ω_{FCN}	1.002346	±	0.00011	1.002171	[cycles/sid.day]
P_{FCN}	426.3	±	20.3	460.5	[sid.days]
second degree, semidiurnal periods					
h_{22}	0.600	±	0.001	0.609	[/]
l_{22}	0.0875	±	0.0001	0.0852	[/]
third degree, all periods					
h_3	0.281	±	0.048	0.291	[/]
l_3	0.0151	±	0.0048	0.0149	[/]

Table 5: Correlation coefficients between the estimates of the resonance parameters.

	h_{RS}	$l_{21}(\omega_{O_1})$	l_{RS}	ω_{FCN}
$h_{21}(\omega_{O_1})$	0.48	0.57	0.36	0.02
h_{RS}		0.27	0.26	0.80
$l_{21}(\omega_{O_1})$			0.64	0.01
l_{RS}				0.12

Table 5 gives the correlation coefficients between the estimated resonance parameters. The strongest correlation with 0.80 was obtained between the FCN frequency ω_{FCN} and the resonance strength factor

h_{RS}. Correlations between the five resonance parameters and the six parameters of the other parts of the tidal band are less than 0.04. The estimates of h_{20}, l_{20} are correlated by 0.62, of h_{22}, l_{22} by 0.21 and of h_3, l_3 by 0.15. All other correlations, i.e. between the parameters of different parts of the tidal spectrum, are less or equal 0.03.

Figures 5 and 6 show the diurnal frequency band: the clear resonance at a period of 426 sidereal days can be seen in comparison to the resonance period of 461 sidereal days in Wahr's theoretical model. The latter is plotted by thin lines in figures 5 and 6 while the thick lines represent our results including the error ranges of the five-parameter model.

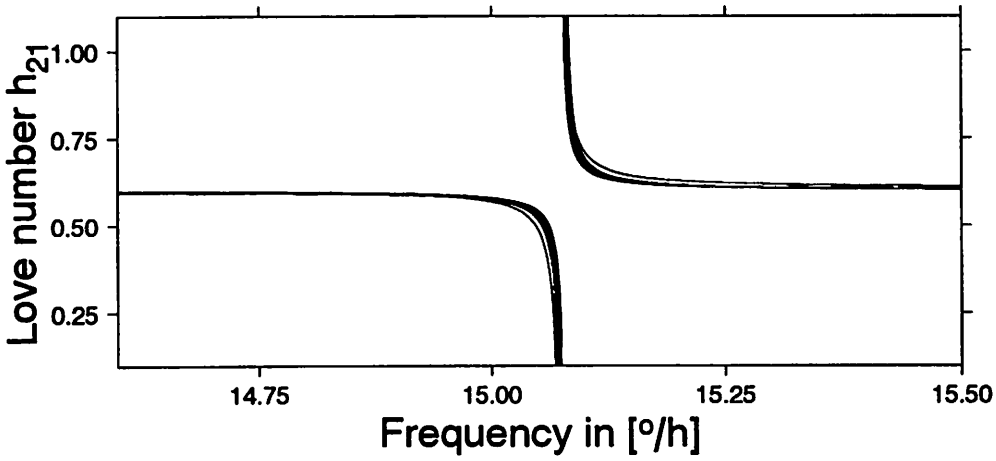

Figure 5: Estimates of resonance model parameters for Love numbers h_{21} including the error ranges (thick lines) and Wahr's theoretical model (thin lines).

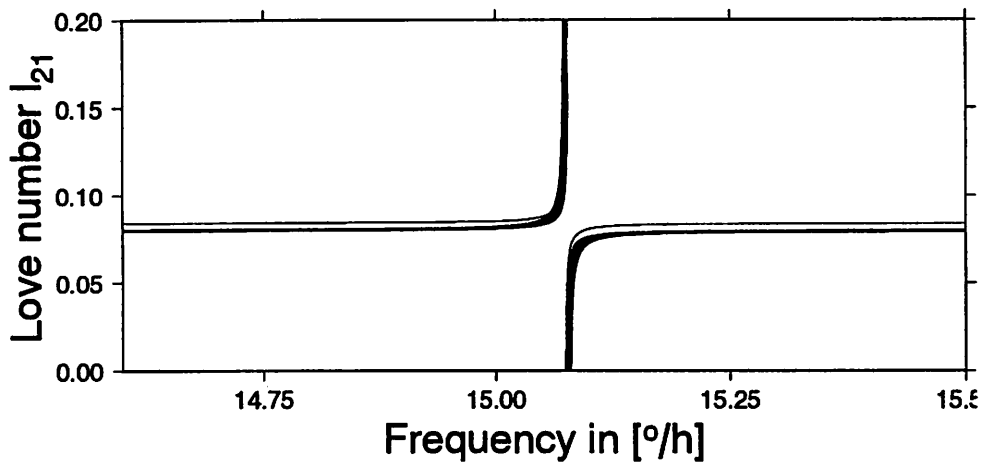

Figure 6: Estimates of resonance model parameters for Love numbers l_{21} including the error ranges (thick lines) and Wahr's theoretical model (thin lines).

5.2 Anelastic Earth

The parameters which represent the FCN resonance in the second degree diurnal tides, i.e. the resonance strength factors h_{RS}, l_{RS} and the FCN frequency ω_{FCN} in equations (7) and (8) can be treated as complex parameters, too. This allows to determine the complex eigenfrequency ω_{FCN} and the so-called quality factor Q as defined at the end of section 2. The results from the direct determination of the resonance parameters via tidal defomations observed by VLBI are shown in table 6. Table 6 shows again the correlation coefficients between the estimated complex resonance parameters. The strongest correlations were obtained between the imaginary part of the FCN frequency $\Im(\omega_{FCN})$ and

the imaginary part of the resonance strength factor $\Im(h_{RS})$ with 0.91 and with 0.83 between the real parts of these parameters.

The FCN period was determined to 430.1 ± 21.6 days and the quality factor Q was determined to 1400 (1000 < Q < 2100). This is not far from many similar analyses of tidal gravimetric measurements (e.g. DEFRAIGNE ET AL., 1994, FLORSCH ET AL., 1994) which yield results for Q usually between 2000 and 3000. However, a completely different approach for the determination of Q based on nutation data observed by VLBI gave a considerably higher Q of 31000 (24000 < Q < 42800) (DEFRAIGNE ET AL., 1994, 1995). The reason for this discrepancy has to be investigated.

Table 6: Estimates of complex resonance parameters in the diurnal frequency band

	$\Re$	$\Im$	
$h_{21}(\omega_{O_1})$	0.598 ± 0.002	-	[/]
h_{RS}	−0.00162 ± 0.00016	0.00001 ± 0.00015	[/]
$l_{21}(\omega_{O_1})$	0.080 ± 0.0005	-	[/]
l_{RS}	0.00012 ± 0.00003	−0.00011 ± 0.00002	[/]
ω_{FCN}	1.00232 ± 0.00012	0.00036 ± 0.00012	[cycles/sid.day]
P_{FCN}	430.1 ± 21.6		[sid.days]

Table 7: Correlation coefficients between the estimates of the complex resonance parameters.

	$\Re(h_{RS})$	$\Im(h_{RS})$	$l_{21}(\omega_{O_1})$	$\Re(l_{RS})$	$\Im(l_{RS})$	$\Re(\omega_{FCN})$	$\Im(\omega_{FCN})$
$h_{21}(\omega_{O_1})$	0.451	0.010	0.569	0.352	0.021	0.030	0.034
$\Re(h_{RS})$		0.003	0.247	0.212	0.002	0.829	0.003
$\Im(h_{RS})$			0.018	0.019	0.148	0.001	0.908
$l_{21}(\omega_{O_1})$				0.635	0.038	0.005	0.003
$\Re(l_{RS})$					0.074	0.132	0.001
$\Im(l_{RS})$						0.002	0.147
$\Re(\omega_{FCN})$							0.005

6 Discussion and Conclusions

The results show that VLBI data provide valuable information for the independent and direct determination of frequency dependent Love and Shida numbers in the long-period, diurnal and semidiurnal tidal ranges. We started for the case of an elastic Earth. Corresponding to the frequency dependence of second degree Love and Shida numbers we obtained an FCN period of 426 ± 20 sidereal days in the celestial reference frame. An FCN period shorter than that given by Wahr was already derived from nutation observations and gravity tide measurements [e.g. DEFRAIGNE ET AL., 1994, 1995]. In spite of this agreement with other recent investigations the large standard deviation of the FCN period should be noted which is probably due to the strong correlation with the FCN resonance strength. Additionally to the different resonance period, both h_{21} and l_{21} curves are slightly shifted in the total level with respect to the theoretical model. The second degree Love numbers h_{2m} determined from VLBI are in all frequency bands smaller than those given by theory. The largest difference between theoretical models and our results was obtained for the long-period Love number h_{20} which is in the VLBI solution only 0.559. For the second degree Shida numbers l_{2m} no such obvious trend can be seen in our results. It is remarkable that even third degree Love and Shida numbers h_3, l_3 could be determined in good agreement with theoretical models within their error ranges.

In a new VLBI solution presented in this paper we considered an anelastic Earth, i.e. also imaginary parts of the Love and Shida numbers for the most prominent tides were computed, some of them beeing significantly different from zero. By complex Love and Shida numbers a phase lag between the tide generating potential and the tidal deformation can be expressed. The complex eigenfrequency ω_{FCN} of the FCN was determined, with an FCN period of 430 $\pm$ 22 sidereal days and a quality factor Q of 1400 ($1000 < Q < 2100$). Both results agree well with analyses of tidal data sets but for Q they disagree with former analyses of nutation data observed by VLBI.

References

[1] Defraigne, P., V. Dehant, and J. Hinderer: *Stacking gravity tide measurements and nutation observations in order to determine the complex eigenfrequency of the Nearly Diurnal Free Wobble*, J. Geophys. Res., Vol. 99, No. B5, 9203-9213, 1994, with a correction in J. Geophys. Res., Vol. 100, No. B2, 2041-2042, 1995

[2] Florsch, N., F. Chambat, J. Hinderer and H. Legros: *A simple method to retrieve the complex eigenfrequency of the Earth's nearly diurnal-free wobble; application to the Strasbourg superconducting gravimeter data*, Geophys. J. Int., 116, 53-63, 1994

[3] Haas, R. and H. Schuh: *Determination of frequency dependent Love and Shida numbers from VLBI data*, Geophys. Res. Lett., Vol. 23, No. 12, 1509-1512, 1996

[4] Haas, R.: *Untersuchungen zu Erddeformationsmodellen für die Auswertung von geodätischen VLBI-Messungen*, Ph.D. thesis, University of Bonn, 1996

[5] Hartmann, T., and H.-G. Wenzel: *Catalogue HW95 of the tidal potential*, Bulletin d'Information Marées Terrestres, Vol. 123, 9278-9301, 1995

[6] Mathews, P. M., B. A. Buffet, and I. I. Shapiro: *Love numbers for a rotating spheroidal Earth: New definitions and numerical values*, Geophys. Res. Lett., Vol. 22, No. 5, 579-582, 1995

[7] McCarthy, D. D. (ed.): *IERS Standards*, IERS Technical Note 13, Observatoire de Paris, 1992

[8] McCarthy, D. D. (ed.): *IERS Conventions*, IERS Technical Note 21, Observatoire de Paris, 1996

[9] Melchior, P., B. Ducarme, O. Francis: *The response of the Earth to tidal body forces described by second- and third-degree spherical harmonics as derived from a 12 year series of measurements with the superconducting gravimeter GWR/T3 in Brussels*, Phys. of the Earth and Planet. Int., 93, 223-238, 1996

[10] Mitrovica, J. X., J. L. Davis, P. M. Mathews and I. I. Shapiro: *Determination of tidal h Love number parameters in the diurnal band using an extensive VLBI data set*, Geophys. Res. Lett., Vol. 21 No. 8, 705-708, 1994

[11] Neuberg, J., J. Hinderer and W. Zürn: *Stacking gravity tide observations in central Europe for the retrieval of the complex eigenfrequency of the nearly diurnal free-wobble*, Geophys. J. Roy. astr. Soc., 91, 853-868, 1987

[12] Ray, R. D., S. Bettadpur, R. J. Eanes and E. J. O. Schrama: *Geometrical determination of the Love number h_2 at four tidal frequencies*, Geophys. Res. Lett., Vol. 22, No. 16, 2175-2178, 1995

[13] Roosbeek, F.: *RATGP95: a harmonic development of the tide-generating potential using an analytical method*, Geophys. J. Int., Vol. 126, No. 1, pp. 197-204, 1996

[14] Scherneck, H. G.: *A parameterized Solid Earth Tide Model and Ocean Tide Loading Effects for Global Geodetic Baseline Measurements*, Geophys. J. Int., 106, 677-694, 1991

[15] Tamura, Y.: *A harmonic development of the tide-generating potential*, Bulletin d'Information Marées Terrestres, Vol. 99, 6813-6855, 1987

[16] Wahr, J. M.: *Tidal motions of a rotating, elliptical, elastic and oceanless earth*, Ph.D. thesis, University of Colorado, 1979

[17] Wahr, J. M.: *Body tides on an elliptical, rotating, elastic and oceanless earth*, Geophys. J. R. Astron. Soc., 64, 677-703, 1981

[18] Wahr, J. M. and Z. Bergen: *The effect of mantle anelasticity on nutations, earth tides, and tidal variations in rotation rate*, Geophys. J. R. Astron. Soc., 87, 633-668, 1986

Status report on the combination of VLBI and other space geodetic data *

Per Helge Andersen

Norwegian Defence Research Establishment
P.O. Box 25, 2007 Kjeller, Norway
and
Institute of Theoretical Astrophysics
P. O. Box 1029, Blindern, 0315 Oslo, Norway
Email: per-helge.Andersen@ffi.no

Abstract.
The GEOSAT software for geodetic and geodynamic applications of tracking data from satellites and VLBI data from distant radio sources has been under development at the Norwegian Defence Research Establishment (NDRE) since 1982. Among the space geodesy softwares currently on the market, GEOSAT is unique in that one and the same program can, in addition to satellite tracking data, also handle VLBI data. The justification for building the satellite and VLBI applications into the same program, is that both types of application share a common terrestrial reference frame with all the complex motions that geodynamics imposes on it.

With the GEOSAT software it is possible to combine VLBI and any type of satellite tracking data in a simultaneous solution for maximum information extraction from the data. The paper presents results from analyses in a simultaneous combined mode with VLBI, GPS, and SLR data.

1 The GEOSAT software

GEOSAT as currently under development at NDRE, is a state-of-the-art software system for high-precision analysis of satellite and radio source tracking data for geodetic and geodynamic applications. GEOSAT is a multi-station, multi-satellite, and multi-measurement technique system, designed to provide a flexible tool for accuracy analysis related to geodetic studies. The software can be applied either in an estimation mode, a simulation mode or in an error analysis mode.

GEOSAT is a library of subroutines written in the FORTRAN language and presently consisting of approximately 150000 statements. The code is highly portable and can be used on any workstation running under the UNIX operating system. There are virtually no limits on the maximum numbers of satellites and of tracking stations that can be included; these will be limited only by the external storage size and processing time available on the computer.

GEOSAT has a sophisticated mathematical model[1] with equations of motion and measurements formulated either in a solar barycentric or a geocentric frame of reference and corrected for relativistic effects. In this software, the most precise reference frames, dynamical models, and measurement models available are used and updated continually as better information comes along. Sophisticated versions of Bayesian weighted least squares and Kalman filtering techniques are available, and many types of model parameters (listed in Table 1), can either be considered in an error analysis or solved-for in an analysis of real data. Most of these parameters, including dynamical parameters, can be represented by stochastic

*In proceedings of the Eleventh Working Meeting on European VLBI for Geodesy and Astrometry. Edited by G. Elgered, Onsala Space Observatory, 1996.

Station coordinates and velocities Ocean loading amplitudes and phases Eccentricity vectors Atmospheric pressure load coefficients
UT1, length of day, polar motion, nutation, precession Earth gravity field coefficients Solid Earth tidal parameters Ocean tidal amplitudes and phases Amplitudes and phases of tidal variations in Earth orientation Amplitudes and phases of tidal variations in geocenter General relativity parameters
Radio source position Satellite orbital elements
Satellite dynamic scaling parameters
Tropospheric zenith delay Atmospheric gradients Tropospheric mapping function coefficients
Clock parameters Measurement biases

Table 1: GEOSAT solve-for and consider parameters.

models (white or colored noise, or random walk).

GEOSAT can be applied in the analysis of any of the existing high-precision satellite tracking data types available today in addition to VLBI data. Table 2 shows the validation status of each technique and the datasets applied in the validation tests. Table 3 presents a summary of the results from the analyses.

Daily variations in baseline length to Westford (left) and baseline length differences between the mean GEOSAT solution over all 12 days during the CONT'94 VLBI campaign and the ITRF'93 solution (right) are shown in Fig. 1. The daily baseline length repeatability is 0.8 mm + 0.67 ppb.

2 Combination of techniques

The different techniques can be combined to get improved and perhaps more realistic estimates and error estimates of geodetic parameters. The usual but in general non-optimal approach, is to perform a separate analysis for each of the techniques and then combine the aposteriori state vectors and variance-covariance matrices from each of the solutions to obtain a multi-technique solution.

Assume, as an example, that we have data from a number of 24-hour VLBI sessions, and that some of the sites also are equipped with GPS receivers which are connected to the same hydrogen-maser clocks as the VLBI electronics. The usual way of analyzing such a combined data set is to reduce separately the GPS and the VLBI data on a session-by-session basis and finally determine a combined solution. In the analysis of both of the datatypes, clock and tropospheric parameters must be estimated from the data in order to obtain results of high quality. This standard strategy does not take into account the fact that the VLBI and GPS signals, in principle, are experiencing the same atmosphere and Earth orientation, and that the station clocks will influence the two types of measurements in an, in principle, equivalent manner.

Another related problem is that different softwares are applied in the analysis of data from the different techniques. We have already mentioned that GEOSAT is the only single software capable of reducing all the existing types of high-precision data. This means in practice that slightly inconsistent models might

GEOSAT MEASUREMENT TECHNIQUES			
Technique	Status	Satellite system	Campaigns
VLBI	Validated	Radio sources	CONT94, ERDE, R&D
GPS	Validated	GPS	CONT94, GIG91
SLR	Validated	LAGEOS1 & 2	Oct. 92 - Sept. 93
	Validated	ETALON1 & 2	Oct. 92 - Sept. 93
	Validated	ERS-1	Selected arcs
	Validated	ERS-2	Selected arcs
	Validated	METEOR-3	Selected arcs
PRARE	Validated	METEOR-3	Selected arcs of range and doppler data
	Validated	ERS-2	Selected arcs of range and doppler data
DORIS	Validated	TOPEX	Selected arcs
XALT	Validated	ERS-1	Selected arcs
	Validated	ERS-2	Selected arcs
Ephemeris	Validated	GPS	IGS-orbits
	Under testing	ERS-1	GEODYN II orbits
WVR	Validated		CONT94/Onsala

Table 2: Measurement techniques presently available in GEOSAT, validation status, and satellite systems involved in the tests. Ephemeris means that it is possible to treat orbits generated by an external software as measurements either to compare orbital models or to generate a reference orbit for later applications in the filter. XALT means crossover radar altimetry data.

GEOSAT SOFTWARE VALIDATION		
Technique	Satellite system	Precision of results
VLBI[3]	Radio sources	Baseline length repeatability: 0.8 mm + 0.7 ppb
		Polar motion and nutation: 0.1 - 0.5 mas
		UT1: 0.01 - 0.04 ms
		Source coordinates: 0.1 - 0.3 mas
GPS[2]	GPS	Baseline length repeatability: 1 mm + 1.4 ppb
		Satellite orbit precision: 10 cm in each coordinate
SLR[4]	LAGEOS/ETALON	Station coordinates: 1 -2 cm
		Polar motion: 0.2 mas
		UT1: 0.02 ms
SLR/PRARE/XALT[5]	ERS-1/2	SLR residuals: 5 - 8 cm
		PRARE range residuals: 5 - 8 cm
		PRARE doppler residuals: $\sim$ 0.3 mm/s
		XALT residuals: 11 - 18 cm
		Radial orbit precision : 5 - 7 cm
		Along-track orbit precision : $\sim$ 20 cm
		Cross-track orbit precision : $\sim$ 10 cm
DORIS	TOPEX	DORIS residuals: 1.5 mm/s
		Cannon-ball satellite model

Table 3: Status of the GEOSAT software validation.

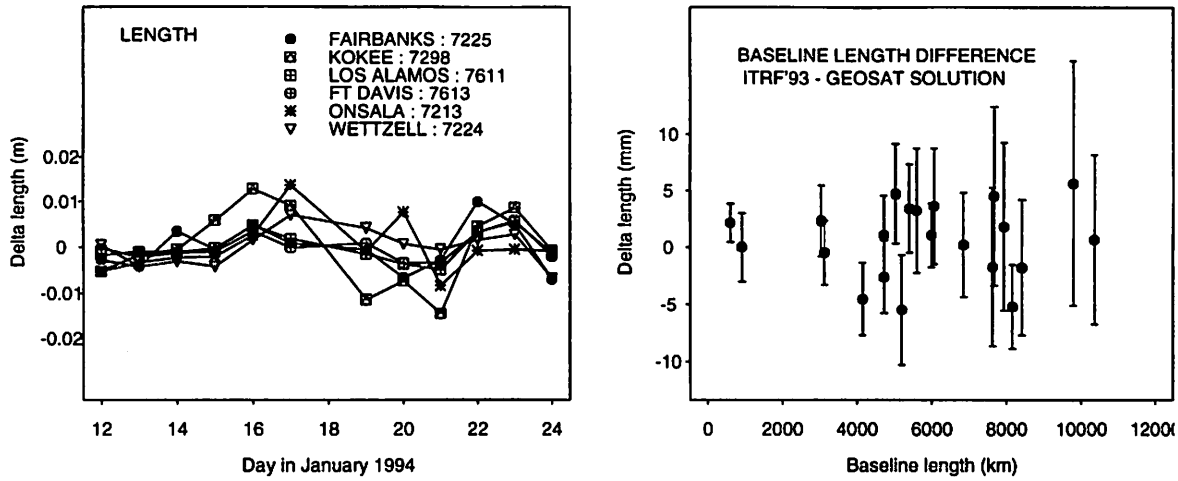

Figure 1: Daily variations in baseline length to Westford (left) and baseline length differences between the mean GEOSAT solution over all 12 days during the CONT'94 VLBI campaign and the ITRF'93 solution (right). The error bars are 1-σ values derived from the observed baseline length repeatabilities. The RMS of the differences is 3.8 mm.

PARAMETER OBSERVABILITY							
Technique	Nut	UT1	LOD	Xp	Yp	Geoc	Pos
VLBI	xx	xx	xx	xx	xx		xx
GPS			xx	xx	xx	x	xx
GLONASS			xx	xx	xx	x	xx
SLR			x	x	x	xx	xx
LLR			x	x	x	x	x
PRARE			xx	xx	xx	xx	xx
DORIS			x	x	x	x	x

Table 4: Parameter observability for the different techniques. x (and xx) means good (or extra good) observability either in accuracy or in temporal resolution.

have been used in the analyses, implying that the results will be given in different reference systems which complicate comparisons.

On the session level, an improved approach would be to analyze the VLBI and GPS datasets for each session simultaneously with the same clock and tropospheric model parameterization and with common estimates for these parameters. The two techniques will complement each other, especially with respect to the troposphere, since GPS acquires signals simultaneously from many spatial directions and typically down to 15 to 20 degrees while VLBI often measures all the way down to an elevation of 2 to 3 degrees. The addition of SLR would, in principle, help in the decoupling of the tropospheric parameters from the others, since this technique does not sense the wet part of the troposphere.

We may expect that some extra parameters must be introduced to soak up systematic differences, but this would certainly give new insight into the sources of such errors. In fact, this simultaneous strategy is the only practical way of detecting and correcting systematic technique-dependent errors.

The observability of different important geodetic parameters is technique-dependent. Table 4 shows that VLBI is the only technique capable of determining the nutations, precession, and the siderial angle (represented by UT1) and thus realize a long-term stable celestial reference frame. The satellite-based techniques cannot in general be used to determine UT1 since this quantity is indistinguishable from the right ascension of the ascending node. The advantage of SLR, and to a certain extent GPS, is the ability to determine the location of the geocenter. The sampling interval, redundancy and measurement simultaneity and precision of GPS make it possible to estimate the motion of the instantaneous Earth rotation axis

relative to a terrestrial reference frame with high precision and resolution in time. The combination of VLBI with other techniques might in some cases make it possible to resolve the ambiguities of some of the VLBI phase delay measurements, which would give access to phase measurements with a precision of around 1 mm or better. This should certainly increase the possibility of performing high-precision EOP analysis with high resolution in time.

A very important practical aspect of a combined analysis is that it is possible to determine geodetic and geodynamical parameters in a common reference frame. Furthermore, the GPS satellite ephemerides will be given in a long-term stable celestial reference frame with the orientation realized by the radio sources present in the VLBI dataset. The combined processing of VLBI and GPS can reduce the network-dependency seen in some of the VLBI-results especially with datasets containing misbehaving stations.

The simultaneous analysis of different datatypes, due consideration of the physical interrelations, and presentation of results in a common reference system, are the main ideas behind the developement of the GEOSAT software.

The GEOSAT scheme for processing daily batches of data is shown in Fig. 2. The first step is to establish measurement files and other files with apriori information. The measurements are ordered passwise before entering GEOSAT. Since the filter program MUDFILTER (Multi-satellite Upper Diagonal factorized kalman FILTER) must have the measurements ordered chronologically, the IMUDFILTER program must be executed first to establish a mapping between the two ordering schemes. The next step is to run the main program GEOSAT to generate residuals and partial derivatives of the measurements with respect to the solve-for and consider parameters. A sophisticated three-level Bayesian weighted least squares estimator is available if some of the parameters need improvement before the filtering. The calculations in the main program GEOSAT are in the case of GPS, based on reference orbits obtained from a preliminary fit to JPL/IGS GPS orbits. The purpose of the SOCUP program is to update the values of model parameters based on the new parameter estimates. The MUDFILTER program can then be applied to obtain results based on only a single technique. In case of a simultaneous analysis of many types of data the residuals and partials of each techniques are input to the CMUDFILTER program which generates a mapping between the passwise ordering and a chronological ordering of all the residuals and partial derivatives. Then the MUDFILTER is executed to generate a daily multi-technique UD matrix including the state vector.

Fig. 3 illustrates how daily UD matrices can be combined into global multi-year solutions using the CSRIF (Combined Square Root Information Filtering) program. With this program it is possible to treat the parameters at four different levels. Examples of parameters for each level are shown in the figure. New levels can easily be incorporated.

3 A combined VLBI, GPS and SLR data analysis

The combined analysis included VLBI (the R& D network) and GPS data (the IGS network), and SLR data for LAGEOS 1 & 2, from January 13-15 and from January 20, 1994. Data from 2 collocated VLBI/GPS/SLR stations, 4 VLBI/GPS stations, 28 GPS-alone stations and 12 SLR-alone stations were applied in the analysis.

No steps were taken in the analysis to optimize the relative data weighting between the three techniques. Typically 40000 GPS pseudorange measurements with a weight based on σ = 1 m, 40000 GPS phase measurements with a weight based on σ = 7 mm, 6000 VLBI group delay measurements with a weight based on σ = 7 mm, and 300 SLR measurements with a weight based on σ = 5 cm, were analyzed for each day.

All parameters were estimated simultaneously in a free network mode. One common set of station coordinates were derived for each collocated station with contributing data from all techniques when available. Table 5 presents the coordinate repeatability of collocated stations with high-precision eccentricity vectors. It can be seen that the repeatability in baseline length is almost independent of the distance between the stations.

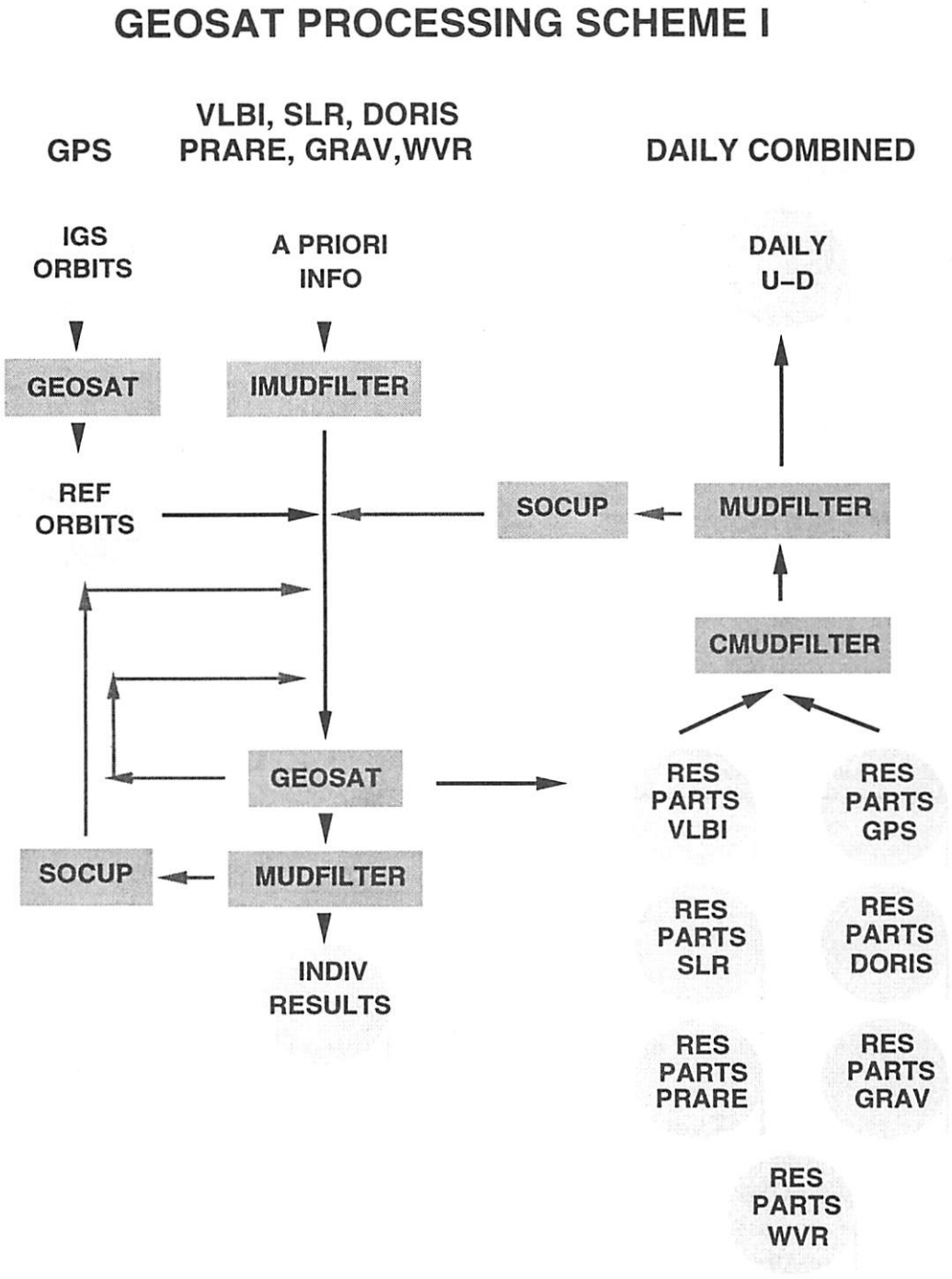

Figure 2: Processing of individual techniques in batches of one day.

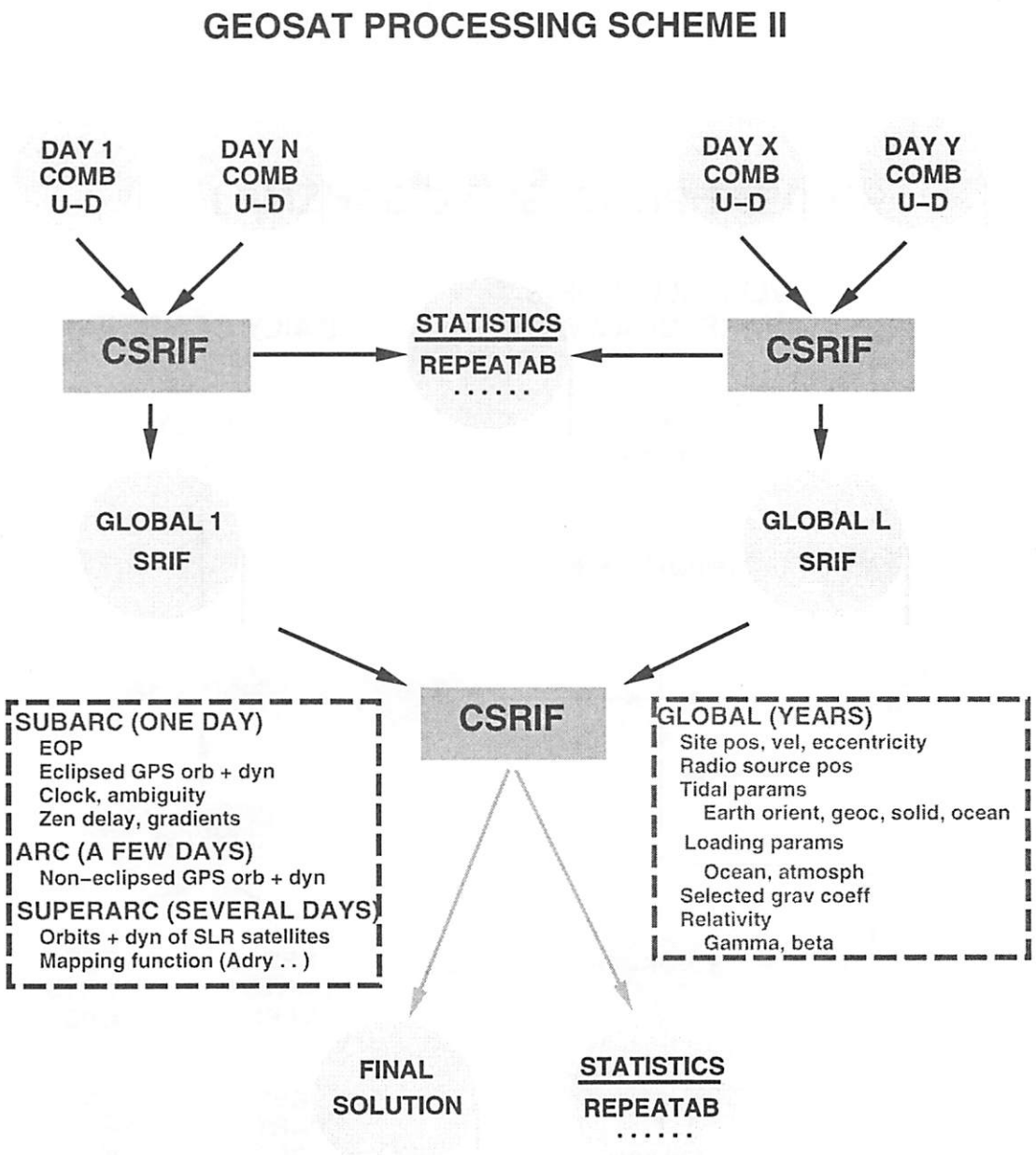

Figure 3: Combination of daily multi-technique state vectors and covariances to global solutions.

Eccentricity vectors from VLBI to GPS and/or SLR were also estimated with an *a priori* sigma in accordance with the given precision of the ground tie. The difference between VLBI to GPS eccentricity vectors estimated by GEOSAT and the vectors applied by IERS in the derivation of ITRF'93 is shown in Table 6. The sigmas are based on the actual daily repeatabilities.

Individual estimates of troposphere and clock parameters were determined for each technique in the analysis. Some of the results are presented in Fig. 4 which shows that it should certainly be possible to apply a common tropospheric parameter representation for the collocated stations. It should also be possible to estimate a common clock drift parameter at each collocated station. The clock estimates from the GPS data show a peculiar periodic behaviour relative to the VLBI estimated clock solutions. Since the period is around 12 hours, it is expected that this phenomena is closely related to the orbital motion of the GPS satellites with the same revolution period. This effect is presently being investigated.

REPEATABILITY				
$\sigma = a + bL$	South	East	Height	Length
a(mm)	1.7	2.1	4.2	2.3
b(ppb)	0	0	0	0.18

Table 5: Coordinate repeatability of collocated stations with high-precision eccentricity vectors in a combined VLBI/GPS/SLR analysis of data from the CONT94 campaign. Two of the stations, Ft. Davis (MDO1) and Wettzell (WETT), had also some passes of SLR data.

GPS ECCENTRICITY CHECK			
Station	Comp	Diff (mm)	σ (mm)
ONSA	X	0.8 ± 1.5	3
	Y	3.6 ± 0.5	3
	Z	0.5 ± 1.4	3
WETT	X	-2.8 ± 1.3	3
	Y	-3.8 ± 1.7	3
	Z	-1.3 ± 0.6	3
KOKB	X	0.8 ± 1.5	3
	Y	0.6 ± 1.3	3
	Z	-0.5 ± 2.0	3
MDO1	X	-0.5 ± 1.9	12
	Y	2.2 ± 2.4	12
	Z	-0.6 ± 2.2	12

Table 6: The difference between VLBI to GPS eccentricity vectors estimated by GEOSAT and the vectors applied by IERS in the derivation of ITRF'93. The given error estimates are the daily repeatabilities. The last column shows the precision of the ground tie.

The next step will be to repeat the combined analysis with a common solution, not only for the station coordinates, but also for some of the troposphere and clock parameters. In that analysis I will also include WVR (Water Vapor Radiometry) data from the Onsala station.

4 Conclusions

The combined multi-technique analysis strategy has been demonstrated with very promising results. The solutions for the antenna phase center coordinates of the different techniques seem to be consistent at the few mm-level for stations with precisely determined ground ties (better than 12 mm, 1σ, in each direction).

The proposed strategy will be very powerful for the study of technique-dependent systematic errors, for the detection of errors in ground ties, and for the recovery of geophysical, geodetic and geodynamical parameters.

Acknowledgements

The author is grateful to Statens kartverk for the continuous financial support of the project during many years.

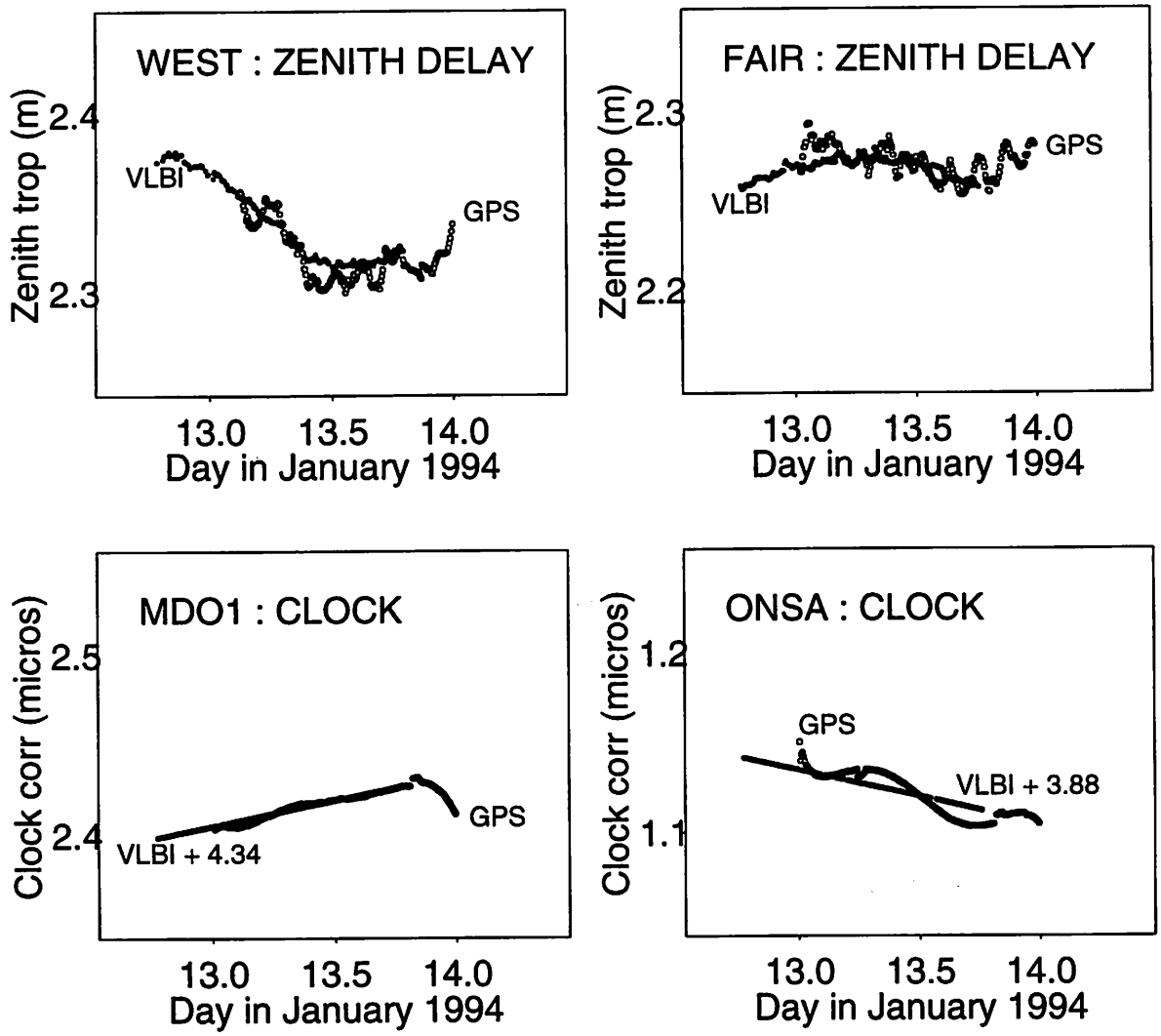

Figure 4: Total tropospheric zenith delay and clock corrections relative to the Westford clock (in milliseconds), estimated with GPS and VLBI data.

References

1. Andersen, P. H. (1994). High-precision Station Positioning and Satellite Orbit Determination, PhD. thesis, the University of Oslo, NDRE/PUBL-95/01094, The Norwegian Defence Research Establishment.

2. Andersen, P. H., S. Hauge and O. Kristiansen (1993). GPS relative positioning at the level of one part per billion. Bulletin Geodesique, Vol. 67, No. 1, pp. 91-106.

3. Andersen, P. H., S. Rekkedal (1995). VLBI data analysis with the GEOSAT Software. Bulletin Geodesique, Vol 69, No. 3, pp. 125-134.

4. Andersen P. H. (1995). Measuring rapid variations in Earth orientation, geocenter and crust with satellite laser ranging. Bulletin Geodesique, Vol. 69, No. 4, pp. 233-243.

5. Andersen, P. H., K. Aksnes, and H. J. Karlsen (1996). ERS-1 & 2 Tandem Mission Orbit Determination. Presented at the XXI General Assembly of the European Geophysical Society, The Hague, The Netherlands, 6-10 May.

Determination of metric coefficients with VLBI

Klaus Boerger, Geodetic Institute, University of Bonn, Nussallee 17, 53115 Bonn
e-mail: boerger@uni-bonn.de

August 1996

Abstract:
At the very beginning the physics of VLBI was modelled by means of Newtonian mechanics and Euclidian geometry. With increasing accuracy one left the domain in which this physical theory, i.e. physical laws and geometry, is valid. This progress led to the introduction of Einstein's Special Theory of Relativity and later this first step to relativity was accomplished by using General Relativity.
Naturally geodesists are dealing with geometry; geometry of surfaces, geometry of 3-dimensional Euclidian spaces and last but not least the geometry of 4-dimensional spacetimes. This Pseudo-Riemannian geometry as space-model for General Relativity has a particular meaning, because all forms of matter, energy and momentum generate geometry. Therefore the geometry of a geocentric spacetime, represented by the metric tensor, includes all well-known forces of Newtonian physics like gravitational forces of earth, tidal forces, coriolis forces and so on.
VLBI considered in this context gets new perspectives that is to say relativity serves not only as a tool for correction of the classical model, but relativity can be used to get new informations. For instance there exists a theoretical chance to determine components of the metric tensor. These theoretical thoughts will be presented.

1 Fundamentals of Geometry

A great field for geodesists is the solution of geodetic problems, i.e. in the first place the **Direct or First Geodetic Problem** and secondly the **Inverse or Second Geodetic Problem**. And dealing with these problems means to observe geometric quantities, for example distances and angles, and to determine coordinates or vice versa. Using the geometric principles, which are valid for 2D-, 3D- and 4D-geometry, one is enabled to solve the mentioned problems. These principles of geometry are the

Presented at the 11th Working Meeting on European VLBI for Geodesy and Astrometry, Onsala, Sweden, 1996

First Fundamental Form:

$$ds^2 = g_{\alpha\beta}\, dx^\alpha\, dx^\beta$$

which gives a relation between measured distances ds and coordinate differentials dx^α. (Einstein's summation convention is used. An index occuring twice - as subscript and superscript - means to execute summation)

The First Fundamental Form is easy explained by a simple example, e.g. a triangle within a plain. By choosing a plain, one gets a simple geometry, i.e. simple metric coefficients $g_{\alpha\beta}$. Then applying the First Fundamental Form yields the well-known Pythagoras.
A further important relation is the

Transformation of the metric tensor:

$$g^{\alpha\beta} = x^\alpha_{,\bar{\mu}}\, x^\beta_{,\bar{\nu}}\, \bar{g}^{\mu\nu},$$

by which one proves the invariance of geometric quantities, like distances and angles. With known metric tensors this equation serves as determination equation for the transformation matrices $x^\alpha_{,\beta}$.

Finally one needs to know the definition of geodesic lines, which is given by the

Differential equation of geodesic lines:

$$\frac{d^2x^\alpha}{dq^2} = \Gamma^\alpha_{\beta\gamma}\, \frac{dx^\beta}{dq}\, \frac{dx^\gamma}{dq}$$

$$\Gamma^\alpha_{\beta\gamma} = F(g_{\mu\nu}) = \text{Christoffel symbols}$$

$$dq = \text{affine parameter.}$$

Note that the distances, which connect points, are measured along so-called **geodesic lines**. These geodesic lines are defined as those lines on which free particles (e.g. photons) or bodies move and in general these lines are curved. This fact emphasizes the importance of geometry, expressed by the metric tensor $g_{\alpha\beta}$, because geometry determines the structure of space and therefore defines geodesic lines. Within 3D-euclidian geometry these lines are straight lines, but in analogy to 2D-geometry geodesic lines in 4D-geometry - so called **geodesic world lines** - are curved, which is in opposition to the euclidian idea. And this curvature is caused by gravity or more general by all forms of energy and momentum.

Up to now only spatial aspects were mentioned, but dealing with 4-dimensional geometry one especially has to consider the time, which now has the character of a coordinate. Thus in an arbitrary 4-dimensional spacetime coordinates are defined according to

$$x^\alpha = (ct, x^i)^\alpha \quad ,$$

and the first fundamental form reads

$$ds^2 = (cd\tau)^2 = g_{\alpha\beta}\, dx^\alpha\, dx^\beta \quad ,$$

or in equivalent form

$$d\tau = (g_{00} + \frac{2}{c} g_{0i} \frac{dx^i}{dt} + \frac{1}{c^2} g_{ij} \frac{dx^i}{dt} \frac{dx^j}{dt})^{\frac{1}{2}} dt \quad .$$

These equations show, that there's a distinction between the **coordinate time** t and the **proper time** τ and the equations above (First Fundamental Form) arrange the relation of these times. The last equation again demonstrates the influence and importance of geometry. Apart from the velocity of a clock it is geometry which causes the difference between coordinate time and proper time.

All these considerations make clear, there is an absolute need to know geometry, and in case of 4D-geometry it means to know the structure (and thus curvature) of space and time to solve the above mentioned geodetic problems. In order to determine this geometry one has to solve the **field equations**, which are determination equations for the unknown metric tensor. These field equations are elementary part of a metric theory.

Besides **Einstein's gravitation theory** there are some different metric theories, like the metric theory of Brans-Dicke-Jordan or Ni's metric theory. All these theories are valid and all these theories (Einstein's gravitation theory included) can be submitted to one theory, which is named the **Parametrized Post Newtonian (PPN) metric theory**. By setting the parameters in a certain way one obtains the individual theories. Nevertheless all theories are equivalent (because all are valid), therefore it is permitted to use Einstein's gravitation theory as metric theory and then the field equations read

$$R^{\alpha\beta} = \kappa (T^{\alpha\beta} - \frac{1}{2} g^{\alpha\beta} T) \quad , T := T^{\alpha}_{\alpha} \quad .$$

with

$$\begin{aligned} R^{\alpha\beta} &= \text{Riccitensor} \quad , \\ T^{\alpha\beta} &= \text{energy-momentum tensor} \quad , \\ \kappa &= \text{coupling constant} \quad . \end{aligned}$$

These differential equations represent determination equations for the the unknown metric. In order to solve them some a priori considerations are necessary:

- First one has to choose the origin of spacetime. Astronomers often use a barycentric spacetime and a non-rotating coordinate system. This is not convenient for geodetic applications. Therefore the metric is required for a geocentric spacetime with a rotating coordinate system.
- Because of the non-linearity and the under-determinacy one has to linearize the field-equations and to introduce an appropriate gauge condition.

With these steps done one starts to develop the Christoffel symbols $\Gamma^{\alpha}_{\beta\gamma}$ (which contain derivatives of the metric tensor) and then with these quantities given the Riccitensor $R^{\alpha\beta}$ can be written as function of the Christoffel symbols. Thus expressions for the left side of the field equations are given. Now the right side, which depends on the energy-momentum-tensor $T^{\alpha\beta}$ and represents the relativistic matter-model, can be developed. This matter-model is known, so that with all quantities inserted in

the field equations one gets determination equations for $g_{\alpha\beta} = \eta_{\alpha\beta} + h_{\alpha\beta}$, which then have to be integrated. The solution reads:

$$
\begin{aligned}
g_{00} &= 1 - \frac{2}{c^2}(U_E - W_{TH} + U_{ZF}) + \frac{2}{c^4}U_E^2 + \Theta \\
&\quad - \frac{4}{c^4}\left(\frac{k}{r^3}\epsilon_{ijk.}\,\epsilon_{ilm.}\,\overset{E}{w}_{j.EI}\,\overset{E}{D}_{l.}\,\overset{E}{x}_{k.}\,\overset{E}{x}_{m.}\right) \\
&\quad + \frac{2}{c^4}\epsilon_{ijk.}\,\epsilon_{ilm.}\,\overset{E}{w}_{j.EI}\,\overset{E}{w}_{l.EI}\,\overset{E}{x}_{k.}\,\overset{E}{x}_{m.}\,(W_{TH} - U_E) \\
g_{0i} &= -\frac{1}{c}\epsilon_{ijk.}\,\overset{E}{w}_{j.EI}\,\overset{E}{x}_{k.} - \frac{2}{c^3}\left\{\frac{k}{r^3}\epsilon_{ijk.}\,\overset{E}{D}_{j.}\,\overset{E}{x}_{k.} + \epsilon_{ijk.}\,\overset{E}{w}_{j.EI}\,\overset{E}{x}_{k.}\,U_E\right\} \\
&\quad - \frac{1}{c^3}\left\{\epsilon_{ijk.}\,\overset{E}{w}_{j.EI}\,\overset{E}{x}_{k.}\,U_{ZF} + \Psi_{i.}\right\} \\
g_{ij} &= -\delta_{ij.} - \frac{2}{c^2}\left(\delta_{ij.}\,U_E + \frac{1}{2}\delta_{ij.}\,U_{ZF} + \Upsilon_{ij.}\right) \quad .
\end{aligned}
$$

with

$$
\begin{aligned}
U_E &= \text{earth gravitational potential} \quad , \\
W_{TH} &= \text{tidal potential} \quad , \\
U_{ZF} &= \text{centrifugal potential} \quad , \\
D_{i.} &= \text{angular momentum vector} \quad , \\
w_{i.} &= \text{earth rotation velocity} \quad .
\end{aligned}
$$

Now the geometry of a geocentric earthbound spacetime is known, but VLBI observations are done at local places. Thus within the framework of a relativistic VLBI modelling one has to define local spacetimes. These local spacetimes (the spacetimes of the antennas) are introduced as flat topocentric spacetimes with a pseudo-euclidian metric, which is an admissible action, because for little scopes of space and time geometry can be replaced by geometry of Special Relativity, i.e. Minkowski metric. The relation between the global and local spacetime is given by the above mentioned transformation law of the metric tensor. Now with given metric tensors one obtains the following transformation matrices, which depend on the metric coefficients $h_{\alpha\beta}$:

$$
\begin{aligned}
x^i_{,\bar{0}} &= 0^i \\
x^i_{,\bar{j}} &= 1 - \frac{1}{2}\left\{-h_{ii\,(2)} + h_{0i\,(1)}\,h_{0i\,(1)} + 2\,h_{0i\,(1)}\,h_{0i\,(3)} - h_{ik\,(2)}\,h_{ik\,(2)}\right\}\delta^i_j \\
x^0_{,\bar{i}} &= -h_{0i\,(1)} - h_{0i\,(3)} + h_{0i\,(1)}\,h_{00\,(2)} + h_{ik\,(2)}\,h_{0k\,(1)} \\
&\quad - \frac{1}{2}\left\{(h_{0i\,(1)})^3 - h_{0i\,(1)}\,h_{ii\,(2)}\right\} \\
x^0_{,\bar{0}} &= 1 + \frac{1}{2}\left\{-h_{00\,(2)} - h_{00\,(4)} + h_{00\,(2)}\,h_{00\,(2)}\right\} \\
&\quad - \left\{h_{0i\,(1)}\,h_{0j\,(1)}\,h_{00\,(2)} + h_{0i\,(1)}\,h_{0k\,(1)}\,h_{jk\,(2)}\right\}\Delta^{ij} \\
&\quad + \frac{1}{2}\left\{h_{0i\,(1)}\,(h_{0j\,(1)})^3 - h_{0i\,(1)}\,h_{0j\,(1)}\,h_{jj\,(2)}\right\}\Delta^{ij} \quad .
\end{aligned}
$$

2 Relativistic Analysis

With the preliminary of the last section one is enabled to derive a relation that provides the observed delay as function of metric coefficients. Given is the situation as shown in the figure and in order to

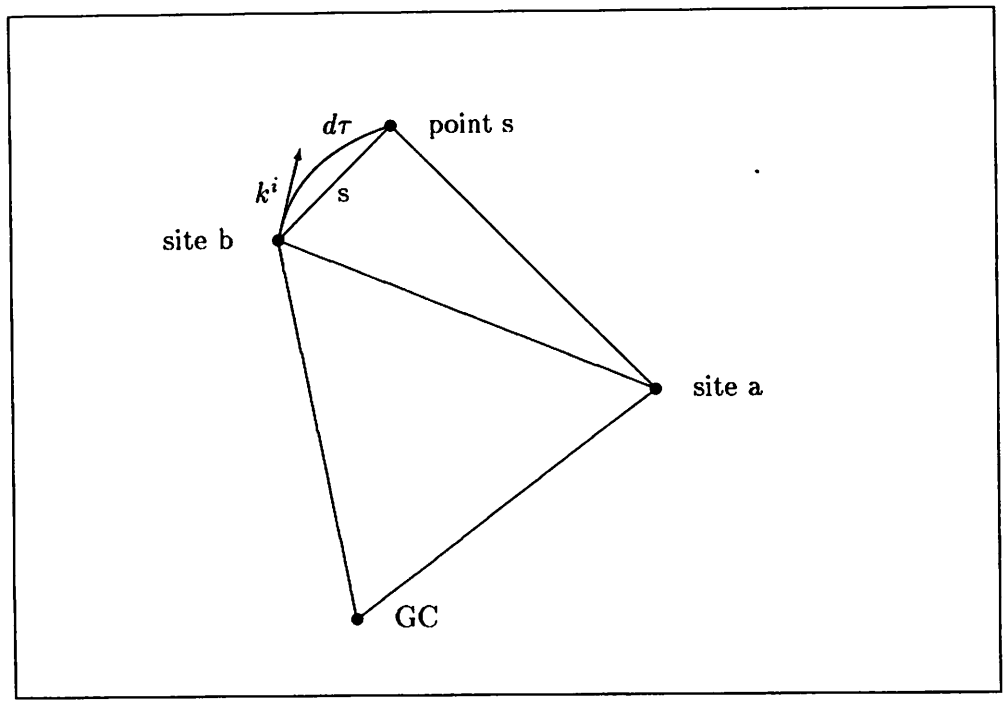

fig. 1: geometric situation

get an observation equation which represents the observed delay as function of the metric, one starts with the following ansatz:

$$x_s^i = x_e^i + \left(\frac{\partial x_H^i}{\partial t}\right)_b \Delta t + \frac{1}{2}\left(\frac{\partial^2 x_H^i}{\partial t^2}\right)_b \Delta t^2 + \dots \quad ,$$

with

x_s^i = spatial coordinates of point s ,

x_e^i = spatial coordinates of site b ,

x_H^i = spatial coordinates of a signal ,

k^i = direction vector to source ,

Δt = time interval ,

respectively

$$\Delta x^i = x_s^i - x_e^i = (v_H^i)_b \Delta t + \frac{1}{2}(b_H^i)_b \Delta t^2 + \dots \quad ,$$

with

v_H^i = velocity of a signal ,

b_H^i = acceleration of a signal .

Now building the root

$$s \;=\; (\Delta_{ij}\,\Delta x^i\,\Delta x^j)^{\frac{1}{2}}$$

one obtains with the above power series inserted

$$s \;=\; (v_H)_b\,\Delta t \;+\; \frac{1}{2}\left(\frac{\Delta_{ij}\,v_H^i\,b_H^j}{v_H}\right)_b \Delta t^2 \;+\; \frac{1}{8}\left(\frac{b_H^2}{v_H}\right)_b \Delta t^3$$

and solved for the delay provides

$$\Delta t \;=\; \left(\frac{s}{v_H}\right)_b \;-\; \frac{1}{2}\left(\frac{\Delta_{ij}\,v_H^i\,b_H^j}{v_H^2}\right)_b \left(\frac{s}{v_H}\right)_b^2 \;-\; \frac{1}{8}\left(\frac{b_H}{v_H}\right)_b^2 \left(\frac{s}{v_H}\right)_b^3 \quad .$$

This equation has to be expressed in the geocentric earthbound spacetime. For this purpose the velocity is to transform from the local topocentric spacetime Σ_n into Σ_E. Finally one gets the delay as function of the metric coefficients. In first approximation and neglecting refraction the observation equation reads:

$$c\,\Delta t \;=\; s\,(1 \;-\; h_{00(2)} \;-\; \frac{1}{c}\,(h_{0j(1)}\overset{n}{v}{}_H^j) \;-\; \xi) \;+\; \cdots \quad ,$$

with

$$\xi \;=\; \text{rest term} \quad .$$

Now, a relation is found, which provides the observed delay Δt as function of the metric coefficients $h_{\alpha\beta}$. In first approximation the delay is given by the euclidian distance. But geometry influences the delay, what can be interpreted as a kind of scaling. Of special interest is the temporal metric coefficient $h_{00(2)}$, which contains gravity. The mixed metric coefficient $h_{0i(1)}$ contains earth rotation.

3 Discussion

General Relativity is still included in VLBI by the so-called Consensus Model, but in a different way, because the ideas shown in this paper are straightened to one special aspect, that is to say the determination of gravitation respectively gravity. And these theoretical thoughts show, that this is in principle possible. Now numerical and practical investigations have to follow in order to show whether the ideas have practical meaning.

The metric coefficient $h_{00(2)}$ is about $1.39 * 10^{-9}$ (concerning only Earth gravitation) and the accuracy of the observed delay is about $1 * 10^{-11}$. Thus the observation clearly contains the signal, which is to determine. The further quantities in the observation equation are all known like the scalar product $h_{0i}\overset{n}{v}{}^i$ and the quantity s, which represents the square root of coordinate differences and thus can be approximated with sufficient accuracy by the euclidian distance.

The CGS VLBI EUR96 Geodetic Solution.

R. Lanotte[1], G. Bianco[2], M. Fermi[3], P. Rutigliano[1] and G.R. Verdone[1]

[1]*Nuova Telespazio S.p.A, Centro di Geodesia Spaziale "G.Colombo", Matera, Italy*
[2]*Agenzia Spaziale Italiana, Centro di Geodesia Spaziale "G.Colombo", Matera, Italy*
[3]*Nuova Telespazio S.p.A, Roma, Italy*

Abstract. The EUROPE project started in 1990 to monitor the tectonic behaviour of the western European region using a network of fixed VLBI stations. Six years of VLBI data have been analysed to estimate the motion of the stations participating to this campaign. The computed site velocities are compared to those predicted by the NUVEL1A plate model. Onsala, Effelsberg, Wettzell and Madrid show a very good agreement with respect to the model and no intraplate motion is evident for these stations while the Italian sites, Medicina, Matera and Noto show significant discrepancy with respect to the model. In particular the Matera motion cannot find the right arrangement into the model.

Introduction

Since 1990 regular VLBI observing sessions are being carried out in the western Europe using fixed stations to monitor the tectonic motion of this region; starting from 1995, two more stations joined the original network, namely Ny-Alesund (Norway) and Crimea (Ukraine), extending the network towards north and east. This analysis focuses on the original network that includes stations in the western part of the Eurasian plate. Table 1 lists the site locations, the managing agencies and the antenna sizes of the stations participating to the Europe project.

Site name	Antenna diameter (m)	Agency	Location
CRIMEA	22	Crimean Radio Astrophysical Observatory	Crimea, Ukraine
DSS65	34	Deep Space Network	Madrid, Spain
EFLSBERG	100	Max Planck Institute for Radioastronomy	Effelsberg, Germany
KARLBURG	MV2		Karlsburg, Germany
MATERA	20	Italian Space Agency (ASI)	Matera, Italy
MEDICINA	32	University of Bologna	near Bologna, Italy
NOTO	32	University of Bologna	Noto, Sicily, Italy
NYALES20	20	Geodetic Institute of the Norwegian Mapping Authority	Ny Alesund, Norway
ONSALA	20	Onsala Space Observatory	Onsala, Sweden
TOULOUSE	MV2		Toulouse, France
WETTZELL	20	German Institute for Applied Geodesy (IfAG)	Bavaria, Germany
YEBES	13.7	National Astronomical Observatory of Spain	Yebes, Spain

Table 1. Description of the stations participating to the Europe campaign.

Data processing

Data acquired from 1990 up to 1995 in the geodetic Mark III [Rogers et al., 1983; Clark et al., 1985] VLBI experiments from the EUROPE campaign have been analysed in the CGS_VLBI/EUR96 solution, including 26 sessions, each lasting 24 hours. Figure 1 summarises the overall session statistic, station by station. YEBES, TOULOUSE and KARLBURG which participated only to one experiment will not be taken into account in the solution. All the other stations in the network show a statistic strong enough to recover a reliable tectonic motion except for CRIMEA and NYALES20 which have six experiments but over a relatively short lapse of time.

Presented at the 11th Working Meeting on European VLBI for Geodesy and Astrometry, Onsala, Sweden, 1996

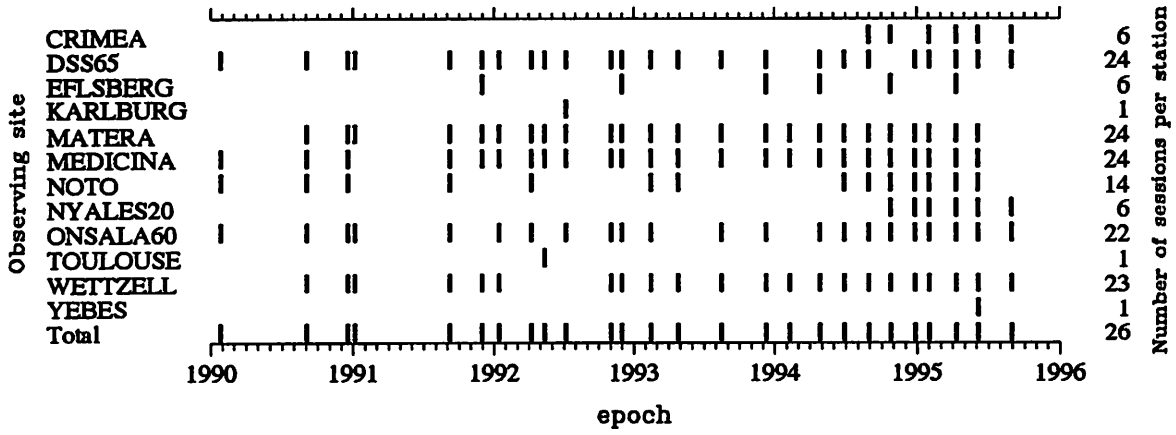

Figure 1. Data coverage record.

Figure 2 schematically shows the logical flow of data processing. The databases, correlated at the Max Planck Institute for Radio Astronomy in Bonn, have been acquired from the NASA-CDDIS (Crustal Dynamic Data Information System) up to 1992 and from the Bonn correlator for the period 1993-1995.

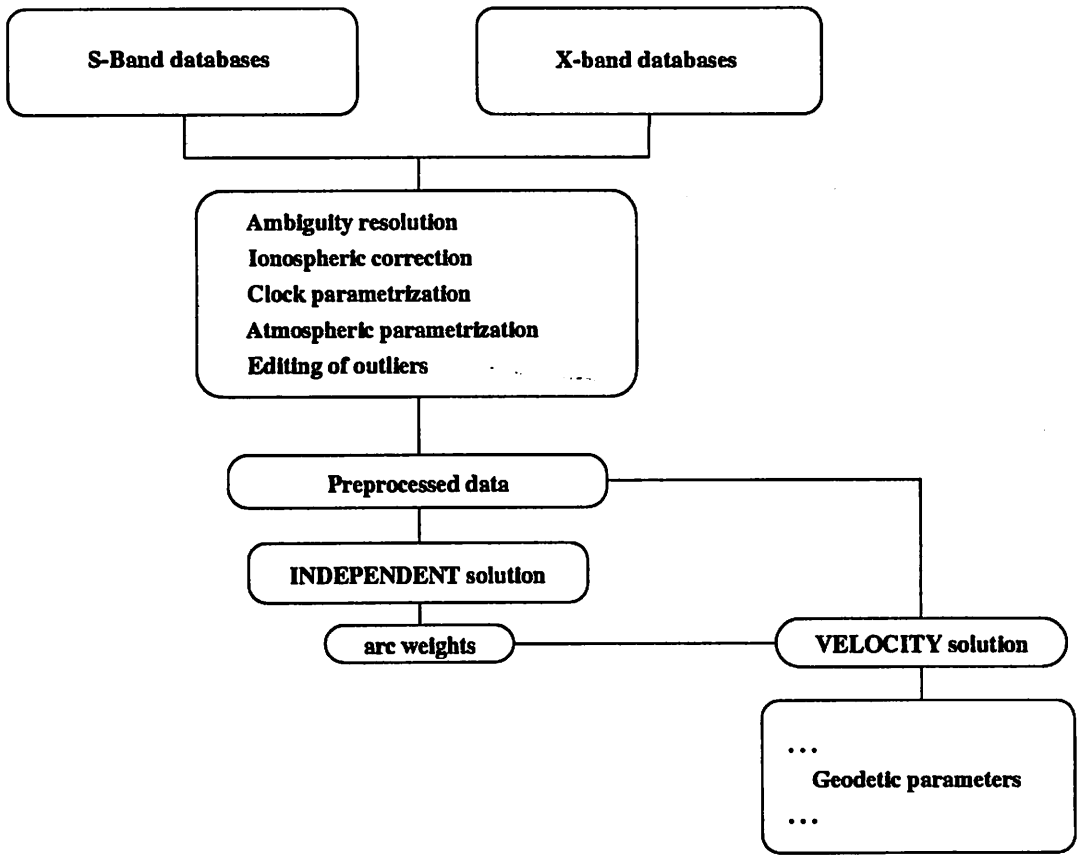

Figure 2. Data processing scheme.

The analyses have been carried out by means of the CALC/SOLVE software system developed at the NASA Goddard Space Flight Center, on an HP755 workstation.
In the first step of the analysis the databases have been preprocessed estimating ambiguities; ionospheric delays have been removed using both the data acquired on the S (2.3 GHz) and X (8.4 GHz) bands. Clocks were estimated using a reference station and modelling the

differences between the reference clock and the others with an unconstrained second order polynomial plus a continuous piecewise linear function with duration of the linear sections of 60 minutes and $5 \cdot 10^{-14}$ constrained in slope.
To take into account the tropospheric delay we have to separate it into its dry and wet components. The dry delay for each observation was estimated at the zenith using the Saastamoinen model and then mapped to the elevation of the observation with the MTT dry model [Harring, 1992]. Wet tropospheric delay was estimated using a continuous, piecewise linear function with duration of the linear sections of 60 minutes and 50 ps/h constrained in slope.
After removal of these systematic effects, the outliers have been edited inspecting directly the data.
Two solutions, using SOLVE in GLOBL mode [Ma et al., 1990], were computed: the first was an independent solution to generate the arc weights used to reweight the observations for the subsequent velocity solution, where site positions and velocities for European stations were estimated as global parameters.
The models used in the analysis are based on the International Earth Rotation Service (IERS) standards [McCarthy, 1989].
The regional extension of the network under investigation does not allow to reliably determine parameters such as the celestial source positions as well as Earth rotation parameters. For this reason they have been kept fixed using: the IERS celestial reference frame ICRF92 for the source coordinates, the IERS series 90 C 04 for the Earth Orientation Parameter and nutation series .[IERS A.R. 1992]. For precession, the J2000.0 model has been used.

Independent solution

In the independent solution the so called "reweighting process" is performed for each session by estimating a constant formal error. This constant added to the variance of the observations (derived in the correlation process) has to satisfy the condition that the overall reduced χ^2 of the residual delays in the session was equal to unity. The reweighting process, in principle, allows to take into account for unmodelled effects in the data.
The independent solution, using the reweighted observations, provides the time series of the geodetic parameters and in particular the baseline vector components.
Figure 3 shows the baseline length variations for all the baselines relevant to Wettzell. These baselines can be considered as representatives for all the baselines in the independent solution.
The high error rate for the baselines CRIMEA-WETTZELL and NYALES20-WETTZELL, one order of magnitude higher than those present on the other baselines, is a feature characterising all the baselines including these stations and may be ascribed to the short lapse of time covered by both stations. These considerations led us to not estimate the velocities for CRIMEA and NYALES20 in the velocity solution.
The time series of the parameters resulting from the independent solution have been used to check the reliability of the solution and to be confident of the goodness of the results that will be carried out in the following velocity solution.

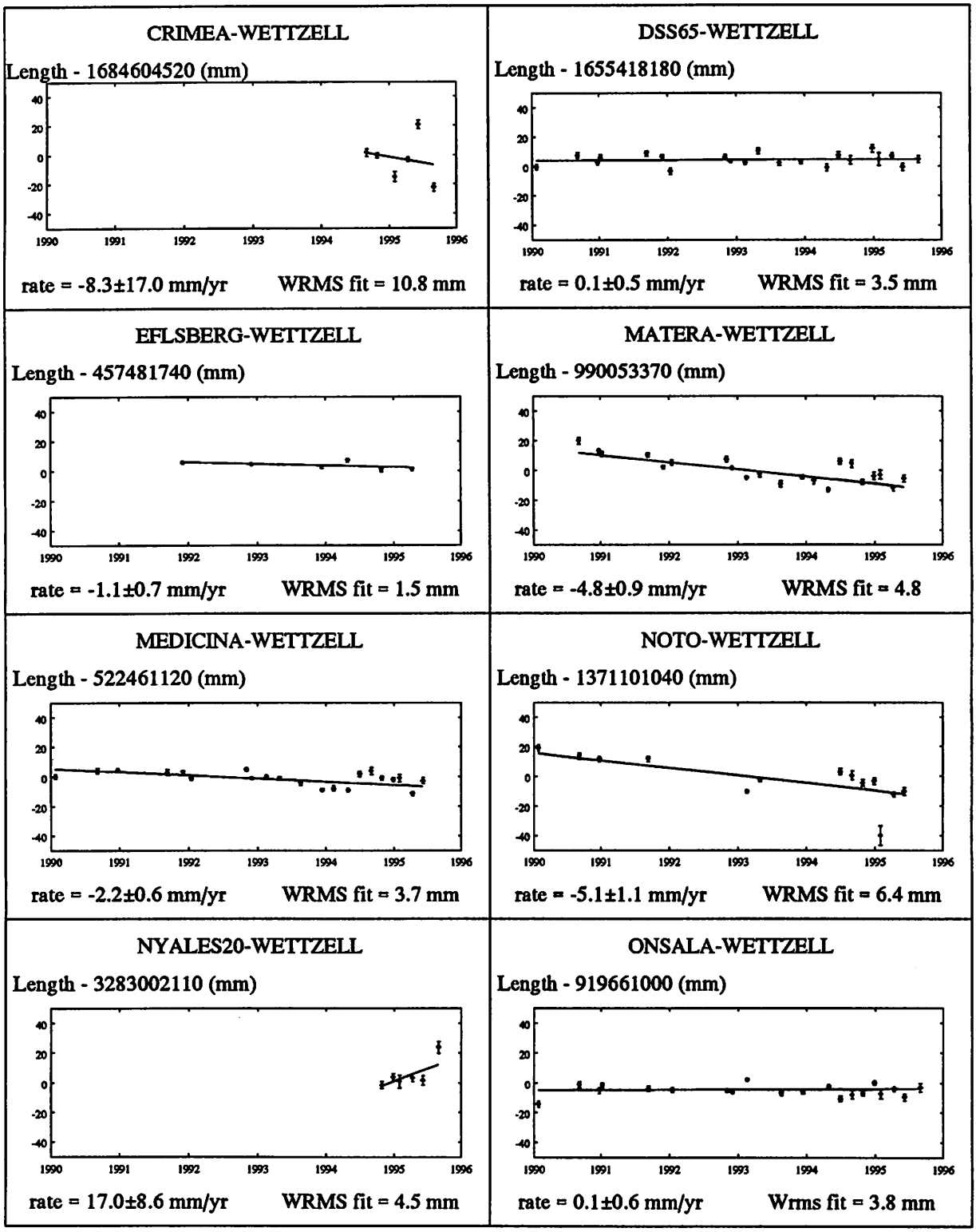

Figure 3. Length variation of the baselines including the Wettzell site. The points are the calculated value of the baseline at an epoch with one sigma formal error bar. The straight line on the plots is the line of best fit by least squares. The rate, error rate and WRMS fit is on the bottom of each plot.

Velocity solution

The velocity solution applies the previously obtained arc weights to the preprocessed databases to estimate the parameters of interest considering station positions and velocities as global parameters, i.e. common to all the analysed sessions.
The solution is constrained moving the Wettzell site according to the NUVEL1A model [De Mets et al., 1994] and fixing its position to the value of the IERS Terrestrial Reference Frame ITRF92 [Boucher et al., 1993] at the epoch January 1, 1988.
We also fixed the positions of the KARLBURG, TOULOSE, CRIMEA and NYALES20 sites to the values of the ITRF92 and the velocities of these sites to the NUVEL1A model.
The overall solution statistics is summarised in table 2.
Table 3 shows the estimated station velocities and the ones provided by the NUVEL1A model in the topocentric Up, East and North reference frame. Looking at the North and East components DSS65, EFLSBERG and ONSALA show a very good agreement with to the NUVEL1A model assuming the stations on the Eurasian plate. NOTO, MATERA and MEDICINA seems to be in disagreement to the model assuming NOTO on the African plate, MEDICINA on the Eurasian one and MATERA on the Eurasian or on the African plate. The Up rates are affected by higher variances which are generally four times those of the horizontal components. All the stations doesn't show significant Up rates except DSS65 and ONSALA.
The horizontal velocity of the stations is highlighted in table 4 where is more evident the behaviour of the stations with respect to the model. These results show that Madrid, Effelsberg, and Onsala belong to the Eurasian plate and no intraplate deformation is acting among these stations.
NOTO shows good agreement for the rate and a discrepancy in the azimuth while MEDICINA shows good agreement for the azimuth and a discrepancy in the rate. For MATERA the estimated vector doesn't agree with the one predicted by the NUVEL1A model assuming this site either on the African or on the Eurasian plate.

Total time span	5.6 years
Total number of data	53171 delay observations
Number of global parameters	69
Number of arc parameters	7470
Overall WRMS fit	42 ps
Reduced χ^2	1.08

Table 2. Overall statistics for the velocity solution.

Site	Up rate (mm/yr)	East rate (mm/yr)	North rate (mm/yr)	NUVEL 1A Up rate (mm/yr)	NUVEL 1A East rate (mm/yr)	NUVEL 1A North rate (mm/yr)	Assigned Plate
DSS65	7.4 ± 0.9	19.4 ± 0.2	16.2 ± 0.2	0.0	18.7	15.6	Eurasian
EFLSBERG	2.5 ± 1.6	19.5 ± 0.3	13.4 ± 0.3	0.0	19.0	14.3	Eurasian
MATERA	-1.4 ± 1.0	23.8 ± 0.2	18.3 ± 0.3	0.0	19.2	20.5	African
				0.0	22.0	12.7	Eurasian
MEDICINA	-2.7 ± 0.8	23.2 ± 0.2	15.7 ± 0.2	0.0	20.8	13.6	Eurasian
NOTO	0.4 ± 1.0	21.9 ± 0.2	18.7 ± 0.3	0.0	19.8	20.5	African
ONSALA	5.0 ± 0.8	18.4 ± 0.2	13.2 ± 0.2	0.0	18.7	13.6	Eurasian
WETTZELL	0.0	20.4	13.4	0.0	20.4	13.4	Eurasian

Table 3. Site velocities in the local topocentric reference frame. The estimated Up, East and North rates are compared with those predicted by the NUVEL1A model. For Matera are reported both the vectors assuming this site on the African or on the Eurasian plate.

Site	Horizontal rate (mm/yr)	Horizontal azimuth (deg)	NUVEL1A Horizontal rate (mm/yr)	NUVEL1A Horizontal azimuth (deg)	NUVEL1A Assigned Plate
DSS65	25.3 ± 0.3	50.3 ± 0.4	24.4	50.1	Eurasian
EFLSBERG	23.6 ± 0.3	55.6 ± 0.7	23.8	53.0	Eurasian
MATERA	30.1 ± 0.2	52.5 ± 0.5	28.1	43.1	African
			25.5	60.0	Eurasian
MEDICINA	28.0 ± 0.2	55.9 ± 0.4	24.9	56.8	Eurasian
NOTO	28.8 ± 0.2	49.5 ± 0.5	28.5	44.1	African
ONSALA	22.6 ± 0.2	54.3 ± 0.6	23.1	54.0	Eurasian
WETTZELL	24.4	56.7	24.4	56.7	Eurasian

Table 4. Horizontal motion. The horizontal velocities are compared with those predicted by the NUVEL1A model. As in table 3, the model values for Matera are determinated assuming this station either on the African or on the Eurasian plate.

Figure 4 shows the horizontal velocity residuals with respect to the model with their three sigma error ellipses. For MATERA both the NUVEL1A residuals are reported assuming this station on the African or Eurasian plate. NOTO shows 2.7 mm/yr residual velocity in the S-E direction with respect to the purely African motion, MEDICINA shows 3.2 mm/yr residual velocity in the N-E direction with respect to the European motion and MATERA shows 5.8 mm/yr in the N-E direction with respect to the Eurasian plate and 5.1 mm/yr in the S-E direction with respect to the African plate.

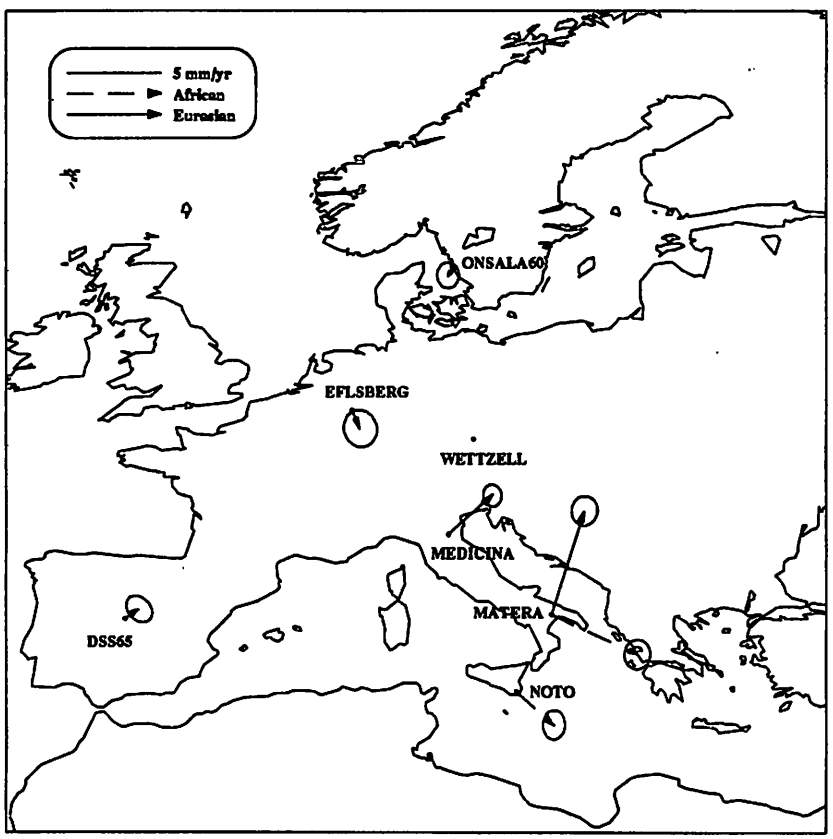

Figure 4. Residual horizontal velocities relative to the NUVEL1A model. For each site is shown the difference vector between the estimated velocity and the one predicted by the NUVEL1A model. For MATERA both the differences assuming this site on the Eurasian or on the African plate are reported. The associated error ellipses are three scaled standard deviation.

Interpretation of the results and conclusions

Our analysis of six years of VLBI data acquired by a regional network of fixed stations shows the capability of this technique to detect regional motion at a few mm/yr level.
For the stations in northern and central Europe the estimated horizontal VLBI motions cleary agree with the ones provided by NUVEL1A model and the motions of Onsala, Effelsberg, Wettzell and Madrid are consistent with the hypothesis that Europe moves like a rigid plate.
For the station in the central Mediterranean area the estimated motions are in disagreement with respect to the forecast. These differencies can be ascribeded to the low detail level presents in the NUVEL1A model for the tectonic of the central Mediterranean area modelled just considering the presence of two major plates, Africa and Eurasia.
Matera seems to be representative of the Adriatic platform showing strong differences from the motion predicted for this station by the model and, in our opinion, its estimated N-NE motion is representative of the mean motion of the Adriatic microplate while the mean motion estimated at Medicina may not be representative of the motion of the Adriatic block.
Noto is located in an area of complex tectonic structure, the boundary of African and Eurasian plate, [Di Geronimo et Al. 1978, Finetti et Al. 1986]. This station is usually assumed as belonging to the African plate but our results show a disagreement with respect to the motion provided by NUVEL1A.
Vertical movements seems to be in effect for Madrid and Onsala.
For Ny-Alesund and Crimea further acquisition are necessary to improve the data statistics.

References

Boucher, C., Z. Altamimi, and L. Duhem, ITRF 92 and its associated velocity field, Central Bureau of IERS, Paris Observatory, October 1993.

Clark, T.A., B.E. Corey, J.L. Davis, G. Elgered, T.A. Herring, H.F. Hinteregger, C.A. Knight, J.I. Levine, G. Lundqvist, C. Ma, E.F. Nesman, R.B. Phillips, A.E.E. Rogers, B.O. Ronnang, J.W. Ryan, B.R. Schupler, D.B. Shaffer, I.I. Shapiro, N.R. Vandenberg, J.C. Webber, and A.R. Whitney, Precision Geodesy Using the Mark-III Very Long Baseline Interferometry System, *IEEE Transactions on Geoscience and Remote Sensing, GE-23*, 438, 1985.

DeMets, C., R.G. Gordon, D.F. Argus, and S. Stein, Effect of recent revisions to the geomagnetic reversal time scale on estimates of current plate motions, *Geophys. Res. Lett.*, in press, 1994

Di Geronimo I., F. Ghisetti, F. Lentini, L. Vezzani, Lineamenti neotettonici della Sicilia orientale, *Mem. Soc. Geol. It.*, 19, 543-549, 1978

Finetti I. and A. Del Ben Geophysical study of the Tyrrhenian opening, *Boll. Geofis. Teor. Appl.*, 110, 75-156, 1986

Herring, T.A., Proceedings of the Symposium on Refraction of Transatmospheric Signals in Geodesy: Modelling Atmospheric Delays in the Analysis of Space Geodetic Data, *Publications on Geodesy, No. 36*, edited by De Munck, J.C. and T.A.Th.Spoelstra, Netherland Geodetic Commision, Delft, Netherlands, 1992.

IERS Annual Report 1992, Central Bureau of IERS, Paris Observatory, July 1993.

Ma, C., J.M. Sauber, L.J. Bell, T.A. Clark, D. Gordon, W.E. Himwich, and J.W. Ryan, Measurement of Horizontal motions in Alaska Using Very Long Baseline Interferometry, *J. Geophys. Res., 95*, 21,991-22,011, 1990.

McCarty, D.D., IERS Technical Note 3 - IERS Standards (1989), Central Bureau of IERS, Paris Observatory, November 1989.

Rogers, A.E.E., R.J. Cappallo, H.F. Hinteregger, J.I. Levine, E.F. Nesman, J.C. Webber, A.R. Whitney, T.A. Clark, C. Ma, J.R. Ryan, B.E. Corey, C.C. Counselman, T.A. Herring, I.I. Shapiro, C.A. Knight, D.B. Shaffer, N.R. Vandenberg, R. Lacasse, R. Mauzy, B. Rayhrer, B.R. Schupler, and J.C. Pigg, Very Long Baseline Radio Interferometry: The Mark III system for geodesy, astrometry, and aperture synthesis, *Science, 219*, 51-54, 1983.

International Radio Interferometric Surveying - South: Results of the first 100 sessions

Axel Nothnagel[1], Rüdiger Haas[1], Hermann Seeger[2]

[1]Geodetic Institute of the University of Bonn, Nussallee 17, D-53115 Bonn
E-mail: nothnagel@uni-bonn.de
[2]Institute for Applied Geodesy, Richard-Strauß-Allee 11, D-60598 Frankfurt

Abstract. In March 1996 the 100th session of the IRIS-S project (International Radio Interferometric Surveying - South) was observed by the VLBI observatories of Wettzell in Germany, Hartebeesthoek in South Africa, Westford in the USA and Fortaleza in Brazil. This series was initiated in 1986 when a Mark III Data Acquisition Terminal was made available temporarily to the Hartebeesthoek Radio Astronomy Observatory (HartRAO) in South Africa. In those days this undertaking made it possible for the first time to extend the high accuracy geodetic VLBI network into the southern hemisphere. Over the years the IRIS-S network has undergone a number of modifications but the basic triangle of Wettzell, HartRAO and Westford was maintained almost throughout. For a number of years now the series is organized and correlated by the VLBI group at the Geodetic Institute of the University of Bonn. In this paper we present baseline length and station displacement results achieved so far.

1. Introduction

In January 1986 the first few Mark III geodetic VLBI sessions with the Hartebeesthoek Radio Astronomy Observatory (HartRAO) were observed which mark the start of the IRIS-S (International Radio Interferometric Surveying - South) campaign. Due to the lack of other Mark III compatible observatories in the southern hemisphere the first sessions of the IRIS-S campaign were scheduled only with northern hemisphere stations like Wettzell Geodetic Fundamental Station (Bavarian Forest, Germany), Onsala Space Observatory (Gothenburg, Sweden), Westford Observatory (near Boston, MA, USA) and Richmond (Florida, USA) (Carter et al., 1988).

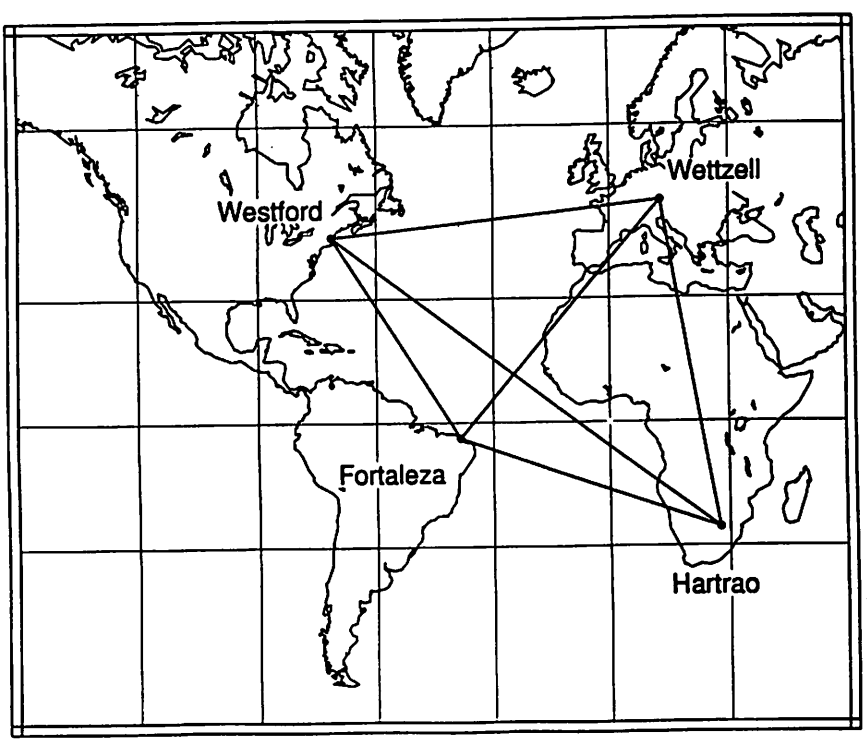

Fig. 1; Current IRIS-S network

Presented at the 11th Working Meeting on European VLBI for Geodesy and Astrometry, Onsala, Sweden, 1996

With more high accuracy geodetic VLBI observatories coming up elsewhere and in the southern hemisphere in particular the network configuration changed over the years about a basic triangle of stations consisting of HartRAO, Wettzell and Westford which missed only about 18 months of the series. By now the network is complemented by the station of Fortaleza in Brazil which adds a fourth station on a fourth continent (Fig. 1).

The first 6 IRIS-S sessions took place in January and February 1986 with follow up campaigns of similar time spans in 1987 and 1988. Since December 1989 IRIS-S sessions are scheduled and observed in monthly intervals. The tenth anniversary of the series coincided with the occurrence of the 100th session.

2. Data Analysis

The IRIS-S sessions are analyzed at the Geodetic Institute of the University of Bonn with the Calc/Solve/Globl software package developed at the NASA Goddard Space Flight Center in cooperation with a number of other institutions (Ryan et al., 1993). The least squares adjustments of VLBI sessions is divided into two groups of estimation strategies.

The first one is the combined processing of all IRIS-S sessions in one single least squares adjustment. The parametrization of this solution is set up estimating station coordinates at a reference epoch and time derivatives of the coordinate components (dx/dt, dy/dt, dz/dt) which reflect continuous station displacements mainly due to global tectonics. In this solution the Earth rotation parameters and nutation angle offsets relative to the IAU 1980 Nutation Model (Wahr, 1981) are estimated for each session.

In order to avoid singularities in the normal equation the Earth orientation parameters for the epoch April 2, 1988 and the coordinates of Wettzell are kept fixed. All other station coordinates may then be estimated. The time evolution of the terrestrial system is predefined by constraining a) the station of Wettzell to move according to the NUVEL-1A model (DeMets et al., 1994), b) the evolution of the Wettzell - Westford baseline according to the NUVEL-1A model and c) the height evolution of the Hartebeesthoek Radio Astronomy Observatory to be fixed to zero. The validity of these assumptions has been manifested with world-wide VLBI and SLR data.

The delay observables of a single VLBI session with typically 100 to 200 observations per baseline generally are not sufficient to reliably estimate all the parameters on which the observables depend. Although radio source positions and station coordinates can be estimated with the observations of a single session the resulting accuracy is still far away from the potential of a greater number of observations gathered with large observing networks over a longer time span. For this reason radio source positions are determined in a zero order least squares adjustment of all available Mark III geodetic VLBI fixed station dual frequency sessions since January 1984. These radio source positions are used for consecutive analyses of VLBI data subsets like e.g. the IRIS-S sessions.

In the second solution all sessions are adjusted separately estimating station coordinates for all stations except for one reference station at each epoch. From the station coordinates, series of baseline lengths can be infered which may be used for a detailed analysis of individual sessions. Earth rotation parameters are taken from the IERS Rapid Service Series which do not affect baseline length results because they are invariant to rotation of the terrestrial frame.

3. Baseline Length Results

From the site coordinates for each epoch, which were estimated in the second type of solution, individual baseline lengths were computed. Figures 2 to 7 depict the results of those baselines which are observed in the current network. Each graph contains a solid line representing the straight line fit of the observed lengths while a dashed line describes the evolution as predicted by the NUVEL-1A model. Since Fortaleza joint the network only in early 1993 the time series for baselines with Fortaleza are shorter than the others.

Looking at the Hartebeesthoek - Wettzell baseline (Fig. 2) it is immediately obvious that the repeatability of the results improved at the end of 1991 when cooled low-noise amplifiers were installed at HartRAO. From this time onwards only two sessions deviate extraordinarily from the general scatter. The reason is a significant loss of observations due to hardware problems.

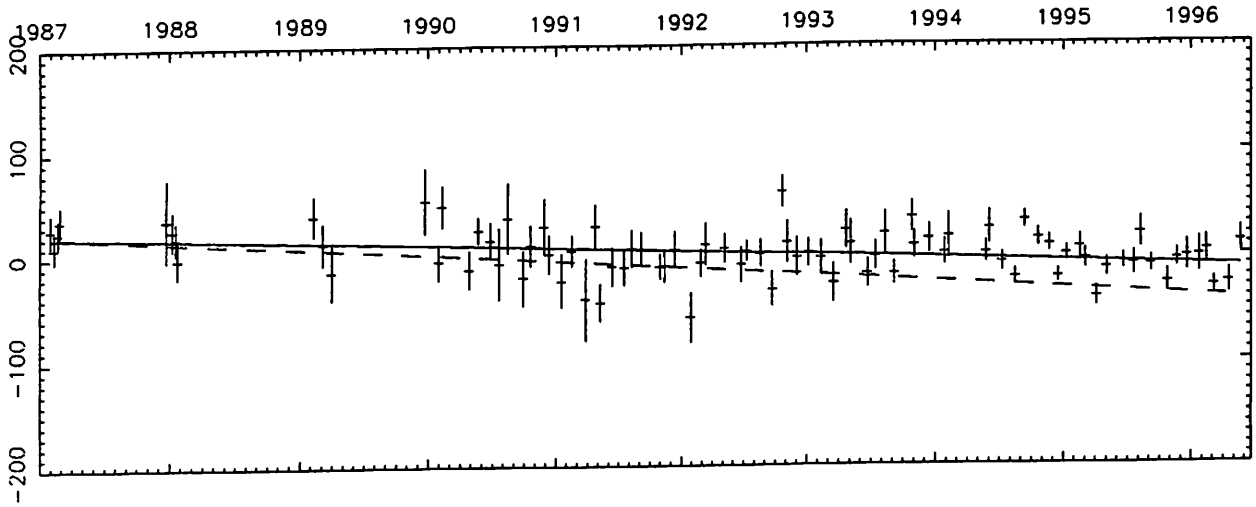

Fig. 2; Baseline Length: Wettzell - HartRAO, Observed rate -3.3 ± 0.9 mm/yr, WRMS = 18.2 mm
7832 km, NUVEL-1A model rate -6.4 mm/yr

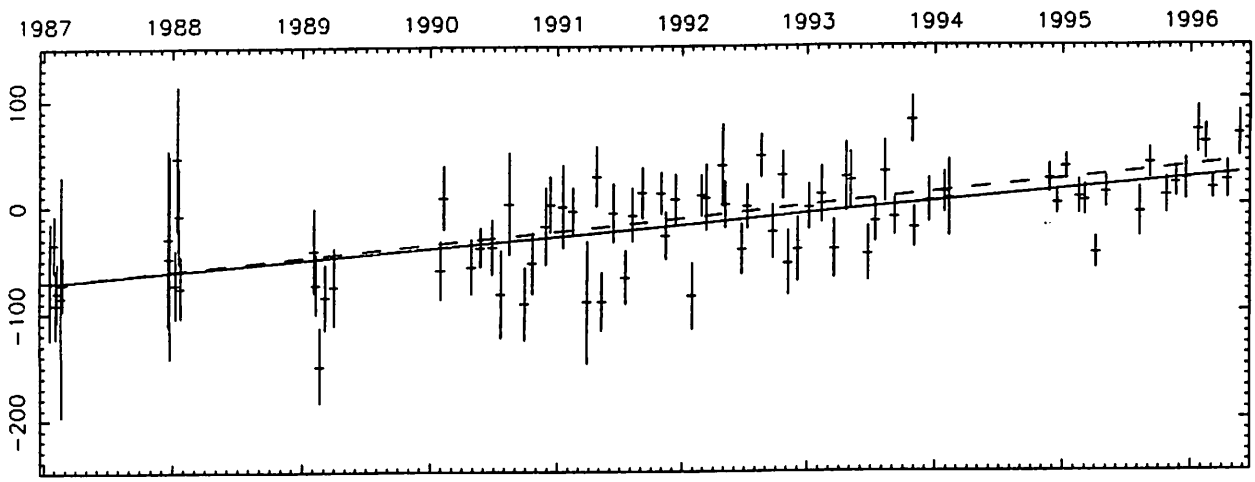

Fig. 3; Baseline Length: Westford - HartRAO, Observed rate 10.8 ± 1.3 mm/yr, WRMS = 28.6 mm
10658 km, NUVEL-1A model rate 11.6 mm/yr

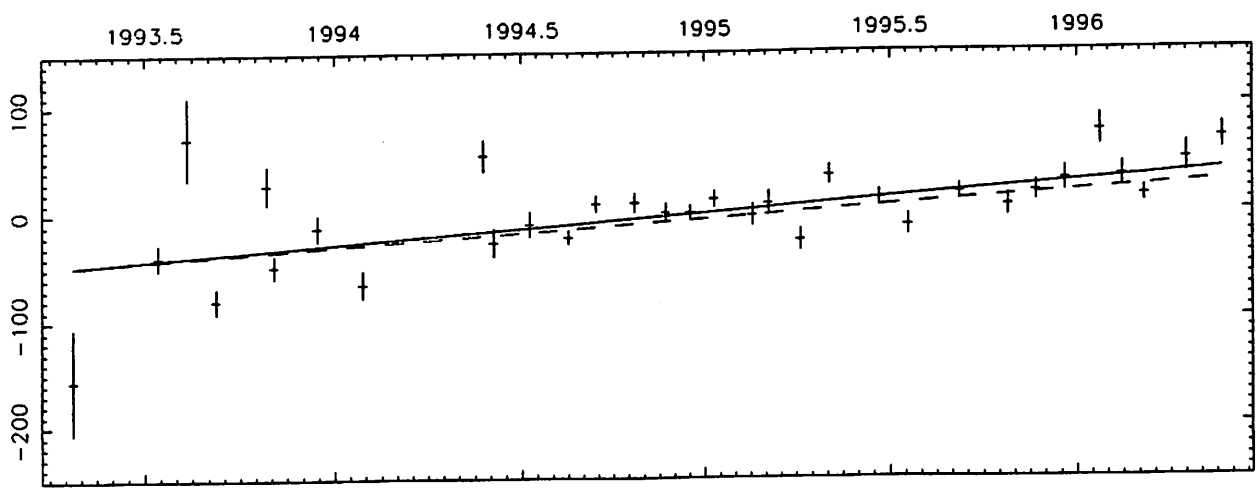

Fig. 4; Baseline Length: Fortaleza - HartRAO, Observed rate 27.9 ± 2.8 mm/yr, WRMS = 21.1 mm
7025 km, NUVEL-1A model rate 23.7 mm/yr

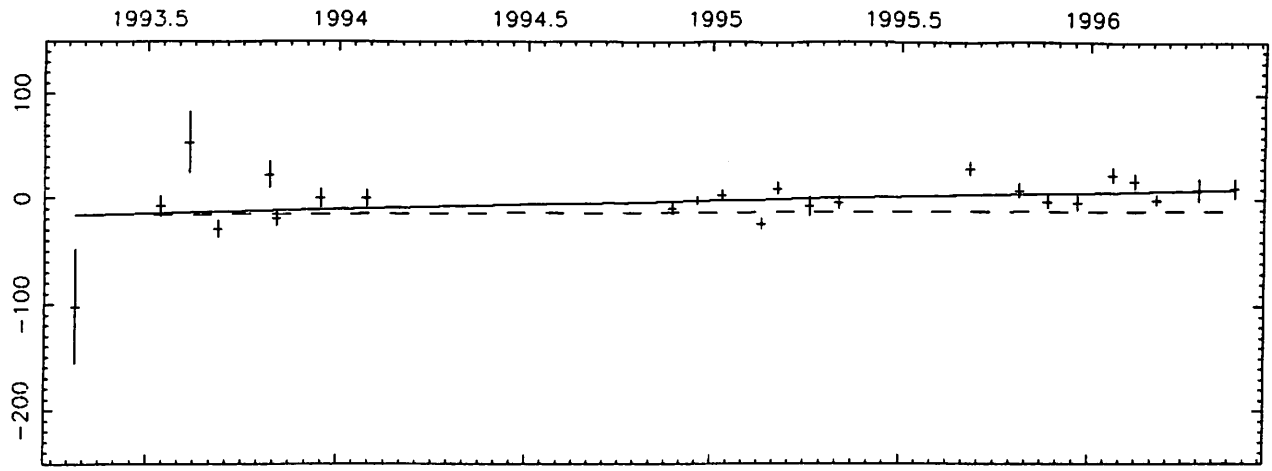

Fig. 5; Baseline Length: Fortaleza - Westford, Observed rate 8.3 ± 3.4 mm/yr, WRMS = 12.4 mm
5897 km, NUVEL-1A model rate 1.6 mm/yr

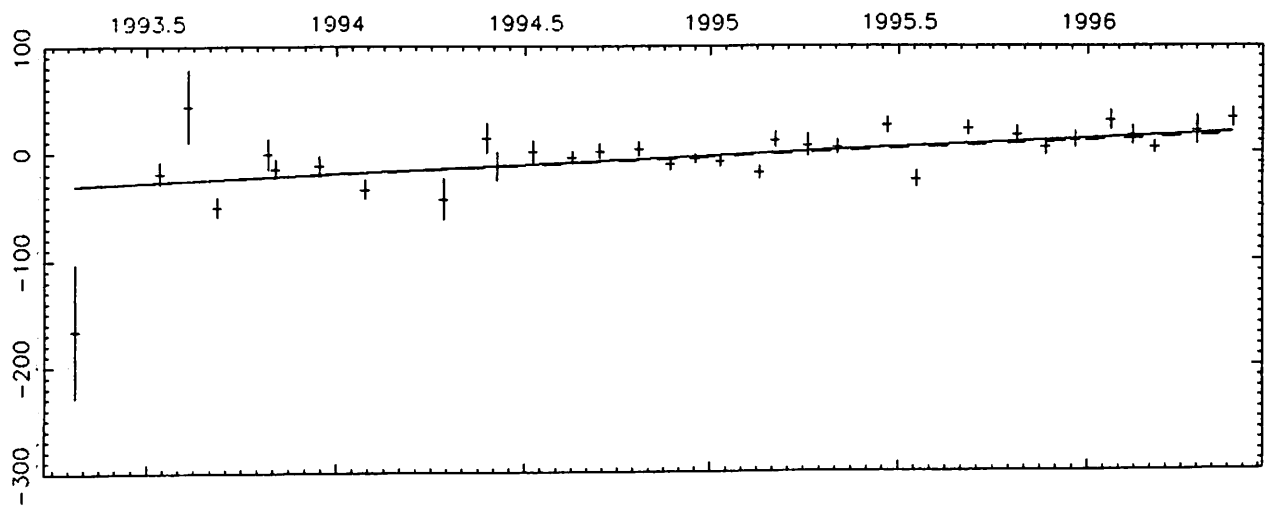

Fig. 6; Baseline Length: Fortaleza - Wettzell, Observed rate 16.0 ± 3.2 mm/yr, WRMS = 12.9 mm
7215 km, NUVEL-1A model rate 14.7 mm/yr

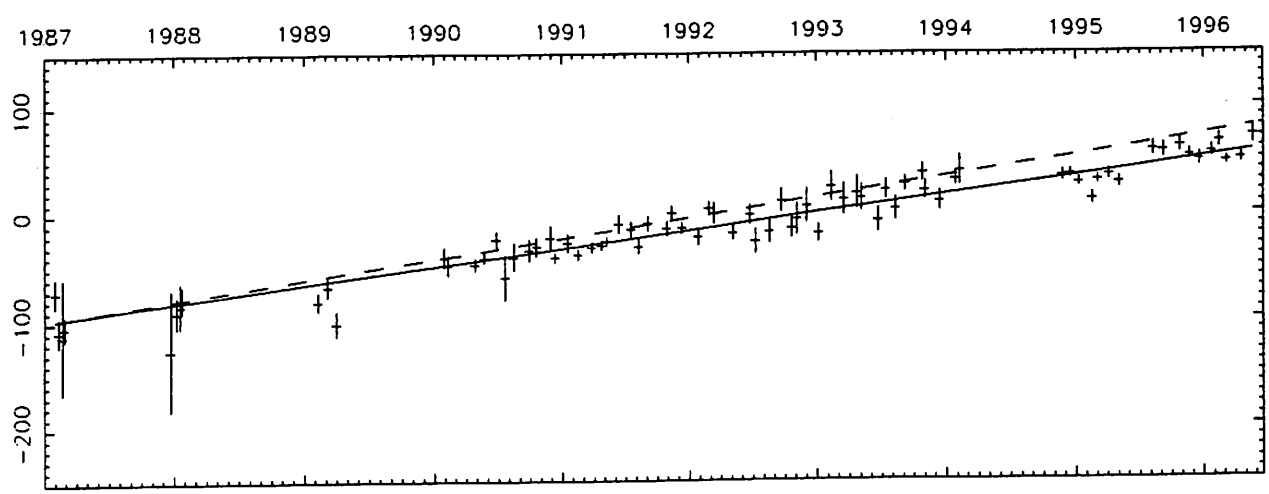

Fig. 7; Baseline Length: Wettzell - Westford, Observed rate 16.5 ± 0.5 mm/yr, WRMS = 10.2 mm
5998 km, NUVEL-1A model rate 18.2 mm/yr

On the baselines with Fortaleza (Fig. 4 - 6) the high level of scatter in the first months of its participation reduces considerably in the later part of the observing period. Again, this originates from technical problems at Fortaleza at the beginning of its operation.

The evolution of the baseline lengths agrees rather good with the NUVEL-1A model rates. Only the baselines HartRAO - Wettzell, HartRAO - Fortaleza and Fortaleza - Westford disagree by more than 2 mm/year. For the baselines with Fortaleza this discrepancy can easily be attributed to the short data span and some influence of the very first session which generally seems to produce too short baseline lengths with Fortaleza. The trend of the HartRAO - Wettzell baseline, however, appears to be sufficiently stable indicating a displacement which disagrees with the global plate tectonic model.

4. Displacement Vector Results

Table 1 lists the magnitude and the direction of the displacement vector for the two stations HartRAO and Fortaleza together with their model values and deviations from the model. Figure 8 depicts these results graphically. The tips of the annual displacement vectors are emphasised with their error ellipses while the NUVEL-1A model numbers are displayed as simple vectors.

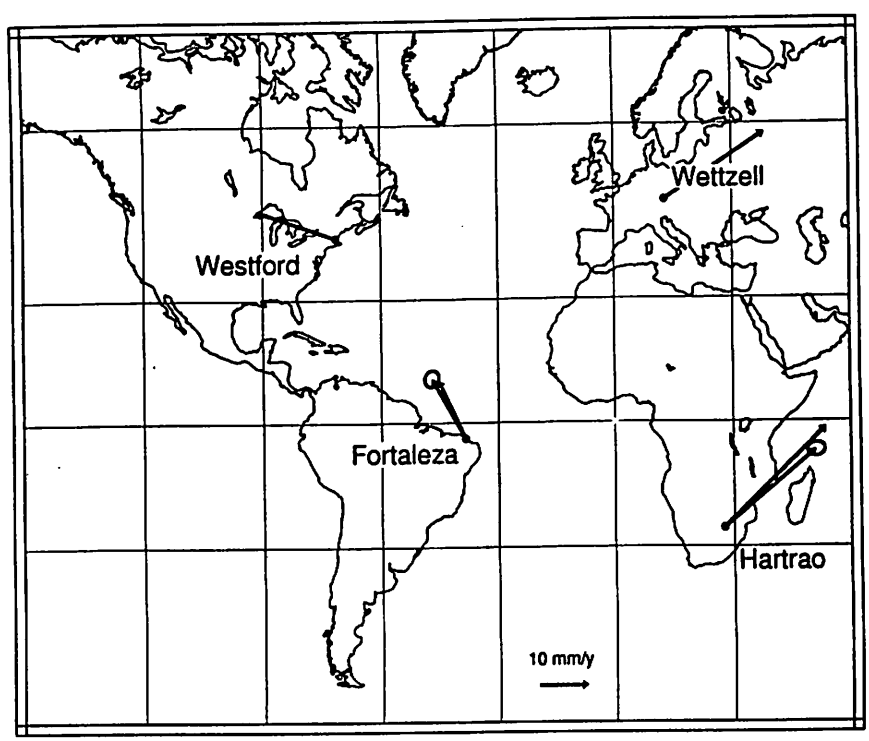

Fig. 8; Estimated annual displacement vectors with error ellipses together with their NUVEL-1A model velocities

The estimated displacement rate for Fortaleza agrees very well with the model. However, as was already to be expected from the baseline lengths the displacement vector of HartRAO significantly deviates from the model in a south-westerly direction. Since HartRAO is not considered to be located near a plate boundary or fracture zone this discrepancy has either to be attributed to a contemporary plate motion which is considerably different to what it was over geological time scales or it has its origin in local or regional deformations.

Table 1, Estimated Horizontal Velocities

Station		Direction		Magnitude	
HartRAO	estimated	50.2	± 1.5 deg	24.3	± 0.7 mm/yr
	NUVEL-1A	44.2		28.9	
	Deviation	203.8	± 8.1 deg	5.0	± 0.6 mm/yr
Fortaleza	estimated	330.2	± 2.6 deg	13.9	± 0.7 mm/yr
	NUVEL-1A	334.8		12.9	
	Deviation	283.8	± 27.2 deg	1.4	± 0.6 mm/yr

5. Conclusions

The IRIS-S network is now well established. With stations in both hemispheres and long baselines in east-west as well as in north-south direction it provides a favorable geometry for the determination of reliable and consistent station coordinates and displacement vectors. The kinematics of the two observing stations in the southern hemiphere, HartRAO and Fortaleza, can now be studied with a high level of confidence. The discrepancy of the HartRAO displacement rate vector from the NUVEL-1A model has still to be investigated. Local or regional deformations may be the most probable cause for this.

Acknowledgements

The authors are greatful to William E. Carter and the staff at NOAA's Geodetic Research Lab who made the data aquisition terminal available over all these years. We thank all individuals and institutions at Fortaleza, HartRAO, Westford and Wettzell who participated in IRIS-S too numerous to name them personally for their indespensable efforts to ensure successful observations. The correlation of the data was mostly done by Arno Mueskens and his students at the correlator of the Max-Planck-Institute for Radio Astronomy (MPIfR) jointly operated by MPIfR and the Geodetic Institute of the University of Bonn. For the last two years the tape shipments to the observatories have been financed by the Institute for Applied Geodesy (IfAG), Frankfurt.

References

Carter, W.E., D.S. Robertson, A. Nothnagel, G.D. Nicolson, H. Schuh, J. Campbell; IRIS-S: Extending Geodetic VLBI Observations to the Southern Hemisphere; Journal of Geophysical Research, Vol. 93, No. B12 p. 14947 - 14953; 1988

DeMets C., R.G. Gordon, D.F. Argus, S. Stein; Effect of Recent Revisions to the Geomagnetic Reversal Time Scale on Estimates of Current Plate Motions; GRL, Vol. 21, No. 20 p. 2191-2194; 1994

Ma, C., J. Sauber, L. Bell, T. Clark, D. Gordon, W. Himwich, J. Ryan; Measurement of horizontal motions in Alaska using VLBI; JGR Vol. 95, p. 21991-22011, 1990

Ryan, J.W.,C. Ma, D.S. Caprette; NASA Space Geodesy Program - GSFC Data Analysis - 1992, Final Report of the Crustal Dynamics Project VLBI Geodetic Results 1979-91; NASA Technical Memorandum 104572, Greenbelt, 1993

Wahr, J.M.; The Forced Nutations of an Elliptical, Rotating, Elastic and Oceanless Earth; Geophys. Journ. of Royal Astron. Society, Vol. 64, p. 705, 1981

Wessel, P., W.H.F. Smith; Free Software Helps Map and Display Data; EOS Trans. Amer. Geophys. U., Vol. 72, pp. 441, 445-446, 1991

The Geodetic VLBI Observations at CRIMEA Station and Some Results of the Analysis

A. Bajkova, A. Finkelstein, A. Ipatov, D. Ivanov,
V. Mardyshkin, T. Pyatunina

Institute of Applied Astronomy RAS
St. Petersburg, Russia

In June 1993 representatives of Institute of Applied Astronomy RAS (IAA), Crimean Astrophysical Observatory (CRAO), Goddard Space Flight Center NASA (GSFC) and Institute of Space Research RAS (IKI) devel-

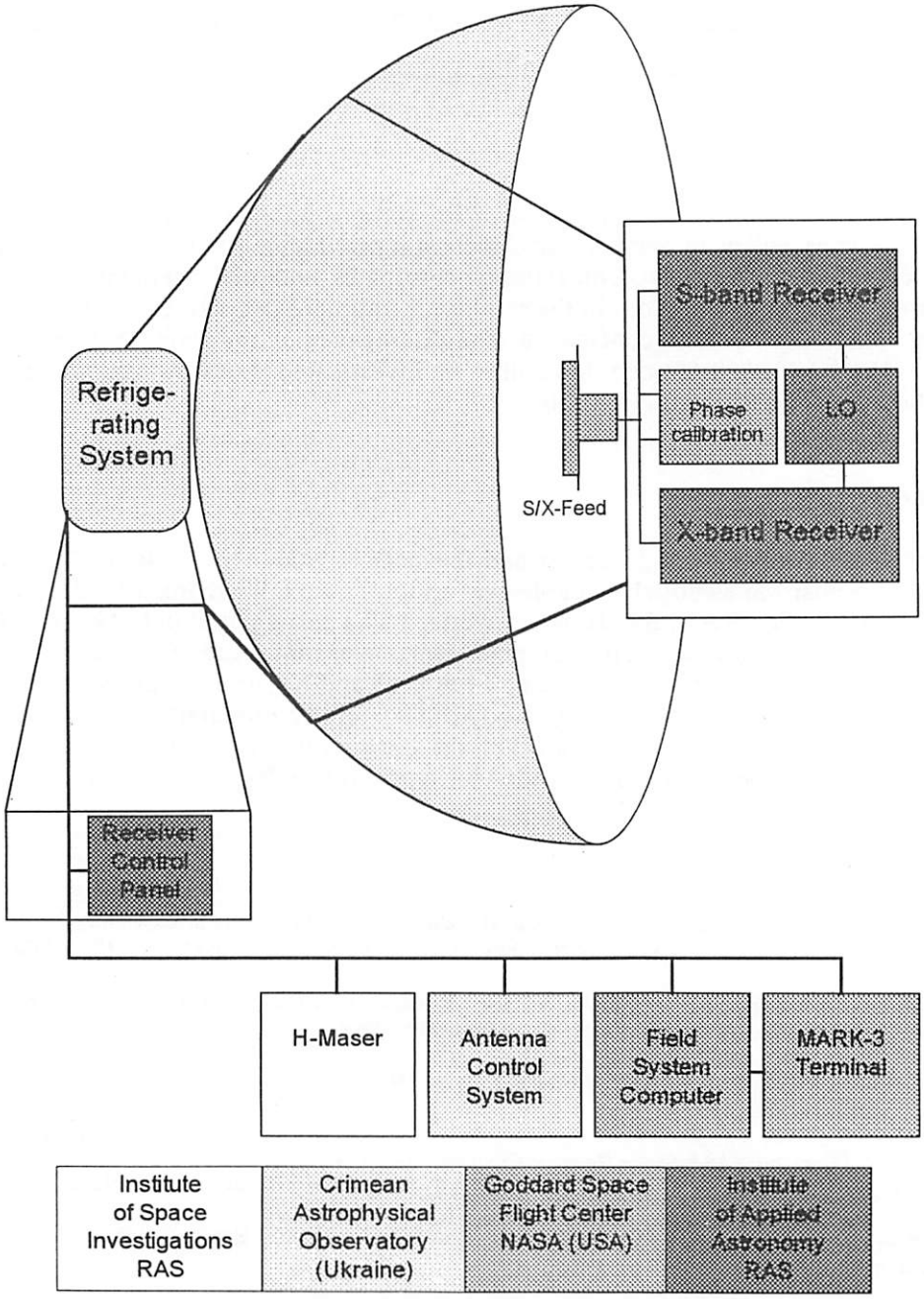

Fig. 1. International cooperation by the construction of VLBI geodynamic Station "Simeiz"

Presented at the 11th Working Meeting on European VLBI for Geodesy and Astrometry, Onsala, Sweden, 1996

oped a plan of the construction of VLBI geodynamic station on the base of 22-meter dish of CRAO (Fig. 1) [1].

It was very instructive experience of international cooperation and it gave new pulses for development of VLBI geodetic investigations in IAA.

We began to work as a team – CRAO supplied the radiotelescope, IAA – microwave hardware, GSFC – MK-III terminal and control computer, IKI – H-maser. CRAO and IAA supplied observational sessions with operators.

The 22-meter radioteloscope is situated on the bank of Blue Gulf of Black Sea in South part of Crimea peninsula. It was constructed in 1966 and participated in the first VLBI observations in 1969 in cooperation with the USA. The radiotelescope has azimuthal mounting and can operate from 1 to 40 GHz (S/X combined horn into primary focus of the dish is installed). It is equipped with MK-III terminal, H-maser and GPS-receiver for time synchronization.

In June 1994 the efforts of our international team were crowned with success – during two test sessions VLBI response were received and the system equivalent flux density (SEFD) of radiotelescope that was quite satisfactory was investigated. The noise temperature or the system is presented in Fig. 2. In the Table 1 the antenna parameters of VLBI stations are given for comparison.

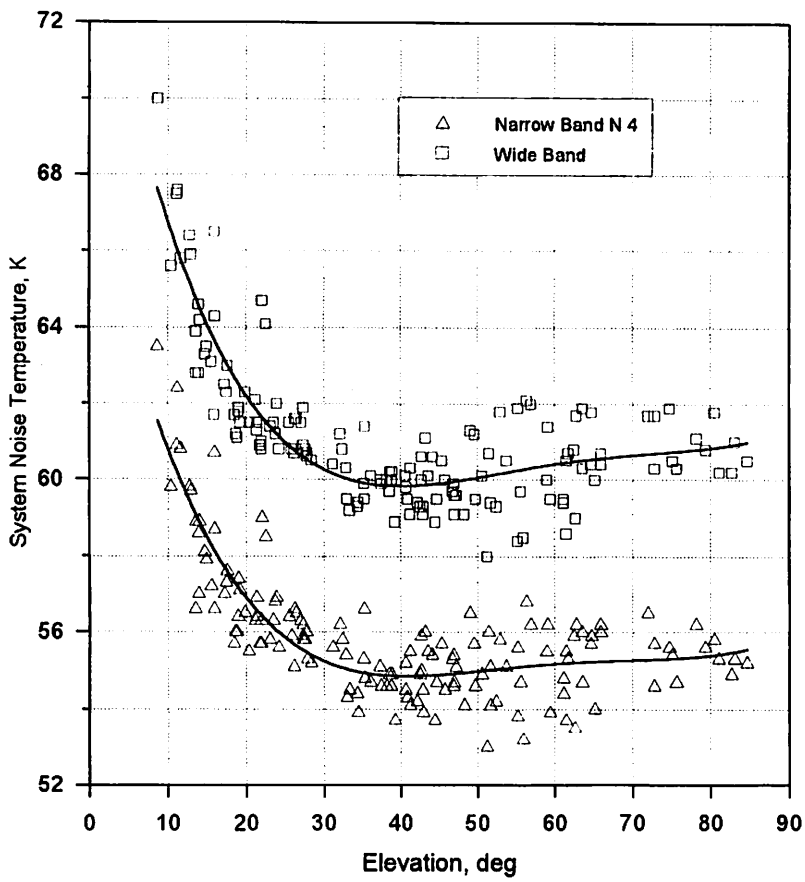

Fig. 2. System noise temperature against elevation. Simeiz, X-band

Table 1. Antenna parameters of VLBI stations

		SEFD Jy	Eff. %	T_{sys} K	T_{rcv} K	T_{sky} K	T_{feed} K	Tso K	D_a m
VLBA	S	350	70	35	9	7	14	5	25
VLBA	X	400	66	39	18	10	5	6	25
Hat Creek	S	525	50	50	8	7	30	5	26
Hat Creek	X	460	51	45	25	10	5	5	26
Fairbanks	S	800	42	65	8	7	30	20	26
Fairbanks	X	750	42	60	25	10	5	20	26
Simeiz	S	1100	51	78	25	7	26	20	22
Simeiz	X	780	56	61	30	10	6	15	22
"Quasar"	S	200	70	41	13	7	16	5	32
"Quasar"	X	250	70	50	15	10	20	5	32

Already in 29 June 1994 we participated in EUROPE-3 geodynamic program as a associated member of EVN.

From this moment VLBI Simeiz station is operating regularly as a member of various VLBI networks.

The main scientific objectives of these programs are traditional and include:

- monitoring of celestial and terrestrial reference systems;
- monitoring of the Earth rotation parameters and global tectonics;
- mapping of radio sources.

To the present time Simeiz station has participated in more than 30 observational sessions (Table 2) in cooperation with 20 radio telescopes. 76 radio sources have been observed and more that 30.000 group time-delays have been obtained.

All the observation data were processed in IAA using IAA software package VORIN for secondary analysis of astrometric and geodetic VLBI observations [2], CALTECH VLBI PROGRAMS and IMAGE package of IAA [3] for source mapping.

VORIN is the package developed by Dr. L. Petrov (IAA) is intended for analysis of astrometric and geodetic VLBI observations.

15 experiments from 16 were processed to 01-AUG-1996. Tapes were correlated in Haystack and Bonn. Databases with measured group time delays and delay rates were acquired using INTERNET. Further analysis was carried out at the IAA by Dr. L. Petrov [2].

Since CRIMEA station participated in various programs there are no baselines with long observational history. To produce sufficiently long series of the station positions we used the following approach: we separated a list of station participated in VLBI experiments together with CRIMEA in two sets. The first set contains the fiducial stations with long observational history whose positions and velocity were fixed to the values from the catalogue GLB979: DSS15, GILCREEK, WETTZELL, DSS65, NOTO, ON-

Table 2. International VLBI experiments with "Simeiz" station, 1994–1996

Date	Session	Base Network	Duration, hours	Number of stations	Subject
25.06.94	CRIMEA-1		24	5	geo
28.06.94	CRIMEA-2		24	3	geo
29.06.94	EUROPE-3	EVN	24	6	geo
25.08.94	POLAR-N1	NASA	24	8	geo
29.08.94	NAVEX-43	NASA	24	12	geo
31.08.94	EUROPE-4	EVN	24	7	geo
12.09.94	C-ASIA1	APT	24	6	geo
24.10.94	NAVEX-44	NASA	24	12	geo
26.10.94	EUROPE-5	EVN	24	9	geo
07.11.94	C-ASIA2	APT	24	6	geo
07.12.94	EUROPE-6	EVN	24	8	geo
19.12.94	NAVEX-45	NASA	24	12	geo
23.01.95	GLOBAL TRF-1	NASA	24	10	geo
01.02.95	EUROPE-1	EVN	24	8	geo
09.02.95	C95X1 "CAL"	EVN	1	5	astro
09.02.95	EA6A "NEARBY STARS"	EVN	12	5	astro
10.02.95	EA6B "NEARBY STARS"	EVN	13	5	astro
12.02.95	ER1 "1308+328"	EVN	13	5	astro
13.02.95	C95X1 "CAL"	EVN	1	5	astro
06.03.95	GLOBAL TRF-2	NASA	24	10	geo
12.04.95	EUROPE-2	EVN	24	9	geo
13.04.95	CASIA-1	APT	24	6	geo
24.04.95	XASIA-1	APT	24	8	geo
08.06.95	EUROPE-3	EVN	24	9	geo
31.08.95	EUROPE-4	EVN	24	6	geo
09.11.95	EUROPE-5	EVN	24	7	geo
13.03.96	TRANS ASIA-1	APT	24	5	geo
23.04.96	GLOBAL TRF-10	NASA	24	10	geo
25.04.96	EUROPE-2	EVN	24	5	geo

SALA60, EFLSBERG, MEDICINA, FORTLEZA, PIETOWN, SC-VLBA, KASHIM34, KOKEE, HARTRAO, KASHIMA, MATERA, WESTFORD. The second set contains the stations with short observational history and their positions were estimated: CRIMEA, NRAO85~3, NYALES20, SANTIA12, SESHAN25, URUMQI, YEBES.

Earth orientation parameters, coordinates of some sources, troposphere path delay in zenith and clock functions for each station modelled by linear splines with one-hour segments were also estimated by Dr. L. Petrov [2].

Fig. 3 shows evolution of the station position, vertical performance of the CRIMEA position appeared to be poor while the horizontal performance is reasonably good. It is not clear now what is the reason of apparent "jumps" in vertical direction. It is known that the performance of H-maser were worsening. Frequent power breaks were making a clock to go out of

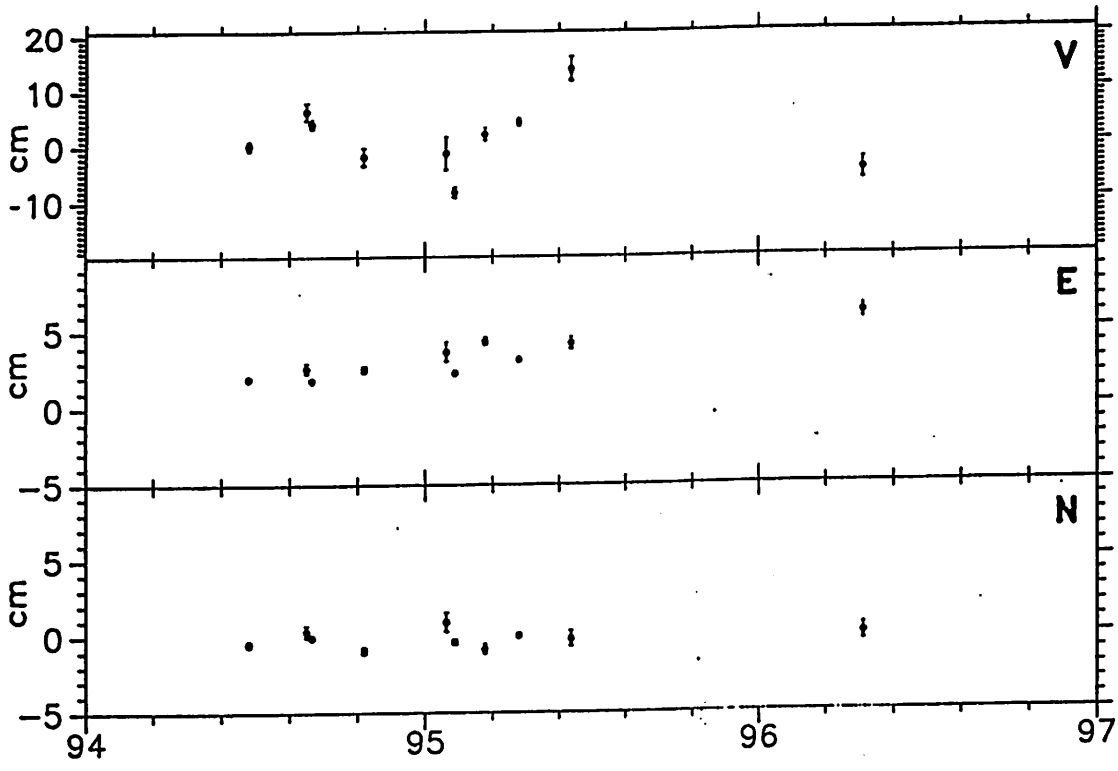

Fig. 3. Evolution of the Crimea station position

normal mode of work. Another source of error in measurements of vertical position maybe stipulated particularity of local topography. The station located in 50 meters of seashore. Plato of Crimean mountains breaks on the height 1000 meters in 5–10 km in north from the station. Rays go through the wet sea air in south direction and under dry steppe air in north direction. The contrast of meteorological conditions is especially strong at spring and autumn. Used troposphere model may be inadequate for this case.

The position of the station to the epoch of the first observation and values of the velocity were found by Dr. L. Petrov from these data using linear fit. The Table 3 contains the results of linear fitting and weighted standard deviations form the line.

Table 3

Comp	Position, (mm)	Velocity, (mm/yr)	Deviation, (mm)
V	10±24	−13±36	48.7
E	17.7±2.0	17.9±3.1	4.1
N	−4.6±1.5	2.3±2.5	3.0

Model NNR-NUVEL1A predicts east and north velocity 23.9 mm/yr and 9.1 m/yr respectively. We should notice that obtained estimates of horizontal velocity are rather formal. It is too few session to judge whether the disagreement between obtained estimates and NNR-NUVEL1A is real.

It is well known that the structure of a source brings into the group time delay an appreciable contribution that should be taken into account for precise reduction. This requires imaging of sources. Nevertheless poor UV-coverages achieved in VLBI geodetic observations (Fig. 4) the mapping is of great interest for investigation source structure dynamics both for astrometric and astrophysics problems. At present IAA Imaging group (Pyatunina and Bajkova) is doing catalogue of compact extragalactic radio sources using VLBI geodetic data at 8.2 GHz. First results are to be appear soon in [4].

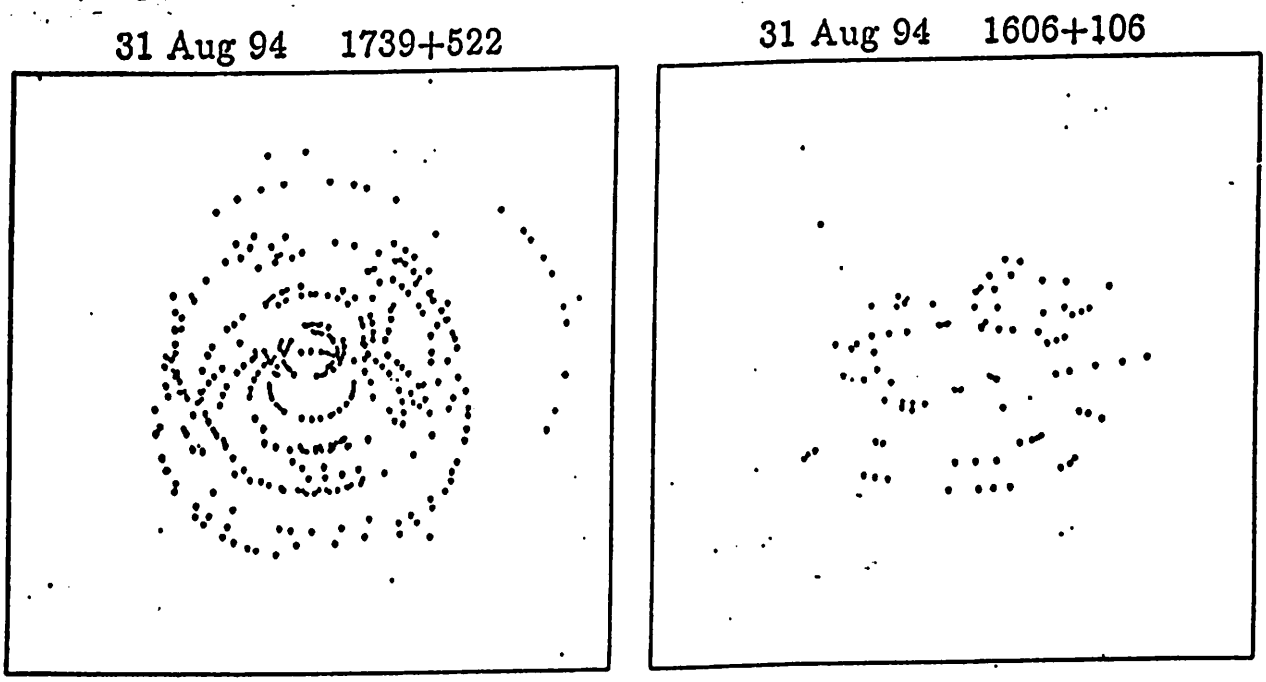

Fig. 4. UV-plane coverage for the geodetic VLBI

As a basic software for mapping the well known CALTECH VLBI PROGRAMS are used. But in IAA independent IMAGE program package was elaborated by Bajkova for VLBI modeling and investigation of new effective image reconstruction procedures. Nowadays IMAGE program package contains besides CLEAN algorithm new reconstruction procedures based on generalized information methods and phaseless procedures as well. The IMAGE package is adapted to work in combination with CALTECH VLBI PROGRAMS. So it is possible to use different reconstruction procedures of the IMAGE package in the cycle of hybrid mapping or selfcalibration of the CALTECH package. It allowed to be sure in reliability of the maps obtained.

Radio maps of the first sample of 39 sources (see Table 4) are made using geodetic VLBI observations in the framework of some programs with Crimea station participation and basically of NEOS program. These maps are obtained with high angular resolution of 0.6–0.8 mas, what allowed to

Table 4. Sources list

Source	Alias	Ident.	z	m_v	S_6, Jy	$S_{3.5}$, Jy
0014+813	S5 0014+81	QSO	3.384	16.5	0.551	1.355
0016+731	S5 0016+73	QSO	1.781	18.0	1.7	1.9
0059+581	–	–	–	–	–	2.8
0133+476	S4 0133+47, DA 55	QSO	0.859	19.0	3.3	2.9
0202+149	4C+15.05, NRAO 91	QSO	–	21.9	2.4	3.1
0229+131	4C+13.14	QSO	2.067	17.03	1.0	1.9
0336–019	CTA 26	QSO	0.852	18.41	2.5	2.8
0400+258	–	QSO	2.109	18.0	1.8	1.4
0402–362	–	QSO	1.417	17.17	1.4	–
0440+345	–	–	–	–	–	–
0454–234	–	QSO	1.003	16.6	2.0	1.9
0458–020	4C–02.19	QSO	2.286	19.5	1.9	3.1
0528+134	–	QSO	2.07	20.3	3.9	4.5
0552+598	DA 193	QSO	2.365	18	5.4	5.7
0615+820	–	QSO	0.71	17.5	0.999	0.9
0642+214	3C 166, 4C+21.21	G	0.245	19.5	1.1	–
0716+714	–	LAC	–	15.5	1.121	0.6
0735+178	OI 158	LAC	0.424	16.22	1.8	1.9
0804+499	OJ 508, S4 0804+49	QSO	1.43	17.5	2.1	0.9
0917+624	OK 630	QSO	1.446	19.5	0.996	1.5
0955+476	OK 492	QSO	1.873	18	0.739	0.7
1014+615	–	BSO	–	18.1	0.631	0.571
1101+384	Mkn 421	G	0.031	13.1	0.725	0.7
1128+385	OM 346.9	QSO	1.733	16	0.771	0.9
1219+285	W Com, ON 231	LAC	0.102	16.11	2.0	0.7
1308+326	AU CVn	LAC	0.996	19.0	1.5	3.7
1357+769	–	QSO	–	19.0	0.844	0.6
1606+106	4C+10.45	QSO	1.226	18.5	1.4	1.6
1637+574	OS 562	QSO	0.751	17	1.4	1.7
1638+398	NRAO 512	QSO	1.666	16.5	1.16	1.5
1739+522	4C+51.37, OT 566	QSO	1.375	18.5	2.0	1.2
1741–038	–	QSO	1.057	18.6	3.0	3.0
1745+624	4C+62.29	QSO	3.886	18.7	0.580	0.480
1803+784	–	LAC	0.684	16.4	2.6	2.4
1823+568	4C+56.27	LAC	0.664	18.4	1.7	2.1
2145+067	4C+06.69	QSO	0.990	16.47	4.5	8.6
2200+420	BL Lac	LAC	0.068	14.72	4.8	5.9
2201+315	4C+31.63	QSO	0.297	15.79	2.3	2.5
2230+114	CTA 102, 4C+11.69	QSO	1.037	17.66	3.6	3.6

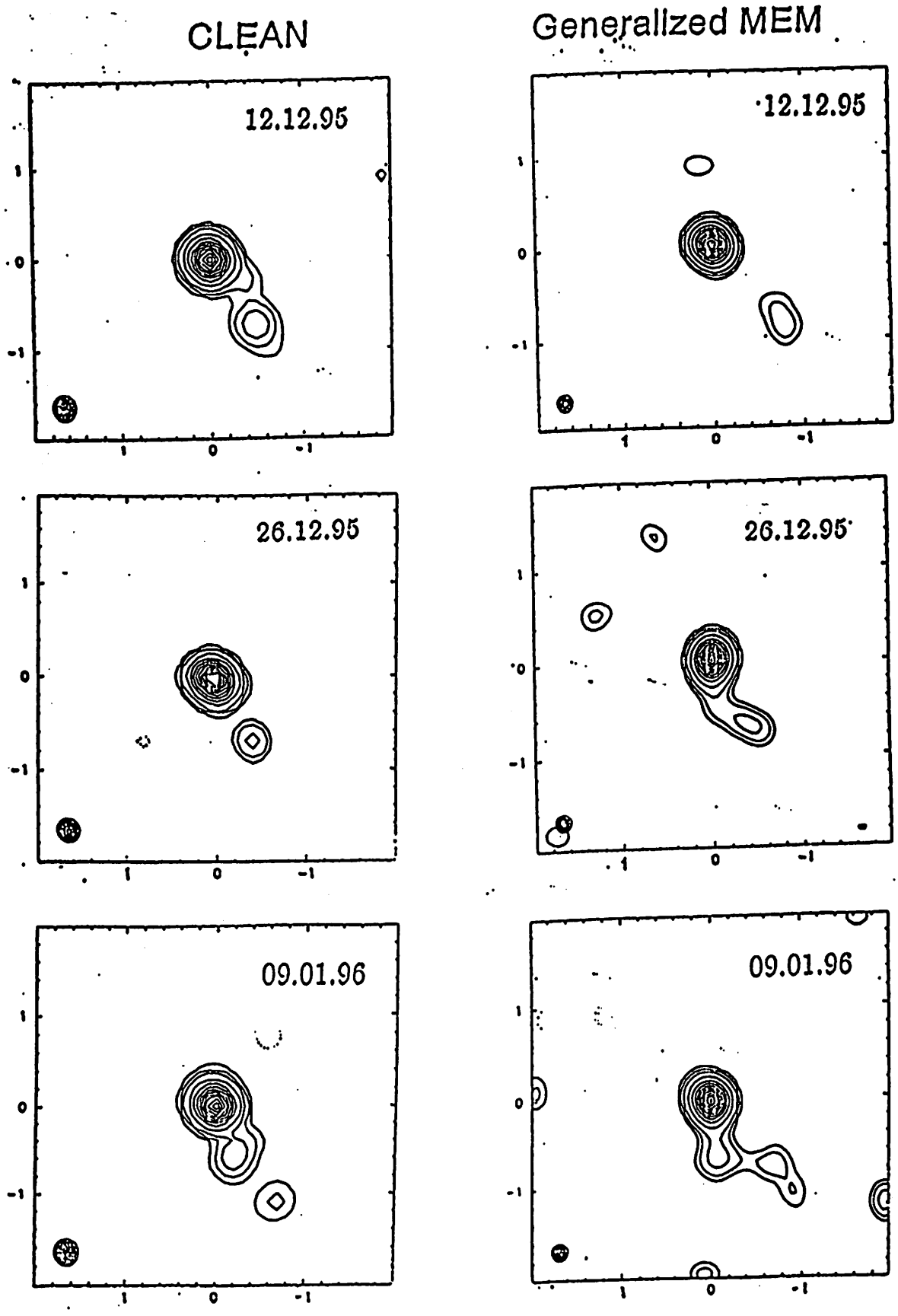

Fig. 5. Radio Source 0059+581

reveal new structure details on the scale less than 1 mas in more than a half of the sample. Short time structure variability of the sources (for example, 0059+581, 0202+149, 1308+326) was detected as well. Most interesting preliminary results are obtained concerning the source 0059+581. The source reveals some details moving with apparent velocity of about 0.7 mas/year. There is no optical identification of this source and we do not know its redshift value. But even if we suppose z–0.1 the apparent velocity of the components are superluminar v/c=3, that means that physical velocity is ultrarelativistic. These results require further investigation and now long series of data are under processing. Some of preliminary results obtained using both CALTECH VLBI PROGRAMS and IMAGE program package are shown in Fig. 5.

References:

[1]. A. V. Stepanov, L. I. Matveenko, A. V. Ipatov. VLBI Station "Simeiz". Proc 2nd EVN/JIVE Symposium, Torun, October 21. 1994. p. 117.

[2]. L. Petrov. This issue.

[3]. Bajkova A. T. Scientific software package "IMAGE" for image reconstruction in radio interferometry (Users manual). Messages of IAA AS USSR, N22, 1990. (in Russian).

[4]. Bajkova A. T., Pyatunina T. B., Finkelstein A. M. Radio Maps of 39 compact extragalactic radio sources on geodynamic VLBI data. – Transactions of the IAA RAS. "Astrometry and Geodynamics", issue 1, 1996. – in press. (in Russian).

A NEW MAPPING METHOD FOR ASTROMETRY OF CLOSE SOURCE PAIRS

Richard W. Porcas [1] and María J. Rioja[2]
[1]*Max-Planck-Institut für Radioastronomie, Bonn, Germany*
[2]*Joint Institute for VLBI in Europe, Dwingeloo, The Netherlands*

Abstract: We review the analysis of VLBI visibility phase in astrometric and astronomical studies, and describe new VLBA observations of the close source pair 1038+52A,B. Unlike observations at previous epochs, the analysis of the new data has been performed with the AIPS software package. The astrometric estimates have been obtained using the phase-reference mapping technique, and also using a new method, "hybrid double mapping", in which a composite visibility function is formed and mapped.

1 Introduction

The geodetic VLBI community regularly uses its growing data base of global observations to solve for both geodetic and geophysical parameters and for astrometric coordinates of radio sources. In general, uncertainties in the model of the propagation medium, geometric and instrumental delays preclude the direct use of the visibility phase; the less accurate frequency derivative of phase, the group delay, is used for this purpose instead. However, the phase difference between a pair of sources which are close together on the sky and observed simultaneously may be used for relative astrometry, since the model errors are almost the same for both sources.

The quasar pair 1038+52A,B (Owen, Porcas and Neff, 1978) consists of two flat-spectrum radio sources, with redshifts 0.678 and 2.296 (Owen, Wills and Wills, 1980), separated on the sky by only 33 arcsec. Because of their close angular proximity, errors in the model delay are "diluted" by a factor of $\sim$ 6000 in the phase difference, and this pair thus provides a unique opportunity to measure the separation between two objects at different cosmological distances, using the precision provided by VLBI relative phase measurements (Marcaide and Shapiro, 1983). Simultaneous observations at 2.3 and 8.4 GHz have permitted a relatively unambiguous registration of maps at different frequencies (Marcaide and Shapiro, 1984) and observations at three different epochs spanning 9 years have allowed an investigation of the stability of the separation, and of temporal changes within both source structures (Marcaide, Elosegui and Shapiro,1994; Rioja, 1993; Rioja et al, 1996.)

We first review the general ideas behind the use of VLBI visibility phase for astrometric and astronomical analysis. Then we describe results from new observations of 1038+52A,B made with the VLBA, and two different analysis methods used for measuring the astrometric separation.

2 Residual and Model Phase

When VLBI data is correlated, a model must be used to compute the wavefront pathlength difference for each telescope pair, ij, for each time t, to compensate for the delay between the signals.

Presented at the 11th Working Meeting on European VLBI for Geodesy and Astrometry, Onsala, Sweden, 1996

The visibility function, V, has a phase which reflects the difference between the actual and model delays, and in some cases is corrected after correlation if a better model is available. The resulting residual phase can only be measured modulo 360 degrees. When expressed in delay units, this is sometimes referred to as the residual "phase delay".

The residual phase, R(ij), for a baseline i-j is expressed here as the sum of three terms of interest :

```
R(ij) =     E(ij)      +      X(ij)       +       S(ij)

          MODEL ERRORS     POSITION OFFSET     SOURCE STRUCTURE
```

where E is the phase contribution from model errors in the interferometer geometry, stations clocks, propagation medium, etc

X is the contribution from the offset of the assumed source position from the true position of a reference feature in the source structure

S is the contribution of source structure terms, evaluated with respect to the reference feature.

Note that the assignment of contributions between X and S depends on the (arbitrary) choice of a reference position for the source.

3 Astrometric Phase

For a close pair of sources, a and b, which are strong, and which are observed simultaneously, the DIFFERENCED RESIDUAL PHASE can be formed :

```
R(b)-R(a)     =   E(b)-E(a)   +   X(b)-X(a)   +  S(b)-S(a)
```

For a sufficiently close source pair and a good model, the differenced model error cancels to zero. For true "point" sources (e.g. pulsars) both source structure terms may also be set to zero, and the differenced residual phase may be modelled directly for the "residual separation". If this is larger than the lobe-spacing on the longest baselines, then it is also necessary to determine the additional number of full turns to be added to each differenced residual phase before fitting. For realistic situations involving extragalactic sources, however, one may expect significant structure terms on long baselines. Strong sources can have only limited compactness because the inverse-Compton process limits the maximum possible brightness for synchrotron sources (Kellermann and Pauliny-Toth, 1969), and many are known to have an asymmetric "core-jet" morphology. Although the source structure contributions have only a small effect on the interferometer group delay analysed by geodesists (e.g. Gontier et al, 1993), they may form a very significant contribution to the phase. Therefore it is necessary to map the radio source structures, in order to determine their contributions to the observed interferometer phases, and to define reference features within the structures to which the astrometric measurements refer.

4 Astronomical Phase

For many VLBI investigations the astronomical interest lies in the fine-scale structure of the radio emission, and not in its absolute position on the sky. The HYBRID MAPPING technique (e.g. Cornwell and Wilkinson, 1983) is generally used in this situtation. This makes use of two properties:

- for an n-antenna array, the model error and positional offset terms in the residual phases, R(ij), for the set of n*(n-1) baselines ij, ik, jk... can be reduced to a set of only (n-1) antenna error phases, T(i), with respect to a reference antenna, since they arise from path-length differences between each antenna pair

$$R(ij) = T(i) - T(j) + S(ij)$$

- the visibility function, V(ij), for each baseline and at each time, is a sample, V(u,v), of the Fourier transform of the source brightness distribution, after its phase has been corrected for model error terms:

$$V(ij) = A(ij) \exp iR(ij)$$

$$= \underbrace{[A \exp iS](u,v)}_{\text{F.T. ==> map}} * \exp i(E(ij)+X(ij))$$

The antenna error phases are first estimated from this equation using an initial model visibility function derived from a trial map (often a point source). This step is referred to as phase "self-calibration". (Note that the position offset terms, X(ij), are entirely absorbed as antenna error phases if the reference feature is at the origin of the map.) The corrected, measured visibility function is then transformed to form a new source map, and this procedure is iterated until the quality of the map and the fit to the antenna error phases indicate that the antenna and source structure phase terms have been well separated. It is fundamental to this process that the signal-to-noise ratio of the V(ij) is > 1.

5 New Observations of 1038+52A,B

Here we describe results from a new VLBI observation of 1038+52A,B. This fourth epoch measurement was made with the VLBA in November 1995. The pair was tracked for a total of 13 hours, alternating every 13 minutes between observations in dual 2.3/8.4 GHz mode and observations at 15 GHz. The 100m telescope at Effelsberg was also included in the array for the 2.3/8.4 GHz scans. VLBA record terminals were used at all sites, recording a total of 64 MHz bandwidth for each scan, using 1-bit sampling. For the dual 2.3/8.4 GHz scans, 4 channels each 8 MHz wide were recorded for each band; at 15 GHz 8 channels of 8 MHz were recorded. The data was correlated at the VLBA correlator in Socorro, NM. Both quasars are well within the primary beams of all antennas at all observing frequencies, but correlation at two field centres using separate passes was required. The two separate visibility functions were preaveraged to 2s in time and 1 MHz

in frequency before subsequent analysis using the AIPS package. The amplitudes of the visibility functions were calibrated using the gain and system temperature measurements provided for each antenna.

6 Analysis of New Observations

Analysis of the observations of 1038+52A,B at previous epochs was done using the differenced residual phase technique, making source structure corrections, S(a) and S(b), derived from hybrid maps. Both quasars, 1038+52 A and B, exhibit extended mas-scale structures at all three frequencies observed. Quasar A has a typical core-jet structure. The structure of quasar B consists of at least 3 co-linear components in pa 130 degrees, with the extreme NW component having a strongly inverted spectrum. In previous epochs, the peak of the "core" component in quasar A was chosen as its reference feature. For quasar B the peak of the central component (which is the dominant component at 2.3 GHz) was used. For continuity we adopted the same reference features. The maps made in our analysis have pixel sizes of 0.5 mas at 2.3 GHz, and 0.15 mas at 8.4 and 15.0 GHz. The CLEAN restoring beams are 1.8 mas and 0.5 mas.

For the astrometric analysis of this fourth epoch data, we first used the technique known as PHASE-REFERENCE MAPPING (e.g. Alef 1989). In this method one first makes a hybrid map of the stronger source, a, (1038+52A) in order to separate the source structure terms from the antenna error terms in the residual visibility phase.

$$V(a) = \frac{[A(a)\exp iS(a)](u,v) * \exp i(E(a) + X(a))}{\text{F.T. ===> a-map}}$$

The antenna error phases are then used to rotate the phase of the visibility function of the weaker source, b, and the corrected function, V'(b), is then Fourier transformed to form a map of b.

$$V'(b) = [A(b)\exp iS(b)](u,v) * \exp i(E(b) + X(b)) * \exp -i(E(a) + X(a))$$

$$= \frac{[A(b)\exp iS(b) * \exp i(X(b)-X(a))](u,v)}{\text{F.T. ===> b-map with position offset}}$$

As with the differenced residual phase method, the difference of the model errors phases, E(b)-E(a), is assumed to be negligible. (This is a reasonable assumption for data from the VLBA correlator, which uses CALC8 to compute the model phase). If the reference feature is at the centre of the hybrid map of a, the reference feature of b is offset from the centre by the residual separation; otherwise one must correct this by the offset of the a reference feature.

In the actual analysis within the AIPS software package, the final hybrid map of 1038+52A (Fig. 1a) was given as an input model to the fringe-fitting task, FRING, in which the source structure

terms are used to derive antenna-based error phases, and phase derivatives (delay and rate), from the 1038+52A visibility data. These were then used to correct the 1038+52 A and B visibility functions; this ensures that identical corrections are made for both sources, and permits the visibility functions to be averaged in time and frequency before making the final maps of 1038+52 A and B (Fig. 1b,c).

The astrometric analysis consists of estimating the positions of the reference features in the a and b maps with respect to the centres. The maps themselves are composed of pixels, of separation typically 1/3 or 1/4 of the interferometer beam. A precise definition of the reference feature position must in general involve some form of interpolation between pixels. One method is to define a centroid of the relevent "CLEAN components" which make up the reference feature. This method was used to define the reference feature positions in the analysis of the previous three epochs. Another method is to fit a smooth function to the peak pixel and the surrounding 8 pixels in the CLEAN map (which is derived from the CLEAN components by convolution with the CLEAN beam). We adopted this method for the fourth epoch, using the AIPS task MAXFIT, and made measurements of the reference feature positions in both A and B maps at all frequencies. The difference of the offsets from the map centres for the two sources is the residual separation, an astrometric correction to the source separation used in the correlator model.

7 A New Analysis Method

The phase-reference mapping method can be used when one of the sources is too weak for an explicit analysis of the differenced residual phase, or for using the hybrid mapping technique to separate source and antenna phases. However, for the 1038+52A,B pair, either source can in principle be used for determining the antenna phase errors by hybrid mapping. We have devised a new method in which the (common) antenna error phases and both source structure phases are determined simultaneously from the two visibility functions. We term this method "hybrid double mapping". It relies on the usual assumption that the difference of the model error terms is negligible and, in addition, that the (u,v) coordinates for both sources are almost the same for simultaneous measurements. In this case we can form the SUM of the visibility functions, V(a) and V(b) :

$$V(a)+V(b) = A(a)\exp iS(a) * \exp i(E(a)+X(a)) + A(b)\exp iS(b) * \exp i(E(b)+X(b))$$

$$= [A(a)\exp iS(a) + A(b)\exp iS(b) * \exp i(X(b)-X(a))] * \exp i(E(a)+X(a))$$

This visibility function sum can be thought of as representing observations of a composite source c, whose brightness distribution consists of a superposition of that of a, and that of b offset by the residual separation.

$$V(a)+V(b) = \underbrace{[A(c)\exp iS(c)](u,v)}_{\text{F.T. ==> c-map}} * \exp i(E(a)+X(a))$$

We then use the hybrid mapping technique to separate the antenna error phases and the source structure phase S(c), and make a hybrid map of c. The astrometric measurement of the relative

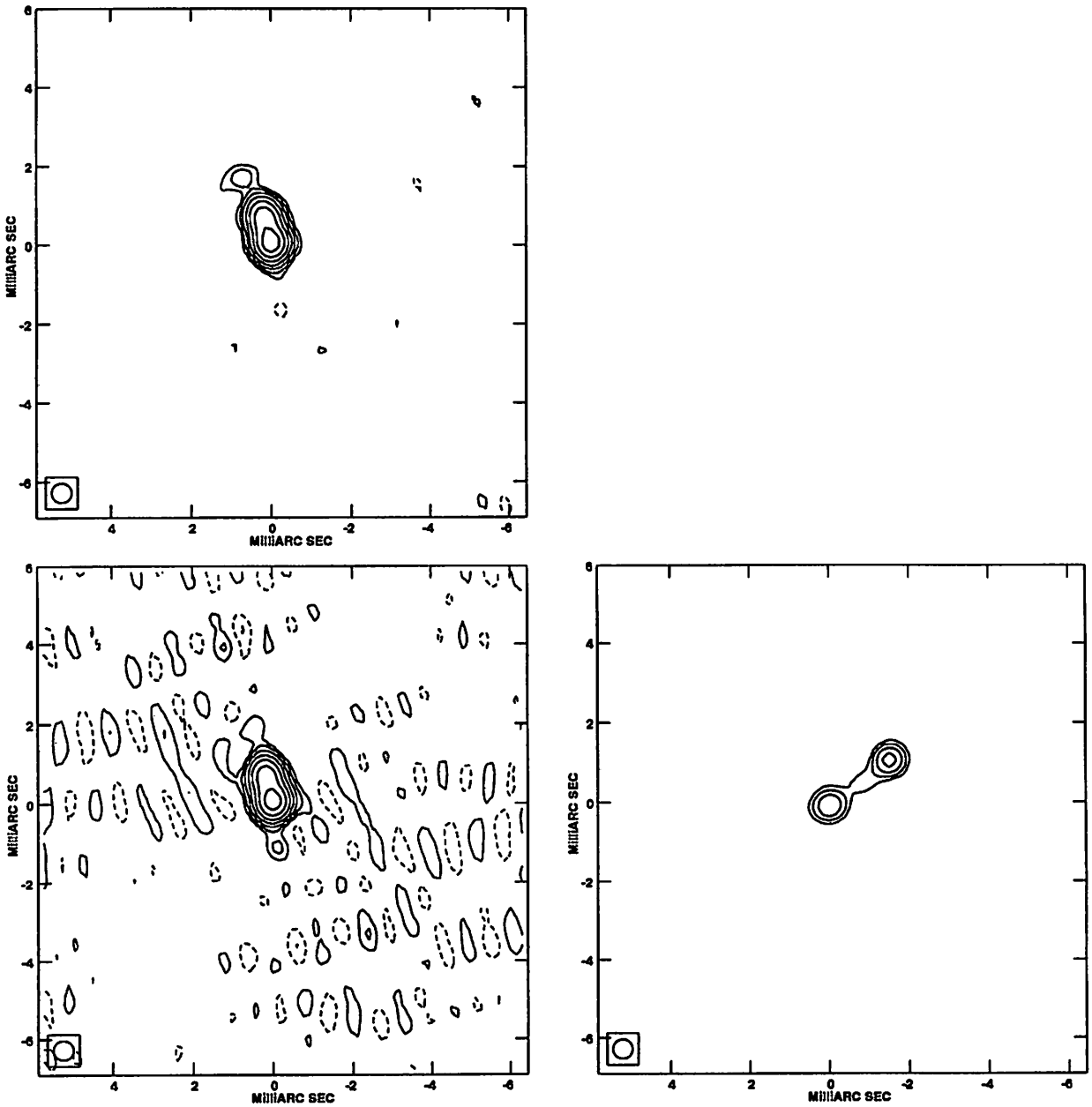

Figure 1: 8.4 GHz maps of 1038+52A,B. Lowest contour level 3 mJy/beam, increasing in factors of 2. **Top (a):** Final hybrid map of 1038+52A, used as input to FRING; **Bottom left (b):** Final map of 1038+52A, used for astrometry; **Bottom right (c):** Final phase-referenced map of 1038+52B, used for astrometry.

position of the reference features of a and b can then be made within the single "hybrid double map" of c.

There are some practical aspects to be considered. If the source coordinates used in the correlator model are very precise, then the residual separation may be less than the interferometer beamwidth, and the two source distributions will lie on top of each other. For our analysis we introduced an artificial position offset to the 1038+52B source visibility function before forming the visibility sum, to ensure that the A and B reference features were well separated in the hybrid double map. One should also arrange that the peak of one source does not lie on the sidelobe response of the other in the "dirty" map, as this may degrade the CLEAN process. Another important consideration is that the averaged samples of the summed visibility function contain equal contributions from both source visibility functions. When both sources are observed simultaneously this will normally be the case, except when different amounts of data are lost in the two separate correlator passes needed for the two source positions. It is important to edit the data sets carefully to fulfil this condition. The range of validity of the assumption that the (u,v) coordinates for the two sources are the same depends on the "dilution factor", i.e. the reciprocal of the source separation, measured in radians. The (u,v) value assigned to the summed visibility will be incorrect for either source by roughly 1 part in the dilution factor (1 in 6000 for 1038+52A,B). Scaling errors of this order occur in the hybrid double map, so the residual separation should be << beamwidth * dilution factor.

In the actual analysis in AIPS, we first made a rough correction to the phase of the summed visibility of 1038+52 A + B, using the antenna phase and phase derivative errors from running FRING on 1038+52A, using a point source model. (However, there is no reason why one should not run FRING on the summed visibility function directly). We then used the hybrid double mapping method on the corrected, summed visibility function to form a hybrid double map of 1038+52 A + B after many self-calibration iterations (Fig 2a,b). We again used the AIPS task MAXFIT to estimate the positions of the reference features of both A and B quasars in the hybrid double map. Their separation in the map represents the residual separation plus the additional offset used to separate the structures.

8 Applications of Hybrid Double Mapping

The hybrid double mapping method has some advantages over the differenced residual phase and phase-reference mapping analyses. When hybrid maps are made of a and b to determine structure corrections for the differenced residual phase method, the antenna error phases are not constrained to be the same. Furthermore, errors in this phase separation process increase the phase "noise" in the differenced residual phase, and in the referenced phase of the weaker source visibility function in the phase-referencing method. In hybrid double mapping we use both source structures simultaneously to separate the (common) antenna error phases from that of a single "structure" in which the a and b reference points are spaced by the residual separation.

The hybrid double mapping method can in principle be applied whenever two (or more !) radio sources are observed simultaneously, but must be correlated at separate field centres. When both sources are strong, as with 1038+52A,B, both sources effectively are used to separate out the

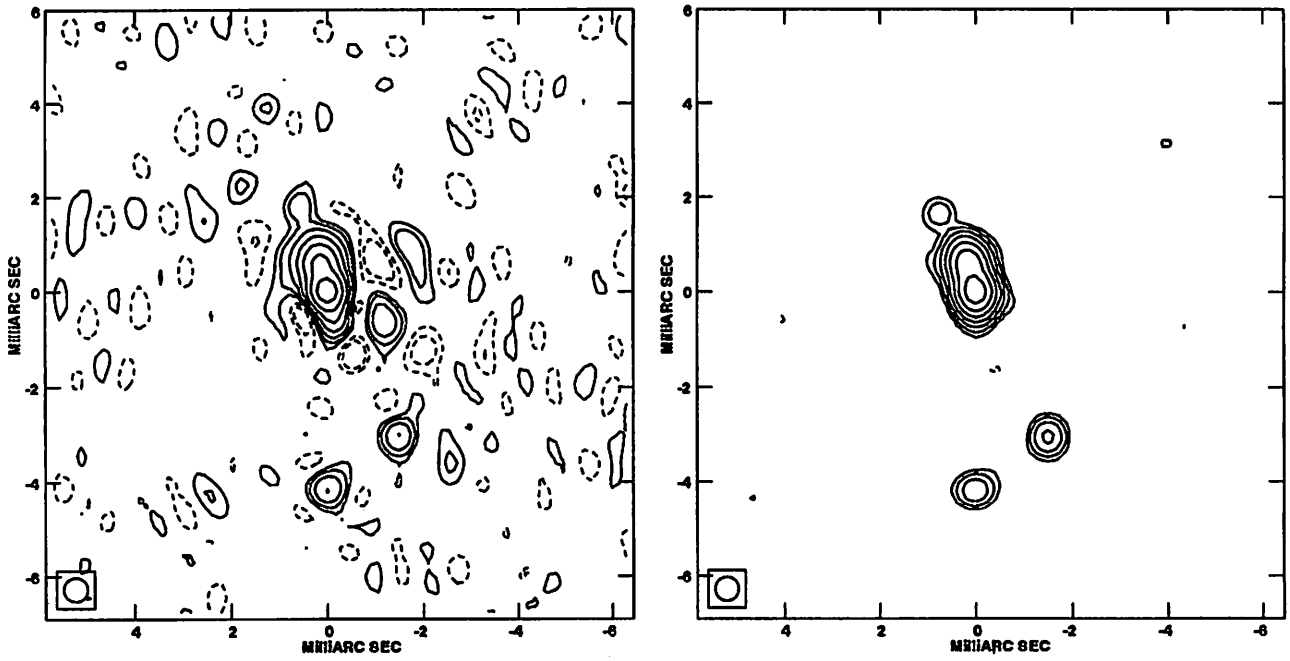

Figure 2: 8.4 GHz hybrid double maps of 1038+52 A+B. Lowest contour level 3 mJy/beam, increasing in factors of 2. **Left (a):** After single "point-source" phase self-cal in FRING; **Right (b):** After 14 hybrid double mapping iterations.

antenna error phases. When one source is very weak, there is probably little to be gained over phase-reference mapping. One field of application is in the VLBI mapping of gravitational lens systems with wide image separations (e.g. the "double quasar" 0957+561; see Garrett et al, 1994).

When the separation between the two sources of a pair exceeds the telescope primary beamwidths, observations must be switched between the sources, and the visibility phase of at least one of the sources must normally be interpolated in the observing gap (e.g. see Rioja and Porcas, these proceedings). The condition that must be fulfilled in this case is that an equal number of observations of both sources must be added to form an average visibility function for the length of the "solution interval" in the phase self-calibration step of hybrid double mapping. This is generally set by the coherence time of the atmosphere, and would imply a very fast switching cycle in most cases. Another situation where close sources are observed simultaneously is in "cluster-cluster" VLBI (see e.g. Rioja et al, 1995) and hybrid double mapping might be applied for the analysis of such data.

9 Preliminary Astrometric Results and Discussion

In Figure 3a we plot our preliminary measurements of the fourth epoch separation between the reference features in the two quasars (in the sense 1038+52A - 1038+52B) at all frequencies, along with the previously published values for the other 3 epochs. The origin represents the separation at epoch 1 (1981.2) at 8.4 GHz. Epochs 2,3 and 4 are at 1983.4, 1990.5 and 1995.8, respectively. The main features to notice are (i) the well known offset between the 2.3 GHz and 8.4 GHz points in pa ca. 30 degrees: (2) the gradual motion of the 8.4 GHz points with time (some 240 micro-a.s.

in 15 years) in p.a. -45 degrees and (3) the near coincidence of the epoch 4 separations at 8.4 and 15.0 GHz.

Figure 3a reflects the results of structural changes with time and frequency in both quasars. Rioja (1993) and Rioja et al (1996) have noted that the motion and p.a. of the 8.4 GHz points corresponds to a slow, outward motion of the reference component in 1038+52B with respect to its flat-spectrum core, which is measureable directly in hybrid maps at 8.4 GHz. In Figure 3b we plot the same measured separations as in Fig. 3a, but corrected for the outward motion of the reference feature in 1038+52B. The remaining separations between points at different frequencies and times are close to the p.a. of the jet in 1038+52A, presumably indicating temporal and spectral changes along its axis. A more extensive discussion of the astrophysical results of this work will be given later (Rioja and Porcas, in preparation).

10 Acknowledgements

We thank Dave Graham for his assistence in making the observations in Effelsberg, and Tony Beasley for help at the VLBA. Tha VLBA is operated by NRAO, which is operated by Associated Universities Inc. under a cooperative agreement with the NSF. María J. Rioja acknowledges support for her research by the European Union under contract CHGECT920011.

11 References

Alef, W., 1989, in "Very Long Baseline Interferometry", ed. Felli, M. and Spencer, R., Kluwer, p261

Cornwell, T.J. and Wilkinson, P.N., 1981, MNRAS, 196, 1067

Garrett, M.A. et al, 1994, MNRAS, 270, 457

Gontier, A-M. et al, 1993, Proc. 9th Working Meeting on European VLBI for Geodesy and Astrometry, ed. Campbell, J. and Nothnagel, A., Bonn, p167

Kellermann, K.I. and Pauliny-Toth, I.I.K., 1969, ApJL, 155, L71

Marcaide, J.M. and Shapiro, I.I., 1983, AJ, 88, 1133

Marcaide, J.M. and Shapiro, I.I., 1984, ApJ, 276, 56

Marcaide, J.M., Elosegui, P. and Shapiro, I.I., 1994, AJ, 108, 368

Owen, F.N., Porcas, R.W. and Neff, S.G., 1978, AJ, 83, 1009

Owen, F.N., Wills, B.J. and Wills, D., 1980, ApJ(L), 235, L57

Rioja, M.J., 1993, Proc. 9th Working Meeting on European VLBI for Geodesy and Astrometry, ed. Campbell, J. and Nothnagel, A., Bonn, p152

Rioja, M.J. et al, 1995, Proc. 10th Working Meeting on European VLBI for Geodesy and Astrometry, ed. Lanotte, R. and Bianco, G., Matera, p160

Rioja, M.J. et al, 1996 (in preparation)

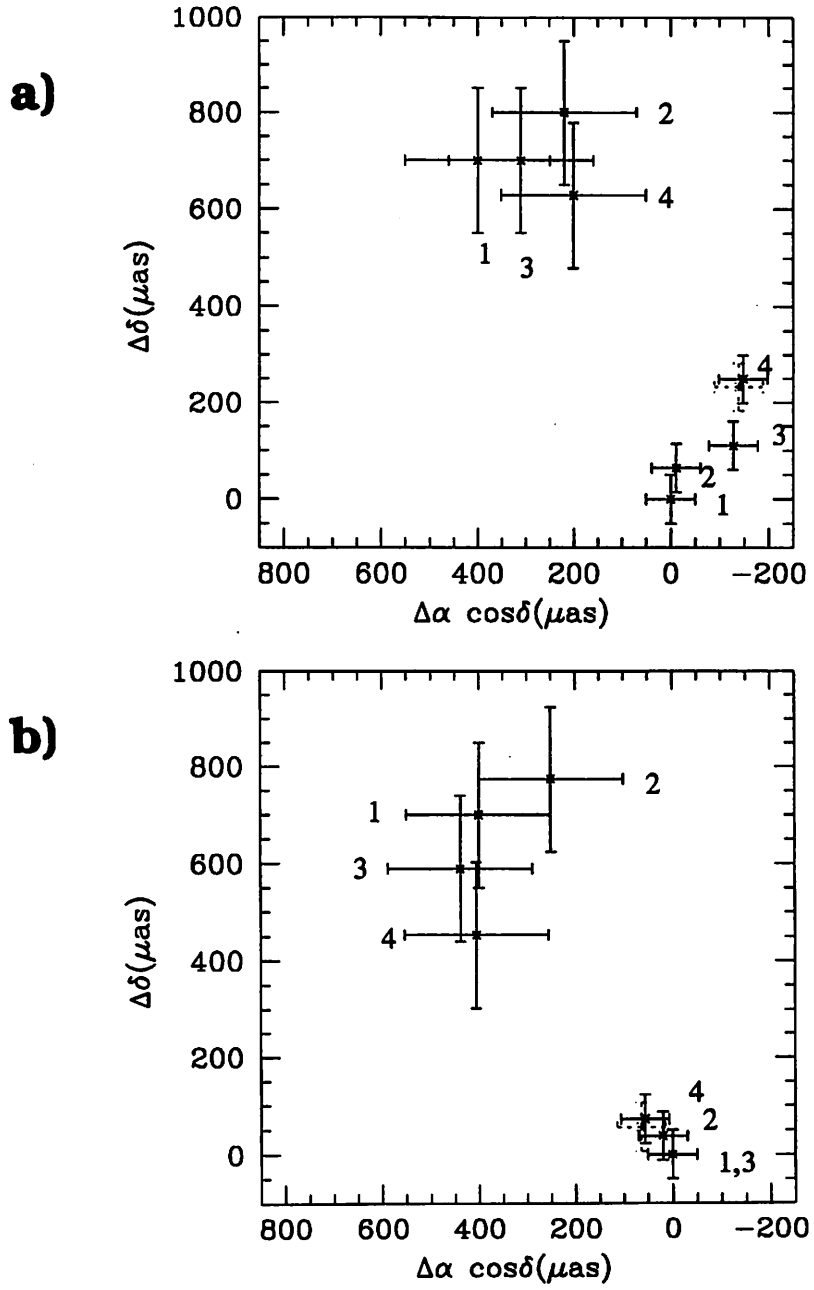

Figure 3: **a)** Summary of relative position measurements between 1038+52 A,B. Large crosses = 2.3 GHz, small crosses = 8.4 GHz and hatched cross = 15 GHz. Numbers indicate epoch number. Origin corresponds to 8.4 GHz separation at epoch 1. **b)** Same as **a)** but positions corrected for outward motion of reference feature in 1038+52B.

Comparative VLBI Astrometric Analysis of the pair 1308+326 and 1308+328

María J. Rioja[1] and Richard W. Porcas [2]
[1]*Joint Institute for VLBI in Europe, Dwingeloo, The Netherlands*
[2]*Max-Planck-Institut für Radioastronomie, Bonn, Germany*

Abstract: We present the results from the analysis of first-epoch VLBI observations of the radiosources 1308+326 and 1308+328, 14.4' apart. The source 1308+328 was not detected in surveys prior to 1975, and has been suggested as a good candidate for a 'new' radiosource. Our VLBI observations show that its structure is extraordinarily compact. We have used different approaches for the astrometric data reduction and have been able to measure the separation between the sources to sub-mas precision. We present the results along with a discussion of some technical aspects of the various analysis paths.

1 Introduction

The extragalactic object 1308+328 ($z \sim 1.65$) is highly variable in its radio, optical (3-3.5 mag) and X-ray emission (Machalski and Engels, 1994). The source brightness at frequencies above 10-15 GHz has been decreasing since 1990 and seems to correlate with changes of the optical brightness. X-ray emission has been found from EINSTEIN, EXOSAT and ROSAT archive data which also shows variability. Its radio detection dates only from 1983, so it can be considered as a 'new' radio source. With this in mind we carried out VLBI observations in order to investigate the early stages of activity in AGNs. Given that it is fortuitously close (14') to the strong BL Lac object 1308+326, we interleaved observations of 1308+328 and 1308+326 to make full use of phase reference and differential techniques.

2 Observations

We observed 1308+328 and 1308+326 in February 1995, simultaneously at λ 3.6 (X-band) and 13cm (S-band), using the MK3 VLBI recording system in Mode A, with an array of 11 telescopes (antenna diameters and locations in parentheses): Effelsberg (100m, Germany), Ny Aalesund (20m, Spitzbergen), Medicina (32m, Italy), Wettzell (20m, Germany), Onsala (20m, Sweden), Noto (32m, Italy), Matera (20m, Italy), Hartebeesthoek (26m, South Africa), Simeiz (22m, Ukraine), Shanghai (25m, China) and Kashima (34m, Japan). Unfortunately, due to technical problems the data recorded at Simeiz had to be discarded.

Observations of the two sources were alternated in a repeated cycle throughout the 13 hours duration of the experiment: about 3 minutes pointing at the target source, 1308+328, and 2 minutes pointing at the reference, 1308+326. The data processing was done at the VLBI correlator center at the MPIfR in Bonn (Germany).

Presented at the 11th Working Meeting on European VLBI for Geodesy and Astrometry, Onsala, Sweden, 1996

3 Data Analysis

Both sources were detected in all scans on all baselines at both frequencies. The data reduction has been done using 3 softwares: AIPS (see e.g. Beasley and Conway, 1995), VLBI3 (Robertson, 1975) and SPRINT (Lestrade et al., 1990). All of them use the phase-delay quantities with different techniques, differenced residual phase or phase-reference mapping, to provide an estimate of the angular separation with sub-mas precision. See the contribution of Porcas and Rioja in these proceedings for a qualitative description of these two approaches.

AIPS and SPRINT use a phase-referenced approach where the observations of the reference source, 1308+326, are used to "steer" the analysis of the data on the target source, 1308+328; then, a Fourier Transform of the phase-corrected visibility function for 1308+328 will produce a phase-referenced map of its brightness distribution, where the offset from the center is astrometrically meaningful. The analysis with AIPS uses the Bonn correlator model (which includes no correction for the ionospheric delay) plus an additional correction for antenna axis offsets. The analysis with SPRINT uses a full theoretical geophysical and relativistic model. The results from SPRINT presented here also include an ionospheric correction derived from the Klobuchar model (Klobuchar, 1975).

VLBI3 uses instead a differenced-phase approach, with a least squares fit to the unambiguous differential phase-delay values, to estimate the relative separation. The analysis with VLBI3 also uses a full theoretical model. Nevertheless, the results from VLBI3 presented here are not final since they do not include the ionospheric and source structure corrections to the observed phases.

We were able to produce hybrid maps of both sources, at X and S-bands, using self-calibration techniques in AIPS. Figure 1 shows the calibrated visibility amplitudes for 1308+326 and 1308+328, versus baseline length, at X-band.

4 Results and Discussion

The structure of 1308+326 is resolved on the longest baselines at X-band. It can be modelled by a gaussian component with size 0.4 x 0.2 mas, in position angle -37^0. The structure of 1308+328 remained unresolved, showing that its emission arises from an unusually compact region. From the visibility data in Figure 1 we estimate that $\sim$ 95% of the source flux density at X-band ($\sim$ 0.7 Jy) arises from components smaller than 0.5 mas, and probably at least 90% of the source flux density is in components on $\sim$ 0.1 mas scale.

Figure 2 shows the referenced phases for 1308+328 at X-band, estimated using the antenna phase solution from 1308+326 in AIPS, along with the phase-referenced map of this source produced after Fourier Transform of the phase-referenced visibility function. The peak fluxes in the phase-

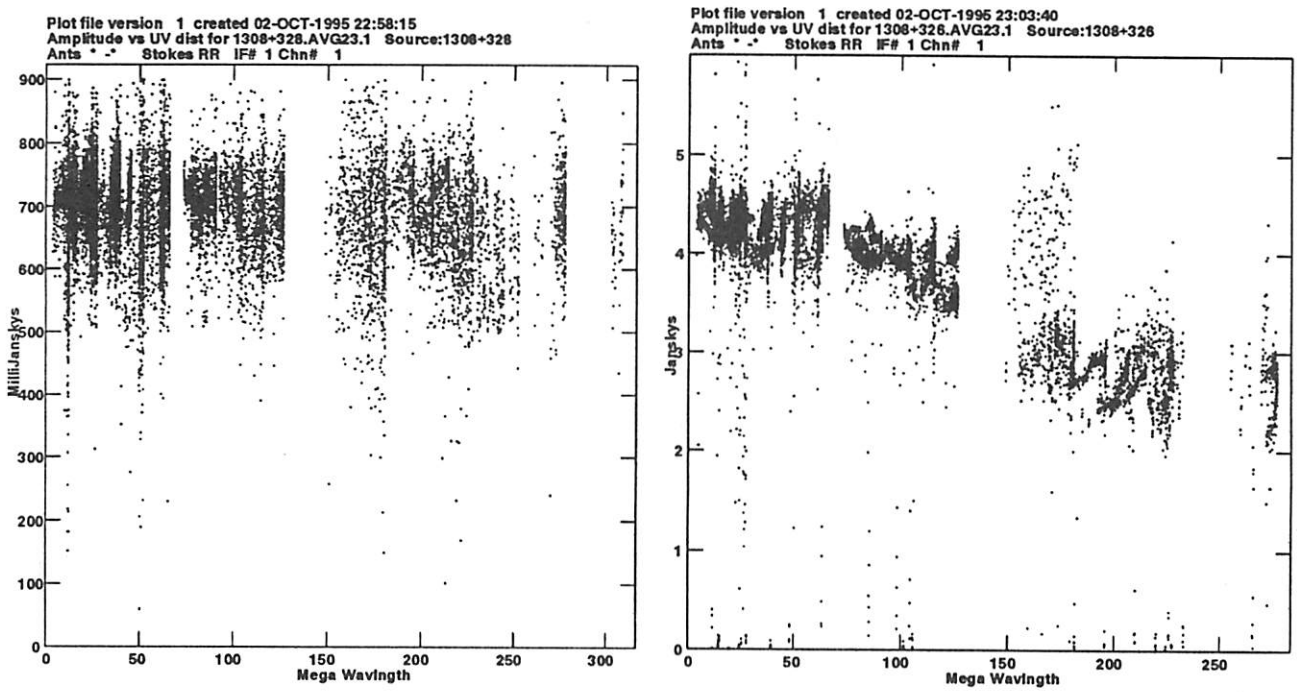

Figure 1: Visibility amplitudes of 1308+328 (*Left*) and 1308+326 (*Right*), versus baseline length, at X-band.

referenced maps produced by AIPS ($\sim$ 0.4 Jy at X-band and $\sim$ 0.14 Jy at S-band) are lower than in the hybrid maps by about 30% at X-band and 50% at S-band, indicating considerable ordered or random errors in the referenced phases. All the flux in the maps is recovered after 1 iteration of phase self-calibration on the phase-referenced data sets. Figures 3 and 4 show the improvement of the phase-referenced maps of 1308+328 after 1 iteration with phase self-calibration, at X and S-bands. The antenna phases resulting from this iteration, at X-band, are plotted in Figure 5. An analysis of these phases will permit an investigation of the relative importance of interpolation errors and model errors in the AIPS phase-reference analysis.

The peak fluxes in the AIPS hybrid maps of 1308+328, and in the phase-referenced maps produced by SPRINT, at X and S-bands, are equivalent ($\sim$ 0.7 Jy at X-band and $\sim$ 0.3 Jy at S-band). We used 2 types of reference phase interpolation, LIND (LINear Double) and PCON (Phase CONnection). LIND makes a forward and reverse extrapolation in time of the phases of the 2 reference source scans adjacent to the target source scan, using the residual fringe rate. If the difference of the 2 extrapolated phases is smaller than a cutoff value (in our case, 100^0), their average is used for differencing with the phase of the corresponding target source scan. PCON makes a linear interpolation between the phases of the 2 adjacent reference source scans, after first using the residual rates to determine the unknown number of full turns of phase between them. Both methods provided similar results.

Figure 6 shows a comparison of the relative positions of 1308+328 with respect to 1308+326 de-

termined using AIPS, SPRINT and VLBI3; we have chosen as the origin of the figure the angular separation between 1308+328 and 1308+326 determined from the geodetic program run by USNO. The error bars in Figure 6 are provisionally set to 100μas for X-band and 300μas for S-band (except for the USNO value which is derived from group delays). A proper error analysis is needed for a realistic estimation of the error bars.

The angular separations determined from different softwares are compatible, within the provisional error bars. We do not detect any significant spectral dependence of the measured angular separation.

More epochs of VLBI observations on this pair will allow changes in the parsec-scale structure of 1308+328 to be monitored with respect to an external reference.

5 Acknowledgements

We wish to thank the personnel at each telescope for making possible these observations. We are grateful to Walter Alef for support in exporting the correlator data and Jean-Francois Lestrade for assistence with SPRINT. María J. Rioja acknowledges support for her research by the European Union under contract CHGECT920011.

6 References

Beasley, A.J. and Conway, J.E., 1995, *Very Long Baseline Interferometry and the VLBA, ASP Conference Series*, Vol. 82, p. 327, eds. Zensus, J.A., Diamond, P.J. and Napier, P.J.

Klobuchar, J.A., 1975, *Air Force Cambridge REsearch Laboratories* Report No. AFCRL-TR-75-0502 (NTIS ADA 018862).

Lestrade, J-F, Rogers, A.E., Whitney, A.E.E., Niell, A.R., Phillips, R.B., Preston, R.A., 1990, *Astron. J.*, **99**, 1663-1673.

Machalski, J., and Engels, D., 1994, *Mon. Not. R. Astron. Soc.*, **266**, L69-L72

Robertson, D.S., 1975, PhD Thesis, MIT.

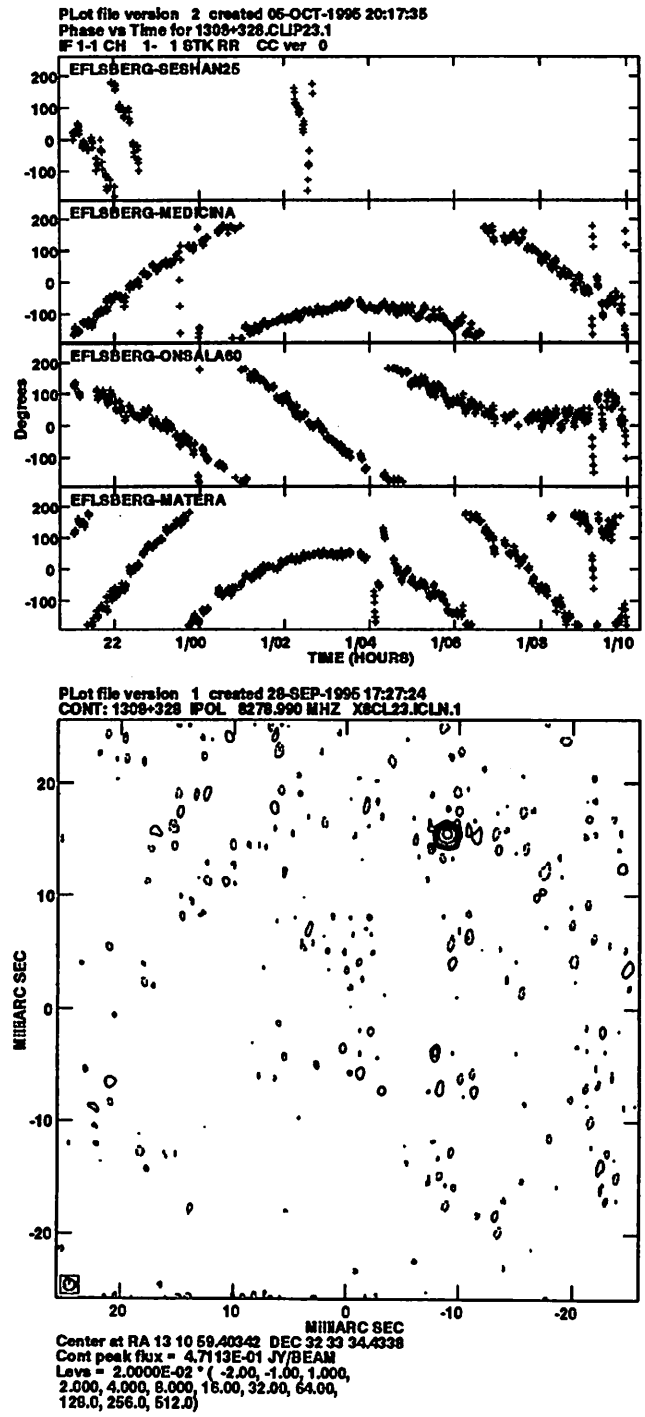

Figure 2: *Top:* Referenced phases for 1308+328 estimated using the interpolated antenna phase solution of the reference source, 14.4' away, in AIPS. *Bottom:* Phase-referenced map of 1308+328 at X-band produced with AIPS.

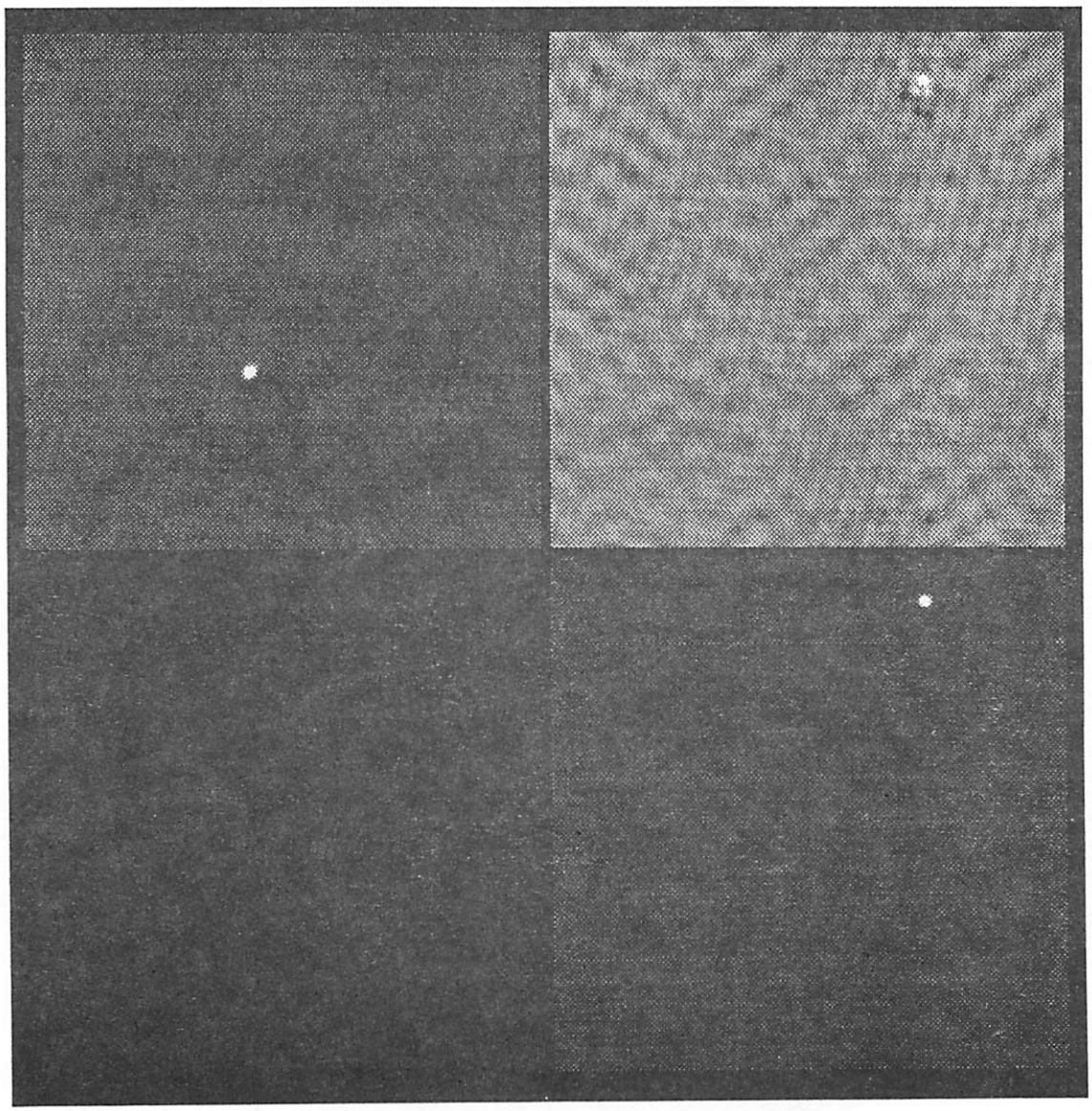

Figure 3: *Top left corner:* Hybrid map of 1308+326 at X-band. *Top right corner:* Phase-referenced map of 1308+328 at X-band. *Bottom right corner:* Map of 1308+328 after 1 iteration of phase self-calibration on the phase-referenced data set at X-band.

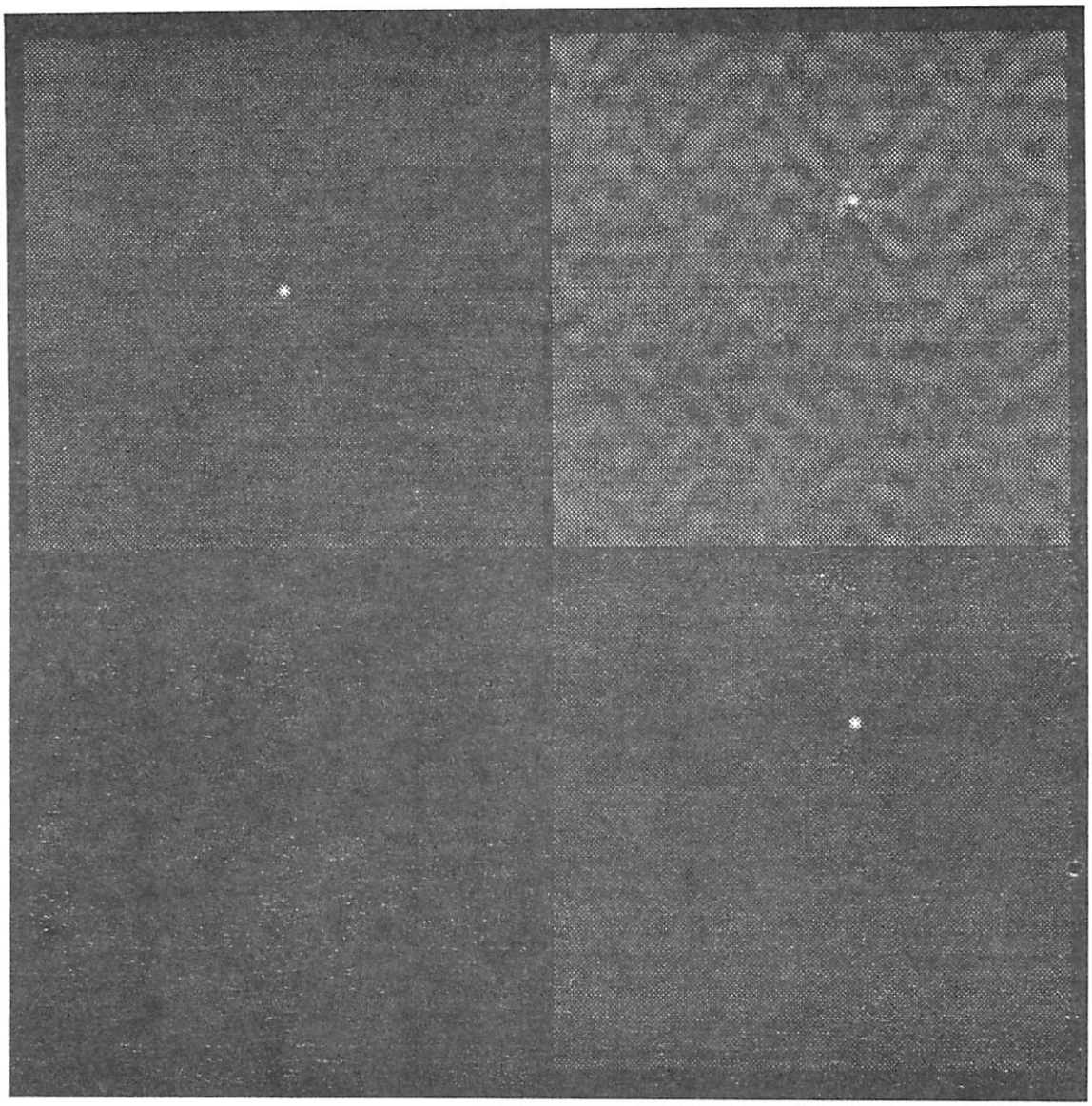

Figure 4: *Top left corner:* Hybrid map of 1308+326 at S-band. *Top right corner:* Phase-referenced map of 1308+328 at S-band. *Bottom right corner:* Map of 1308+328 after 1 iteration of phase self-calibration on the phase-referenced data set at S-band.

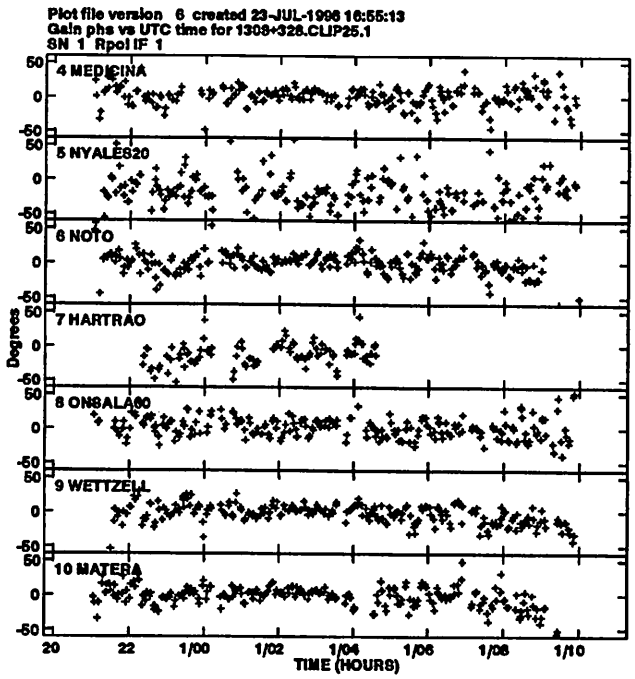

Figure 5: Antenna phases derived after one iteration of phase self-calibration on the phase-referenced data set of 1308+328 at X-band.

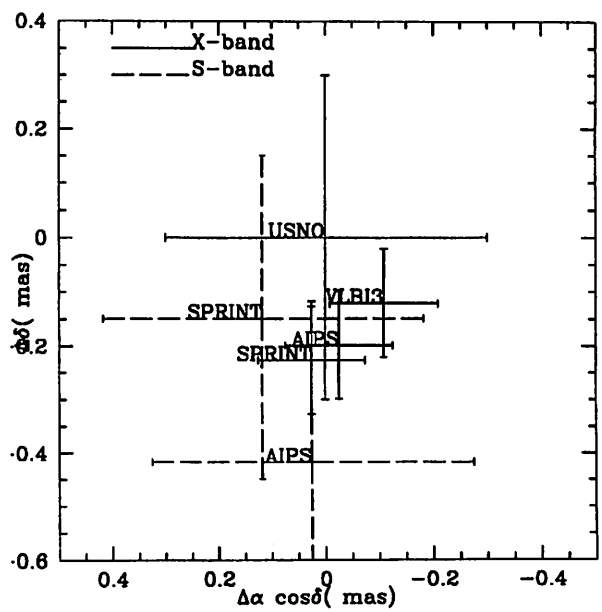

Figure 6: Summary of measurements of the angular separation between 1308+328 and 1308+326 derived with different softwares at X-band (continuous lines), and at S-band (dashed lines); the origin of the plot corresponds to the relative position of 1308+328, with respect to that of 1308+326, given by USNO at X-band.

MEASUREMENT OF VERTICAL CRUSTAL MOTION IN EUROPE BY VLBI - Further Support of the European Geodetic VLBI Network by the European Union

James Campbell, Geodetic Institute of the University of Bonn, Germany

1. Introduction

The current operational phase of the European Geodetic VLBI Network (Phase I, 1993-1996) has been supported by the EU under the title "European VLBI for Crustal Dynamics". In this first phase the work has been concentrated on the measurement of horizontal crustal motions caused by tectonic stresses in the European region *(see Nothnagel in these proceedings)*.

The proposal for a continuation and expansion of the project has been recently accepted by the European Commission under the "Training and Mobility of Researchers (TMR)"-programme, enabling a second phase of geodetic VLBI observations to start with new funding in from October this year. This second phase stresses the determination of vertical site motions, which are much more difficult to detect. Accordingly, the project contains an expanded work programme with increased observations, new VLBI stations and, most importantly, GPS data collection and processing. Together with the already existing series of observations, the entire project will achieve a total observation time span of almost 10 years. With a refined modelling of the atmospheric path delay this longer data set should yield significant results for vertical motions on the order of a few millimeters per year.

The data set will be of high significance for the monitoring of land uplift and subsidence, sea level changes, glaciology and other vertical motion applications. The results will contribute to the evaluation of global climatic changes and other environmental effects.

The training scheme, which is an intrinsic part of the TMR programme, will be implemented chiefly through employment of visiting young post-doctoral researchers from the EU-member states. Plans are also to make ample use of the possibility of temporal exchange of staff members and part-time students between the participating institutions in order to stimulate the interest of young talents in the new developments in the geosciences.

2. The Challenge of Determining Vertical Crustal Motion

In most cases, vertical crustal motions caused by isostatic and/or tectonic processes in the earth's crust are much smaller than horizontal motions, i.e. at most about 10 mm/year. However, on the local scale man-induced vertical changes (i.e. by withdrawal of natural gas, oil or groundwater) may be much larger. Moreover, volcanic activities are often associated with local height changes of considerable size (e.g. Pozzuoli near Naples). With global or regional-seize VLBI networks it will therefore be difficult to interpret any significant vertical station motions in a meaningful way without having recourse to GPS- and levelling data.

But up to now the detection of significant vertical motions in global and regional geodetic networks has yet to be demonstrated (see e.g. Macmillan and Ray 1991). The difficulties encountered by the users of the space techniques are well known: the errors in the vertical tend to be several times larger than in the horizontal due to the unmodeled effects of atmospheric path delays which contaminate primarily the vertical component of point position. Although in recent years significant progress has been made to improve the models for correcting the atmospheric path delay, a true panacea for solving the problem has not yet been found. Therefore one of the main areas of research in the new project has to concentrate on the validation of correction models for the atmospheric path delay.

From recent work in this area it has become apparent that one of the most useful strategies is to analyse the results of solutions as a function of the elevation cut-off. Up to now, the (invariant) baseline length has been used almost exclusively in such tests, because on long baselines the instabilities of the

Presented at the 11th Working Meeting on European VLBI for Geodesy and Astrometry, Onsala, Sweden, 1996

reference frame will inevitably introduce tilts in the baseline vectors and thus contaminate the vertical component. However, at present the Earth Orientation Series are said to be accurate to the level of a few tenths of a milliarcsecond, and at this level, a 2000km baseline will not experience any tilts greater than a few millimeters (0.1mas -- 1mm). One particular aspect of the European network as opposed to the global networks considered in most of the existing studies is the relatively small size of the network, which allows to investigate the behaviour of the vertical component in a direct way as it changes with different cut-offs used in the solution.

Another problem is of course the wet component of the path delay which is hard to estimate due to its rapid variations during the observing session. Measurements of humidity at the site are of little use if they are to represent the situation up in the atmosphere. Water Vapour Radiometry has been successful to a certain degree, but so far the technique has been difficult and costly to operate. For radio sondes the situation is similar: they are available only at a few locations and cannot be used routinely during the experiments *(see e.g. A. Niell in these proceedings)*. With the advent of GPS, however, new possibilities arise to infer the wet path delay contribution from the GPS measurements themselves *(see Carlsson, Elgered and Johansson in these proceedings)*. This will be another area of concentrated research in the new project.

The increased potential for high precision geodetic positoning of the GPS will in itself form a major contribution in the second phase of the project. From 1992 onwards permanent receivers have been installed at most of the VLBI/SLR-stations and at other geodynamically interesting sites. The network is being operated globally as the IGS network and will provide data sets of the colocated European GPS sites. This will enable us to produce independent GPS site motions which can be compared to the VLBI results. These comparisons will be of particular importance for the validation of the vertical motions of the fiducial sites.

In recent years, several denser networks have been set up to study regional phenomena. Thus, in Scandinavia, a permanent network of GPS stations has started operating with the aim of determining the Fennoscandian post-glacial uplift. Similar networks are being set up in the Netherlands and other European countries with the aim of connecting tide gauges to primary GPS sites and to the levelling networks (e.g. the Eurogauge Project). For these networks the inherent properties of VLBI as an essentially non-mobile but very precise measurement system with high long-term stability guaranteed by extra-galactic radio sources will form the ideal reference standard. In this way, the European VLBI-network will be perfectly suited to serve as a reference net for GPS densification campaigns aimed at the detection of regional crustal deformations, the connection of tide gauges and regional geoid studies.

3. Research Teams in the European Network

At present, the European Network consists of six core stations *(see map in M. Sorgente, these proceedings)*. A new 20m antenna erected at Ny Ålesund on the arctic archipelago of Spitsbergen by the Norwegian Mapping Agency has been taking part routinely in the European VLBI experiments since Oct. 26 1994. The 15m antenna of the Instituto Geografico Nacional at Yebes, about 80km east of Madrid, has recently been equipped for geodetic VLBI and made its first test run in the geodetic VLBI network *(see Lopez-Fernandez in these proceedings)*. With the help of NASA the station of Simeiz on Crimea (Ukraine) has become operational in the MkIII mode in 1994 and has taken part in several of the European geodetic sessions *(see Petrov et al. in these proceedings)*. Also, those European radio astronomy observatories that are almost exclusively committed to astrophysical work, such as Effelsberg (Germany) and Westerbork (The Netherlands) are or will be taking part occasionally in the geodetic campaigns.

The observations are being taken care of by the participating observatories using their own staff. The scheduling, sending out of tapes and the correlation is accomplished by the Bonn VLBI-group of the Geodetic Institute. The geodetic analysis is shared by all participants in this project, using the different available software packages, and contributing further developments needed to obtain the optimal accuracy in the results.

In the second phase of the EU funding scheme, the TMR-network comprises eight participants, with one organisational change concerning the new affiliation of Matera and a newcomer, i.e. the Norwegian station of Ny Alesund. The profiles of the 8 participants in the TMR programme are given below. Of course, a close cooperation also exists with those groups and institutions that have not been eligible to take part in the present EU programme.

1. Geodetic Institute of the University of Bonn, Germany (Coordinator)

The VLBI group at the Geodetic Institute of the University of Bonn (GIUB) will continue to act as a coordinator of the network operations and as the principal processing and data analysis center. The MKIIIA correlator of the Max-Planck-Institute for Radioastronomy (MPIfR) which is located in proximity of the Geodetic Institute provides the crucial capability for on-the-spot data processing and quality assessment. A special agreement between the Geodetic Institute, IfAG, and MPIfR for the allocation of geodetic VLBI correlation time exists.

The VLBI-specific activities of GIUB include the creation and sending out of observing schedules, the management of the tape pool, the timely supply of the participating stations with tapes, the correlation of the raw data and the geodetic post-processing of the correlated data. GIUB is also responsible for updating and maintaining the data bases and for compiling the reports. Once or twice per year the participation of the Effelsberg 100m-telescope of the MPIfR is organised in the framework of the astronomical S/X-campaigns of the EVN.

2. CNR-Istituto di Radioastronomia Bologna, Italy

The "Istituto di Radioastronomia" (IRA) participates as a shared facility for both astronomy and geodesy in the proposed project, joining the network with two 32 meter dishes located in Medicina (near Bologna) and in Noto (near Syracuse). Its project-related activities include operational work, checks on antenna stability and geodetic data processing with the CALC/SOLVE software. The group at Noto will also be concerned with astrometric aspects of the VLBI data collected in the European campaigns. GPS receivers are now operating permanently at both the Medicina and Noto sites.

3. CNR/ITIS - Matera, Italy

The "Istituto di Tecnologia Informatica Spaziale" (ITIS, Institute of Information and Technology for Space) Geodesy (CGS) near Matera. ITIS-CNR will contribute as a participating organization to the project in cooperation with the Italian Space Agency (ASI). Its activities include the VLBI and ancillary data acquisition and recording at the 20 m antenna at the Matera CGS, using the operational interface standard MARKIIIA, the maintenance of a local geodetic control network around the VLBI antenna. The precise control network includes the Satellite Laser Ranging (SLR) station and the fixed Global Positioning System (GPS) receiver currently operating at the CGS. At CGS the VLBI geodetic data analysis using the CALC/SOLVE package is currently being used. The results will be compared with SLR and GPS data analysis results also processed at CGS.

4. CSIC - CEAB, DSS65 Madrid, Spain

The Consejo Superior de Investigaciones Cientificas - Centre d'Estudis i Avancats de Blanes (CSIC-CEAB) continues its involvement in geodetic and astrometric VLBI activities on the observational and scientific levels using the DSS65 antenna of the NASA Madrid Deep Space Communications Complex (MDSCC) at Robledo near Madrid under the host country agreement. The VLBI group is responsible for the carrying out of the observing sessions and performs its own analysis using the OCCAM geodetic VLBI software. In addition, the geodetic control network around the antenna including the ties to the GPS-monument will be maintained.

5. Rijkswaterstaat - Delft (RWS)

The Survey Department is a division of the Rijkswaterstaat specialized in Surveying/Mapping and Geodesy. In connection with the responsibility of the maintenance of the NAP (Amsterdam Height Datum), it is charged with all matters related to height information in The Netherlands. The Survey Department participates in a number of governmental bodies for coordination of research and in actual research projects. Examples are research on land subsidence from national levellings (with the Geological Survey of the Netherlands), determination of sea level rise (with the National Institute for Coastal and Marine Management of Rijkswaterstaat) and precise geoid determination (with Delft University of Technology). At present, the most prominent themes for research and development in the field are the maintenance of the Geometrical Infrastructure in the Netherlands (e.g. by setting up a so-called Active GPS Reference System) and detection and interpretation of subsidence due to

anthropogenic (gas/water extraction) and natural (compaction, neo-tectonics) influences. Moreover, the Survey Department operates in close connection with other institutes in Europe, e.g. in the project "Relative sea level changes and extreme flooding events in Europe" which is also supported by the EU. In close cooperation with the Netherlands Foundation for Research in Astronomy (NFRA) the Survey Department plans to use the Westerbork Radio Telescope (WSRT) in dedicated VLBI campaigns for height determination. The frequency of the measurements will depend on the availablity of S/X receiving capability at the WSRT. The upgrade of the WSRT is now scheduled for 1998.

6. Onsala Space Observatory near Göteborg, Sweden

Onsala Space Observatory (OSO) is the Swedish National Facility for Radio Astronomy, financed by the Swedish Natural Science Research Council and operated by Chalmers University of Technology (CUT). OSO has pioneered geodetic and astronomical VLBI since the early seventies. Besides its regular participation in the geodetic VLBI experiments using the 20m telescope at Onsala, OSO concentrates its research work on the following areas in order to contribute to the estimation of vertical crustal motion: More sensitive observations through the introduction of the Mark-IV VLBI system which offers a wider recorded bandwidth and hence an improved precision of the fundamental observables. The research in the area of the wet part of the atmospheric path delay will use independent instruments such as microwave radiometers to study, model and correct for this effect. Comparisons with estimated delays obtained from the VLBI and GPS observables using the Kalman filter technique will also be done. Further studies of the stability of the antenna mount at the millimetre level is necessary. Models of the thermal expansion will be developed based on length versus temperature measurements. Comparison of VLBI and GPS data in northern Europe will be an important task to eliminate systematic error sources. The fundamental and accurate VLBI technique and the much denser (in time and space) observational technique of GPS are in many respects complementary. Separation of vertical crustal motions related to different geophysical phenomena is fundamental for the interpretation of the observations. Of special interest is the vertical crustal response to atmospheric and ocean loading.

7. Institut für Angewandte Geodäsie - Satellitenbeobachtungsstation Wettzell (IfAG)

The Satellite Observation Station of Wettzell, which includes a VLBI facility with a 20 m radio telescope will participate in the proposed project as far as its other commitments towards NASA (Crustal Dynamics Project) and NGS (IRIS - Earth Rotation Monitoring) will permit, i. e. with at least three 24 h-experiments per year. Moreover the geodetic control network around the station will be maintained. The precise link between the VLBI and the SLR sites will permit a comparison between VLBI and Laser results. The IfAG, in partnership with the Technical University of Munich, has been operating the Wettzell Fundamental Station since the mid-seventies and is concerned with maintaining and updating the station systems to ensure the highest possible data quality. The IfAG is responsible for surveying and mapping on the nation-wide scale in Germany, but its research program also includes the full spectrum of global geodynamics activities, such as Earth Rotation Monitoring and Crustal Motion Determination. The use of VLBI in pursuing these goals form one of the corner stones of the research programs. Therefore the proposed project is fully consistent with the institutional involvement in this field.

8. Geodetic Institute of the National Mapping Agency - Statens Kartverk (GI/NMA) Hönefoss, Norway

The Geodetic Institute of the Norwegian Mapping Authority (GI/NMA) will contribute to this project by making observations with its new 20 m VLBI antenna at Ny-Ålesund Space Geodetic Observatory, and by carrying out geodetic analyses of the data from the European network. The Geodetic Institute is responsible for the operational VLBI tasks. Possible upgrade to Mark IV data acquisition may take place during the project period. Further activities include the monitoring of antenna stability once per year by means of local geodetic surveys in Ny-Ålesund. This will also include the GPS site participating in IGS (since 1991) and the VLBI data analysis at the Geodetic Institute i Hönefoss. The GI/NMA is responsible for geodetic infrastructure in Norway and is the national facility for space geodetic research. Initial training in VLBI observations were received when GI/NMA operated a mobile VLBI unit on loan from NOAA during 1991-93, partly as a semi-permanent observatory in Trysil, Norway, and partly during European campaigns in the summer. A permanent observatory was built at Ny-Ålesund, on the arctic archipelago of Spitsbergen, in 1992-94, and is now in regular operation. The Space Geodesy Research Group of GI/NMA, led by Dr. Bjørn Ragnvald Pettersen,

administrates the Ny-Ålesund Space Observatory and performs geodetic analyses of data from GPS and VLBI networks at the NMA headquarters in Hönefoss. Areas of particular interest are development of analyses techniques, and applications to geodynamics and geodetic environmental monitoring. Participation in global networks takes place in close cooperation with NASA; USNO, and other institutions. NASA supports the Space Geodetic Observatory through loan of instrumentation and data recording equipment. VLBI operation and analysis is consistent with the goals and programs of GI/NMA.

4. Training aspects of the project

The VLBI-technique as a tool to measure deformations of the Earth's crust stands at the cross-roads between a considerable number of different fields of research, among which the most important are astronomy, geodesy, geophysics, electrical engineering, statistics and computer science. In this situation the introduction of young researchers has always involved a great deal of additional education and training before the level of productive work could be reached. Much of this introductory training has been achieved through doctoral fellowships, but by the time a good level of knowledge and experience was achieved the young researcher had to abandon his scientific career due to the lack of appropriate positions.

In the present second phase of the EU-support 5 temporary post-doc positions have been created for the full 4 years of the duration of the project. The positions will be installed at the coordination and processing center in Bonn and with those participants who are able to provide training assistance, i.e. Onsala, Madrid, Bologna and Matera. The post-doc researchers are eligible to spend a certain amount of their time at the correlation and processing center in order to complement the training and assist in the processing workload. A strong emphasis will be laid on regular exchanges and group meetings in order to ensure the best possible coherence and cooperation among all participants.

5. Outlook

The expected achievement of the proposed project will consist of the first reliable estimates of changes in the vertical position of the stations in the European VLBI-network. These estimates will be based on VLBI measurements started by NASA in 1989/90 and continued under the coordination of the Bonn VLBI group with support by the EU in the Science Program and presently in the TMR program.

The importance of the project is determined by two aspects. On the one hand, the results derived from the campaigns will constitute the much needed basis for the geophysical interpretation of sea level changes and other vertical motion applications. On the other, the establishment of an organisational structure to carry out regular VLBI measurements will guarantee the maintenance of the geometric framework for monitoring geotectonic as well as man-induced changes in the environment. Contacts with geophysicists will be sought and intensified in order to make the results available for interpretational analysis in combination with the broad spectrum of other geophysical data.

In view of the ongoing development of the new MKIV data acquisition and correlation system, which is to be completed in 1998, there are hopes that the increase in delay resolution will have a sizable effect on the accuracy of the results. There are also other benefits of the new system, such as a faster throughput and a bigger number of stations that can be correlated in one passage.

Still the fact remains that the determination of vertical changes heavily relies on the capability to correctly model the atmospheric path delays, the prime error source in geodetic VLBI measurements.

6. References

Macmillan, D.S., J.R. Ray: Current Precision of VLBI Vertical Determinations. Proc. AGU Chapman Conference on Geodetic VLBI: Monitoring Global Change. NOAA Techn. Report NOS 137 NGS 49, p. 428-436, 1991

The competition

1. Which country earned most medals per capita in the Olympics 1996 ?

   1) Australia
   X) Fidji Islands
   2) USA

2. Which Swedish softdrink can be associated with the Onsala Space Observatory ?

   1) Coca Cola
   X) Pommac
   2) Champagnebrus

3. When was the land you are standing on last time at the equator ?

   1) 900 million years ago
   X) 350 million years ago
   2) Never

4. How far is it between the 20 m antenna and the 25 m antenna here at Onsala ?

   1) 1000 m
   X) 800 m
   2) 600 m

5. At what height above the WGS-84 ellipsoid is this paper ?

   1) 13 m
   X) 41 m
   2) - 5 m

6. Why does the church in Onsala have two towers ?

   1) To make way for a marriage
   X) Two priests wanted their own tower
   2) When building the second tower they forgot that there already existed one

7. How long can a tooth of a narwhal (sea-unicorn) be?

   1) 1.8 m
   X) 3 m
   2) 0.6 m

8. What kind of rock is this ?

   1) Basalt
   X) Granite
   2) Gabbro

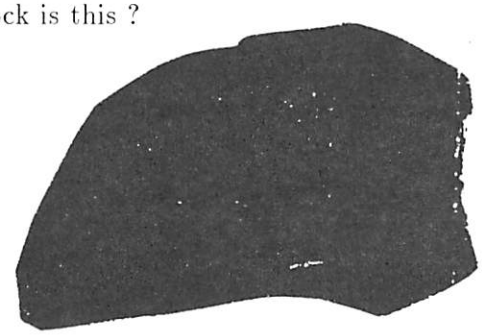

9. Where was the 6th European VLBI conference held ?

   1) Bologna
   X) Dwingeloo
   2) Onsala

10. From which VLBI experiment is this bar code?

   1) CRIMEA June–94
   X) EUROPE 1–96
   2) R&D 10–94

The correct answers

1. **X**, Fidji Islands won a silver medal in boxing, USA for example would have needed some 2000 medals to beat them.
2. **X**, Albert Wilhelm Nummelin, the grand grandfather to Albert Nummelin, Ph D student at the observatory, invented the softdrink Pommac.
3. **X**, 350 million years ago. However, we experienced a tropical night between Friday and Saturday during the meeting. Meteorologists define a tropical night as a night when the temperature never goes below 20°C. This happens very seldom in Sweden.
4. **2**
5. **X**
6. **1**, when "Lasse i Gatan", a famous pirate living in Onsala, asked Ingela to marry him, she answered "—Not until the church has two towers I will marry you". As he was a rich man he built another tower on the church, which still stands, and they married.
7. **X**
8. **2**, gabbro is a rock typical for the lower crust. That we find it here at the surface can only be explained as the consequence of major tectonic events a long time ago ($\approx$ 800 Myr).
9. **1**
10. **X**

PARTICIPANTS IN THE ELEVENTH WORKING MEETING ON EUROPEAN VLBI FOR GEODESY AND ASTROMETRY

Per Helge Andersen
Norwegian Defence
Research Establishment
Box 25
N–2007 Kjeller
Norway
Per-Helge.Andersen@ffi.no
+47 63 80 74 07
+47 63 80 72 12(fax)

Klaus Boerger
Geodetic Institute of the Univ. of Bonn
Nussallee 17
D–53115 Bonn
Germany
kboerger@kuestner.geod.uni-bonn.de
+49 228 733562
+49 228 732988 (fax)
alternative 733281 (fax)

Roy Booth
Onsala Space Observatory
Chalmers University of Technology
S–43992 Onsala
Sweden
roy@oso.chalmers.se
+46 31 772 5520
+46 31 772 5590 (fax)
Sweden

Jörgen Börjesson
Onsala Space Observatory
Chalmers University of Technology
S–43992 Onsala
Sweden
ajb@oso.chalmers.se
+46 31 772 5575
+46 31 772 5590 (fax)

James Campbell
Geodetic Institute of the Univ. of Bonn
Nussallee 17
D–53115 Bonn
Germany
campbell@sn-geod-1.geod.uni-bonn.de
+49 228 733565
+49 228 732988 (fax)
alternative 733281 (fax)

Ragne Carlsson
Onsala Space Observatory
Chalmers University of Technology
S–43992 Onsala
Sweden
rtc@oso.chalmers.se
+46 31 772 5575
+46 31 772 5590 (fax)

Giuseppe Colucci
Nuova Telespazio S.p.A.
Centro di Geodesia Spaziale
P.O. Box 155
I–75100 Matera
Italy
colucci@geodaf.mt.asi.it
+39 835 377 291
+39 835 334 951 (fax)

John Conway
Onsala Space Observatory
Chalmers University of Technology
S–43992 Onsala
Sweden
jconway@oso.chalmers.se
+46 31 772 5503
+46 31 772 5590 (fax)

Fredrik Darin
Onsala Space Observatory
Chalmers University of Technology
S–43992 Onsala
Sweden
cfd@oso.chalmers.se
+46 31 772 5566
+46 31 772 5590 (fax)

Gunnar Elgered
Onsala Space Observatory
Chalmers University of Technology
S–43992 Onsala
Sweden
kge@oso.chalmers.se
+46 31 772 5565
+46 31 772 5590 (fax)

Lubomir Gradinarski
Onsala Space Observatory
Chalmers University of Technology
S-43992 Onsala
Sweden

lbg@oso.chalmers.se
+46 31 772 5575
+46 31 772 5590 (fax)

Barbara Görres
Geodetic Institute of the Univ. of Bonn
Nussallee 17
D-53115 Bonn
Germany

goerres@uni-bonn.de
+49 228 733570
+49 228 732988 (fax)
alternative 733281 (fax)

Rüdiger Haas
Geodetic Institute of the Univ. of Bonn
Nussallee 17
D-53115 Bonn
Germany

haas@uni-bonn.de
+49 228 733562
+49 228 732988 (fax)
alternative 733281 (fax)

Bert Hansson
Onsala Space Observatory
Chalmers University of Technology
S-43992 Onsala
Sweden

bert@oso.chalmers.se
+46 31 772 5555
+46 31 772 5590 (fax)

Hayo Hase
Institut für Angewandte Geodäsie
Fundamentalstation Wettzell
D-93444 Kötzting
Germany

hase@wettzell.ifag.de
+49 9941 603 0 resp. -104
+49 9941 603 222 (fax)

Alexandr V. Ipatov
Institute of Applied Astronomy
Zhdanovskaya st. 8
Sanct-Petersburg, 197042
Russia

ipatov@ipa.rssi.ru
+7 812 230 74 14
+7 812 230 74 13 (fax)

Kenneth Jaldehag
Swedish National Testing
and Research Institute
Box 857
S-50115 Borås
Sweden

kenneth.jaldehag@sp.se
+46 33 16 54 08
+46 33 12 50 38

Per Jarlemark
Onsala Space Observatory
Chalmers University of Technology
S-43992 Onsala
Sweden

poj@oso.chalmers.se
+46 31 772 5566
+46 31 772 5590 (fax)

Jan Johansson
Onsala Space Observatory
Chalmers University of Technology
S-43992 Onsala
Sweden

jmj@oso.chalmers.se
+46 31 772 5558
+46 31 772 5590 (fax)

Richard Kilger
Fundamental Station Wettzell
Sackenrieder Strasse 25
D-93444 Kötzting
Germany

kilger@wvax1.wettzell.ifag.de
+49 9941 603 263
+49 9941 603 222 (fax)

Roberto Lanotte
Nuova Telespazio S.p.A
Contrada Terlecchia
P.O. Box 155
I–75100 Matera
Italy

lanotte@hp755.mt.asi.it
+39 835 377238
+39 835 334951 (fax)

Isaac Lopez-Fernandez
Centro Astronomico de Yebes
Observatorio Astronomico Nacional
Apartado 148
E–19080 Guadalajara
Spain

isaac@cay.oan.es
+34 49 290311/37
+34 49 290063 (fax)

Ronald Molendijk
Survey Department
P.O. Box 5023
NL–2600 GA Delft
The Netherlands

r.e.molendijk@mdi.rws.minvenw.nl
+31 15 2691 464
+31 15 2618 962 (fax)

Arno Mueskens
Geodetic Institute of the Univ. of Bonn
Nussallee 17
D–53115 Bonn
Germany

am@hp.mpifr-bonn.mpg.de
+49 228 733562
+49 228 732988 (fax)
alternative 733281 (fax)

Gaetano Nicotra
Istituto di Radioastronomia del CNR
p.o. box 141
I–96017 Noto (SR)
Italy

nicotra@ira.noto.cnr.it
+39 931 835622
+39 931 573265 (fax)

Arthur Niell
Haystack Observatory
Westford, MA 01886
USA

aen@bashful.haystack.edu
+1 508 692 4764
+1 617 981 0590 (fax)

Biörn Nilsson
Onsala Space Observatory
Chalmers University of Technology
S–43992 Onsala
Sweden

bin@oso.chalmers.se
+46 31 772 5557
+46 31 772 5590 (fax)

Axel Nothnagel
Geodetic Institute of the Univ. of Bonn
Nussallee 17
D–53115 Bonn
Germany

nothnagel@uni-bonn.de
+49 228 733562
+49 228 732988 (fax)
alternative 733281 (fax)

Leonid Y. Petrov
Institute of Applied Astronomy
Zhdanovskaya st. 8
Sanct-Petersburg, 197042
Russia

petrov@ipa.rssi.ru
+7 812 230 74 14
+7 812 230 74 13 (fax)

Björn Ragnvald Pettersen
Geodetic Institute
Norwegian Mapping Authority
Kartverksveien 21
N–3500 Hönefoss
Norway

bjornrp@gdiv.statkart.no
+47 32 11 81 00
and +47 32 11 83 15
+47 32 11 81 01 (fax)

Richard Porcas
MPIfR
Auf dem Hügel 69
D–53121 Bonn
Germany
porcas@mpifr-bonn.mpg.de
+49 228 525 288
+49 228 525 229 (fax)

Maria J. Rioja
JIVE
Postbus 2
NL–7990 AA Dwingeloo
The Netherlands
rioja@nfra.nl
+31 521 595226
+31 521 597332(fax)

Antonio Rius
IEEC/CSIC Research Unit
LAEFF INTA
Edif. NEXUS,104
Gran Capita, 2–4
E–08034 Barcelona
Spain
rius@ieec.fcr.es
+34 72 336102
+34 72 337806 (fax)

Bernt Rönnäng
Onsala Space Observatory
Chalmers University of Technology
S–43992 Onsala
Sweden
bor@oso.chalmers.se
+46 31 772 5530
+46 31 772 5590 (fax)

Hans-Georg Scherneck
Onsala Space Observatory
Chalmers University of Technology
S–43992 Onsala
Sweden
hgs@oso.chalmers.se
+46 31 772 5556
+46 31 772 5590 (fax)

Harald Schuh
DGFI, Abt. I
Marstallplatz 8
D–80539 München
Germany
schuh@dgfi.badw-muenchen.de
+49 89 23031 214
+49 89 23031 240 (fax)

Mauro Sorgente
Geodetic Institute of the Univ. of Bonn
Nussallee 17
D–53115 Bonn
Germany
sorgente@kuestner.geod.uni-bonn.de
+49 228 733562
+49 228 732988 (fax)
alternative 733281 (fax)

Alexander A. Stotskii
Institute of Applied Astronomy
Zhdanovskaya st. 8
Sanct-Petersburg, 197042
Russia
stotskii@isida.ipa.rssi.ru
+7 812 230 7340
+7 812 230 74 13 (fax)

Oleg Titov
Institute of Applied Astronomy
Zhdanovskaya st. 8
Sanct-Petersburg, 197042
Russia
titov@ipa.rssi.ru
+7 812 230 74 14
+7 812 230 74 13 (fax)

Vincenza Tornatore
Istituto di Radioastronomia de CNR
C.P. 141
I–96017 Noto (SR)
Italy
tornatore@astbo1.bo:cnr.it
+39 931 835622
+39 931 573265 (fax)

Gino Tuccari
Istituto di Radioastronomia de CNR
C.P. 141
I–96017 Noto (SR)
Italy
tuccari@ira.noto.cnr.it
+39 931 835622
+39 931 573265 (fax)